ION SENSING AND MOLECULAR LOGIC IN

SUPRAMOLECULAR SYSTEMS

A THESIS SUBMITTED TO
THE GRADUATE SCHOOL OF NATURAL AND APPLIED SCIENCES
OF
MIDDLE EAST TECHNICAL UNIVERSITY

BY

ALİ COŞKUN

IN PARTIAL FULFILLMENT OF THE REQUIREMENTS
FOR
THE DEGREE OF DOCTOR OF PHILOSOPHY
IN
CHEMISTRY

SEPTEMBER 2007

Approval of the Thesis:

ION SENSING AND MOLECULAR LOGIC IN SUPRAMOLECULAR SYSTEMS

submitted by **ALİ COŞKUN** in partial fulfillment of the requirements for the degree of **Doctor of Philosophy in Chemistry Department, Middle East Technical University** by,

Prof. Dr. Canan Özgen _____
Dean, Graduate School of **Natural and Applied Sciences**

Prof. Dr. Ahmet Önal _____
Head of Department, **Chemistry**

Prof. Dr. Engin U. Akkaya _____
Supervisor, **Chemistry Dept., METU**

Examining Committee Members:

Prof. Dr. J. Fraser Stoddart (USA) _____
Chemistry Dept., University of California, at Los Angeles

Prof. Dr. Engin U. Akkaya _____
Chemistry Dept., METU

Prof. Dr. Metin Balcı _____
Chemistry Dept., METU

Prof. Dr. Ayhan S. Demir _____
Chemistry Dept., METU

Prof. Dr. Adil Denizli _____
Chemistry Dept., Hacettepe University

Date: _____

I hereby declare that all information in this document has been obtained and presented in accordance with academic rules and ethical conduct. I also declare that, as required by these rules and conduct, I have fully cited and referenced all material and results that are not original to this work.

Name, Last name : Ali Coşkun

Signature :

ABSTRACT

ION SENSING AND MOLECULAR LOGIC IN SUPRAMOLECULAR SYSTEMS

Coşkun, Ali

Ph.D, Department of Chemistry

Supervisor: Prof. Dr. Engin U. Akkaya

September 2007, 168 pages

Supramolecular chemistry is an emerging field of chemistry which has attracted much attention in recent years as a result of its broad applicability in many areas. Thus, the design of functional supramolecular systems is strongly in demand in this field. For this purpose, we have developed ratiometric fluorescent chemosensors for ion sensing and mechanically interlocked structures for their application in molecular logic.

In the first part, we report a novel dimeric boradiazaindacene dye which can be converted in one step to an efficient resonance energy transfer (RET) dyad. In addition, if this modification is done with appropriate ligands, RET can be coupled to

ion sensing. The utility of this approach is demonstrated in a highly selective, emission ratiometric chemosensor for Ag(I).

In the second part, boradiazaindacene dyads designed as energy transfer casettes were modified to signal cation concentrations ratiometrically. If the energy transfer efficiency is increased by changing spectral overlap on cation binding, an enhancement of emission signal ratios can be obtained. A larger range of ratios results in highly improved sensitivity to analyte concentrations. We demonstrate this approach in a *de novo* design of a novel and highly selective ratiometric chemosensor for Hg(II) ions.

In the last part, we synthesized a two-station [2]catenane composed of an π-electron rich bis-1,5-dihydroxynapthalene[38]-crown-10 (1/5DNPC10) ring interlocked with a second macrocycle containing two π-electron deficient unit, namely, napthodiimide (NpI) and bipyridinium (BIPY)$^{2+}$ unit using the Cu(I)-catalyzed Huisgen 1,3-cycloaddition reaction. The resulting bistable [2]catenane is isolated as a single co-conformation which is comprised of the 1/5DNP[38]C10 ring around the NpI unit. Thermal activation of the pure NpI-isomer at 70˚C for 60 h leads to the formation of the BIPY^{2+}-isomer by virtue of the circumrotation of the crown-ether ring along the backbone of the other macrocycle over the steric barrier of the tetra-aryl methane units. The energy barrier for the circumrotation is 28.5±0.3 kcal/mol. Electrochemistry of a 1:1 mixture of the two possible isomers shows that the [2]catenane cannot be switched mechanically on account of the large steric barriers presented by the tetra-aryl methane groups on the electron-accepting ring.

Keywords; boradiazaindacene, molecular logic gate, ion recognition, energy transfer, catenane

ÖZ

SÜPRAMOLEKÜLER SİSTEMLERDE İYON ALGILANMASI VE MOLEKÜLER MANTIK KAPILARI

Coşkun, Ali

Doktora, Kimya Bölümü

Tez yöneticisi: Prof. Dr. Engin U. Akkaya

Eylül 2007, 168 sayfa

Süpramoleküler kimya geniş uygulama alanlarından dolayı, son yıllarda kimyanın, hızla gelişen bir dalı haline gelmiştir. Bunun sonucu olarak da, fonksiyonel supramoleküler yapıların dizaynın da ve geliştirilmesine oldukça fazla ihtiyaç vardır. Bu amaçla, iyon algılayıcı sistemlerde kullanılmak üzere, oranlanabilir floresans moleküler algılayıcılar ve moleküler elektronik alanında uygulanmak üzere birbiri içine geçmiş yapılar geliştirilmiştir. Bu çalışmada, tek bir basamakta etkin bir enerji transfer diyadına çevirilebilen, yeni dimerik borodiazaindasen boyar maddeleri hazırlanmıştır. Bunun yani sıra, eğer bu modifikasyon uygun ligand ile yapılırsa, enerji transferi iyon algılanmasıyla birleştirilebilir. Bu yaklaşımın uygulanabilirliği, Ag(I) katyonuna oldukça yüksek selektivite gösteren emisyon orantılamalı bir moleküler algılayıcı ile gösterilmiştir. İkinci bölümünde, enerji transfer kaseti seklinde bulunan boradiazaindasen diyadları, orantısal olarak katyon

konsantrasyonu'nu sinyalleyebilecek bir biçime dönüştürülebilir. Eğer enerji transferinin etkinliği, katyon bağlanması sonucunda spektral örtüşmeyi değiştirerek arttırılırsa, emisyon sinyali oranlarında bir artış elde edilebilir. Bu oranlardaki artış, moleküler algılayıcının analit konsantrasyonuna duyarlılığını arttırır. Biz bu yaklaşımı, Hg(II) katyonuna oldukça yüksek seçicilik gösteren, yeni moleküler algılayıcımızda göstermiş bulunmaktayız. Bu çalışmamızın son bölümünde, 2 istasyona sahip bir [2]-Katenan sentezlemiş bulunmaktayız. Bu iç içe geçmiş halkalardan biri π-elektronca zengin bis-1,5-dihidroksinaftalin38-crown-10 (1/5DNPC10), diğeri ise naftodiimid (NpI) ve bipiridinyum (BIPY)$^{2+}$ birimlerini içermektedir. Bu birimler Cu(I) katalizörlüğünde, Huisgen 1,3-siklo katılması olarak da bilinen metotla birleştirilmiştir. Elde edilen [2]Katenan, tek bir konformasyonda izole edilmiştir, bu konformasyonda 1/5DNP38C10 halkası tamamıyla NpI birimi üzerindedir. Saf NpI izomerinin 70°C ve 60 saat sure ile termal aktivasyonu sonucunda, halka, tetra-arilmetan birimlerinden kaynaklanan sterik bariyeri asarak, BIPY^{2+}-izomerini oluşturmuştur. 1:1 karışım üzerinde yapılan elektrokimyasal çalışmalar bize, aradaki sterik bariyerler nedeniyle, elde edilen [2]katenan'ın mekanik olarak hareket ettirilemeyeceğini göstermiştir.

Anahtar kelimeler: boradizaindasen, moleküler mantık kapısı, iyon algılayıcı, enerji transferi, katenan

To my parents

ACKNOWLEDGEMENTS

TABLE OF CONTENTS

xii

LIST OF TABLES

TABLE

LIST OF FIGURES

FIGURE

xvi

LIST OF ABBREVIATIONS

CV :   Cyclic voltammetry

ET: Electron transfer

PET: Photoinduced electron transfer

PCT: Photoinduced charge transfer

TICT: Twisted internal charge transfer

FRET: Fluorescence resonance energy transfer

TFA: Trifluoroacetic acid

MSTJ: Molecular switch tunnel junction

NpI: Naphthalenedimide

BODIPY: Boradizaindacene
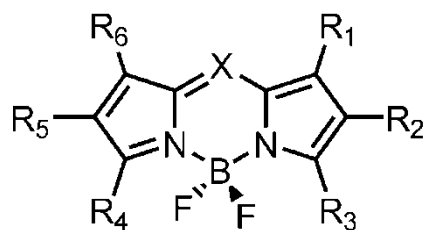
R = H or any group
X = C or N

CHAPTER 1

INTRODUCTION

1.1 Definition of Supramolecular Chemistry

Supramolecular chemistry can be defined as 'chemistry beyond the molecule' where a supermolecule is a species that is held together by noncovalent interactions between two or more covalent molecules or ions. It can also be described as 'Lego^{TM} chemistry', in this definition each lego brick represents one of the molecular components that held together by noncovalent interactions. [1]
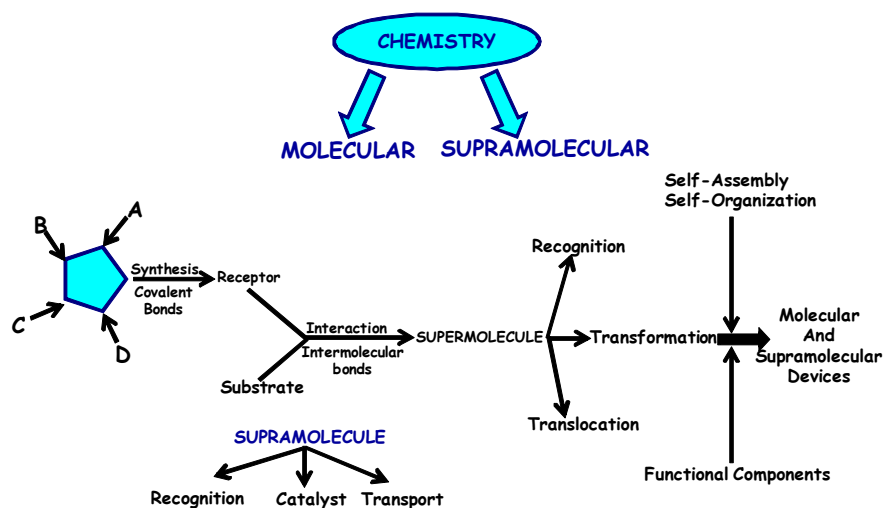
Figure 1. Comparison between molecular and supramolecular chemistry according to J.M. Lehn.[2]

These noncovalent interactions are mainly electrostatic interactions (ion-ion, ion-dipole and dipole-dipole), hydrogen bonding, π-π interactions, dispersion and induction forces (van der waals forces), hydrophobic or solvatophobic effects.

Supramolecular chemistry is defined as chemistry beyond the molecule, which means supramolecular chemistry is a multidisciplinary field which has strong interactions with other disciplines (Figure 1). Organic chemistry and inorganic chemistry are used as tools for the synthesis of the receptor molecules for the desired analyte and physical chemistry to understand the properties of supramolecular systems. Interaction of a receptor molecule with the appropriate analyte would yield a functional supermolecule. This formed supermolecule can perform mainly three operations, these are recognition, transformation and translocation. Finally, with the help of self-assembly, self-organization and appropriate functional components, one can obtain functional molecular and supramolecular devices. A great deal of biological chemistry involves supramolecular concepts and in addition a degree of technical knowledge is required in order to apply supramolecular systems to the real world. Supramolecular chemistry can be divided into two main categories: these are host-guest chemistry 'The study of large host molecules that are capable of enclosing smaller guest molecules via non-covalent interactions', and self-assembly 'The spontaneous and reversible association of two or more components to form larger supermolecules with the help of non-covalent interactions'. If one molecule is significantly larger than another and can wrap around it, then it is termed as 'host' and the smaller molecule as its 'guest', which is surrounded by host. One definition of hosts and guests was given by Donald Cram, who said 'The host component is defined as an organic molecule or ion whose binding sites converge in the complex'. [3] The guest component is any molecule or ion whose binding sites diverge in the complex. Molecular self-assembly is a key concept in supramolecular chemistry since assembly of the molecules is directed through noncovalent interactions, such as hydrogen bonding, metal coordination, hydrophobic forces, van der Waals forces, π-π interactions, and/or electrostatic effects. Simple examples include the formation of a micelle or a Langmuir monolayer by surfactant molecules in solution. More advanced examples of supramolecular assemblies demonstrate that a variety of different shapes and sizes can be obtained using molecular self-assembly. Nature itself is full of supramolecular systems and the inspiration for many supramolecular species designed and developed by chemists has come from biological systems.

1.2 Supramolecular Interactions

In general, supramolecular chemistry concerns noncovalent bonding interactions. Noncovalent interactions represent the energies that hold supramolecular species together. Noncovalent interactions are considerably weaker than covalent interactions, which can range between ca. 150 kj mol^{-1} to 450 kj mol^{-1} for single bonds. Noncovalent bonds range from 2 kj mol^{-1} for dispersion interactions to 300 kj mol^{-1} for 'ion-ion' interactions. However, when these interactions are used in a co-operative manner a stable supramolecular complex can form. The term 'noncovalent' is an enormous range of attractive and repulsive forces.[4] These forces can be summarized as follows;

1.2.1 Ionic and dipolar interactions

These interactions can divided into three sub-categories:(i) ion-ion interactions, (ii) ion-dipole interactions and (iii) dipole-dipole interactions, which are based on the Coulombic attraction between opposite charges (See Figure 2). The strongest one of these interactions is the ion-ion interaction, which is comparable with covalent interactions. In comparison to ion-dipole and dipole-dipole interactions, ion-ion interactions can occur in any orientation. It is the one of reasons why ion-ion interactions are stronger than directional interactions. Despite being the weakest directional interaction, dipole-dipole interactions are useful for bringing species into alignment, as the interaction requires a specific orientation of both

| ion-ion | ion-dipole | dipole-dipole |
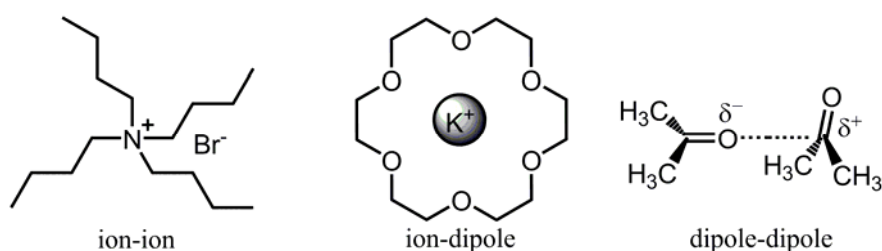
Figure 2. Examples of electrostatic interactions.

entities. Electrostatic interactions play an important role in understanding the factors that influence high binding affinities, particularly in biological systems in which there is a large number of recognition processes that involve charge-charge interactions; indeed these are often the first interactions between a substrate and enzyme. [5]

1.2.2 Hydrogen bonding

A hydrogen bond may be regarded as a particular kind of dipole-dipole interaction in which a hydrogen atom attached to an electronegative atom (or electron withdrawing group) is attracted to a neighbouring dipole on an adjacent molecule or functional group. Because of its relatively strong and highly directional nature, hydrogen bonding is the key interaction for supramolecular chemistry. Typically, the strengths range from 4 to 120 kj mol^{-1}, with the vast majority being under 60 kj mol^{-1}. There are a number of naturally occurring 'building blocks' that are a rich source of hydrogen bond donors and acceptors (e.g. amino acids, carbohydrates and nucleobases). In particular, hydrogen bonds are responsible for the overall shape of many proteins, recognition of substrates by numerous enzymes, and for the double helix structure of DNA.
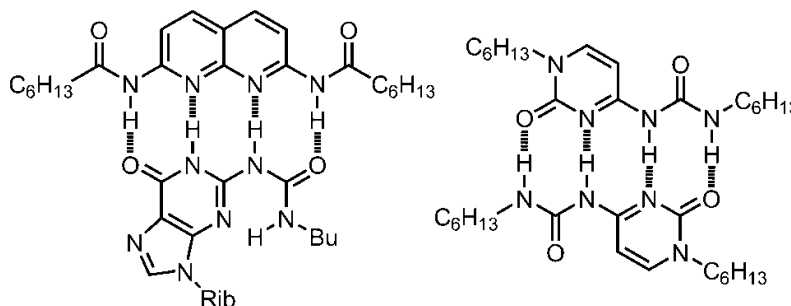
Figure 3. Four-point dimers developed by Zimmerman and Hailes.

The addition of extra hydrogen bonds to a monomeric recognition unit is another effective means of enhancing the association of dimeric ensembles based on functionalized nucleobases.[6](See Figure 3).

1.2.3. π interactions

There are two main π-interactions that can be found in supramolecular systems, namely (i) cation- π interaction [7] and (ii) π-π interactions [8]. Cation- π interactions are well known in the field of organometallic chemistry, whereby olefinic groups are bound to transition metal centers, for example, ferrocene, but these are not regarded as noncovalent interactions. For example, the interaction of potassium ions with benzene has a similar energy to the K^+-OH_2 interaction. The potassium cation is more soluble in water than in benzene, however, as it is not sterically possible to fit as many benzene molecules around the metal ion as water molecules.

The two types of π- π interactions are face to face, whereby parallel ring systems, separated by ca. 3.5Å, are offset and the interaction is between the centre of one ring and the corner of another, and edge-to-face, whereby a hydrogen atom from one ring interacts in a perpendicular orientation with respect to the centre of another ring. These π-π interactions arise from the attraction between the negatively charged π-electron cloud of one conjugated system and the positively charged σ-framework of a neighbouring molecule.

1.2.4 Van der Waals forces

Van der Waals interactions arise from the polarization of an electron cloud by the proximity of an adjacent nucleus, resulting in a weak electrostatic attraction. They are nondirectional an hence possess only limited scope in the design of specific hosts for selective complexation of particular guests. In general, van der Waals interactions provide a general attractive interaction for most polarisable species. Van der Waals interactions may be divided into dispersion (London) and exchange-repulsion terms. The dispersion interaction is the

attractive component that results from the interactions between fluctuating multipoles in adjacent molecules. The attraction decreases very rapidly with distance and is additive with every bond in the molecule contributing to the overall interaction energy. [9]

1.2.5 Hydrophobic effects

Hydrophobic effects [10] arise from the exclusion of non-polar groups or molecules from aqueous solution (Figure 4). This situation is more energetically favorable because water molecules interact with themselves or with other polar groups or molecules. This phenomenon can be observed between dichloromethane and water which are immiscible. The organic solvent is forced away as the inter-solvent interactions between the water molecules themselves are more favorable than the 'hole' created by the dichloromethane. Hydrophobic interactions play an important role in supramolecular chemistry, for example, the binding of organic molecules by cyclophanes and cyclodextrins in water. Hydrophobic effects can be split into two components, namely an enthalpic hydrophobic effect and entropic hydrophobic effect. Enthalpic hydrophobic interactions occur when a guest replaces the water within a cavity. Entropic hydrophobic interactions come about when there are two or more organic
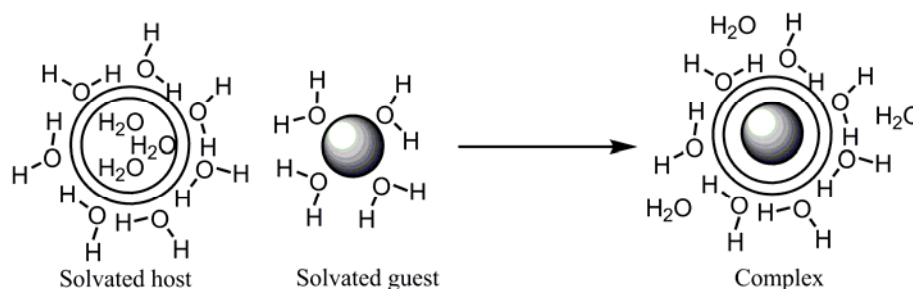
Figure 4. Hydrophobic binding of organic guests in aqueous solution.

aqueous solution, the combination of host with the guest molecule replaces the water molecules which placed interior of host molecule. It can be aasumed that

6

there is initially two species in the medium. When supramolecular complex forms, displacement of the water molecules both around the guest and inside host will increase the number of independent species, thus, it will increase the total entropy of the system.

1.3 Molecular recognition

Molecular recognition is defined by the energy and the information involved in the binding and selection of substrates by a given receptor molecule. Binding is no recognition, but the recognition is a binding with a purpose. Recognition processes works through set of intermolecular interactions. Binding of receptor to analyte forms a complex or supermolecule characterized by its (thermodynamic and kinetic) stability and selectivity, by the amount of energy and of information brought into operation.Molecular recognition implies the molecular storage and supramolecular read out of molecular information. Information may be stored in the architecture of the receptor, in its binding sites and in the ligand layer surrounding bound analyte; its read out is related to the rate of formation and dissociation of the supermolecule. The binding sites are characterized by their electronic properties (charge, polarity, polarisability, van der Waals attraction and repulsion), their size, shape, number and the arrangement in the receptor framework.

Gathering information is a key notion of supramolecular chemistry which may be considered as a chemical information science or molecular informatics concerned with the molecular storage and the supramolecular reading and processing of the information via the structural and temporal features of molecules and supermolecules.

Recognition implies geometrical and interactional complementarity between the associating partners, optimal information content of a receptor with respect to a given analyte. This interpretation amounts to a generalized double complementarity principle extending over energetic features, as well as over the geometrical ones represented by the 'lock and key' concept of Emil Fischer. [11]

In order to achieve large differences in affinity several factors must be taken into account:

- Steric (shape and size) complementarity between receptor and analyte.
- Interactional complementarity, presence of complementary binding sites (electrostatic such as positive-negative, charge-dipole, dipole-dipole, hydrogen bond, etc.) in the correct disposition on receptor and analyte
- Large contact areas between receptor and analyte
- Multiple interaction sites, since noncovalent interactions are rather weak compared to covalent bonds
- Strong overall binding, in order to achieve efficient recognition. Both high stability and high selectivity, strong binding of receptor and analyte is required.

In addition, medium effects play an important role through the interaction of solvent molecules with receptor and analyte as well as each other; thus, the two partners should present geometrically matched hydrophobic-hydrophobic or hydrophilic-hydrophilic domains.

1.4 Molecular Sensors

In biology, chemistry, and material sciences, analyte recognition, the determination of local environmental properties or the operation of molecular-scale switches, requires the efficient transduction of an event into a measurable signal. Depending on the actual location of the source and the properties of the surrounding medium, the signal generated by such an event should ideally be detectable both in close vicinity as well as at remote distances and should strongly differ from any signals from an unspecific background, the unbound sensor, or the switch in the 'ZERO' or 'OFF' position. Moreover, a rational application implies that the desired information is only reported upon request. Random and uncontrolled generation of the analytically important output by, for instance, changes of other environmental and physical parameters or by unintended chemical processes, which are likely to occur in the biological, natural or artificial medium of operation, have to be avoided.

Among the numerous analytical methods that are available for the detection of various analytes, flame photometry, atomic absorbtion spectrometry, ion sensitive electrodes, etc. are expensive, often require samples of large size and do not allow continuous monitoring. So, the molecular sensors gains primary importance in this area. Molecular sensors can be split into two major categories: These are electrochemical sensors and optical sensors. Electrochemical sensors, can be obtained with the attachment of redox active unit to the receptor moiety. Complexation can be signaled by direct coordinate bond formation between the redox centre[12], induced conformational perturbation of the redox centre caused by guest complexation [13] and through-bond electrostatic communication. [14] These changes can be monitored cyclic voltammetry (CV) technique.

Although the most common type of the optical sensors are fluorescent sensors, there are also colorimetric, [15] and electron-transfer (ET) path selective sensors,[16]. The responses in the last two examples are followed according to changes in their absorbances. Whereas absorbance measurements for colorimetric sensors can reliably determine concentrations only as low as several tenths of a micromolar, fluorescence techniques can accurately measure concentrations one million times smaller, at pico and even femtomolar concentrations. The methods based on fluorescent sensors offer distinct advantages in terms of sensitivity, selectivity, response time, local observation (e.g. by fluorescence imaging spectroscopy). Moreover, remote sensing is possible by using optical fibers with a molecular sensor immobilized at the tip. Therefore, considerable efforts are being put to develop selective fluorescence sensors.

1.5 Fluorescent signaling phenomena

Fluorescent sensors consist of a fluorophore linked to a receptor (Figure 5). These fluoroionophors can signal various analytes such as anions, cations and neutral species. In the design of sensors, the most important part is the recognition and signaling moieties. The signaling moiety acts as a signal transducer, it converts the information into an optical signal expressed as the changes in the photophysical characteristics of the fluorophore. These changes are

due to the perturbation (by the bound analyte) of photoinduced processes such as electron transfer, charge transfer, energy transfer, excimer or exciplex formation or disappearance, etc. these aspects are relevant to the field of photophysics. As regards the recognition moiety, it is responsible for selectivity and efficiency of binding which depend on the ligand topology, on the characteristics of the analyte (charge, size, shape, ….), and on the nature of the solvent (pH, ionic strength, …). These aspects are relevant to the field of supramolecular chemistry. The signaling moiety and the receptor can be attached in two different ways; the receptor is either directly linked to the signaling unit (integrated) or it is linked to the signaling unit via a spacer (spaced). [17]
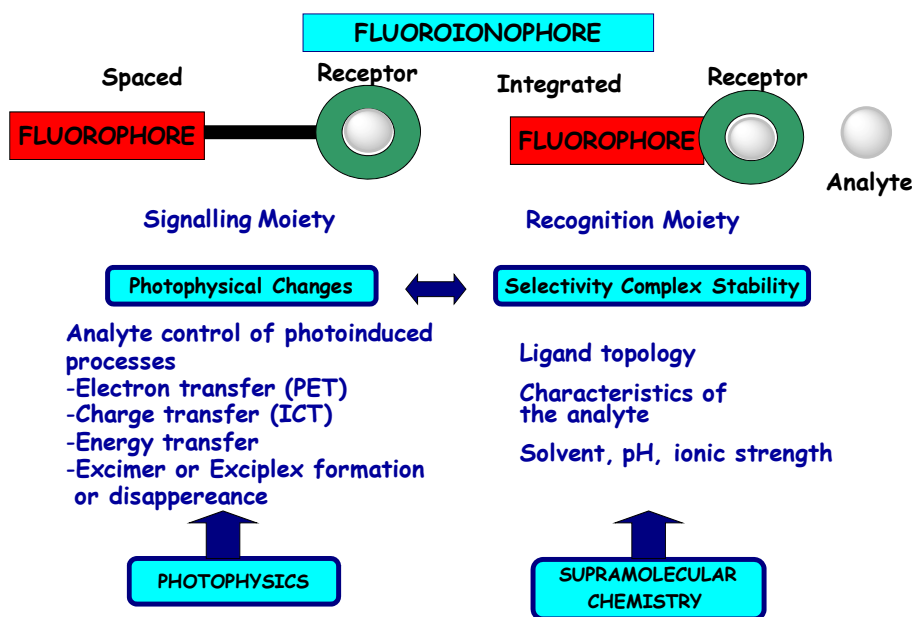
Figure 5. Main aspects of fluorescent molecular sensors.

1.5.1 Photoinduced electron transfer (PET)

Photoinduced electron transfer (PET) is a signaling event which relies on emission quenching or enhancement. This process is involved in many organic photochemical reactions. It plays a major role in photosynthesis and in artificial systems for the conversion of solar energy based on photoinduced charge separation. Besides these, PET is widely used in sensors for the fluorescent

sensing of various analytes (cations, anions, neutral molecules, etc.). the exploitation of this information for the development of fluorescent sensors and switches has been confined to the last two decades with the few pioneering efforts being scattered across the first of these decades. Fluorescent signaling via the PET strategy is distinguished by its intirinsically supramolecular nature since distinct components perform each one of the necessary functions. A fluorophore module is the site of both photonic transactions of excitation and emission. A receptor module is responsible for guest complexation and decomplexation. A spacer module holds the fluorophore and the receptor close to, but separate from, each other. This also means that true molecular engineering applies, the optical,
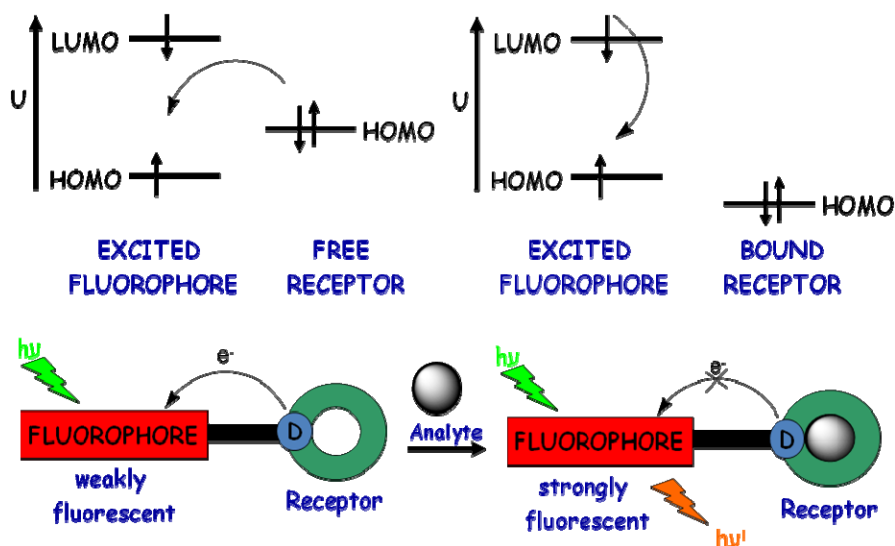
Figure 6. Schematic representation of photoinduced electron transfer (PET).

guest-binding, and redox properties of the components to allow the quantitative prediction of the signaling parameters of the supramolecular system. Further, PET signaling systems have natural switchability: guest-induced "off-on" and "on-off" fluorescence are both designable. Figure 6 explains how an analyte can control PET mechanism in a fluoroionophore in which the receptor is an electron donor (e.g. amino group) and fluorophore plays the role of an acceptor. In this case designed system is an "off-on" type signaling system. Upon excitation of the fluorophore, an electron of the highest occupied molecular orbital (HOMO) is promoted to the lowest unoccupied molecular orbital (LUMO), which enables

PET from the HOMO of the donor (which belongs to the free receptor) to that of the fluorophore, causing the fluorescence quenching of the latter. Upon analyte binding, the redox potential of the donor is raised so that the relevant HOMO becomes lower in energy than that of fluorophore; consequently, PET is not possible any more fluorescence quenching is suppressed. As a result of this, fluorescence enhancement occurs. PET may sometimes occur from acceptor to donor. Then it is called oxidative PET (or reverse PET). After blocking PET by cation binding, excitation energy is transferred from the fluorophore, through the ligand to another bound cation such as Eu(III), Tb(III), Zn(II), etc. It is also known that coordination of anions to the metal center blocks oxidative PET mechanism and as a result of this emission intensity is restored. [18]

There are several laboratories working in this field, these include the groups of Czarnik, Fabbrizzi, Tsien, Kuhn, Deservenge, de Silva, Nagano, Valeur, Shinkai and ourselves.

Some examples of the PET sensors for cation recognition is given in Figure 7, compound **1** [19] is the simplest and first PET sensor which has been synthesized by de Silva et al., its fluorescence quantum yield increases from
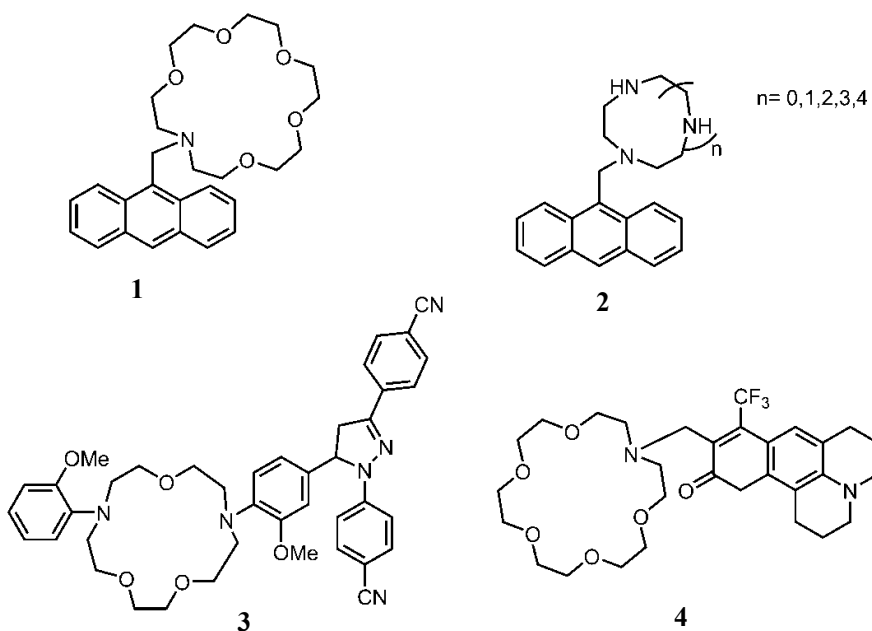
Figure 7. Crown containing fluorescent PET sensors.
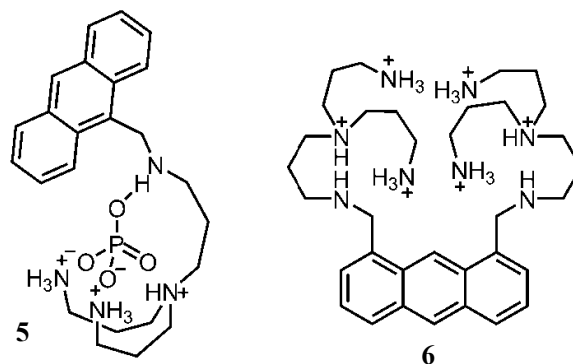
Figure 8. Polycationic PET sensors for anion recognition

0.003 to 0.14 upon binding of K$^+$ in methanol solution. Compound **2** [20] was designed by Czarnik et al. for the recognition of soft metal ions like Zn^{2+}. In **3** [21] the recognition moiety is similar to that of Tsien`s PCT fluorescent sensor, the methoxy groups being in ortho position with respect to the nitrogen atoms of the crown participate in the complexation, so that strong Na$^+$ binding is achieved. Na$^+$ causes decoupling of the nitrogen centers from the rest of the π-electron system of the receptor. Thus, the retardation of PET causes Na$^+$-induced switching `on` of the fluorescence. Compound **4** [22] is one of several examples from Valeur`s group which responds to a variety of metal ions from various regions of the Periodic Table. Charge density control of the metal ion-induced fluorescence enhancement is evident. Another interesting point of compound **4** is that the ICT excited state of the fluorophore is stabilized by the metal ion when bound the receptor. This leads to metal ion induced red shifts in the emission.

Another interesting compound has been synthesized by Czarnik et al., a clever adaptation of a partially protonated polyamine to serve as a receptor whose PET channel is blocked upon arrival of HPO$_4^{2-}$ guest can be seen in complex **5**. [23] Two of these receptor units can be placed on the 1- and 8- positions of an anthracene fluorophore as in **6** [24] in order to create a signaling PET system for pyrophosphate in the form of H$_2$P$_2$O$_5^{2-}$. Both these cases require careful pH control for success. A judicious use of nonmacrocyclic receptors within fluorescent PET "off-on" signaling systems against cationic and anionic targets is

illustrated in Figure 8. One of the recent examples of a PET type thiol sensor is reported by Nagano et al. [25] who designed thiol-reactive fluorescence probe **7** based on BODIPY fluorophore. The fluorescence of this fluorophore is strongly quenched by oxidative PET which was previously explained and examined by our group [26].
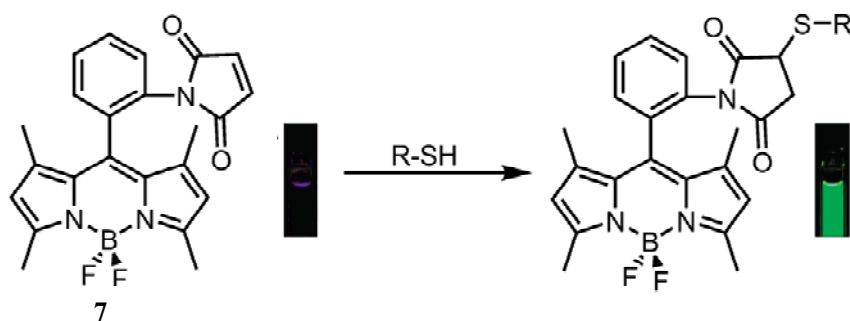
Figure 9. Thiol-reactive BODIPY based on oxidative PET

In this case, electron transfer occurs from the BODIPY fluorophore to the maleimide group, but after reaction with the thiol, the fluorescence of BODIPY is restored, affording a 350-fold intensity increase. The fluorescence quantum yield of BODIPY changes from 0.002 to 0.73 upon reaction with the thiol. Also the position of the maleimide group is important source m- and p- substitutions do not cause the desired change, only the o- substituted one gives an enhancement factor.

1.5.2 Photoinduced charge transfer   (PCT)

In the case of PCT, the spacer module between receptor unit and signaling unit is removed. In contrast to PET, a fluorophore is directly integrated with the receptor so that their orbitals overlaps to such an extent that the joint doesn't show. Then, one terminal tends to be electron rich and the other electron poor. In such 'push–pull' cases, excitation leads to a serious redistribution of electron density, so that a substantial dipole is created.   This excitation causes

intramolecular charge transfer from donor to the acceptor. Binding of a target species, especially a charged one, into the receptor naturally causes an interaction with this excited state dipole. This interaction energy shows up in the emission signature.

The excited state of the fluorophore looks like the resonance form of the ground state. The consequent change in dipole moment results in a Stokes shift that depends on the microenvironment of the fluorophore; polarity probes have been designed on this basis. It can thus be anticipated that cations, in close interaction with the donor or the acceptor moiety, will change the photophysical properties of the fluorophore because the complexed cation affects the efficiency of intramolecular charge transfer. When a group (like an amino group), playing the role of an electron donor within the fluorophore, interacts with a cation, the latter reduces the electron-donating character of this group; owing to the resulting reduction of conjugation, a blue shift of the absorption spectrum is expected, together with a decrease of the extinction coefficient. The photophysical changes upon cation binding can also be described in terms of charge dipole interactions. Excited state will be electronically similar to the resonance forms of the ground state, where the amino group will be positively charged. Thus, the interaction between this moiety and the cation will destabilize the excited state. This event will cause an increase in the energy gap between S_0 and S_1 energy levels. Increasing energy will cause decrease in the wavelength, as a result of this interaction a blue-shift occurs and the desired analyte can be signaled in this way. Conversely, a cation interacting with the acceptor group (like a carbonyl group) enhances the electron-withdrawing character of this group; the absorption spectrum is, thus, red-shifted and the molar absorption coefficient is increased. We can also describe this change in terms of a charge-dipole interaction; when the cation interacts with the acceptor group, the excited state is more stabilized by the cation than the ground state, and this phenomenon leads to a red shift of the absorption and emission spectra. If we consider the resonance structure of the acceptor group, in the excited state carbonyl oxygen to be negatively charged, this situation will increase the interaction between cation and the acceptor group. As a result of this interaction, the excited state is stabilized, and the energy gap between S_0 and S_1 will decrease, causing a red-shift in the spectrum. The

15

fluorescence spectra are, in principle, shifted in the same direction as those of the absorption spectra. In addition to these shifts, changes in quantum yields and lifetimes are often observed. All these photophysical effects are obviously dependent on the charge and the size of the cation, and selectivity of these effects are expected (See Figure 10). [27]
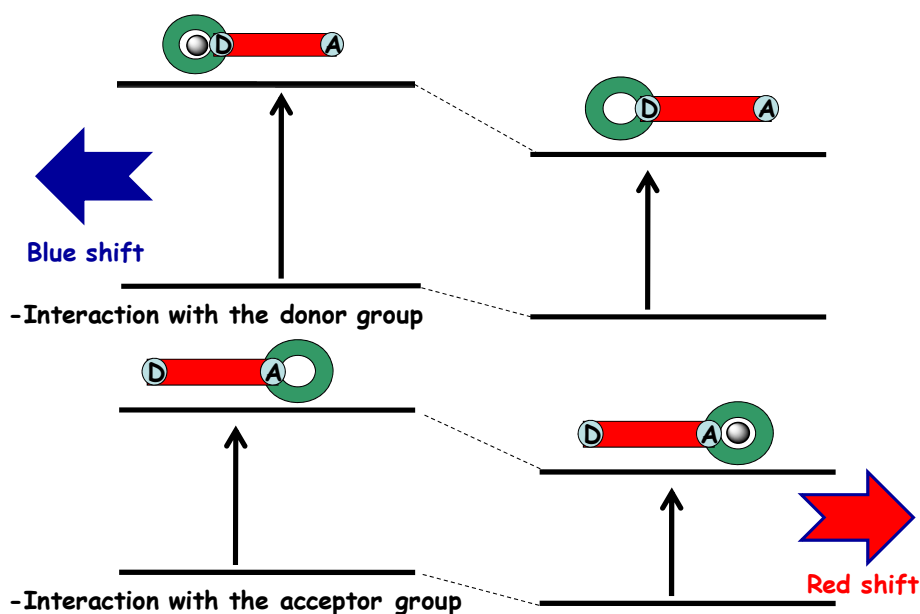
Figure 10. Spectral displacements of PCT type sensors

Many fluoroionophores have been designed according to the following principle: the cation receptor is an azacrown containing a nitrogen atom which is conjugated to an electron-withdrawing group. Compounds **8** to **13** exhibit common features: the blue shift of the absorbtion spectrum is much larger than that of the emission spectrum on cation binding. **8** [28], **9** [29], **10** [30], **11** [31], **12** [32], **13** [33] showed similar affinities towards calcium ion. The PCT reduces the electron density on the nitrogen atom of the crown, and this nitrogen atom becomes a noncoordinating atom because it is positively charged. Therefore, excitation induces a photodisruption of the interaction between the cation and the nitrogen atom of the crown. The fluorescence spectrum is slightly affected because most

of the fluorescence originates from species in which the interaction between the cation and the fluorophore is non-existent or much weaker. Also the quantum yield of this type of fluorophores is quite low on account of the excited state rotation around the double bond between donor and acceptor units. The absence of fluorescence of **14** [34] may be a consequence of the formation of a nonfluorescent TICT state, and an acridinium type fluorescence is recovered upon binding of H+ and Ag(I). In most cases, the changes in fluorescence intensity upon binding of an analyte are not very large in PCT sensors as compared to PET sensors.
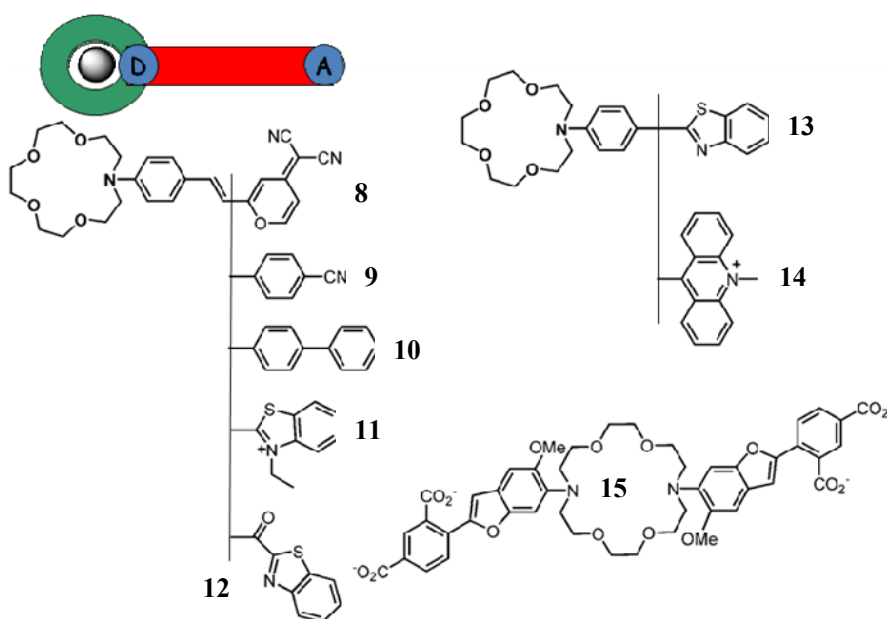
Figure 11. Crown containing PCT sensors.

Compound **15** was synthesized by Tsien et al. In this case, the improvement of selectivity can be achieved by the participation [35] of external groups as shown in Figure 11. In **15**, the oxygen atom of the methoxy substituent of the fluorophore can interact with a cation; the binding efficiency and selectivity are thus better than those of the crown alone. **15** has been designed for probing intracellular sodium ions.

Compound **16** [36] in Figure 12 was synthesized by our group. This compound shows PET and PCT type behavior in a single molecule. This unique

feature of **16** has been used to generate a unimolecular half-subtractor. Addition of a base to the THF solution of this dye, deprotonates the OH group and quenches the fluorescence (PET mechanism). And addition of acid cause a drastic blue-shift (100 nm) both in absorbance and emission spectrum. Upon addition of acid, the fluorescence quantum yield of the compound changes from 0.30 to 0.70.
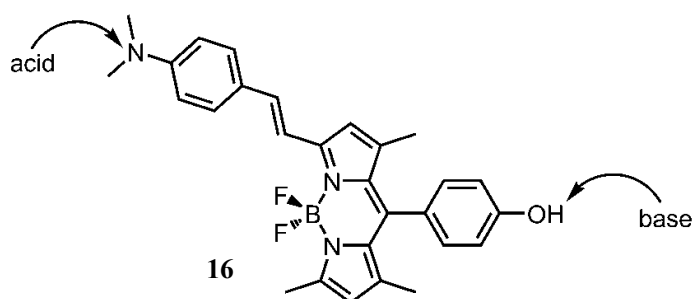
Figure 12. BODIPY based unimolecular half-subtractor

The near-absence of ICT fluorophores responsive to small anionic or neutral molecules is an important fact. Some headway is being made by Shinkai et. al. with **17** [37] which shows a small spectral shift upon binding fructose. It may be symptomatic that similar structural motifs give rise to much larger fluorescence responses when coupled to different photochemical mechanisms. The cyanine dye **18** [38] is more promising. Its ICT excited state is poorly fluorescent until

Figure 13. ICT flurophores responsive to neutral molecules

monosaccharide binding obstructs its torsion.   The switching "on" of the fluorescence by visible excitation and the detection of a previously interactable analyte are two very positive developments.

1.6 Energy Transfer Systems

Fluorescent labels that emit light at wavelengths distant from that of the source used to excite them have many applications in biotechnology. For single dye systems, the difference between the S_0 absorption and the S_1 emission wavelengths is the Stokes` shift.  When the Stokes` shift of a single dye is insufficient for a particular application, strategies that exploit through-space energy transfer between two dyes are frequently used. An absorbing molecular fragment (a donor) is arranged to be proximal to an emitting fragment (an acceptor); the donor is then excited at wavelengths close to its λ_{max} , and the fluorescence of the acceptor is observed. For biotechnological applications, the donor and acceptor units are usually connected via non-conjugated linker systems, hence the predominant energy transfer mechanism is through-space (Förster mechanism). A requirement for Förster energy transfer is that the emission spectrum of the donor must overlap with the absorption spectrum of the acceptor. That requirement places an upper limit on the range of fluorescence wavelengths from two-dye cassettes irradiated using a single excitation wavelength. In contrast to through-space energy transfer cassettes, donor and acceptor units connected by conjugated linker fragments may transfer energy via several pathways. These pathways include through-space energy transfer, but also other pathways that may be collectively referred to as through-bond energy transfer mechanisms, which include Dexter energy transfer and others.

1.6.1 Dexter type energy transfer (through bond)

The literature on molecules that exhibit through-bond energy transfer may be divided into that which deals with oligomeric conjugated materials, and other contributions featuring models for biological systems (e.g. porphyrin-containing

systems).   Energy transfer through bonds does not require the excited energy states of the donor to overlap with the lowest energy excited states of the acceptor. Of course, excitation of any molecule above the S_1 state will lead
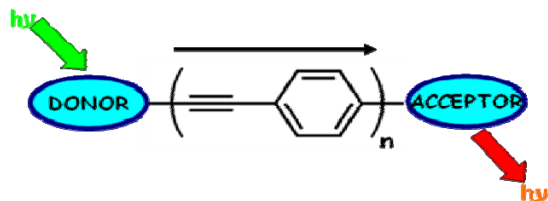
Figure 14. Through-bond energy transfer

to S_1 to S_0 fluorescence, but the higher energy absorption cross sections are often low and they vary considerably between molecules. In conjugated donor-acceptor cassettes, however, a given donor part can be incorporated to absorb strongly at a given wavelength, and the acceptors can be varied to emit at different wavelengths that are distant from that of the source used to excite them. This phenomenon can be exploited in biotechnology. For conjugated cassettes of the type shown in Figure 14, it may not be possible to ascertain how much energy transfer proceeds via through-bond mechanisms relative to the through-space pathways. This situation is very likely to be the case when the donor and acceptor fragments are relatively close together. Nevertheless, the overall rates of energy transfer can be measured; they, in turn, will be influenced by the structure of the donor, acceptor, and linker fragments, and the orientation of the donor-linker-acceptor connectivity.

Compounds **19** [39] and **20** [39] have been synthesized by Burgess et al. It is evident that the orientation of the donor and acceptor fragments will effect the energy transfer efficiency. The key feature for the design of this kind of systems is conjugation.

19 **20**
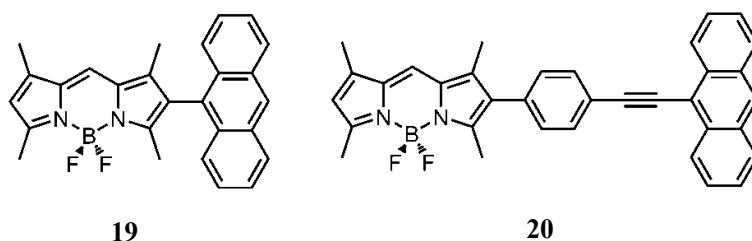
Figure 15. Through bond energy transfer cassettes.

If the system is completely conjugated, then it will not be a true energy transfer cassette. It shows red shifted broad absorbance. But in **19** the anthracene donor and the BODIPY acceptor are directly attached and significant steric interactions preventing the donor acceptor fragments becoming planar. The corresponding steric effects for compound **20** are evident, but not so severe.

Compound **21** [40] (Figure 16) has been designed for intracellular imaging, and the electronic spectra of the compound shows several desirable

21
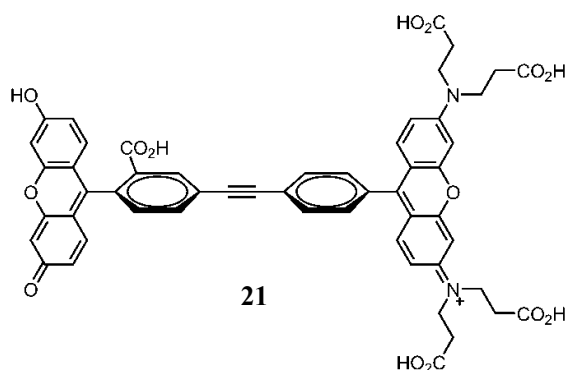
Figure 16. Water-soluble through-bond energy transfer cassette.

characteristics. However, the energy transfer efficiency is not %100. The reason for this is some of the fluorescence leaks from the fluorescein donor rather than being transferred to the acceptor. Compound **21** is used to label the proteins and the labeled proteins are loaded into the living cells, When the cells are excited at

488 nm (to excite the donor), the acceptor fluorescence at 598 nm is observed. The main advantage of this system, namely large Stokes` shifts prevent the likelihood interference and the scattering of the light arising from the condensed media of the cell.

A set of soluble synthetic porphyrin arrays for the construction of light-harvesting model compounds and related molecular photonic devices have been developed by Lindsey et al.[41] These studies suggested that the

22
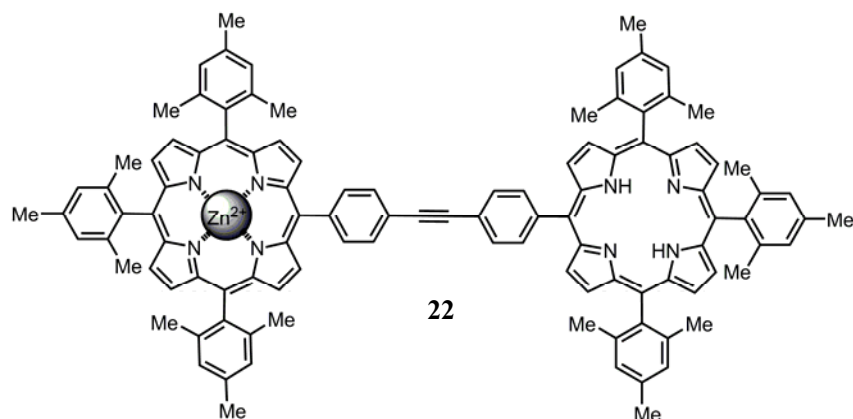
Figure 17. Porphyrin containing energy transfer cassette (Dexter type)

diphenylethyne unit mediates electronic communication between the porphyrins, and that rotation toward a more coplanar geometry of the diphenylethyne with the porphyrins would enhance the communication and thereby increase the energy transfer rate. To investigate this hypothesis, concerning structural control of energy transfer, Lindsey et al. prepared a set of dimeric arrays. Zinc and free base porphyrins (compound **22**) are employed in the arrays. Free-base porhyrins absorb and emit at longer wavelengths than zinc porphyrins and serve as a convenient low-energy trap to which excited-state energy flows.

1.6.2 Förster type (through space)

Fluorescence resonance energy transfer (FRET) is a nonradiative process whereby an excited state donor D (usually a fluorophore) transfers energy to a proximal ground state acceptor A through long-range dipole–dipole interactions. The acceptor must absorb energy at the emission wavelength of the donor, but does not necessarily have to abate the energy fluorescently itself (i.e., dark
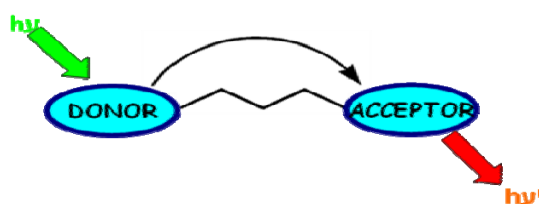
Figure 18. Through-space energy transfer

quenching). The rate of energy transfer is highly dependent on many factors, such as the extent of spectral overlap, the relative orientation of the transition dipoles, and, most importantly, the distance between the donor and acceptor molecules. FRET usually occurs over distances comparable to the dimensions of most biological macromolecules, that is, about 10 to 100 Å. Although configurations in which multiple donors and acceptors interact are increasingly common, the following equations consider energy transfer between a single linked D/A pair separated by a fixed distance r and originate from the theoretical treatment of Förster. The energy transfer rate $k_T(r)$ between a single D/A pair which is dependent on the distance r between D and A can be expressed in terms of the Förster distance R_0. R_0 is the distance between D and A at which 50% of the excited D molecules decay by energy transfer, while the other half decay through other radiative or nonradiative channels. R_0 can be calculated from the spectral properties of the D and A species (Eq. 1).

$$R_0 = 9.78 \times 10^3 [\kappa^2 n^{-4} Q_D J(\lambda)]^{1/6} \quad \text{(in Å)} \qquad \text{Eq. (1)}$$

The factor κ^2 describes the D/A transition dipole orientation and can range in value from 0 (perpendicular) to 4 (collinear/parallel). There has been much debate about which dipole orientation value to assign for particular FRET formats. Only in few cases can the crystal structure of the D/A molecules be determined; there is no other reliable experimental method to measure absolute or fixed κ^2 values, which leads to potential uncertainties in subsequent calculations. Fortunately, the accumulated evidence has shown that the mobility and statistical dynamics of the dye linker lead to a κ^2 value of approximately 2/3 in almost all biological formats. The refractive index n of the medium is ascribed a value of 1.4 for biomolecules in aqueous solution. Q_D is the quantum yield (QY) of the donor in the absence of the acceptor and $J(\lambda)$ is the overlap integral, which represents the degree of spectral overlap between the donor emission and the acceptor absorption. The values for $J(\lambda)$ and R_0 increase with higher acceptor extinction coefficients and greater overlap between the donor emission spectrum and the acceptor absorption spectrum. Whether FRET will be effective at a particular distance r can be estimated by the "rule of thumb" $R_0 \pm 50\%$ R_0 for the upper and lower limits of the Förster distance. The efficiency of the energy transfer can be determined from either steady-state [Eq. (2)] or time-resolved [Eq. (3)] measurements.

$$E = 1 - \frac{F_{DA}}{F_D} \qquad \text{Eq. (2)} \qquad\qquad E = 1 - \frac{\tau_{DA}}{\tau_D} \qquad \text{Eq. (3)}$$

F is the relative donor fluorescence intensity in the absence (F_D) and presence (F_{DA}) of the acceptor, and t is the fluorescent lifetime of the donor in the absence (τ_D) and presence (τ_{DA}) of the acceptor. FRET is very promising for bioanalysis because of its intrinsic sensitivity to nanoscale changes in D/A separation distance (proportional to r^6). This property is exploited in FRET techniques ranging from the assay of interactions of an antigen with an antibody in vitro to the real-time imaging of protein folding in vivo. [42]

Many research groups are currently working in this field, some examples are summarized below. Diederich et al. developed compound **23** [43] which operates as an acid-base switchable energy transfer cassette. They attached two bodipy derivatives onto a resorciarane unit, which is sensitive to acid. To control the efficiency of the energy transfer, rigid analogues of **23** have been synthesized with increasing distance between donor and acceptor BODIPY dye pair. FRET efficiency strongly decreases with increasing length of the rigid spacer from about 98% when the distance r=19 Å (between the B atoms of the dyes), to ≈85% when the distance r=32 Å), and to ≈35% when the distance r=53 Å). Importantly, addition of TFA (up to c=0.3m) does not affect the emission behavior. Upon addition of TFA to compound **23**, the acceptor fluorescence vanishes nearly completely, whereas the donor fluorescence doubles in intensity. In the expanded state, with a separation of donor and acceptor of ≈7 nm, the FRET efficiency is dramatically reduced. Thus, the large-scale expansion/contraction movement of **23** is clearly proven by FRET measurements.
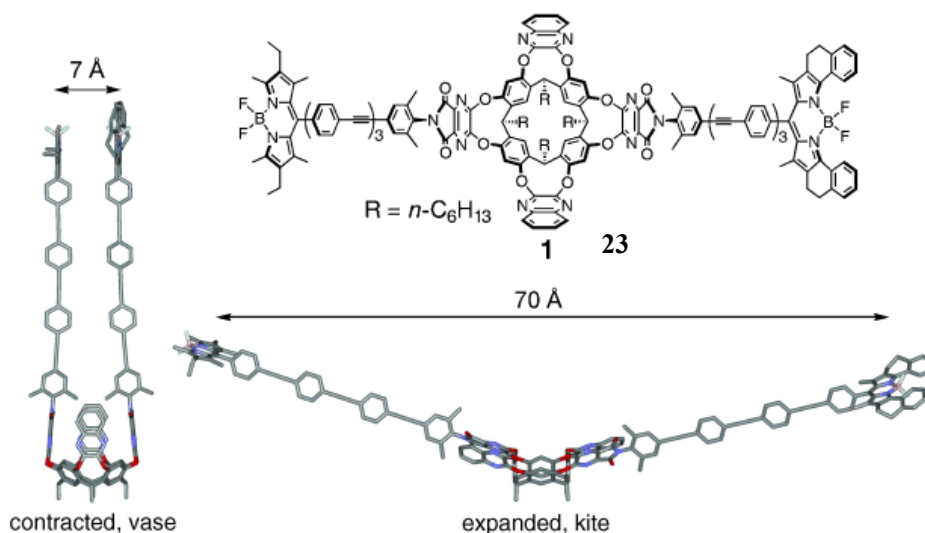
Figure 19. Acid switchable through-space energy transfer cassette. [43]

Incorporating FRET into sensing of biologically important analytes is quite important topic. Recently, Chang et al. [44] designed a system **24** which is

selective for reactive organic species (ROS) (Figure 20). Upon treatment with H_2O_2, excitation at 420 nm produces a bright green fluorescence which is consistent with increased FRET from the coumarin donor to open, colored fluorescein acceptor.
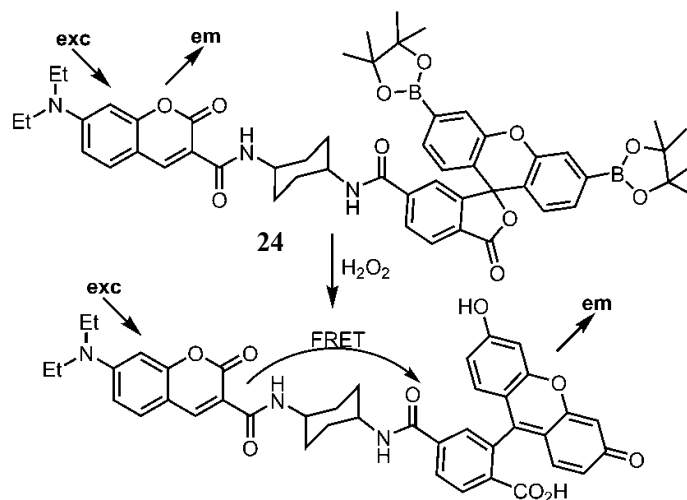
Figure 20. FRET-based approach for the detection of hydrogen peroxide.

This new type of FRET-based reagent features good selectivity for H_2O_2 over other ROS as well as visible wavelength excitation and emission profiles to minimize damage and autofluorescence from biological samples.

Rebek et al. have constructed a mechanically interlocked structure [45] which can be used to detect small motions in mechanically interlocked structures. In chloform solution, they observed very efficient FRET from coumarin D/A pair. Upon addition of DMSO, the hydrogen bonding interactions were obstructed, then the ring will start to move and this will decrease the efficiency of the FRET.
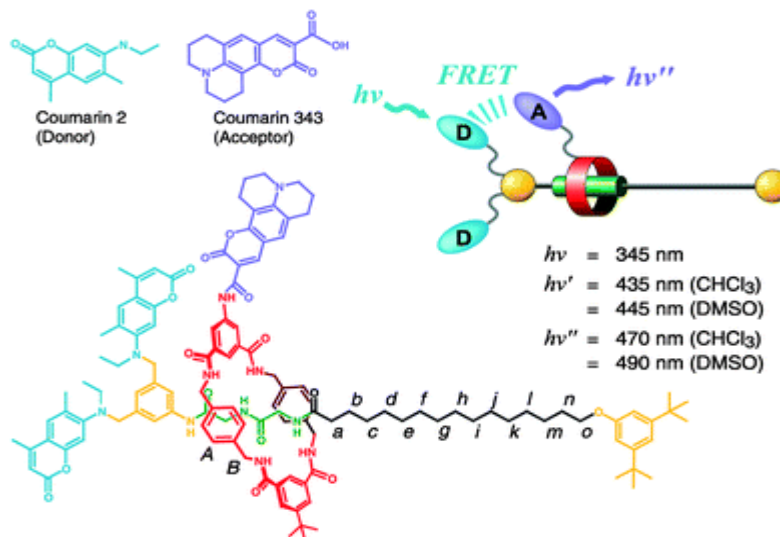
Figure 21. FRET-based approach for the interlocked molecules. [45]

1.7 Cation Binding

Cations play many roles in biological processes. Concentration gradients of cations across cell membranes maintain potentials that are used to transport organic substrates into cells. They trigger muscle contraction and are involved in the transmission of nerve impulses. Metal cations are present at the active sites of many enzymes playing catalytic roles. Additionally, metal cations play vital roles in enzymes, stabilizing the polypeptide tertiary structure.

Medically important metal complexes include complexes of paramagnetic lanthanide (e.g., Gd(III)) that are used as contrast agents in magnetic resonance imaging (MRI) of soft issue. Besides this, it is important to control the serum levels of lithium in patients under treatment for manic depression, and potassium in the case of high blood pressure. Zinc and aluminum are known to have possible implications in Alzheimer`s disease.

The design of receptors which particularly binds heavy metal transition (HTM) elements in the presence of other competitive cations are quite important, concerning the particularly well toxicity and pollutant effects of the cations such as Pb(II), Cd(II), Hg(II), etc. and the early detection in the environment is

27

desirable. There has therefore been a great deal of effort aimed at producing selective receptors for cationic guest species.

Compound **25** [46] is a highly selective chemosensor for Na(I) sensing,
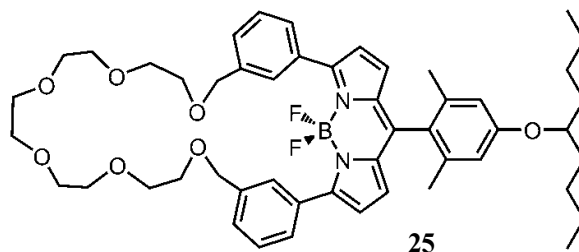
Figure 22. Sodium selective fluoroionophore based on conformational restriction.

although there are many chemosensors for sodium ion which are already used in practice, this chemosensor uses a different sensing mechanism which is called conformational restriction approach besides PET and ICT mechanism. The binding of cation which causes a red-shift in the emission and absorption spectra, is a result of the restriction of phenyl groups which are linked directly to BODIPY fluorophore, and extended conjugation causes red-shift in the spectrum. With the attachment of water soluble molecules instead of alkyl chains this approach can easily be extended to the aqueous media. Selective sensing of soft metals are quite important because of their toxic effects on human metabolism; for this reason, many efforts have been made to develop sensors for Hg(II). Some examples of it are given in Figure 23. Compound **26** [47], developed by Chang et al., is a sulfur containing macrocyle known to be selective soft metal cations. Depending on the size and the shape effect this ligand shows exclusive selectivity towards Hg(II) ion. This compound has been used to detect the mercury levels in fish, and, while demonstrated in fish, the method provides a useful starting point for developing
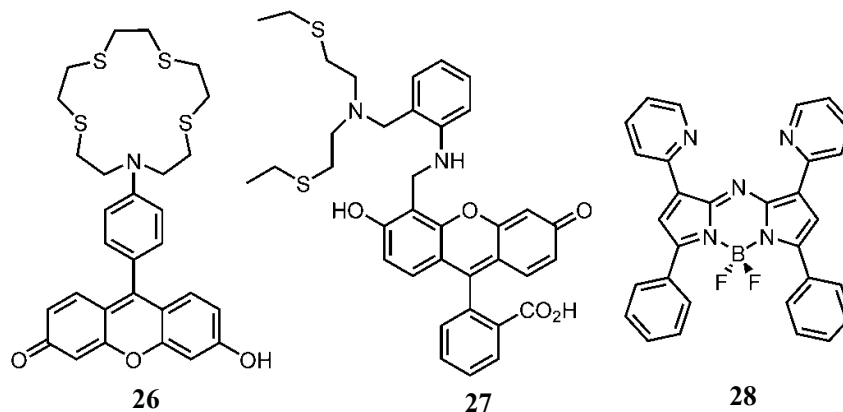
Figure 23. Hg(II) selective fluorescent chemosensors.

new mercury contamination screens for a wide range of biological, toxicological, and environmental samples. This chemosensor is expected to work as a PCT type but, there is only a small amout of change in the emission spectrum. Compound **27** [48] behaves as an PET type chemosensor for Hg(II) ion in aqueous media. Again, this chemosensor uses fluorescein moiety as a reporter unit. Although the ligand shows quite good selectivity over other cations, it shows only small change in the emission spectrum for Cd(II) ion. The latter one developed by Akkaya et al., this compound is the first chemosensor application of these dyes. 2-Pyridyl substituents at positions 1 and 7 create a well defined pocket for metal ion binding. The chemosensor **28** [49] is selective for Hg(II) ions, and both absorbtion and the emission spectra display large changes that would allow ratiometric sensing. It appears that appropriate derivatization of these novel fluorophores would lead to satisfactory chemosensors for other molecular or ionic species of interest. As a bonus, such boratriazaindacenes would have very long wavelength emissions in the otherwise silent region of the electromagnetic spectrum.
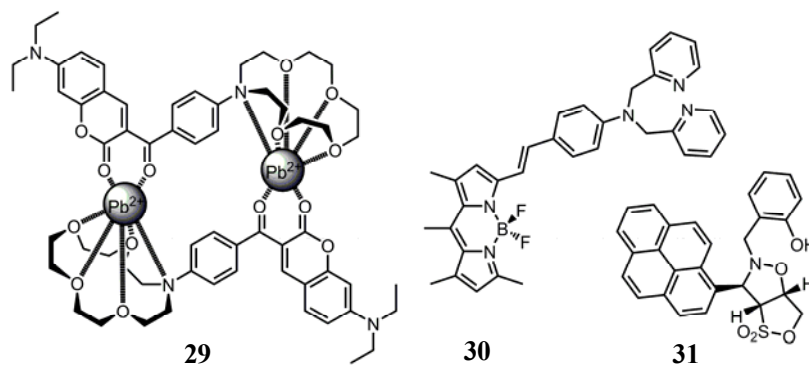
Figure 24. Selective fluorescent chemosensors for Pb(II), Cd(II) and Ag(I).

The selectivity for Pb(II) over Ca(II), Zn(II), Cd(II), Fe(II), Mn(II) and Hg(II) is particularly important because Pb(II) targets both Ca(II) and Zn(II) binding sites in vivo. Chemosensor **29** [50] forms 2:2 complex with Pb(II). The pronounced fluorescence enhancement can be rationalized in terms of PCT and metal binding-induced conformational restriction upon complexation. The magnitude of enhancement in emission and selectivity from **29** are quite high and can be detected visually. Compound **30** [51] is sensitive towards Cd(II) in acetone-water mixture. This type of derivatization of BODIPY dyes was developed by Akkaya and Rurack et al. independently [52, 53]. Dipicolyl amine moiety known to be selective for Zn(II) but it is quite interesting that changing solvent composition would drastically effect the selectivity of the ligand. This chemosensor is also used for *in vivo* detection of Cd(II). Compound **31** [54] one of the very few examples of Ag(I) sensors in literature. It signals Ag(I) concentration upon excimer formation between the pyrene units. Authors proposed 2:1 binding for this chemosensor and support this proposal with Job`s plot. Also –OH group on phenyl unit has great effect on binding, when is it replaced with –H, no excimer formation is observed. This molecule makes it possible to detect the Ag(I) ion ratiometrically, thereby eliminating most or all of the possible variability due to differences in instrumental efficiency and content of effective dye.

Selective and sensitive signaling of Zinc(II) ion is quite important due to its effects on Alzeimer`s disease and human metabolism. Compound **32** [55] is a ratiometric chemosensor for Zn(II). This novel two fluorophore approach gives opportunity for intracellular ratiometric sensing of Zn(II). Coumazin group
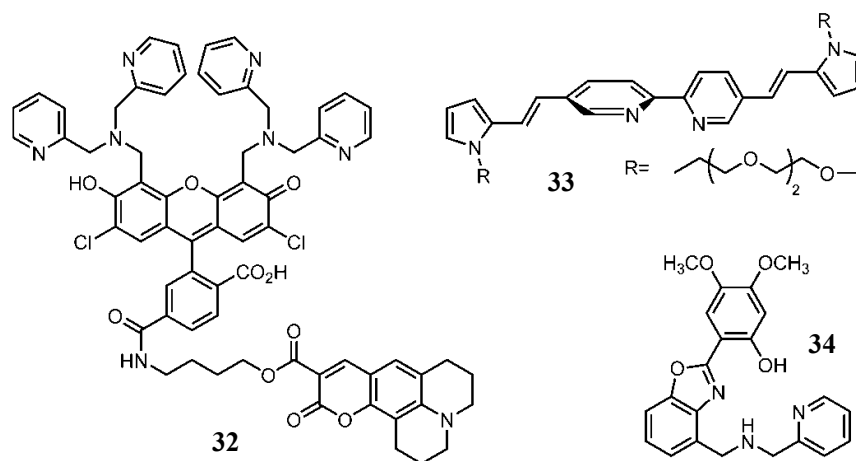
Figure 25. Selective fluorescent chemosensors for Zn(II) ion.

which is attached to fluorescein via ester linkage is hydrolyzed within the cell by esterase enzyme. After hydrolysis, Zn(II) sensitive fluorescein and insensitive coumazin fluorophore is created and Zn(II) concentration can be signaled from the emission signal at 534 nm from fluorescein, emission from hydrolyzed coumazin fluorophore from the emission signal at 488 nm. Thus, ratiometric sensing of Zn(II) is provided. **33** [56] is another example for conformational restriction which is coupled with Zn(II) sensing. Formation of zinc complex with bipyridyl unit causes red-shift in the absorbtion and emission spectra of the **33**. The reported fluorophore facilitate selective ratiometric and visual sensing of Zn(II) in the presence of other competing metal ions. This will allow differential fluorescence imaging of Zn(II) in biological specimens. O`Halloran et al. developed **34** [37], this benzoxazole type fluorescent chemosensor shows great selectivy towards Zn(II) in aqueous media. Emission ration imaging experiments of **34** reveals changes in intracellular zinc availability. These methods are particularly amenable to investigation of live tissue samples in real time and are

being applied to studies of hippocampus, where physiological fluctuations in synaptic zinc concentration are estimated to be as high as 100-300 μM or as low 2 nM. Nagano et al. is also developed many Zn(II) selective probes. [58]

1.8 Anion Binding

Anion recognition chemistry has its roots in work conducted in the late 1960s around the same time that Pedersen reported the synthesis and coordination chemistry of crown ethers and Lehn published the first accounts of cation coordination chemistry by cryptands. In the 1970s, the coordination chemistry of group I and II metal and ammonium cations attracted most interest and consequently cation recognition is now a well-developed area of supramolecular chemistry. In contrast to this, sensing of anions received little attention and only in last twenty years, much attention is given to solve the problems inherent in binding anions. There are a number of reasons for this sudden growth in this new area of supramolecular chemistry. Anions are ubiquitous within the biological systems. They carry genetic information (DNA is a polyanion) and the majority of enzyme substrates and co-factors are anionic. Anions also play roles in the areas of medicine and catalysis, whilst pollutant anions have been linked to eutrophication of rivers (from the over use of phosphate-containing fertilizers) and carcinogenesis (metabolites of nitrate). The production of pertechnetate during the reprocessing of nuclear fuel (and its subsequent discharge into the seas and oceans) is also a matter of environmental concern. The design of anion receptors for this kind of targets is particularly important and challenging. There are a number of reasons for this. Anions are generally larger than cations and therefore have a lower charge to radius ratio. This means that electrostatic binding interactions are less effective than they would be for the smaller cation. Additionally anions are also quite sensitive to pH values, thus receptors must function within the pH window of their target anion (mostly at neutral and physiological pH). Anionic species have a wide range of geometries and therefore a higher degree of design may be required to make receptors complementary to their anionic guest. Solvent effects also play a crucial role in

controlling anion binding strength and selectivity. A potential anion receptor must therefore effectively compete with the solvent environment in which the anion recognition event takes place. It is no coincidence that biological anion receptor systems are optimized to operate in a very specific range of environments where the source of selectivity for the biological anion is the difference in free energy lost on dehydrating the anion and that gained by the interaction of the anion with the binding site. Hydrophobicity can also influence the selectivity of a receptor. The Hofmeister series [59], which was first established through studies on the effect of salts on the solubility of proteins, orders anions by their hydrophobicity (and therefore degree of aqueous solvation). Hydrophobic anions are generally bound more strongly in hydrophobic binding sites.

Anslyn et al. have published several papers on the recognition of tricarboxylate and triphosphate polyanions by trisguanidinium receptor species such as **35** [60] (Figure 26). This molecule contains three guanidinium groups and is therefore complementary to guests containing three carboxylate groups. The stability constant determinations revealed that guests containing three anionic moieties, such as citrate, are bound more strongly than those with fewer anionic
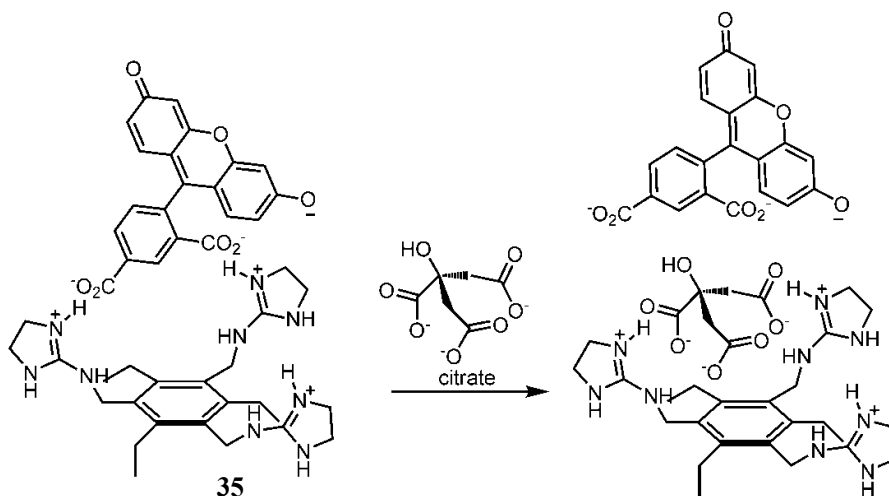
Figure 26. Displacement assay for citrate anion.

groups (for example, acetate). This receptor has been used to produce a displacement-assay-type chemosensor for citrate in beverages. 5-Carboxyfluorescein is a commercially available fluorescent probe containing two carboxylate groups. Its fluorescence is particularly sensitive to changes in pH values. The two carboxylate groups present in fluorescein coordinate to cationic receptor. A citrate ion displaces the carboxyfluorescein from the complex, initially emission of the carboxyfluorescein is lowered and when it is displaced fluorescence enhancement occurs. These changes could be calibrated against standard solutions of citrate to produce a quantitative sensor.

The Cd(II) complex of receptor **36** [61], behaves as an anion sensitive chemosensor in aqueous neutral solutions. Cd(II) was coordinated by the four nitrogen atoms of cyclen and by the aromatic amino group of coumarin. When anions were added to solutions of $[Cd(36)]^{2+}$, the aromatic amino group of coumarin was displaced causing changes in its fluorescence spectrum (see Figure 19). While pyrophosphate and citrate anions were detected with high sensitivity, fluoride and perchlorate induced no response. Four nucleotide monophosphates, AMP, GMP, CMP, and UMP, were added to solutions of $[Cd(36)]^{2+}$. GMP caused fluorescence quenching (ascribed to PET), whereas the other nucleotides caused red shift of the fluorescence band (this effect was most noticeable for AMP; shift of 40 nm, from 340 to 380 nm). On the basis of the fact that addition of cAMP scarcely changed the fluorescence

36
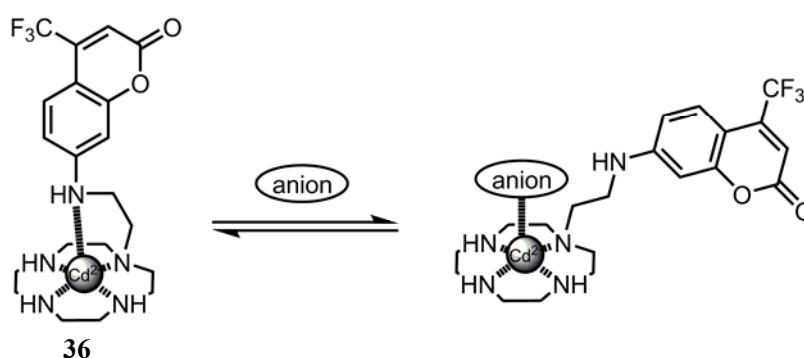
Figure 27. Sensing of anions through metal coordination and displacement.

spectrum of [Cd(**36**)]$^{2+}$, real-time detection of phosphodiesterase 3`:5`-cyclic mononucleotide activity was achieved. This phosphodiesterase catalyzes the conversion of cAMP to AMP. Monitoring the fluorescence increase at 380 nm (band due to the presence of AMP), the activity of this enzyme was detected in real-time.

Sessler et al. developed the compound **37** [42], published many articles on various calixpyrrole derivatives, these compounds are known to be selective towards F⁻ anion. But binding response can only be obtained by displacement or ¹H-NMR data. Appropriate modifications of this backbone can create fluorescent receptors for anions.
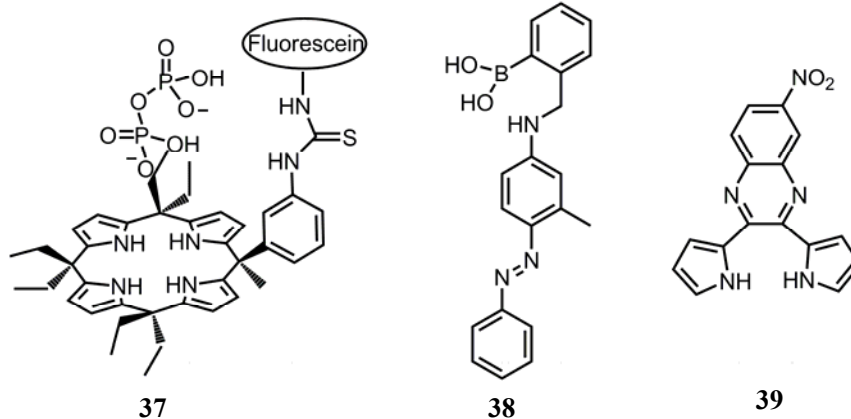
Figure 28. Fluorogenic and Chromogenic sensors for anions.

Compound **37** contains spacers having sulfonamide and thiourea groups in order to provide additional hydrogen bonding. It is quite selective for pyrophosphate, because of this additional hydrogen bonding, interaction of phosphate group with thiourea functionality would change the emission characteristics of fluorescein. Thus, the pyrophosphate concentration can be signaled. Solutions of **38** [63] in methanol exhibited an absorption band centered at 450 nm responsible for the orange color of the solutions. In the presence of chloride, bromide, and iodide, only an increase in intensity of the 450 nm band was observed; in contrast, addition of fluoride resulted in a bathochromic shift from 450 to 563 nm with a simultaneous color shift from orange to dark red. This color change was selective

for fluoride and attributed to the formation of a tetrahedral boronate anion upon reaction with one equivalent of fluoride.

Compound **39** [64] showed a remarkable color change from yellow ($\lambda_{max} =$ 455 nm) to purple ($\lambda_{max} = 560$ nm) upon fluoride addition in dichloromethane or DMSO, whereas chloride and dihydrogen phosphate did not produce any noteworthy color variation. The sensing of fluoride was also monitored by the quenching of the emission fluorescence observed in the presence of this anion. The color change was in agreement with the quite large stability constant found between **39** and F⁻ whereas formation constants with chloride and dihydrogen phosphate were much smaller.
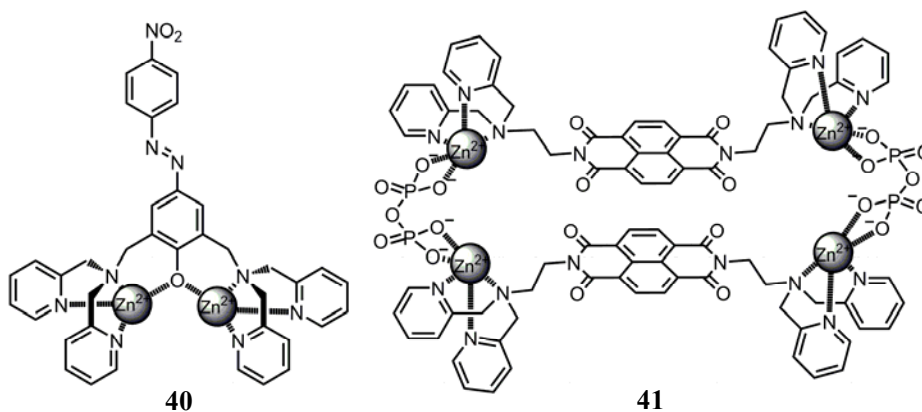
Figure 29. Fluorogenic and Chromogenic pyrophosphate sensors.

Aqueous solutions (10 mM HEPES buffer, pH 7.4) of complex $[Zn_2(\mathbf{40})]^{3+}$ (in which both Zn^{2+} atoms were coordinated with three nitrogen atoms and with the phenolate oxygen) presented an absorption band centered at 417 nm responsible for the yellow color observed.[65] Addition of $H_2PO_4^-$, AcO^-, F^-, HCO_3^-, Cl^-, HPO_4^{2-}, and citrate (up to an excess of 100 equivalents) did not induce remarkable spectral changes. However, addition of pyrophosphate causes a bathochromic shift from 417 to 465 nm and a color change from yellow to red. A 1:1 adduct was formed between the complex and the pyrophosphate anion.

The binding model between $[Zn_2(\mathbf{40})]^{3+}$ and pyrophosphate involves interaction of two oxygen atoms of pyrophosphate with the zinc atoms in the complex to give

two hexacoordinate Zn(II) ions in the adduct. It was suggested that the red shift of the emission maxima, induced by pyrophosphate binding, was due to a weakening of the bond between phenolate oxygen and Zn(II) atoms that increases the negative charge character of the phenolate oxygen, giving a bathochromic shift in the visible band. Compound **41** [66] is reported by Yoon et al., is a highly selective fluorescent chemosensor towards pyrophosphate (PP$_i$) that can function in 100% aqueous solution. This sensor shows an excimer peak at 490 nm only in the presence of PP$_i$. Four zinc sites as well as a π-π interaction induced the unique 2+2 type excimer in the presence of PP$_i$, furthermore, the detection of PP$_i$ is selective over ATP and phosphate.

1.9   BODIPY® dyes

Among the large variety of known fluorescent dyes, the boradiazaindacene family has gained recognition as being one of the most versatile reagents and has found great popularity with chemists, biochemists and physicists. BODIPY has a high molar extinction coefficient and high fluorescence quantum efficiency (Φ_{fl}). Furthermore, it has the advantages of lower sensitivity to solvent polarity and pH than fluorescein-based probes, and its structure can be modified to change its excitation and emission wavelengths. Since various structural modifications are possible, BODIPY-based fluorescence probes have been studied in depth. Since their discovery by Treibs and co-workers in 1968,[67] the number and range of applications have blossomed and include such diverse uses as biomolecular labels, chromogenic probes and cation sensors, drug delivery agents, fluorescent switches, electroluminescent films, laser dyes, light-harvesters and sensitizers for solar cells. The excellent stability, high fluorescence yield, negligible triplet state formation, intense absorption profile, good solubility, and chemical robustness have added to the general attractiveness of these dyes. Furthermore, the field has been extended significantly by the vast number of BODIPY derivatives that can be accessed by attaching secondary units at the pyrrole, meso, and N-ortho positions and this has been further expanded by the recent realization that the boron atom is also amenable to substitution. There

are many research groups working on the derivatization of BODIPY dyes, these groups are those of Akkaya, Rurack, Burgess, Ziessel, Nagano, Boens et al.

1.9.1 Applications of BODIPY® dyes

The excellent thermal and photochemical stability, high fluorescence yield, negligible triplet state formation, intense absorbtion profile, good solubility

Figure 30. Applications of the BODIPY dyes.

and chemical robustness have all added to the general attractiveness of these materials. Also the BODIPY core can be functionalized in many ways, which is shown at the heart of Figure 30. As a result of these functionalization, one can span entire visible spectrum. Due to the versatility of the BODIPY class of fluorophores; in 2006, some 729 patents and 1074 journal articles were published that described the multifarious applications of BODIPY-based dyes.

One of the first applications of BODIPY dyes is the labeling of proteins, [68] due to the high quantum yield and the photostability of these materials.

Photodynamic therapy and singlet oxygen generation are the interesting applications of BODIPY dyes. Distyryl-boradiazaindacenes **42** can be obtained by the condensation of 3,5-dimethyl derivatives with corresponding aldehyde.[69] Extension of the bodipy framework results in longer wavelength emitting dye. Water-solubility is achieved via functionalization with oligoethyleneglycol groups. These materials show good permeability into biological cells and have tumour targeting characteristics that make them interesting candidates for sensitizers in photodynamic therapy. Attachment of heavy atoms to the 2 and 6 positions increase the triplet yields of these dyes. And these heavy atoms favors intersystem crossing to the triplet state. Nagano et al. synthesized compound **43**, compared to the reference dye lacking iodine groups, the fluorescence efficiency drops from 70% to 2%. Under aerobic conditions, $^1O_2$ is generated with modest efficiency on illumination and cellular toxicity has been reported. [70]
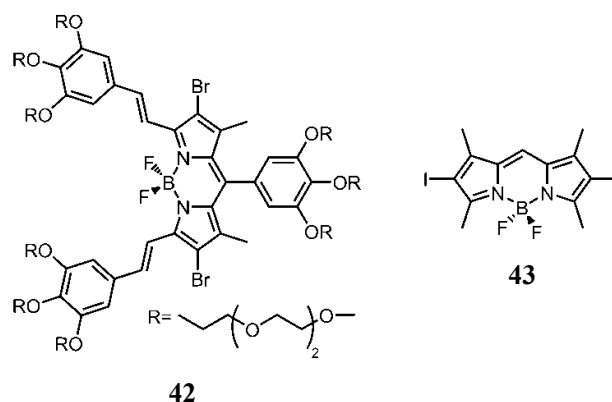
Figure 31. BODIPY based photosensitizers.

A common problem found in organic dyes is that the Stoke`s shift is too small for optimum use in imaging systems. Synthetic strategies have been developed to overcome this problem by covalent attachment of an ancillary light absorber to the BODIPY core. Here, the intention is to channel all photons absorbed by the secondary chromophore, this usually being an aromatic polycycle, to the BODIPY emitter. In this way, there is a large disparity in excitation and emission

wavelengths and the full benefits of the BODIPY emitter are retained. Some examples shown in Figure 32, these compounds are developed by Burgess, **44** [39] and Ziessel, **45**, **46** [71] et al.

44   **45**   **46**
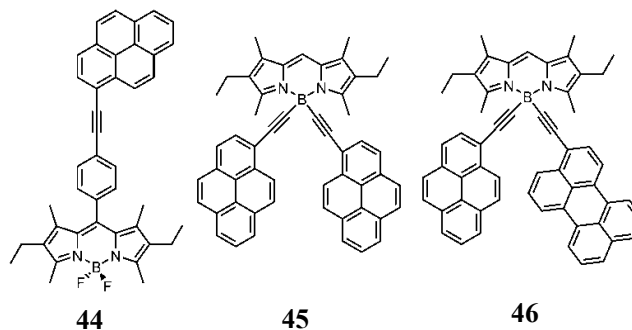
Figure 32. BODIPY dyes with ancillary light absorbers.

BODIPY dyes are also extensively used in the construction of molecular logic gates by Akkaya et. al., a unimolecular half-subtactor (See Figure 25) [36] and XOR gate [72] are reported.
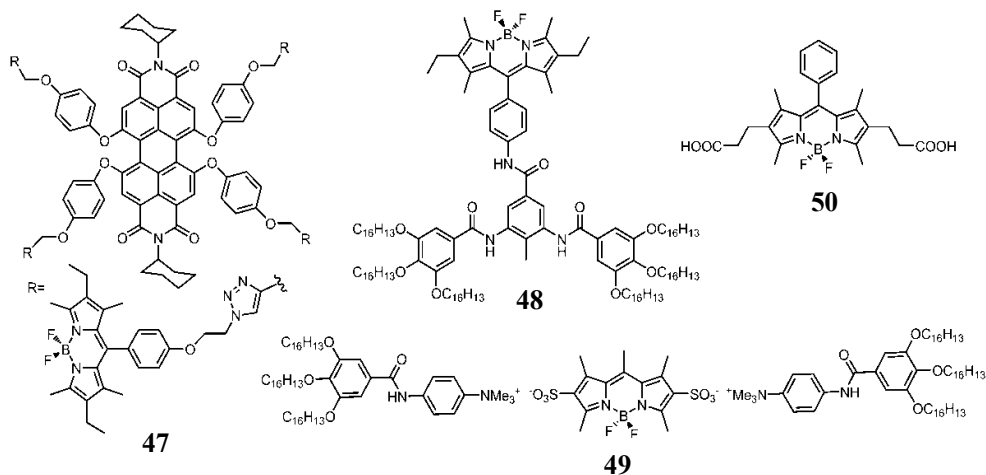
Figure 33. Applications of BODIPY dyes in Liquid crystalline materials, solar energy conversion and light harvesting systems.

Hybrid type BODIPY dye is developed by Akkaya group, [73] this dye is capable of functioning as photon concentrator, which have been engineered around perylenedimide (PDI) frameworks by means of 'click' chemistry. The presence of for BODIPY units in **47** offers a large cross-section for light absorption in the visible region and in this case, energy transfer occurs from the BODIPY unit to the PDI central core, which fluoresces at 618 nm. There is a need to identify new materials that are easily manufactured in bulk and that possess valuable properties in terms of colour and stability, and considerable effort has gone into the systematic modification of the BODIPY architecture to enable its incorporation into such supramolecular systems (liquid crystals, sol gels, etc.). Up to now, entangled three-dimensional networks of fibers entrapping solvent molecules have been produced by grafting paraffin chains onto pre-organized platforms carrying amido functions (Figure 33). Balancing the molar ratio of paraffin chains and the rigid aromatic core provides columnar mesophases, the symmetry of which depends strongly on weak intramolecular interactions (**48**). [74] The ionic self-assembled adducts (**49**) shown in Figure 33 are known to generate columnar liquid crystalline materials and thin films that are stable over a wide temperature range. The flexibility introduced by the ready exchange of ionic components and the use of highly fluorescent templates, like sulfonated bodipy dyes, allows the emergent mesomorphic textures to be monitored by fluorescence microscopy without the need of crossed polarizers. [75] Compound **50** is developed by Nagano group for solar energy conversion. Although, the solar energy efficiency of this dye is quite low, it is the first example of BODIPY dyes for photocurrent generation.[76] There are also many chemosensors and switches which are build by using BODIPY dyes, some of them is already presented within the introduction part(see Figures 12, 22, 23 and 24).

These examples show us that these dyes are highly versatile, and have broad applicability in various fields. The next step will be integration of bodipy-based dyes into all manner of interesting molecular-scale devices.

1.10   Self-Assembly

Self-assembly is one of the core concepts of supramolecular chemistry. It is often defined as the spontaneous formation of higher-ordered superstructures from molecular building blocks. This hypothesis first arose through research into biological systems. As the complex architectures found in living cells were delineated, the concept that such constructs were built by the convergent assembly of smaller subunits was increasingly invoked.

There are many examples of self-assembling biological systems. The formation of the DNA double helix from two complementary deoxyribonucleic acid strands is a striking example. As a result of the reversibility of the process, any errors that may have occurred during assembly can be corrected. The formation of cell membranes, multi-component enzymes, and viruses are paradigms of the way in which nature uses a simple, limited range of interactions to produce very complex molecular assemblies. The tobacco mosaic virus (TMV) consists of an RNA strand and 2130 protein subunits. The protein blocks self assemble around the RNA strand *via* noncovalent interactions to form the virus superstructure.

Self-assembly allows access to new molecular architectures that are inaccessible (or accessible in only very small yields) via traditional multi-step covalent bond making and bond breaking techniques. The new molecular architectures are produced by combining appropriately designed sub-units, which can be quite simple, and yet after the assembly process produce quite complex architectures. A striking example for the Borromean rings (**51**) was developed by Stoddart et al.; in this particular example, 18 components form this molecular structure in one step. [77]
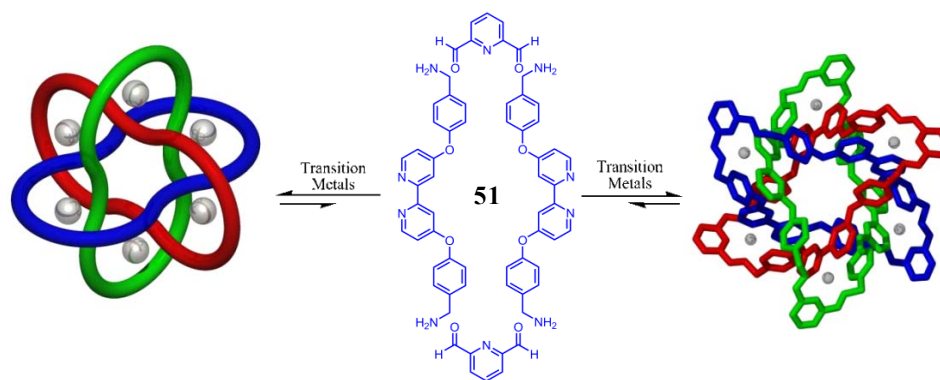
Figure 34. Cartoon and the 3D representation of Borromean rings.

1.10.1 Rotaxanes and Catenanes

A rotaxane consists of a linear molecule which is threaded through a ring with the ends of the thread, or axle, capped in such a manner that the ring cannot slip off (Figure 35). The term 'rotaxane' is derived from the Latin words *rota* and *axis*, meaning wheel and axel, respectively, and is therefore highly descriptive of
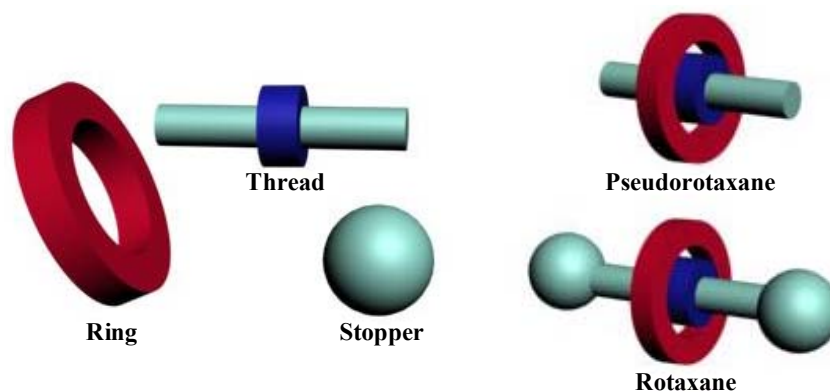
Figure 35. Nomenclature of rotaxanes.

these systems. Closely related to rotaxanes are pseudorotaxanes, which possess no terminal groups at the ends of the thread to prevent dissociation of the ring. Pseudorotaxanes are commonly used as intermediates in the synthesis of rotaxanes (and also catenanes). The nomenclature used for rotaxanes is [n]-

(pseudo)rotaxane, where n is the number of components that comprise the complex. Hence a [2]-rotaxane consists of only two components, a ring and a thread, whereas a [3]-rotaxane consists of two rings positioned along the same thread. The template-directed synthesis of rotaxanes can be achieved through one of four methods;

Threading possibly the most common way in which rotaxanes are be formed uses pseudorotaxane as a precursor. The axle is threaded through the
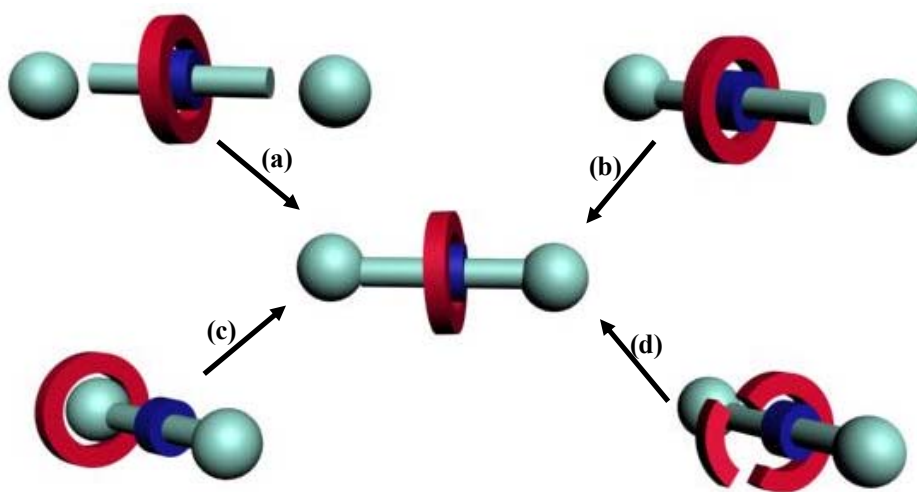
Figure 36. Synthetic pathways for rotaxanes, (a) threading, (b) trapping, (c) slipping, (d) clipping.

wheel (thread), akin to cotton thread through the eye of a needle, and is held in place by one or more templating interactions between the two components. The termini of the thread are appropriately functionalized so that, once the ring is secure, they can readily be capped in a post-assembly synthetic modification step. (Figure 37)

Trapping, if a thread is synthesized in such a way so that, it is already blocked at one end, then only the uncapped end needs to be capped once ring is in place. This approach can be advategous as there is statistically less chance of the ring slipping off of one end of the thread. Furthermore, this synthetic strategy can be used to create non-symmetrical rotaxanes.

Slipping, in some cases, it may be possible for a macrocycle to be forced over one of the blocked ends of a preformed axle at elevated temperatures. This process is referred to as 'thermally induced slippage' or simply 'slipping'.

Clipping, it is possible to form rotaxanes by using a fully assembled axle, complete with bulky terminal groups, as one of the starting components. The wheel can be introduced by closing it around the thread at a suitably templation point. The two ends of the macrocycle may simply be joined together through a covalent reaction or the wheel may be formed from two separate species that combine to form the complete macrocycle.(Figure 37) [78]
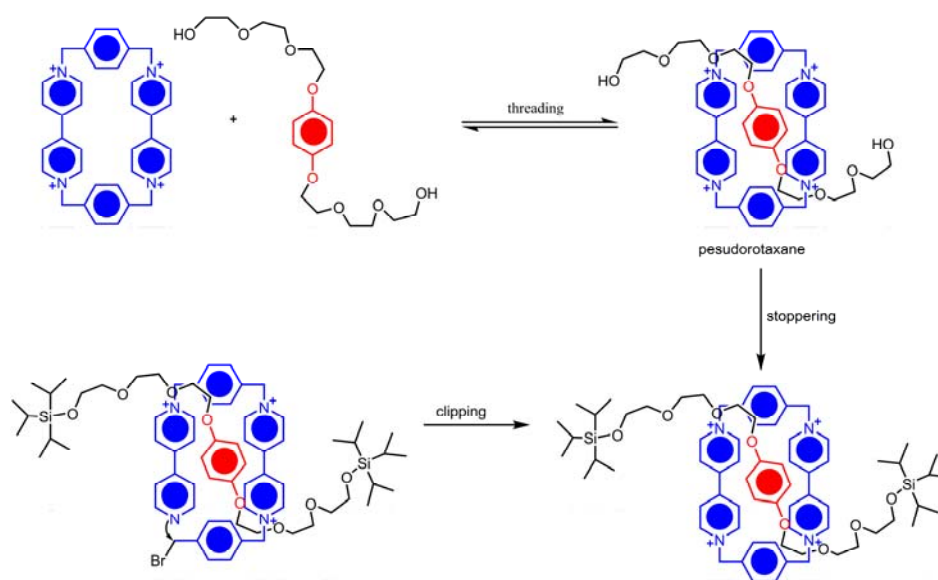
Figure 37. Rotaxane synthesis via clipping and threading pathways.

[n]Catenanes (from Latin: *catena* (chain)) consist of n interlocked macrocyclic species. For example a [2] catenane refers to two interlocking macrocycles. The most fundamental form of catenane is shown in Figure 38 in which only two rings are interlocked. Once a catenane has formed, the only way in which the rings can be removed from one another is by breaking one of the rings open. One can regard the catenane as being held together by a topological bond. Unlike rotaxanes, catenanes represent examples of true topologically connected species. Catenanes can be templated in a variety of ways. These include self-assembly of

aromatic π-donor and π-acceptors,[79] using metal-mediated synthesis,[80] around anionic templates [81] or via hydrogen bonding [82] between the component parts.
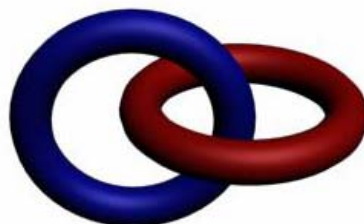
Figure 38. Cartoon representation of [2]catenane.

Catenanes with larger numbers of rings have been produced by analogous methods. The [5] catenane (**52**) which was developed by Stoddart et al. has been dubbed olympiadane because of its similarity to the five interlocked Olympic rings.[83] It provides an elegant example of the power of self-assembly and the use of non-covalent interactions to access complex molecular arrays with high molecular mass.
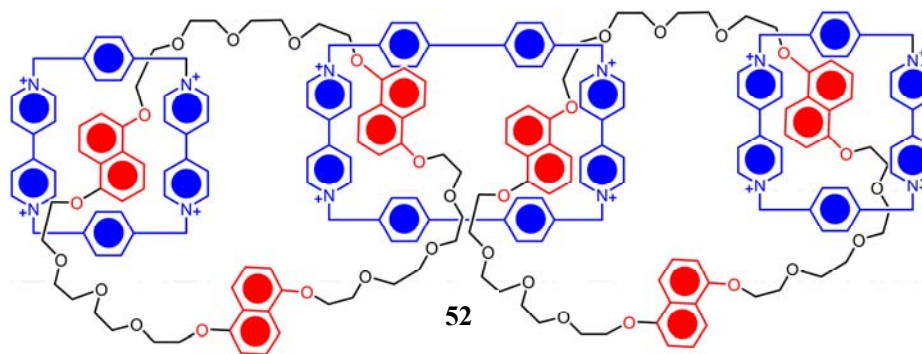
Figure 39. Olympiadane, a [5]catenane.

1.10.2 Molecular Machines

Movement is one of the life`s attributes.[84] Nature provides living systems with complex molecules called motor proteins which work inside a cell like ordinary machines built for everyday needs. These proteins ceaselessly perform duties such as transporting molecular materials, copying and translating the genetic code into proteins, communicating with the other cells, adapting the cell shape to the external environment, and reorganizing its interior to enable complex processes such as cell division and locomotion. Because of these molecular engines we can walk, talk and even think. [85]

Natural molecular-level machines and motors are extremely complex systems; their structures and detailed working mechanisms have been elucidated in a few instances only and any attempt to construct systems of such complexity by use of the bottom-up molecular approach would be hopeless at the present time. What can be done, at present, in the field of molecular-level machines is to construct simple prototypes consisting of a few molecular components capable of moving in a controllable way, and to investigate the challenging problems posed by interfacing artificial molecular machines with the macroscopic world, particularly as far as energy supply and information exchange are concerned. Certainly, the study of motion at the molecular level is a fascinating topic from the viewpoint of basic research and a promising field for novel applications.

Molecular-level machines operate as a result of nuclear movements caused by chemical reactions. Any kind of chemical reaction involves, of course, some nuclear displacement. The term "molecular machine", however, is used only for chemical systems performing reactions that can cause motions of large amplitude, leading to real translocation of some component parts of the system. Mechanical movement within the system can be obtained in the following ways;

- isomerization reactions involving –N=N-, -C=N-, and –C=C- double bonds in covalent supramolecular structures,[86]

- acid-base or redox reactions causing making or breaking of intermolecular bonds (including hydrogen bonds) [87]

- metal-ligand reactions causing the formation of disruption of coordination bonds. [88]

Molecular-level machines must contain a motor which, in principle, consists of a mobile and a stationary part. An external operator should be able, by means of a given input, to induce the displacement of the movable component from the stationary one. In addition to a motor, macroscopic machines contain a great variety of auxilary components such as fasteners, bearings, drive shafts, gears, brakes, rotors, etc. The concepts of machine components can also be extended to the molecular scale.

The first demonstration of macroscopic mechanical motion triggered by shuttling in a rotaxane was recently demonstrated using electroactive [3]rotaxane **53**[8+].[89] Oxidation of the TTF stations (green to pink) results in shuttling of the cyclophanes onto the hydroxynapthalene units (red), significantly shortening the inter-ring separation (Figure 40).
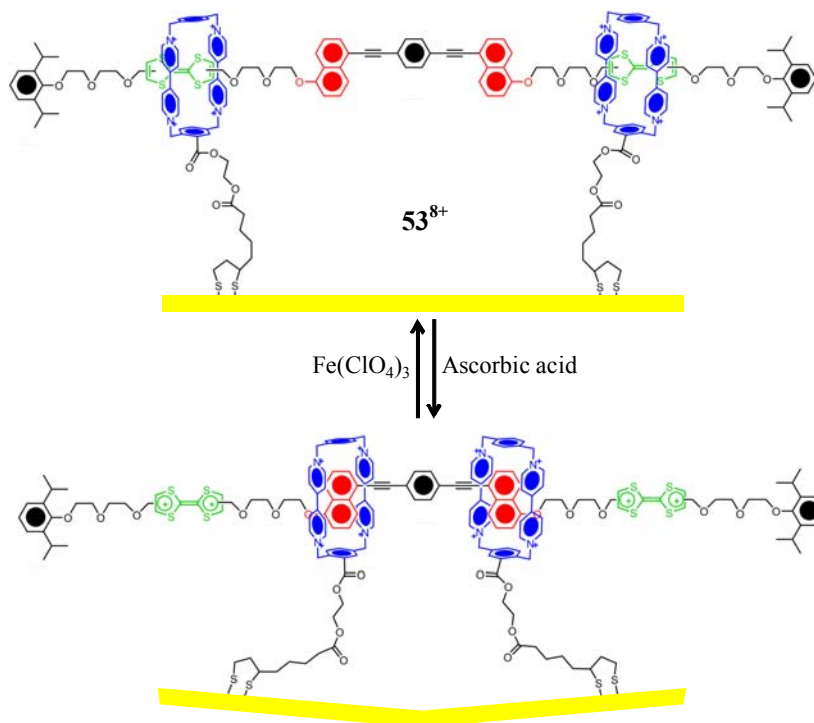
Figure 40. Chemical structure of **53**[8+] [3]rotaxane and schematic representation of its operation as a molecular actuator.

A self-assembled monolayer of **53**[8+] was deposited on an array of microcantilever beams which had been coated on one side with a gold film and the set up then

inserted in a fluid cell. the chemical oxidant $Fe(ClO_4)_3$ was added to the solution and the combined effect of co-conformational change in approximately six billion randomly oriented rotaxanes on each cantilever was an upward bending of the beam by about 35 nm. Reduction with ascorbic acid returned the cantilever to its starting position.

Movement of the droplets was demonstrated using a photo resposive surface based on molecular shuttles. [90] The milimeter-scale directional transport of diiodomethane drops across a surface (Figure 41) was achieved using the biased Brownian motion the components of a stimuli-resposive rotaxane
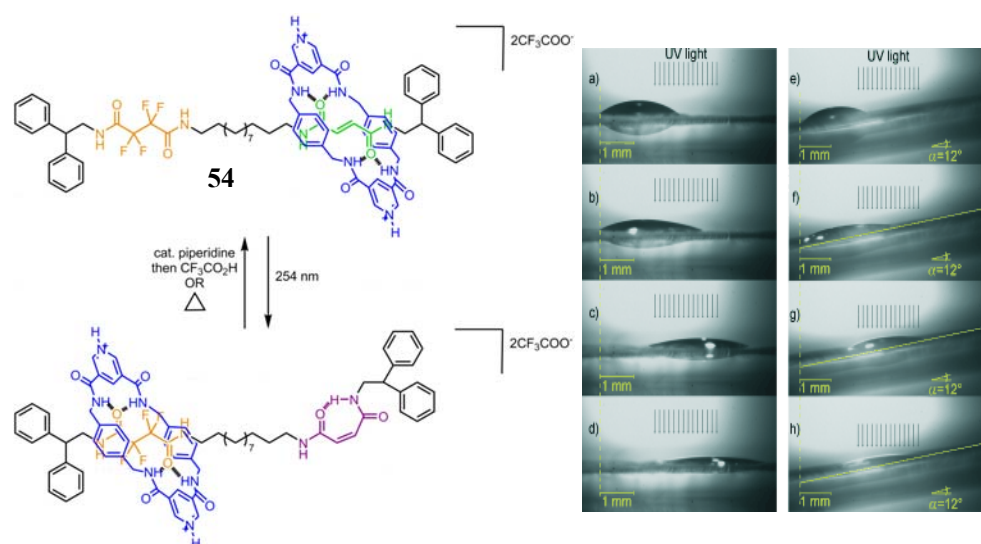
Figure 41. Stimuli-induced positional change of the macrocycle in the fluorinated molecular shuttle 54. [90]

54 to expose or conceal fluoroalkane residues and thereby modify the surface tension. The collective operation of a monolayer of the molecular shuttles attached to a SAM of 11-mercaptoundecaoic acid on Au(111) was sufficient to power the movement of microliter droplet up a twelve degree incline. In doing this, the molecular machines effectively employ the energy of the isomerization photon to do work on the drop against gravity.

55
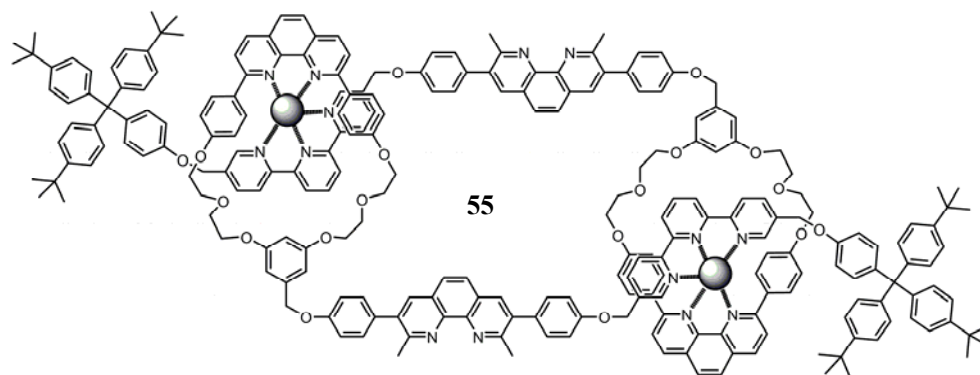
Figure 42. A molecular muscle **55**,[91] in which contraction and expansion is controlled by the coordination of metals with different coordination preferences to determine which binding site on the thread is utilized (figure illustrates Zn(II) complex).

The compound **55** is an example of a hermaphroditic rotaxane, [91] in which the ring and the thread are contained in the same molecule. The species is capable of acting as a `molecular muscle`, able to contract and stretch as a result of the two distinct binding sites within the thread, a bidentate 1,10 phenantroline unit and a tridentate terpyridine group. The rotaxane is synthesized from a smaller pseudorotaxane precursor in which thread terminates after the phenanthroline unit. This pseudorotaxane assembly is templated by two Cu(I) ions which are bound in their preferred tetrahedral geometry between the phenanthroline groups on the thread and in the ring. The terpyridine groups and the bulky stopper are then added in a post-assembly modification step. Once assembled, the complete rotaxane assembly can be demetallated (using KCN). Addition of octahedral Zn(II) induces the formation of a contracted conformation in which the metal is prefentially bound to the macrocycle and to the terpyridine group further along the thread, so reducing the length of the complex by some 20 Å.

In a second generation of devices, bistable interlocked molecules were employed and reversible switching achieved. Structures containing the tetracationic cyclophane CBPQT^{4+} can be ordered in Langmuir films by using an amphiphilic counterion and the monolayers subsequently transferred onto solid substrates by
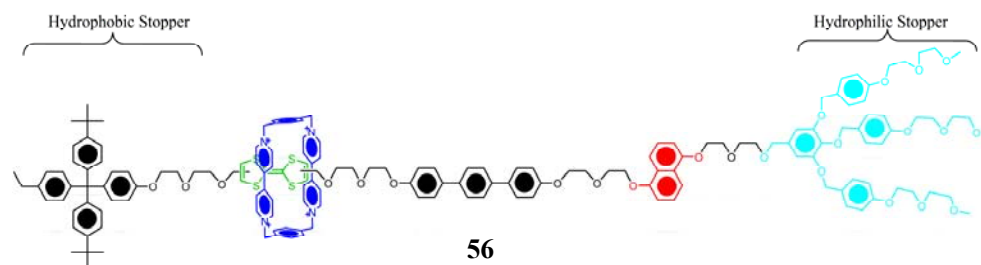
Figure 43. Chemical structure of amphiphilic bistable [2]rotaxane **56** used as the active components MSTJs.

using the LB technique. [92] The process was used to create a molecular switch tunnel junction (MSTJ) in which a monolayer of bistable [2]rotaxane **56** was sandwiched between silicon and titanium/aluminum electrodes. [93] These devices exhibited a moderate increase in conductance after application of an oxidizing potential,while recovery of the initial state occurred after a reducing voltage was applied. Molecular switch tunnel junctions of these rotaxanes possessed stable switching voltages around -2 V and +2 V with reasonable on/ off ratios and switch-closed currents. [94] These favorable characteristics allowed preparation of nanometer-scale devices which displayed properties similar to the original micrometer-sized analogues,thus suggesting a molecular-level mechanism for the MSTJ operation. Furthermore,these devices could be successfully connected to form a 2D crossbar circuit architecture. A breakthrough from Stoddart and coworkers is development of 160,000-bit molecular electronic memory circuit, fabricated at a density of 10^{11} bits cm^{-2} (pitch 33 nm; memory cell size 0.0011 μm^2), that is, roughly analogous to the dimensions of a DRAM circuit projected to be available by 2020. A monolayer of bistable, [2]rotaxane molecules **56** served as the data storage elements. Although the circuit has large numbers of defects, those defects could be readily identified through electronic testing and isolated using software coding. The working bits were then configured to form a fully functional random access memory circuit for storing and retrieving information. [95]

CHAPTER 2

EXPERIMENTAL

2.1 Instrumentation

For the first two parts;

All chemicals and solvents purchased from Aldrich were used without further purification. ^{1}H-NMR and ^{13}C-NMR spectra were recorded using a Bruker DPX-400 in CDCl$_3$ or DMSO-d$_6$ with TMS as internal reference. Absorption spectrometry was performed using a Varian spectrophotometer. Steady state fluorescence measurements were conducted using a Varian Eclipse spectrofluorometer . Column chromatography of all products was performed using Merck Silica Gel 60 (particle size: 0.040–0.063 mm, 230–400 mesh ASTM). Reactions were monitored by thin layer chromatography using fluorescent coated aluminum sheets. Solvents used for spectroscopy experiments were spectrophotometric grade. HRMS (ESI) measurements were done at the Mass Spec & Proteomics Facility, Ohio State University, Columbus, OH, USA.

For the last part;

Starting materials and reagents were purchased from Aldrich and used as received. Compound **72**, **73**, and **78** were prepared following the procedures as described in the literature. All reactions were performed under an argon atmosphere and in dry solvents unless otherwise noted. Analytical thin-layer chromatography (TLC) was performed on aluminum sheets, precoated with silica

gel 60-F$_{254}$ (Merck 5554). Flash chromatography was performed with silica gel 60 (Silicycle). ^{1}H NMR Spectra were recorded on either a Bruker ARX 400 MHz, a Bruker Avance 500 MHz, or a Bruker Avance 600 MHz spectrometer at ambient temperature in appropriate deuterated solvents using tetramethylsilane as an internal reference. UV-Vis spectra were recorded on a Varian 100-Bio UV-Vis spectrophotometer.

Electrochemistry

The electrochemical experiments were carried out in argon-purged MeCN solutions at concentrations ranging from 1.0×10^{-4} to 1.0×10^{-3} M and with 0.1 M tetrabutylammonium hexafluorophosphate (TBAPF$_6$) as supporting electrolyte, using a glassy carbon working electrode (0.08 cm^2, Amel), a Pt-spiral — separated from the bulk solution with a fine glass frit — as the counter electrode, and a silver wire as a pseudo-reference electrode. The surface of the working electrode was polished routinely with a 0.05 µm alumina-water slurry on a felt surface immediately before use. Cyclic voltammograms were obtained with sweep rates in the range 20–1000 mV s^{-1}. In any instance, the full reversibility of the voltammetric wave of the internal standard was taken as an indicator of the absence of uncompensated resistance effects. The reversibility of the observed processes was established by using the criteria of (i) separation of 60 mV between cathodic and anodic peaks, (ii) the close to unity ratio of the intensities of the cathodic and anodic currents, and (iii) the constancy of the peak potential on changing sweep rate in the cyclic voltammograms.

2.2.1 Synthesis of 4,4-difluoro-8-phenyl-1,3,5,7-tetramethyl-2,6-diethyl-4-bora-3a,4a-diaza-s-indacene (57).

Benzoyl chloride (3.95 mmol, 556 mg) and 3-ethyl-2,4-dimethyl pyrrole (8.12 mmol, 1.0 g) were refluxed for 3 h in CH_2Cl_2. The reaction was monitored by TLC (eluent CH_2Cl_2), after 3h, Et_3N (3 ml) and $BF_3.OEt_2$ (3 ml) were added. Immediately after the addition of $BF_3.OEt_2$ bright yellowish fluorescence was observed. Crude product washed three times with water, dried over Na_2SO_4 and concentrated in vacuo. Then crude product purified by silica gel column chromatography (eluent 2 CH_2Cl_2 : 1 Hexane). The orange fraction which has bright yellow fluorescence was collected. Orange solid (810 mg, 54 %).

^{1}H NMR (400 MHz, CDCl$_3$) δ 7.40-7.37 (m, 3H), 7.21-7.17 (m, 2H), 2.45 (s, 6H), 2.22 (q, J= 7.5 Hz ,4H), 1.20 (s, 6H), 0.90 (t, J= 7.5 Hz , 6H);

^{13}C NMR (100 MHz, CDCl$_3$) δ 153.7, 140.2, 138.4, 135.8, 132.7, 130.8, 128.9, 128.7, 128.3, 17.1, 14.5, 14.1, 12.5, 11.6;

FAB-HRMS calcd for 380.2235, found 380.223709 Δ= 0.50 ppm.
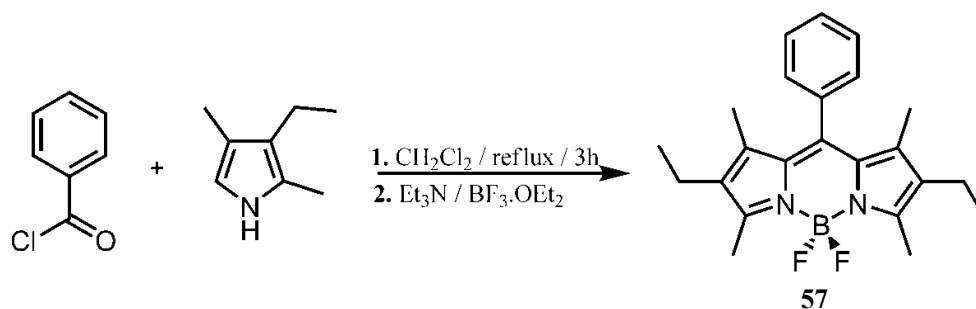
Figure 44. Synthesis of Compound **57**

2.2.2 3-{2'-(4''-dimethylaminophenyl)ethenyl}-4,4-difluoro-8-phenyl-1,3,5,7-tetramethyl -2,6-diethyl-4-bora-3a,4a-diaza-s-indacene (58).

Compound **57** (0.58 mmol, 222 mg) and dimethylaminobenzaldehyde (0.61 mmol, 91 mg) were refluxed in a mixture of toluene (40 ml), glacial acetic acid (440 µl), piperidine (530 µl) and small amount of Mg(ClO$_4$)$_2$. Any water formed during the reaction, was removed azeotropically by heating overnight in a Dean-Stark apparatus. Crude product concentrated under vacuum, then purified by silica gel column chromatography (first CH$_2$Cl$_2$, then CH$_2$Cl$_2$:Hexane (2:1)). The blue colored fraction was collected (124 mg, 42 %).

^{1}H NMR (400 MHz, CDCl$_3$) δ 7.50 (d, *J*= 14.5 Hz, 1H), 7.44-7.36 (m, 5H), 7.25-7.20 (m,2H), 7.14 (d, *J*= 14.5 Hz, 1H), 6.63 (d, *J*= 8.7 Hz, 2H), 2.93 (s, 6H), 2.55-2.49 (m, 5H), 2.24 (q, *J*=7.5 Hz , 2H), 1.23 (s, 3H), 1.20 (s, 3H), 1.07 (t, *J*=7.5 Hz, 3H), 0.91 (t, *J*=7.5 Hz, 3H);

^{13}C NMR (100 MHz, CDCl$_3$) δ 153.2, 150.9, 150.8, 138.8, 138.4, 137.5, 136.2, 136.1, 133.1, 132.8, 132.0, 131.4, 128.9, 128.7, 128.6, 125.8, 115.7, 112.2, 40.3, 18.4, 17.1, 14.6, 14.0, 12.6, 11.6, 11.4;

FAB-HRMS calcd for 511.2970, found 511.297247, Δ= 0.45 ppm.
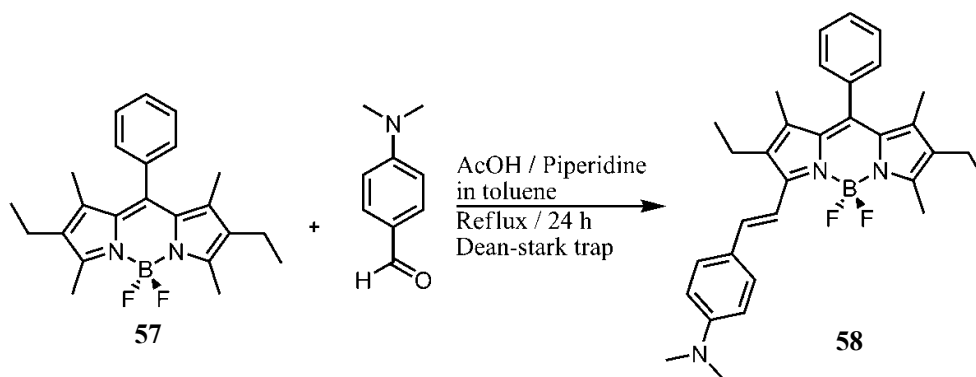
Figure 45. Synthesis of Compound **58**

2.2.3   Bis(1,4-{4',4'-difluoro-1',3',5',7'-tetramethyl   -2',6'-diethyl-4'-bora-3a,4a-diaza-sindacen-8'-yl)}benzene (59):

Terephthaloyl chloride (2.40 mmol, 490 mg) and 3-ethyl-2,4-dimethyl pyrrole (9.74 mmol,1.2 g) were refluxed for 12 h in CH_2Cl_2. The reaction was monitored by TLC (eluent CH_2Cl_2). Once terephthaloylchloride was consumed, Et_3N (3.0 ml) and $BF_3.OEt_2$ (3.0 ml) added. With the addition of $BF_3.OEt_2$, bright yellowish fluorescence was observed. Organic phase was washed three times with water, dried over Na_2SO_4 and concentrated in vacuo. Then crude product was then purified by silica gel column chromatography (eluted first with CH_2Cl_2
then CH_2Cl_2:Hexane (4:1)). The orange fraction which has a bright yellow fluorescence was collected (930 mg , 57 %).

^{1}H NMR (400 MHz, CDCl₃) δ 7.44 (s, 4H), 2.48 (s, 12H), 2.25 (q, *J*= 7.6 Hz, 8H), 1.40 (s, 12H), 0.93 (t, *J*= 7.6 Hz, 12H);
^{13}C NMR (100 MHz, CDCl₃) δ 154.2, 139.2, 137.9, 136.8, 132.9, 130.8, 129.8, 17.1, 14.6, 13.2, 12.5;
FAB-HRMS calcd for 682.4001, found 682.400341 Δ= 0.35 ppm.
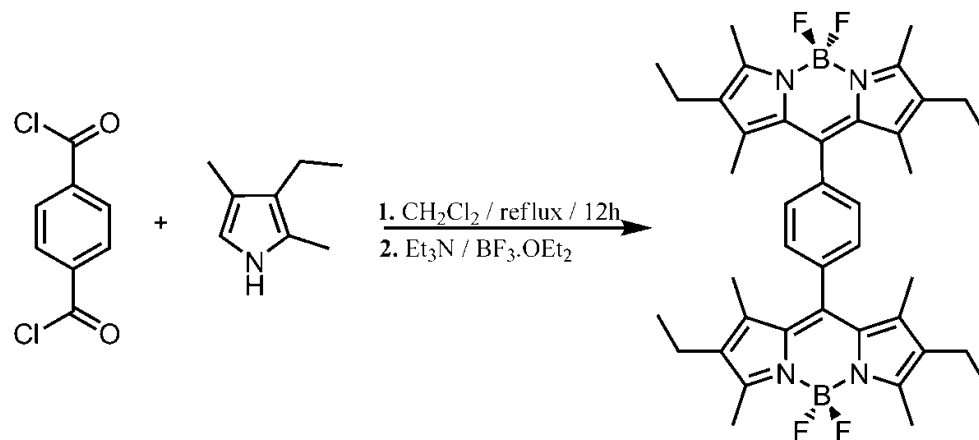
Figure 46. Synthesis of BODIPY dimer **59**

2.2.4 1-{4,4-difluoro-1,3,5,7-tetramethyl-2,6-diethyl-4-bora-3a,4a-diaza-s-indacen-8-yl}-4-[3-{2'-(4''-dimethylaminophenyl)ethenyl}-4,4-difluoro-1,3,5,7-tetramethyl -2,6-diethyl-4-bora-3a,4a-diaza-s-indacen-8-yl]-benzene (60):

Compound **59** (0.188 mmol, 128 mg) and p-Dimethylaminobenzaldehyde (0.19 mmol, 29 mg) were refluxed in a mixture of toluene (30 ml), glacial acetic acid (150 µl), piperidine (180 µl) and small amount of $Mg(ClO_4)_2$. Any water formed during the reaction, was removed azeotropically by heating overnight in a Dean-Stark apparatus. Solvents were removed under reduced pressure, and the crude product was then purified by silica gel column chromatography (first eluted with CH_2Cl_2, then CH_2Cl_2:Hexane (4/1)). The blue colored fraction was collected (57 mg, 37 %).

^{1}H NMR (400 MHz, CDCl$_3$) δ 7.53 (d, J= 16.7 Hz, 1H), 7.47-7.42 (m, 6H), 7.16 (d, J= 16.7 Hz, 1H), 6.65 (d, J= 8.7 Hz, 2H), 2.95 (s, 6H), 2.58-2.49 (m, 11H), 2.29-2.23 (m, 6H), 1.42-1.38 (m, 12H), 1.10 (t, J=7.5 Hz, 3H), 0.96-0.92 (m, 9H);

^{13}C NMR (100 MHz, CDCl$_3$) δ 154.2, 151.4, 139.3, 138.3, 138.0, 137.2, 136.7, 133.3, 132.9, 132.1, 130.8, 130.1, 129.7, 128.8, 112.3, 40.4, 18.4, 17.1, 17.0, 14.6, 14.0, 13.2, 13.0, 12.7, 12.6;

FAB-HRMS calcd for 813.4736, found 813.47592 Δ= 2.86 ppm.
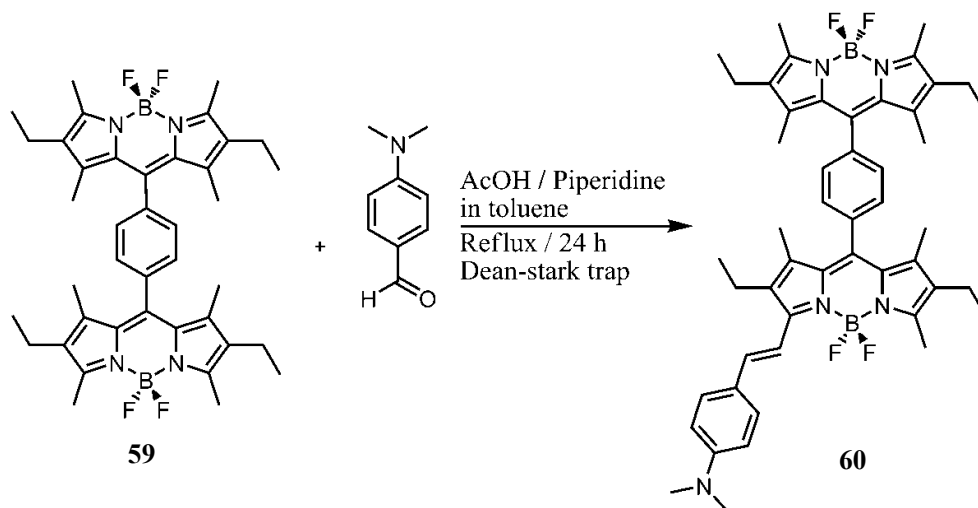
Figure 47. Synthesis of BODIPY dyad **60**

2.2.5 1-{4,4-difluoro-1,3,5,7-tetramethyl-2,6-diethyl-4-bora-3a,4a-diaza-s-indacen-8-yl}-4-[3-{2'-(4''-(9'''-aza-3''',6''',12''',15'''-tetrathiaheptadec-9'''-yl)-ethenyl}-4,4-difluoro-1,3,5,7-tetramethyl -2,6-diethyl-4-bora-3a,4a-diaza-s-indacen-8-yl]-benzene (61):

Compound **59** (0.32 mmol, 218 mg) and 4-(bis(2-(2-(ethylthio)ethylthio)ethyl)aminobenzaldehyde (synthesized according to a literature procedure, starting from 3-N-phenyl-3-aza-1,5-pentanediol; 0.41 mmol, 172 mg) were refluxed in a mixture of toluene (45 ml), glacial acetic acid (240 μl), piperidine (290 μl) and small amount of $Mg(ClO_4)_2$. Any water formed during the reaction, was removed azeotropically by heating overnight in a Dean-Stark apparatus. Solvents were removed under reduced pressure, and the crude product was then purified by silica gel column chromatography (first eluted with CH_2Cl_2, then CH_2Cl_2:MeOH(99:1)). The blue fraction was collected (105 mg, 31 %).

^{1}H NMR (400 MHz, CDCl$_3$) δ 7.53 (d, *J*= 16.6 Hz, 1H), 7.47-7.42 (m, 6H), 7.12 (d, *J*= 16.6 Hz, 1H), 6.65 (d, *J*= 8.7 Hz, 2H), 3.54 (t, *J*= 7.6 Hz, 4H), 2.75-2.66 (m, 12H), 2.57-2.48 (m, 15H), 2.29-2.25 (m, 6H), 1.46-1.41 (m, 12H, 1.25-1.19 (m, 6H), 1.09 (t, *J*=7.5 Hz, 3H), 0.96-0.92 (m, 9H);

^{13}C NMR (100 MHz, CDCl$_3$) δ 154.2, 139.3, 138.3, 137.9, 137.0, 136.7, 133.1, 132.9, 131.9, 131.4, 130.7, 130.0, 129.7, 129.1, 51.7, 32.5, 31.8, 30.9, 29.7, 29.4, 26.1, 18.4, 17.1, 14.8, 14.7, 14.0, 13.2, 13.0, 12.7, 12.6
FAB-HRMS calcd for 1082.5262 (M+H), found 1082.52756 Δ= 1.25 ppm.
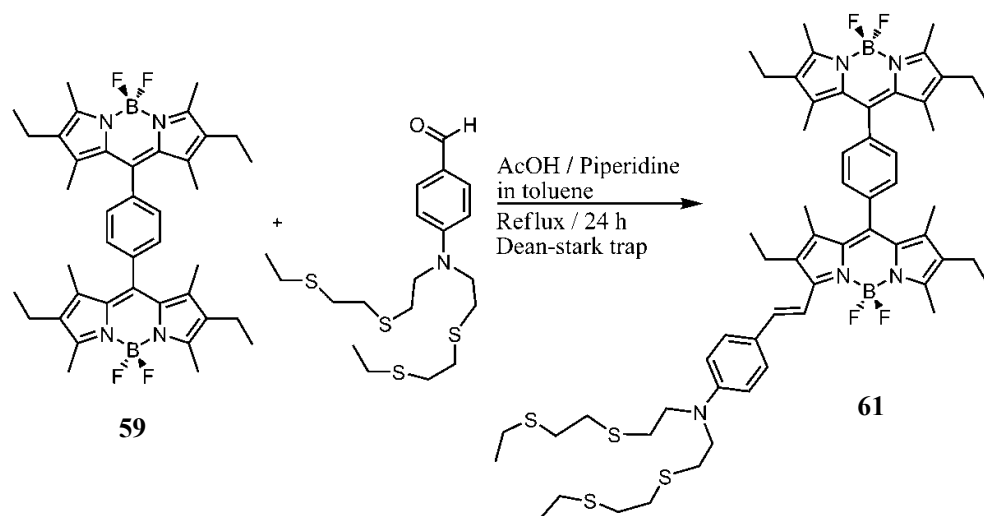
Figure 48. Synthesis of BODIPY dyad **61**

PART II

2.3.1 Synthesis of 2,6-diethyl-4,4-difluoro-1,3,5,7-tetramethyl-8-(4-iodophenyl)-4-bora-3a,4a-diaza-s-inadcene (62):

4-iodobenzoylchloride (7.7 mmol, 2.05 g) and 3-ethyl-2,4-dimethyl pyrrole (15.4 mmol, 1.9 g) were dissolved in CH_2Cl_2 and refluxed for 3 h. After 3 h, Et_3N (5 ml) and $BF_3.OEt_2$ (5 ml) were added. Then bright yellowish fluorescence was observed. Crude product washed three times with water and dried over Na_2SO_4 and concentrated in *vacuo.* Then the crude product purified by silica gel column chromatography (eluent $CHCl_3$). First fraction which has bright yellow fluorescence was collected. Orange solid (2.53 g, 65 %).[ref. 96]
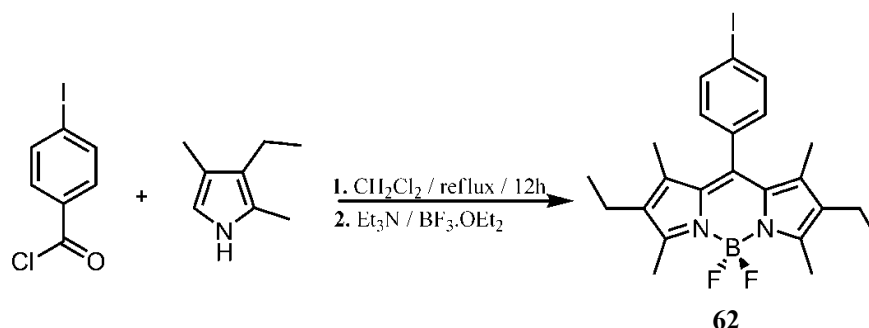
Figure 49. Synthesis of compound **62**

2.3.2 Synthesis of boradiazaindacene dimer 63;

Compound **62** (1.98 mmol, 1 g), 1,4-diethynylbenzene (0.988 mmol, 0.125 g), $PdCl_2$ (0.15 mmol, 27 mg), CuI (0.30 mmol, 57 mg) and PPh_3 (0.60 mmol, 157 mg) were added to the round bottomed flask which was previously flushed with Argon. As a solvent Et_3N (5 ml) and anhyrdous THF (50 ml) was added. The reaction mixture was stirred overnight at r.t.. After completion of the reaction, solvent was removed in *vacuo*. The crude product purified by silica gel column

chromatography (eluent first; CHCl$_3$ then 2 CHCl$_3$: 1 Hexane). Orange solid (724 mg, % 83) .

^{1}H NMR (400 MHz, CDCl$_3$) δ; 7.60 (d, *J*=8.10 Hz, 4H), 7.50 (s, 4H), 7.24 (d, *J*=8.10 Hz, 4H), 2.47 (s, 12H), 2.24 (q, *J*=7.50 Hz, 8H), 1.27 (s, 12H), 0.92 (t, *J*=7.50 Hz, 12H) ;

^{13}C NMR (100 MHz, CDCl$_3$) δ; 154.1, 139.2, 138.2, 136.2, 132.9, 132.3, 131.7, 130.6, 128.7, 123.6, 123.1, 90.8, 90.3, 17.1, 14.6, 12.5, 11.9 ;

ESI-HRMS calcd for [M+Na] 905.4525 found. 905.4495 Δ=3.3 ppm.
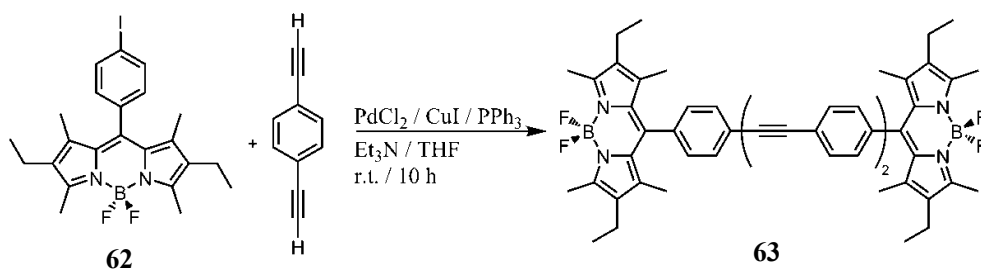
Figure 50. Synthesis of compound **63**

2.3.3 Synthesis of *p*-Dimethylaminostyryl modified boradiazaindacene dimer (64);

Compound **63** (0.283 mmol, 250 mg) and *p*-dimethylaminobenzaldehyde (0.283 mmol, 43 mg) were refluxed in a mixture of toluene (75 ml), glacial aceticacid (220 μl), piperidine (260 μl). Any water formed during the reaction, was removed azeotropically by heating overnight in a Dean-Stark apparatus. The solvent was removed in *vacuo*, then crude product purified by silica gel column chromatography (eluent CHCl$_3$). The blue colored fraction was collected (106 mg, % 37).

^{1}H NMR (400 MHz, CDCl$_3$) δ; 7.60 (d, *J*=7.95 Hz , 4H), 7.56-7.46 (m, 7H), 7.27-7.23 (m, 4H), 7.14 (d, *J*=16.70 Hz, 1H), 6.68 (br, 2H), 2.96 (s, 6H), 2.57-2.47 (m, 11H), 2.30-2.21 (m, 6H), 1.30 (s, 3H), 1.27 (s, 9H), 1.09 (t, *J*=7.55 Hz, 3H), 0.95-0.90 (m, 9H) ;

^{13}C NMR (100 MHz, CDCl$_3$) δ; 153.1, 138.2, 137.2, 136.3, 135.5, 135.1, 132.3, 131.9, 131.2, 131.1, 130.6, 129.5, 127.9, 127.7, 127.6, 122.6, 122.5, 122.1, 122.0, 89.9, 89.8, 89.2, 40.4, 17.4, 16.1, 13.6, 13.0, 11.7, 11.5, 10.8, 10.6 ; ESI-HRMS calcd for [M+Na] 1036.5260 found 1036.5281 Δ=2.0 ppm.
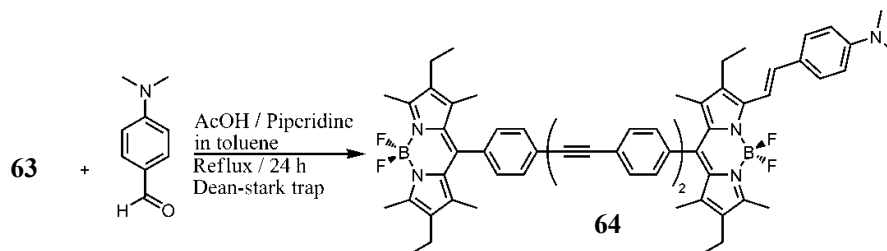
Figure 51. Synthesis of compound **64**

2.3.4 Synthesis of chemosensor 65:

Compound **63** (0.164 mmol, 145 mg) and 4-(1-aza-7,10-dioxa-4,13-dithiacyclopentadecyl)benzaldehyde (synthesized according to literature procedure, starting from 3-N-phenyl-3-aza-1,5-pentanediol [97]; 0.18 mmol, 64 mg) were dissolved in toluene (60 ml), glacial aceticacid (130 μl), piperidine (153 μl). Any water formed during the reaction, was removed azeotropically by heating overnight in a Dean-Stark apparatus. Solvent was removed under reduced pressure and the crude product first purified by silica gel column chromatography (eluent 99 CHCl$_3$: 1 MeOH), then further purified by Preparative thin layer chromatography (PTLC) in the same solvent system. The blue fraction was isolated (82 mg, % 41).

^{1}H NMR (400 MHz, CDCl$_3$) δ; 7.60 (d, J=7.90 Hz, 4H), 7.53-7.43 (m, 7H), 7.27-7.23 (m, 4H), 7.12 (d, J=16.55 Hz, 1H), 6.65 (br, 2H), 3.74 (t, J=5.04 Hz, 4H), 3.65-3.59 (m, 8H), 2.88-2.84 (m, 4H), 2.70 (t, J=5.04 Hz, 4H), 2.56-2.47 (m, 11H), 2.25-2.17 (m, 6H), 1.29 (s, 3H), 1.27 (s, 9H), 1.06 (t, J=7.40 Hz, 3H), 0.92 (t, J=7.40 Hz, 9H) ;

^{13}C NMR (100 MHz, CDCl$_3$) δ; 154.1, 139.2, 138.2, 136.1, 133.3, 132.9, 132.2, 131.6, 130.5, 129.0, 128.9, 128.6, 123.5, 123.1, 90.9, 90.1, 74.2, 70.7, 51.1, 31.9, 31.5, 29.6, 29.2, 21.0, 17.1, 14.5, 14.1, 14.0, 12.5, 11.8, 11.6 ;

ESI-HRMS calcd for [M+Na] 1242.5695 found 1242.5710 Δ=1.2 ppm.
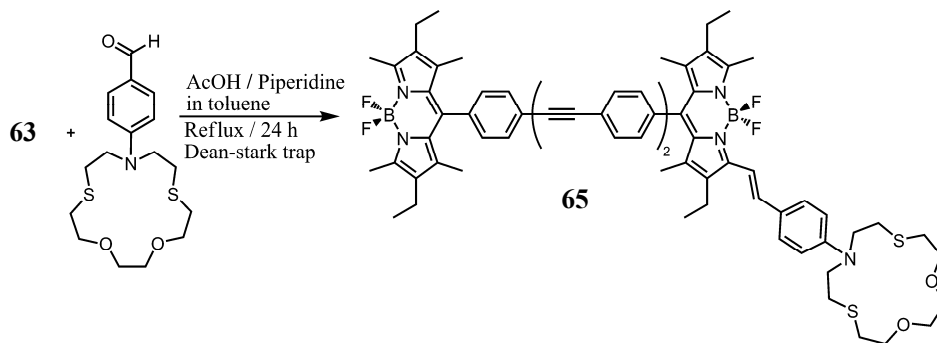
Figure 52. Synthesis of compound **65**

2.3.5 Synthesis of TMS-protected spacer (66):

(2-(4-iodophenyl)ethynyl)trimethylsilane (synthesized acc. to literature procedure [98]; 5.5 mmol, 1.65 g), 1,4-diethynylbenzene (2.75 mmol, 0.35 g), PdCl$_2$ (0.275 mmol, 49 mg), CuI (0.55 mmol, 105 mg) and PPh$_3$ (1.1 mmol, 289 mg) were added to the round bottomed flask which was previously flushed with Argon. As a solvent Et$_3$N (5 ml) and anhyrdous THF (50 ml) was added. The reaction mixture was stirred overnight at r.t. under Ar atmosphere. After completion of the reaction, solvent was removed in *vacuo*. The crude product first purified by silica gel column chromatography (eluent   CHCl$_3$),then further purifed by washing yellowish solid with n-hexane to yield white solid. White solid (1.13 g, % 87) .

^{1}H NMR (400 MHz, CDCl$_3$) δ; 7.43 (s, 4H), 7.39 (s, 8H), 0.19 (s, 18H).
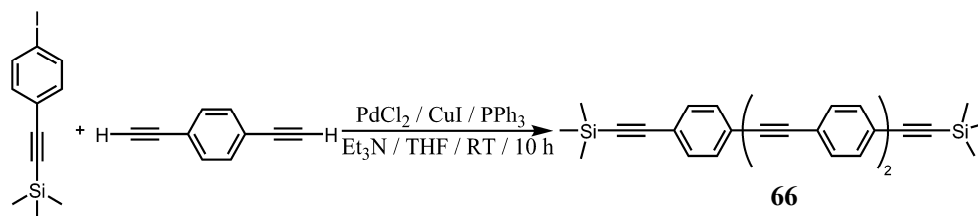
Figure 53. Synthesis of compound **66**.

2.3.6 Deprotection of compound 66:

Compound **66** (1.02 mmol, 480 mg) and anhydrous K_2CO_3 (6.12 mmol, 845 mg) was added to THF/MeOH mixture (50/50 ml) the mixture was stirred for 6h at rt. After completion of the reaction , solvents were removed in *vacuo*. Then the crude product washed with water and dried under vacuum. The yellowish solid was used through next step without further purification.
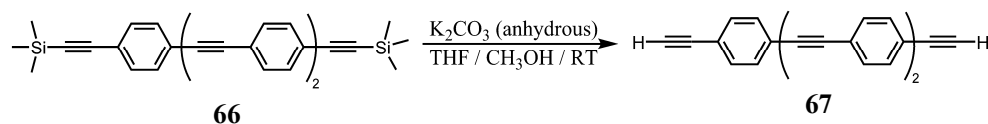
Figure 54. Deprotection of compound **66**.

2.3.7 Synthesis of boradiazaindacene dimer (68):

Compound **62** (0.9 mmol, 456 mg), Compound **67** (0.43 mmol, 140 mg), $PdCl_2$ (0.086 mmol, 16 mg), CuI (0.18 mmol, 34 mg) and PPh_3 (0.36 mmol, 95 mg) were added to the round bottomed flask which was previously flushed with Argon. As a solvent Et_3N (5 ml) and anhyrdous THF (50 ml) was added. The reaction mixture was stirred overnight at r.t.. After completion of the reaction, solvent was removed in *vacuo*. The crude product purified by silica gel column chromatography (eluent CHCl$_3$). Orange solid (354 mg, % 76) .

<super>1</super>H NMR (400 MHz, CDCl$_3$) δ; 7.59 (d, *J*=8.10 Hz, 4H), 7.48 (s, 8H), 7.46 (s, 4H), 7.24 (d, *J*=8.10 Hz, 4H), 2.47 (s, 12H), 2.24 (q, *J*=7.40 Hz, 8H), 1.27 (s, 12H), 0.92 (t, *J*=7.40 Hz, 12H) ;

<super>13</super>C NMR (100 MHz, CDCl$_3$) δ; 154.1, 139.2, 138.2, 136.1, 132.9, 132.3, 132.2, 131.6, 130.5, 128.6, 128.4, 123.6, 123.2, 123.1, 122.9, 91.2, 91.0, 90.8, 90.3, 17.1, 14.6, 12.5, 11.8 ;

ESI-HRMS calcd for [M+Na] 1105.5151 found 1105.5144 Δ=0.6 ppm.
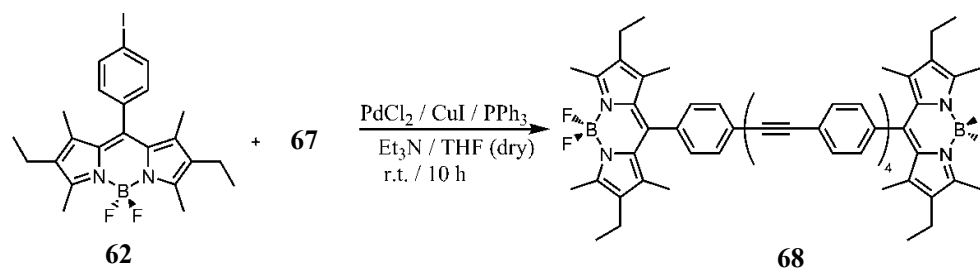
Figure 55. Synthesis of compound **68.**

2.3.8 Synthesis of *p*-Dimethylaminostyryl modified boradiazaindacene dimer (69):

Compound **68** (0.092 mmol, 100 mg) and *p*-dimethylaminobenzaldehyde (0.100 mmol, 15 mg) were refluxed in a mixture of toluene (50 ml), glacial aceticacid (75 μl), piperidine (85 μl). Any water formed during the reaction, was removed azeotropically by heating overnight in a Dean-Stark apparatus. The solvent was removed in *vacuo*, then crude product purified by silica gel column chromatography (eluent first CHCl$_3$, then CHCl$_3$:n-hexane, 2:1, v:v). The blue colored fraction was collected (36 mg, % 32).

<super>1</super>H NMR (400 MHz, CDCl$_3$) δ; 7.63-7.56 (m, 5H), 7.52-7.46 (m, 14H), 7.27-7.23 (m, 4H), 7.14 (d, *J*=16.70 Hz, 1H), 6.83 (br, 2H), 2.98 (s, 6H), 2.55-2.47 (m, 11H), 2.27-2.21 (m, 6H), 1.3 (s, 3H), 1.27 (s, 9H), 1.06 (t, *J*=7.55 Hz, 3H), 0.95-0.90 (m, 9H);

ESI-HRMS calcd for 1213.5988 found 1213.6049   Δ=5.0 ppm
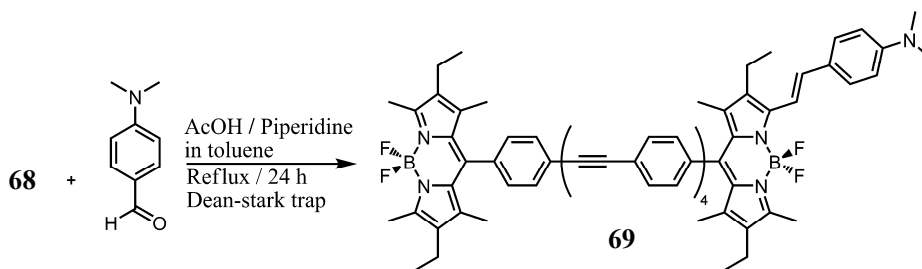
Figure 56. Synthesis of compound **69**.

2.3.9 Synthesis of Chemosensor 70:

Compound **68** (0.096 mmol, 104 mg) and 4-(1-aza-7,10-dioxa-4,13-dithiacyclopentadecyl)benzaldehyde (synthesized according to literature procedure, starting from 3-N-phenyl-3-aza-1,5-pentanediol [97]; 0.105 mmol, 38 mg) were dissolved in toluene (40 ml), glacial aceticacid (75 µl), piperidine (90 µl). Any water formed during the reaction, was removed azeotropically by heating overnight in a Dean-Stark apparatus. Solvent was removed under reduced pressure and the crude product first purified by silica gel column chromatography (eluent 99 $CHCl_3$: 1 MeOH), then further purified by Preparative thin layer chromatography (PTLC) in the same solvent system. The blue fraction was isolated (65 mg, % 48).

^{1}H NMR (400 MHz, $CDCl_3$) δ; 7.59 (d, *J*=8.05 Hz, 4H), 7.52-7.42 (m, 15H), 7.26-7.22 (m, 4H), 7.12 (d, *J*=16.50 Hz, 1H), 6.61 (br, 2H), 3.74 (t, *J*=4.90 Hz, 4H), 3.64-3.58 (m, 8H), 2.85 (m, 4H), 2.69 (t, *J*=4.90 Hz, 4H), 2.54-2.46 (m, 11H), 2.25-2.19 (m, 6H), 1.29 (s, 3H), 1.26 (s, 9H), 1.07 (t, *J*=7.60 Hz, 3H), 0.92 (t, *J*=7.60 Hz, 9H);

^{13}C NMR (100 MHz, $CDCl_3$) δ; 154.1, 139.2, 138.5, 138.2, 137.4, 136.5, 136.1, 133.3, 132.9, 132.5, 132.2, 131.6, 131.2, 130.5, 129.1, 128.9, 128.6, 123.6, 123.5, 123.2, 123.1, 123.0, 122.9, 91.1, 90.8, 90.7, 90.3, 74.2, 70.8, 52.4, 31.9, 31.4, 29.7, 29.4, 22.7, 18.4, 17.1, 14.6, 14.0, 12.5, 11.9, 11.6 ;

ESI-HRMS calcd for [M+ Na+ 3H- $2BF_2$] 1347.6434 found. 1347.9
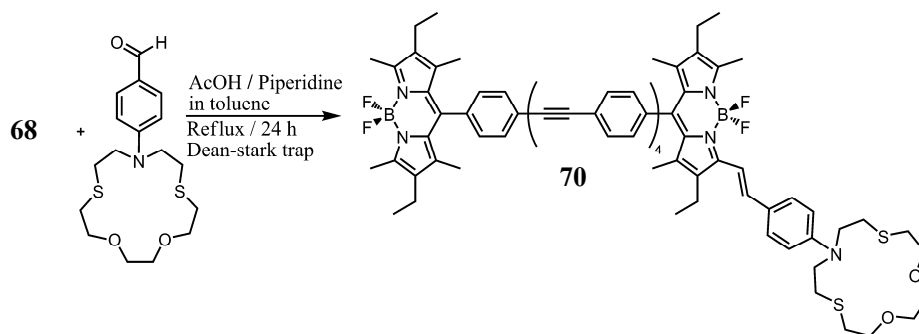
Figure 57. Synthesis of compound **70**.

2.3.10 Reference compound (71):

Compound **57** (0.263 mmol, 100 mg) and 4-(1-aza-7,10-dioxa-4,13-dithiacyclopentadecyl)benzaldehyde (synthesized according to literature procedure, starting from 3-N-phenyl-3-aza-1,5-pentanediol [97]; 0.265 mmol, 95 mg) were dissolved in toluene (50 ml), glacial aceticacid (165 μl), piperidine (190 μl). Any water formed during the reaction, was removed azeotropically by heating overnight in a Dean-Stark apparatus. Solvent was removed under reduced pressure and the crude product purified by silica gel column chromatography (eluent 99 CHCl$_3$: 1 MeOH). The blue fraction was isolated (106 mg, % 56).

^{1}H NMR (400 MHz, CDCl$_3$) δ; 7.49 (d, *J*=16.65 Hz, 1H), 7.43-7.37 (m, 5H), 7.24-7.21 (m, 2H), 7.10 (d, *J*=16.65 Hz, 1H), 6.58 (m, 2H), 3.74 (t, *J*=4.70 Hz, 4H), 3.63-3.58 (m, 8H), 2.84 (m, 4H), 2.69 (t, *J*=4.70 Hz, 4H), 2.52-2.45 (m, 5H), 2.22 (q, *J*=7.50 Hz, 2H), 1.23 (s, 3H), 1.19 (s, 3H), 1.07 (t, *J*=7.50 Hz, 3H), 0.92 (t, *J*=7.50 Hz, 3H);

^{13}C NMR (100 MHz, CDCl$_3$) δ; 153.2, 137.7, 137.4, 136.6, 135.2, 134.7, 132.1, 131.8, 131.0, 130.5, 128.0, 127.9, 127.6, 125.3, 115.6, 114.9, 111.7, 73.2, 69.71, 51.1, 30.4, 28.6, 17.4, 16.3, 13.6, 13.0, 11.6, 10.6, 10.3;

ESI-HRMS calcd for [M+Na] 740.3303 found 740.3325 Δ=3.0 ppm.
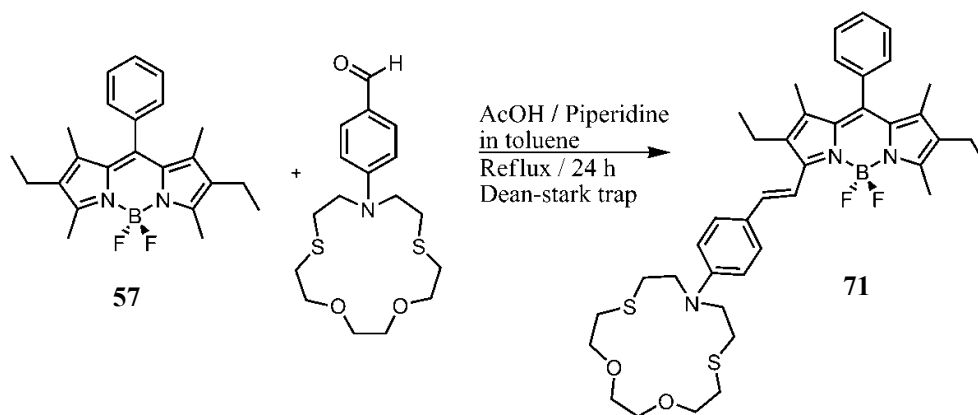
Figure 58. Synthesis of compound **71**.

PART III

2.4.1 Synthesis of NpI Ditosylate (74).

Diethylazodicaboxylate (DEAD) (0.45 ml, 2.6 mmol) was added dropwise at 0°C to a solution of naphthalene diimide **72** (266 mg, 1 mmol), alcohol **73** (1.58 g, mmol), PPh$_3$ (690 mg, 2.6 mmol) in THF, and the reaction mixture was stirred at room temperature for 16 h. The mixture was filtered though silica gel and the solution was evaporated under reduced pressure to obtain the crude product which was then purified by column chromatography (SiO$_2$: CH$_2$Cl$_2$/Me$_2$CO, 100:5) to give the compound **74** as a orange solid (1.5 g, 82 %).

^{1}H NMR (400 MHz, CD$_2$Cl$_2$, 298 K): δ = 1.27 (s, 36H), 1.84–1.57 (m, 24H), 3.86 (br t, 4H), 3.95 (t, 4H, J = 4 Hz), 4.02 (t, 4H, J = 4 Hz), 4.20 (br t, 4H), 6.71–6.76 (m, 8H), 7.08–7.13 (m, 16H), 7.24–7.26 (m, 8H), 7.35 (d, 2H, J = 5 Hz), 7.75 (d, 2H, J = 5 Hz), 8.72 (s, 4H) ppm.

^{13}C NMR (600 MHz, CD$_2$Cl$_2$, 298 K): δ = 21.7, 22.5, 24.1, 28.1, 28.9, 29.0, 29.4, 31.5, 34.6, 41.0, 50.8, 63.2, 67.8, 68.0, 71.0, 113.4, 113.5, 124.6, 127.1, 128.2, 130.3, 130.8, 131.1, 132.3, 139.9, 140.1, 144.9, 145.4, 148.8, 157.3, 157.4, 163.3 ppm.
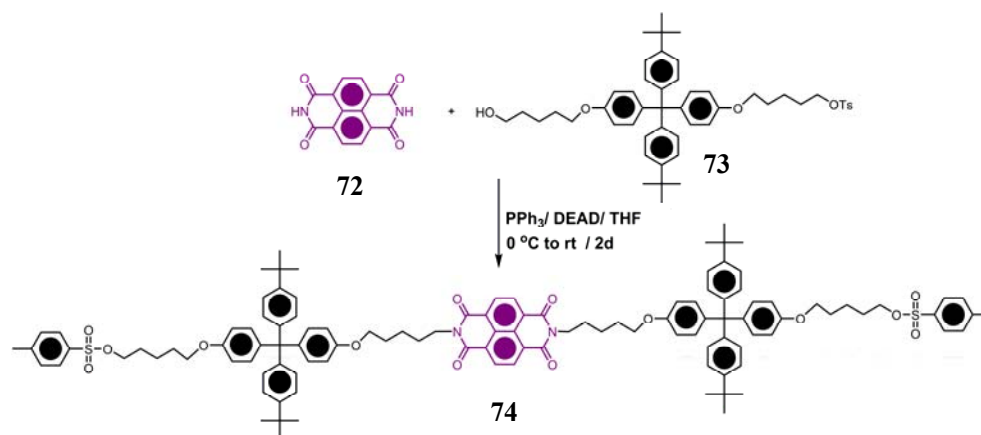
Figure 59. Synthesis of compound **74**.

2.4.2 Synthesis of Diazide 75.

The NpI ditosyl derivative **74** (280 mg, 0.154 mmol) and NaN$_3$ (11 mg, 0.16 mmol) were dissolved in DMF (5 ml). The mixture was heated at 80°C for 12h. After that DMF was removed under reduced pressure, the reaction mixture was dissolved in CH$_2$Cl$_2$ and washed with water (3 × 50 ml). The organic layer was dried over Na$_2$SO$_4$, and evaporated to dryness under reduced pressure to obtain the diazide **75** as a yellowish solid (227 mg, 95 %).

^{1}H-NMR (500 MHz, CDCl$_3$, 298 K): δ = 1.31 (s, 36H), 1.87–1.57 (m, 24H), 3.31 (t, ^3J = 6.8 Hz), 3.97–3.93 (m, 8H), 4.23 (br t, 4H), 6.76 (d, 8H, ^3J = 7.2 Hz), 7.10–7.07 (m, 16H), 7.25 (d, 8H, ^3J = 7.2 Hz), 8.75 (s, 4H) ppm.

^{13}C-NMR (125 MHz, CDCl$_3$, 298 K): δ = 23.5, 23.8, 28.7, 28.9, 29.1, 31.4, 34.3, 40.8, 51.4, 62.8, 67.3, 112.9, 124.1, 126.6, 126.7, 130.7, 131.0, 132.2, 139.5, 144.3, 148.3, 156.8, 162.8 ppm.
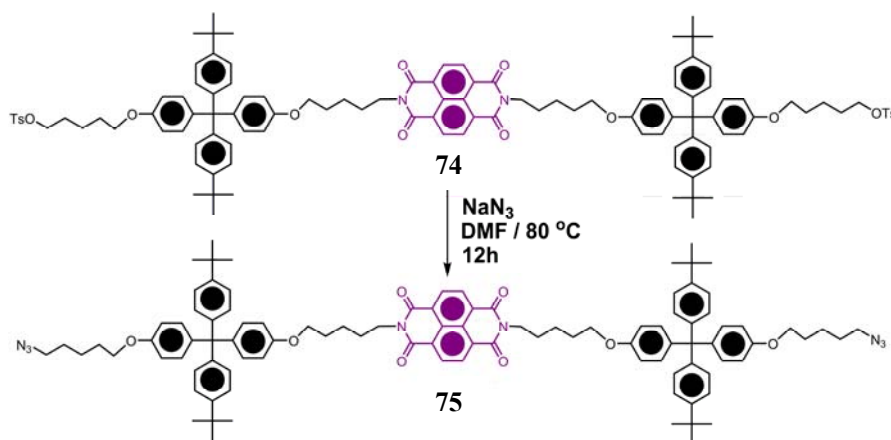
Figure 60. Synthesis of compound **75**.

2.4.3 Synthesis of 1,1'-di(but-3-ynyl)-4,4'-bipyridine-1,1'-diium hexafluorophosphate salt 76.2PF₆.

A solution of 4,4'-bipyridine (260 mg, 1.67 mmol) and *p*-toluenesulfonic acid but-3-ynyl ester (1.5 g, 6.69 mmol) in MeCN (10 ml) was heated to 80°C in a sealed tube for 4 d. The solution was then cooled to room temperature and the resulting precipitate was filtered and washed with MeCN. The yellowish solid was then dissolved in a H_2O/MeCN (3:1) mixture and a saturated aqueous solution of NH_4PF_6 was added to this mixture. The resulting white precipitate was filtered, washed with water, and dried under reduced pressure. The BIPY^{2+}-derivative **76.2PF₆** was isolated as a white powder (645 mg, 95 %).

^{1}H-NMR (500 MHz, CD₃CN, 298 K): δ = 2.45 (s, 2H), 2.97–2.95 (m, 4H), 4.75 (t, 4H, ^3J = 6.4 Hz), 8.41 (d, 4H, ^3J = 7.0 Hz), 8.94 (d, 4H, ^3J = 7.0 Hz).

^{13}C-NMR (125 MHz, CD₃CN): δ = 20.5, 59.3, 73.8, 77.7, 127.0, 145.7, 150.3.
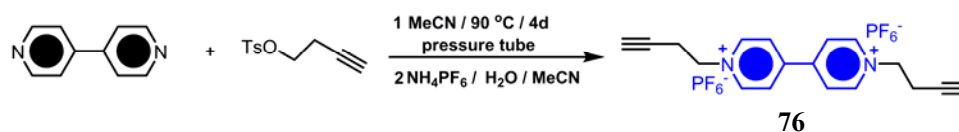
Figure 61. Synthesis of compound **76**.

2.4.4 Synthesis of [2]Pseudorotaxane 77.

The NpI-containing diazide **75** (198 mg, 0.127 mmol) and 1,5-dinaphto[38]crown-10 (400 mg, 0.635 mmol) were dissolved in a CHCl₃/MeOH mixture (9.5 : 0.5). To this solution LiBr (55 mg, 0.635 mmol) was added and heated to reflux for 7 d. During this time, formation of the [2]pseudorotaxane was observed as the solution turned red. Then the solvent was evaporated and the

product was purifed by column chromatography (SiO$_2$: CH$_2$Cl$_2$/EtOAc, 9:1) to obtain the [2]pseudorotaxane **77** as a red solid (42 mg, 15 %).

^{1}H-NMR (500 MHz, CDCl$_3$, 298K): δ = 1.29 (s, 36H), 1.86-1.67 (m, 24H), 3.29 (t, 4H, ^3J = 6.83 Hz), 4.09–3.86 (m, 44H), 6.06 (d, 4H, ^3J = 7.8 Hz), 6.65 (t, 4H, ^3J = 7.8 Hz), 6.73 (d, ^3J = 8.8 Hz), 6.82 (d, ^3J = 8.8 Hz), 6.86 (d, 4H, ^3J= 7.8 Hz), 7.09–7.07 (m, 16H), 7.15 (d, 8H, ^3J = 8.5 Hz), 8.26 (s, 4H) ppm.

^{13}C-NMR (125 MHz, CDCl$_3$, 298K): δ = 23.4, 24.2, 28.7, 28.9, 29.2, 31.4, 34.3, 51.4, 62.8, 67.4, 67.6, 69.8, 71.2, 71.4, 103.4, 112.9, 113.0, 114.1, 123.6, 123.9, 124.1, 124.7, 125.1, 130.5, 130.6, 132.2, 139.5, 139.6, 144.3, 148.3, 153.0, 156.7, 156.9, 163.1 ppm.
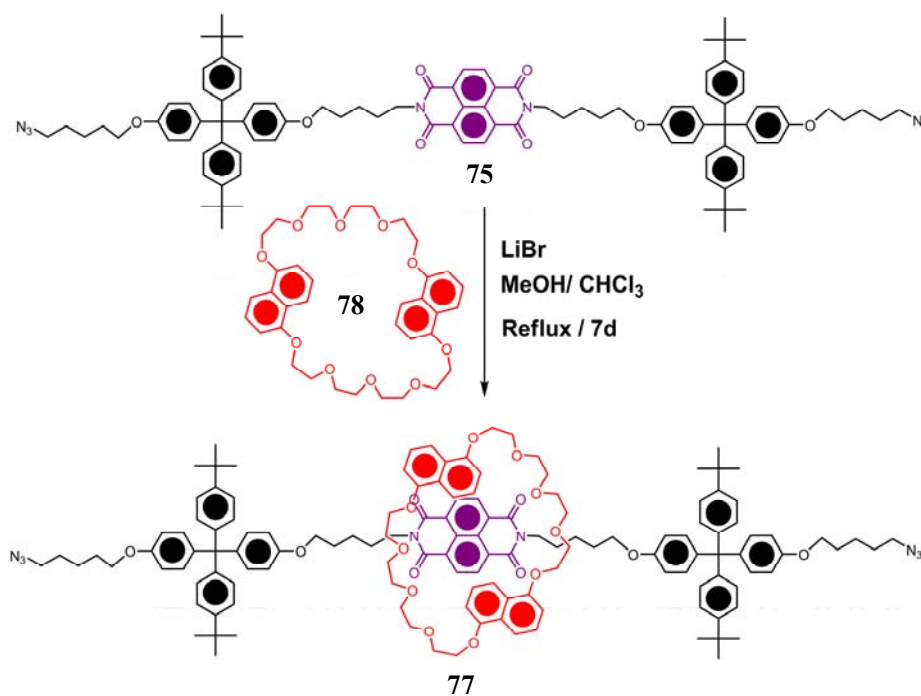
Figure 62. Synthesis of [2]pseudorotaxane **77**.

2.4.5 Synthesis of [2]Catenane 79.2PF$_6$.

A solution of the [2]pseudorotaxane **77** (36 mg, 0.0164 mmol), the BIPY^{2+}-derivative **76**•2PF$_6$ (6.7 mg, 0.0164 mmol), TBTA (1.74 mg, 0.0033 mmol), and Cu(MeCN)$_4$PF$_6$ (1.22 mg, 0.0033 mmol) in dry Me$_2$CO (10 ml) was stirred for 24 h. The solvent was then evaporated and the resulting reddish solid was purified by column chromatography (SiO$_2$: Me$_2$CO to 2% NH$_4$PF$_6$ / Me$_2$CO). The red fraction was collected and washed with H$_2$O (3 × 5 ml), then dried under reduced pressure to obtain the [2]catenane **79**•2PF$_6$ as a red solid (10 mg, 25 %).

^{1}H-NMR (500 MHz, (CD$_3$)$_2$CO, 298 K): δ = 1.23 (s, 36H), 2.03–1.85 (m, 24H), 4.34–3.57 (m, 52H, O-CH$_2$, N-CH$_2$), 5.24 (br t, 4H), 6.11 (d, ^3J = 7.5 Hz, 4H), 6.62–6.59 (m, 8H), 6.75 (d, 4H, ^3J = 8.30 Hz), 6.88 (d, 4H, ^3J = 8.9 Hz), 6.97 (d, 4H, ^3J = 8.90 Hz), 7.03–7.00 (m, 12H), 7.23 (d, ^3J = 8.60 Hz, 8H), 8.22 (s, 2H), 8.71 (s, 4H), 8.70 (d, 4H, ^3J = 6.8 Hz), 9.32 (d, 4H, ^3J = 6.8 Hz) ppm.

^{13}C-NMR (125 MHz, (CD$_3$)$_2$CO, 298 K): δ = 22.7, 23.9, 26.8, 27.3, 29.1, 29.2, 29.3, 29.4, 29.6, 30.6, 33.8, 49.5, 62.5, 67.4, 69.4, 71.0, 103.4, 112.9, 113.1, 113.7, 123.5, 124.0, 124.6, 125.0, 126.7, 130.2, 130.3, 131.6, 131.7, 139.3, 144.2, 146.1, 148.1, 152.9, 156.7, 162.7 ppm.
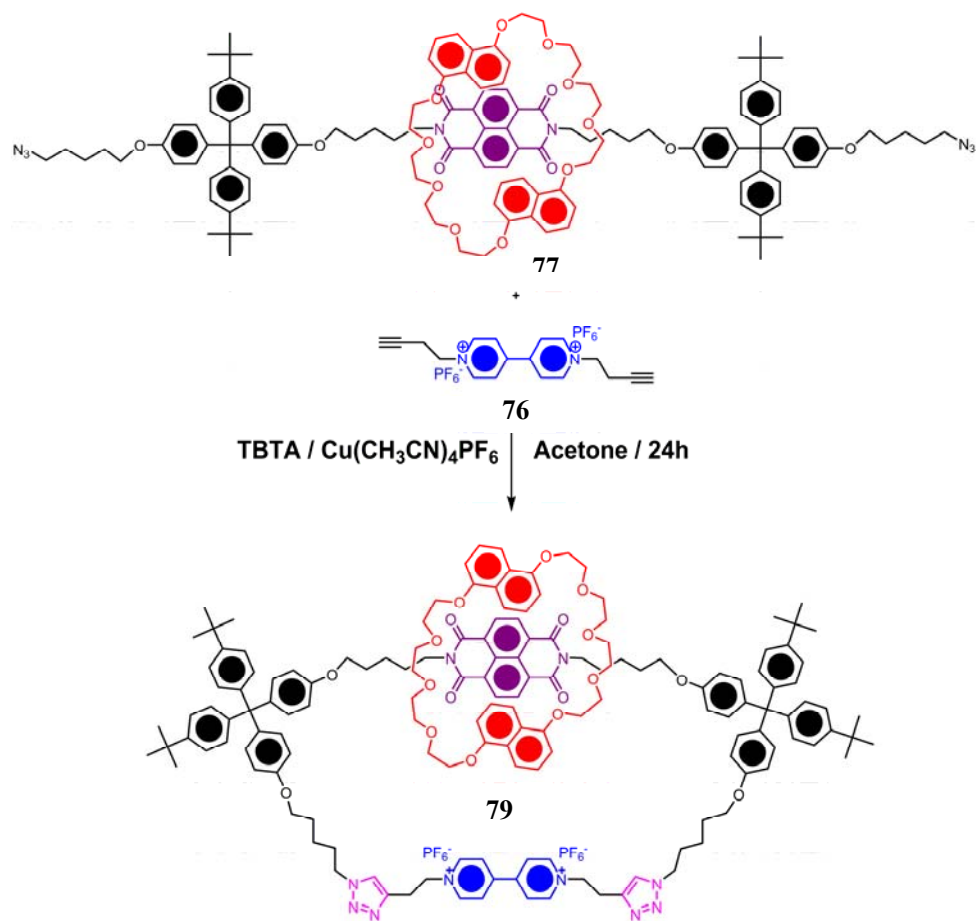
Figure 63. Synthesis of [2]catenane **79**.

CHAPTER 3

RESULTS AND DISCUSSION

3.1 Ion Sensing Coupled to Resonance Energy Transfer: A Highly Selective and Sensitive Ratiometric Fluorescent Chemosensor for Ag(I) by a Modular Approach

Design and synthesis of fluorescent chemosensors with desirable properties is a vibrant field of supramolecular chemistry. Especially, chemosensors targeting heavy and transition metal cations are very important due to the environmental and biological relevance of such metal ions. Fluorescence sensing of cations, such as Hg(II), Pb(II), Ag(I), and Cu(II), is particularly challenging since these ions generally act as quenchers via the electron transfer and facilitated intersystem crossing (isc) processes. Up to now, a number of satisfactory chemosensors for these ions have been reported. Most of them display fluorescence intensity changes (PET type), but only very few of them result in spectral shifts in either absorption or emission spectra (ICT type). This would be a highly desirable property as such spectral changes would allow wavelength ratiometric analyses, canceling likely artifacts due to concentration variations in the analysis media.

Boradiazaindacenes (borondipyrromethenes, BODIPYs, BDPs) are very bright fluorophores with high quantum yields and large extinction coefficients. Structural modifications of these compounds are known to generate dyes with emission peaks spanning part of the visible spectrum from green to the red end. A

number of fluorescent chemosensors were reported based on modified boradiazaindacene dyes. Recently, a very interesting modification converting a standard green emitting dye to a longer wavelength absorbing and red emitting ICT dye was reported. It was also demonstrated that the emission properties can be switched on upon acid addition, opening possibilities for further interesting cation sensing applications with judiciously designed chemosensors.

To this end, we targeted various BODIPY dyes which are shown in Figure 64 and designed a modular chemosensor **61** composed of two fluorophores and a selective ligand. The design allows a facile attachment and derivatization of boradiazaindacene fluorophores geared for efficient energy transfer and modulation of the emission signal.
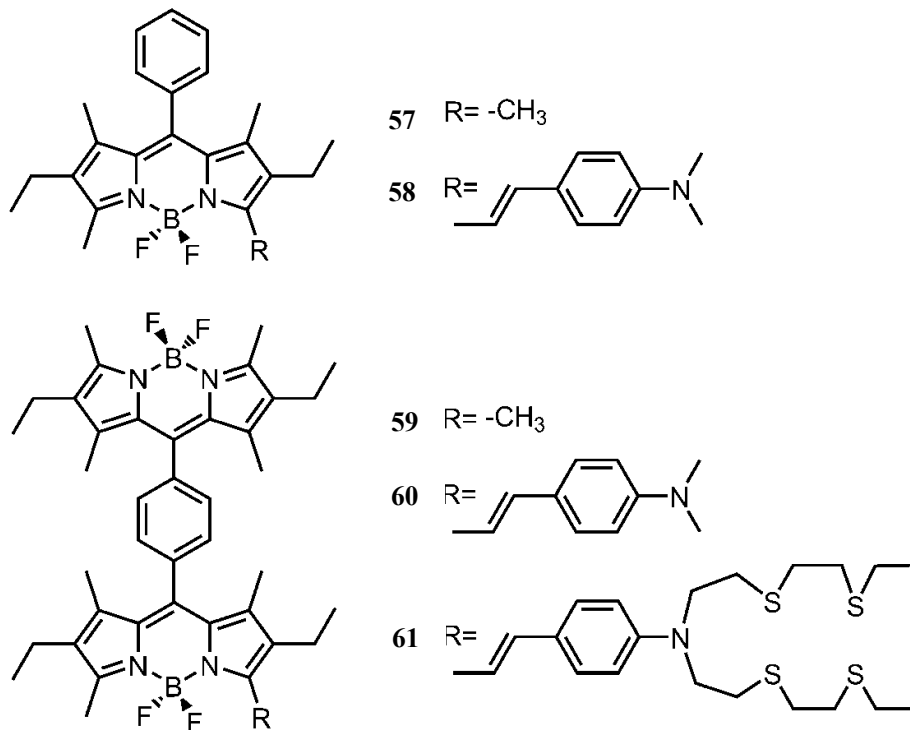
Figure 64. Target BODIPY dyes.

The powerful part of this approach is the modularity of the system. Due to the high symmetry of the BODIPY dimer **59**, any aldehyde containing receptor unit

for the desired analyte can be attached by simple and efficient condensation reaction. Besides this advantage, this system has large Stoke`s shift, which prevents the scattering of light in turbid solutions and likelihood artifacts which can interfere with the emission signal.

Thus, we synthesized compound **59** by the reaction of terephthaloyl chloride with 3-ethyl-2,4-dimethylpyrrole in CH_2Cl_2 at reflux temperature. Then, Et_3N and $BF_3.OEt_2$ added to this solution, respectively. Formation of the bright orange fluorescence indicates formation of the target BODIPY dye **59**.

Energy minimized (MM+, Hyperchem v.7.5), see Figure 73, structure of this compound shows two coplanar boradiazaindacene units with a nearly perpendicular 1,4-phenylene ring as a spacer. Methyl groups on the pyrrole units ensure the perpendicular orientation. Absorption spectrum of **59** correlate well with the presence of two noninteracting chromophores with no evidence of excitonic interactions (see Figure 65). The methyl groups neighboring the BF_2 bridge are slightly acidic, and this property was exploited in the synthesis of compounds **60** and **61**. The condensation reactions between compound **59** and corresponding aldehydes
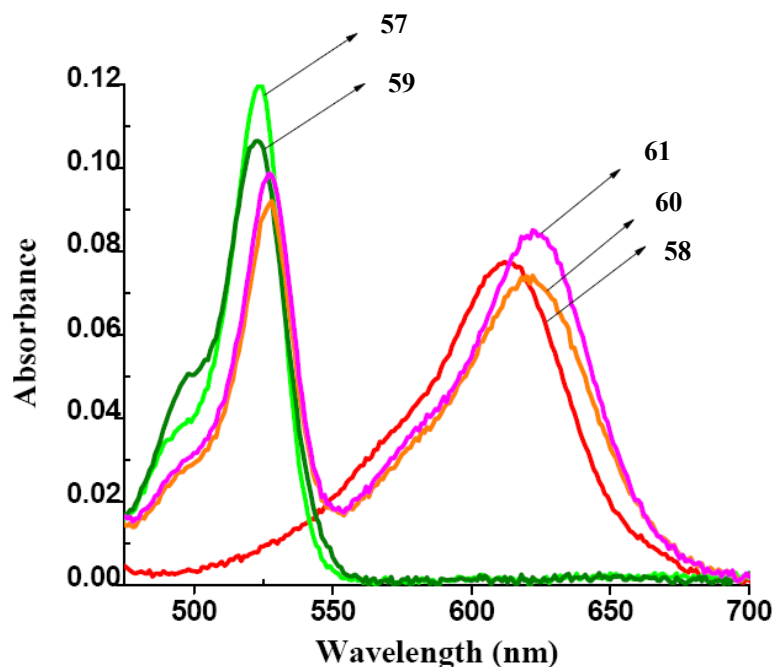
Figure 65. Absorption spectra of compounds **57-61** in THF. Concentrations for **57**, **58**, **60**, **61** was 1.4 μM. For compound **59**, the concentration was 0.7 μM.

were carried out in toluene, with azeotropic removal of water. Slight modifications in the literature procedure resulted in improved yields, facilitating the synthesis of our target compounds and also accentuating the modularity of our approach.

The absorption spectra of compounds **60** and **61** (Figure 63) as expected show two distinct peaks centered near 500 and 600 nm. The shorter wavelength absorption corresponds to the unmodified boradiazaindacene unit, whereas the other unit corresponds to the absorption of extended conjugation PCT chromophore within the same molecule. This evidence strongly shows that two dyes are noninteracting in the ground state. Therefore this synthetic modification enables us to obtain energy transfer cassette in one step.
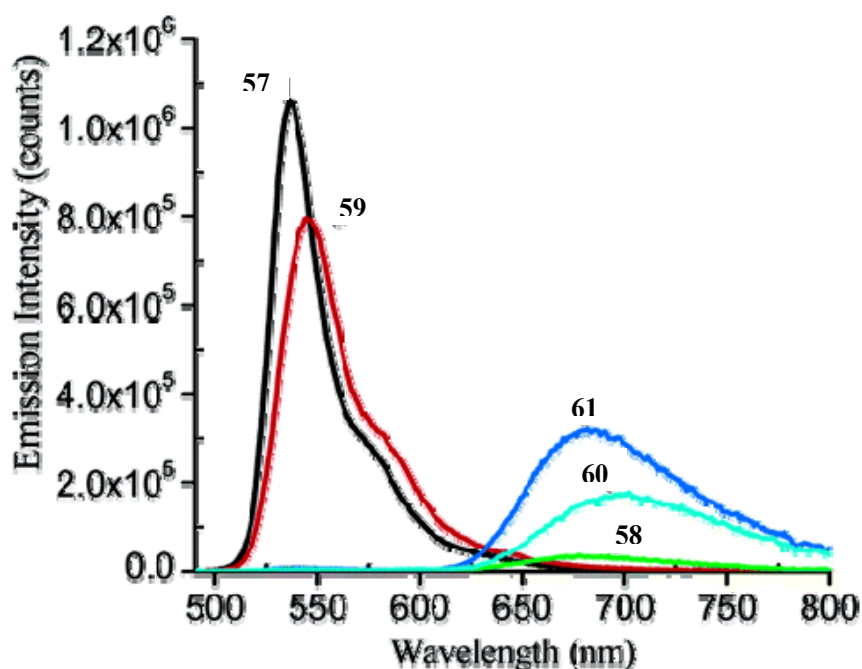
Figure 66. Emission spectra of compounds **57-61** in THF. Excitation was at 480 nm with 5 nm slit widths.

A comparison of the emission spectra of compounds **57-61** (Figure 66) with equal absorbance values at the excitation wavelength (480 nm) for compounds **57** and

78

59-61 was made. For compound **58**, since there is no absorption peak in that region, a comparable concentration of the dye (1.4 μM) was used. The dimeric dye **59** and the monomeric reference compound **57** showed comparable quantum yields (0.73 and 0.76, respectively) with a slight red shift in the emission spectrum of **59**. Most interesting results were obtained on excitation of dyes **58**, **60**, and **61** at 480 nm. Compound **58**, as expected, displayed only a very weak and broad emission peak around 680 nm. This is due to very weak absorption of this dye at the excitation wavelength. However, compounds **60** and **61**, when excited at the same wavelength, show only very weak residual emissions near 550 nm, corresponding to a remarkably decreased quantum yield of this fluorophore from 0.76 in compound **57** to 1.3x 10^{-3} in **60** and 4.1x10^{-3} in **61**. However, as a result of the excitation energy transfer, strong emission peaks centered around 700 and 680 nm, respectively, were obtained from the red emitting dye. Highly diminished emission from the green emitting boradiazaindacene dye clearly demonstrates the efficiency of energy transfer (near 100%) from this dye to the red emitting extended conjugation boradiazaindacene derivative.

Table 1. Quantum yields of the dyes in THF solutions.

Compounds	Quantum yield of dye 1	Quantum yield of dye 2
Parent BODIPY **57**	0.76	-
Extended conj. BODIPY **58**	0.31	-
Dimeric BODIPY **59**	0.73	-
Dimethylaminophenyl BODIPY **60**	0.0013	0.26
Thiazaligand BODIPY **61**	0.0041	0.49
Thiazaligand BODIPY **61**+ Ag(I)	0.0032	0.67

All dyes were excited at 480 nm, and all spectra were corrected, excitation and emission slits were both set at 5 nm. Rhodamine 6G was used as the reference compound in quantum yield measurements, Quantum yield of rhodamine is 0.95

Table 1 (continued), in ethanol. [99] Corrections for refractive indices were done. The last column refers to the quantum yields of long wavelength emission from the energy acceptor dye, assuming %100 percent energy transfer efficiency.

This result encouraged us in developing this system further by attaching a selective soft metal binding ligand. The ligand we chose for further modification of the dimeric dye, *N*-phenyl-9-aza-3,6,12,15-tetrathiaheptadecane, is reportedly a highly selective ligand for Ag(I). Absorption spectra of compound **61** in response to changing Ag(I) concentrations are shown in Figure 67.
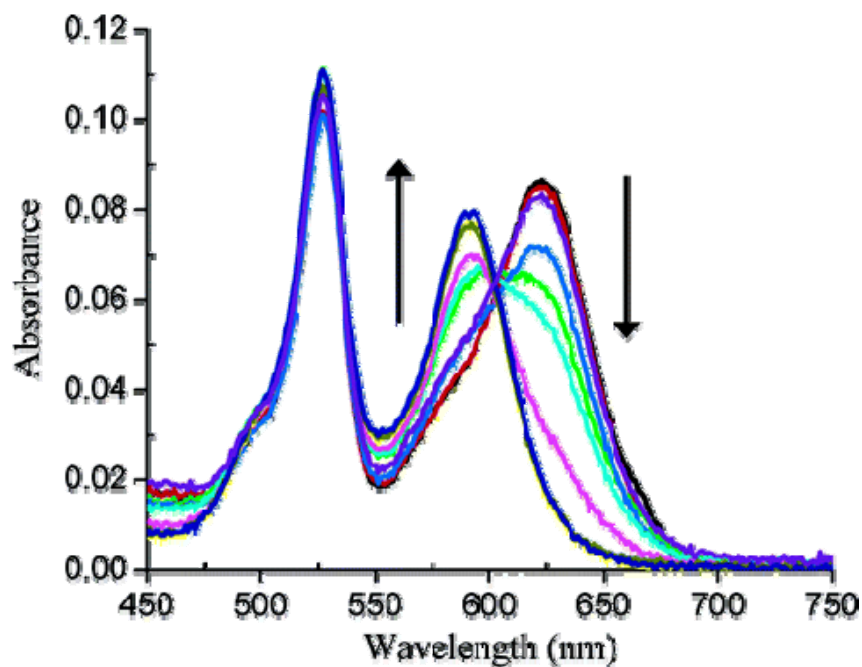
Figure 67. Absorption spectra of compound **61** in the presence of increasing Ag(I) concentrations (0, 0.5, 0.75, 1.0, 1.5, 2.0, 2.5, 4.0, 5.0, 7.5, 10 μM). The concentration of the chemosensor was 1.4 μM.

The binding of Ag(I), in accordance with our design expectations, resulted in a blue shift of the long wavelength peak, which corresponds to the modified

boradiazaindacene dye, whereas no significant change takes place in the absorption peak corresponding to the unmodified dye. This creates multiple opportunities for ratiometric cation analysis. Excitation can be done either at the unmodified boradiazaindacene absorption or at any one of the longer wavelength peaks corresponding to the free and metal-bound form of the chemosensor. To take advantage of larger pseudo-Stokes' shift generated by resonance energy transfer, we have selected to excite the dye close to the absorption peak of the unmodified boradiazaindacene unit. The emission spectra obtained by excitation at 480 nm demonstrate that we have a very efficient emission ratiometric chemosensor working in the long wavelength end of the visible spectrum (Figure 68). Ag(I) binding causes a 41 nm hypsochromic shift which is consistent with
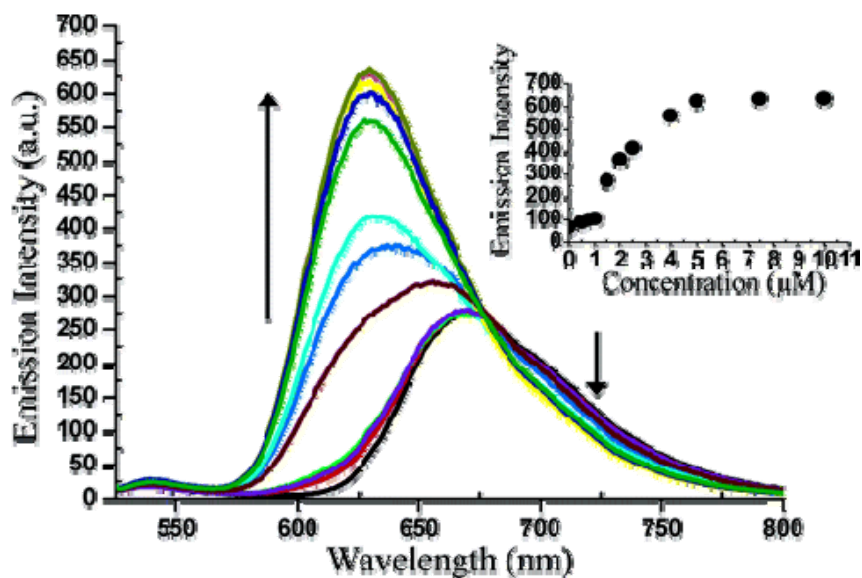
Figure 68. Emission spectra of compound **61** at increasing concentration of Ag(I) (0, 0.5, 0.75, 1.0, 1.5, 2.0, 2.5, 4.0, 5.0, 7.5, 10 μM). Inset: emission change at 630 nm with increasing concentrations of Ag(I). Excitation wavelength was 480 nm with 5 nm slit widths, and spectra were corrected. The concentration of the chemosensor **61** was 1.4 μM.

the PCT nature of the fluorophore (acceptor part). The nitrogen donor atom within the macrocycle, interacts with the cation, thus, destabilizes the excited state and this results in increasing the energy gap between S_0 and S_1 energy levels. And blue shift observed in both emission and the absorbtion spectra. In the excited state system looks like its resonance form, so the nitrogen atom will be positively charged and this situation cause the destabilization. Although the energy transfer efficiency is assumed to be %100, there is small amount of modulation in the efficiency of energy transfer. Quantum yields which are summarized in Table 1 show that binding of silver ion causes a decrease in the quantum yield of the donor from 0.0041 to 0.0032 and increase in the quantum yield of the acceptor from 0.49 to 0.67. This emission spectrum shows that we can signal silver ion
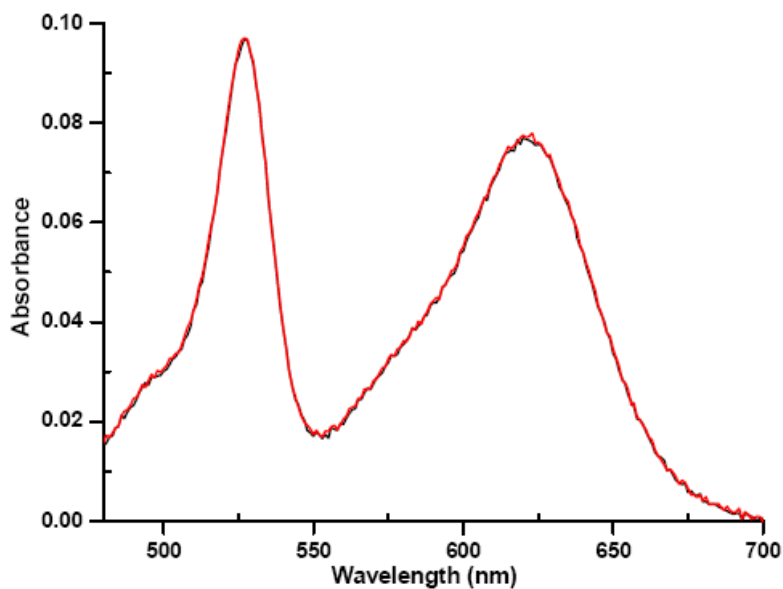
Figure 69. Absorption spectra of compound **60** in the absence (red curve) and presence of 10μM Ag(I) (black curve)

Concentration, up to micromolar regime, ratiometrically. Compound **60** and **61** contain nitrogen donor atoms in their structure. Therefore, we carried out a control experiment, just to show that compound **60** is insensitive towards silver ion and also to show effect of the macrocycle for the binding of Ag(I), control

experiments are shown below which proves that compound **60** is completely insensitive to Ag(I) both in absorbance and the emission spectra.
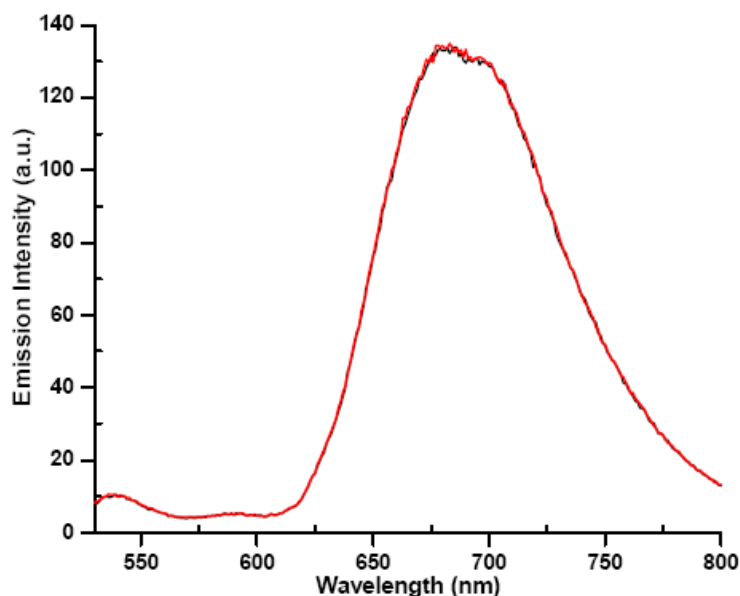
Figure 70. Emission spectra of compound **60** in the absence (red curve) and presence of 10μM Ag(I) (black curve).

Remarkably, all the other metal ions studied caused only insignificant changes in the emission spectrum, not enough for an accurate assessment of the binding constant. It is also remarkable that cations, such as Pb(II), Mn(II), Fe(II), Hg(II), and Co(II), have practically no effect on the emission spectrum, although they are known to be effective HTM (heavy or transition metal) quenchers (See Figure 71). The important point is to consider, the hard soft interaction between the sulfur atoms of the ligand which is soft and the soft metal ions, these are Ag(I), Cd(II), Pb(II), Hg(II). The selectivity arises from the shape of the macrocycle. There is approximately 7 fold ratio change in the emission spectrum.
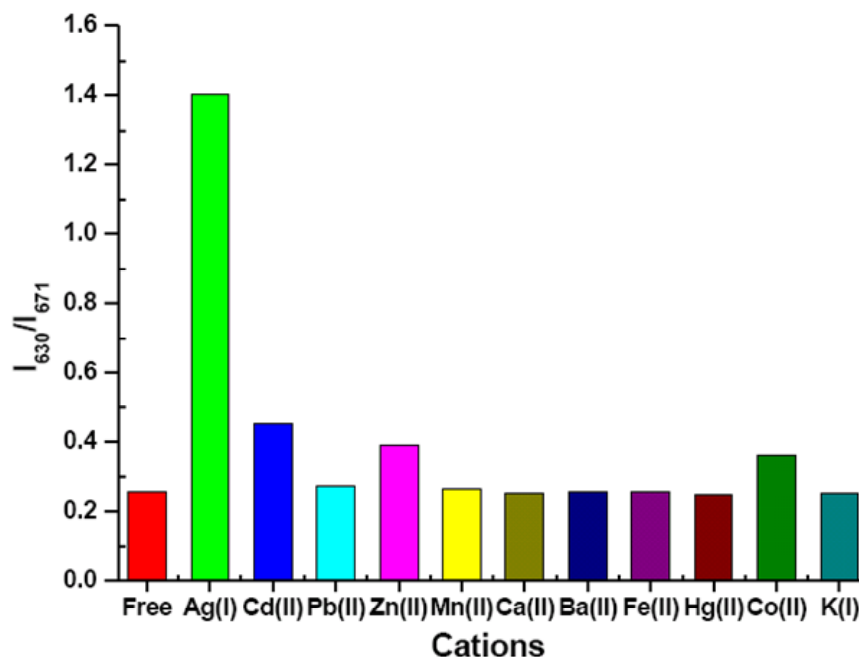
Figure 71. Emission ratios obtained in the presence of different metal cations. The chemosensor **61** was excited at 480 nm and the ratio of the emission data at 630 and 671 nm were calculated. Cation concentration was 5 μM and the chemosensor concentration was 1.4 μM.

As a ratiometric chemosensor, compound **61** is outstanding; emission ratio of intensities at 630 and 671 nm (I_{630}/I_{671}) changes from 0.25 to 1.42 for the free and Ag(I)-bound chemosensor, respectively. The binding constant of silver in THF was determined to be 1.7×10^5 M^{-1} by using Benesi-Hildebrand analysis. According to the least square analysis on absorbance data, the binding constant is calculated as $1.7 \times 10^5 \pm 2.6$, this data shows that we get quite reasonable and high binding affinitiy towards Ag(I) by using chemosensor **61**.
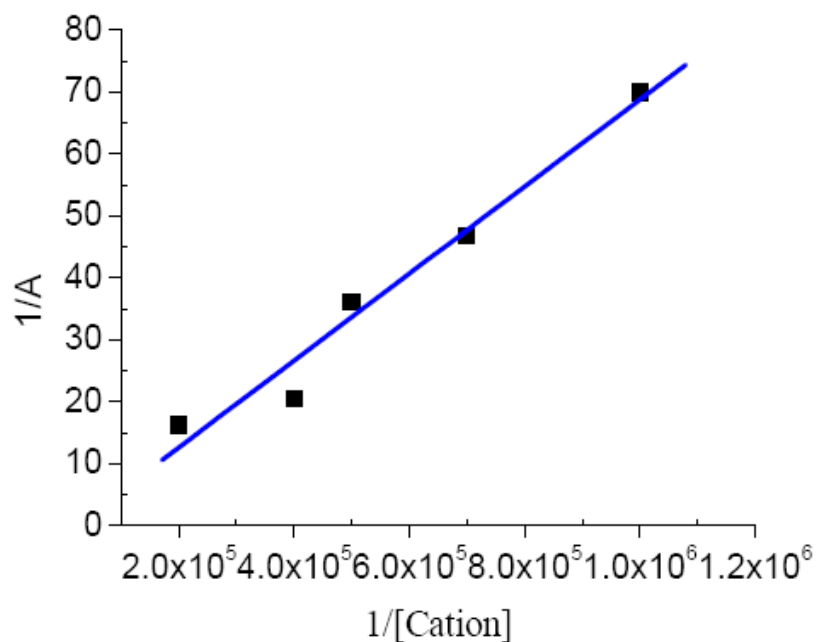
Figure 72. Benesi-Hildebrand analysis of compound **61** with the absorbance data collected at 620nm.

Result of the least square analysis follows:

Equation $Y = AX + B$, $A_0 = 0.085719444$ (absorbance value of the unbound form at 620 nm)

$Y = 7.013E^{-5}X - 1.3762$

$K = 1/(B*A_o) = 166350.1$ (binding constant for Ag(I)

$SD = 1/(SD*A_o) = +/- 2.597684$

     In summary, we have introduced a general strategy for large pseudo-Stokes' shift, ratiometric chemosensors, utilizing efficient energy transfer (See Figure 73). Yet, the synthesis is highly straightforward due to the symmetry of the first precursor. In just one step, this symmetric precursor can be transformed into an efficient RET system, where the choice of the ligand carrying aldehyde would also determine
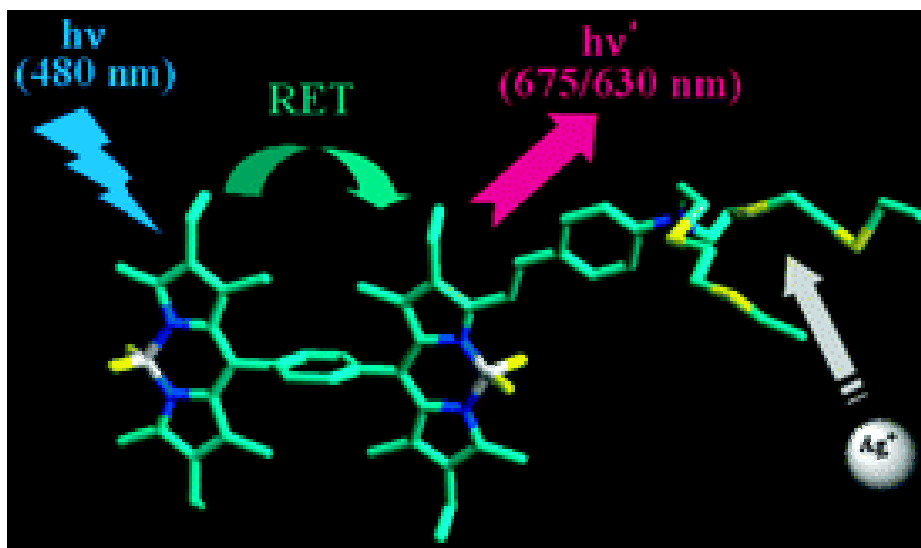
Figure 73. Energy minimized structure of chemosensor **61** and proposed sensing mechanism for Ag(I) ion.

the selectivity of the resulting chemosensor. Also the corresponding energy transfer cassettes are easily accessible considering the synthetic pathway. Figure 74 summarizes our modular approach for the design of ratiometric fluorescent chemosensors coupled with resonance energy transfer (FRET).
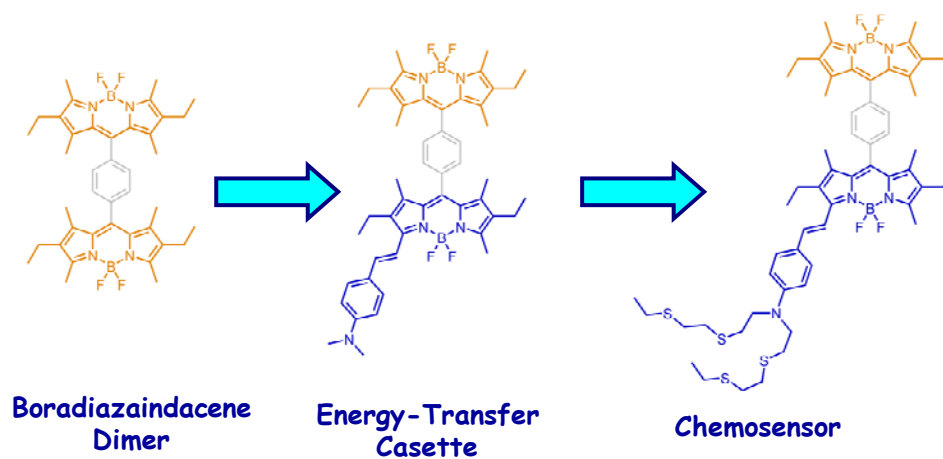
Figure 74. Modular approach.

Considering the multitude of choices in the ligand selection and the large number of energy transfer casettes operating in aqueous solutions, we are confident that this powerful approach can be extended to polar protic solvents, including water, to yield a new class of chemosensors with practical applications in many sensing fields. Because there is a strong demad for the development of chemosensors which has large Stokes` shift and can signal desired analyte, ratiometrically.

3.2 Signal Ratio Amplification via Modulation of Resonance Energy Transfer: Proof of Principle in an Emission Ratiometric Hg(II) Sensor [100]

Fluorescent chemosensor design is an active field of supramolecular chemistry, not only because of potential practical benefits in cell physiology, analytical, and environmental chemistry, but also as a proving ground for manipulation and/or engineering of various photophysical processes toward an ultimate goal of selective and sensitive signaling of targeted molecular or ionic species. Recently, boradiazaindacenes have become the fluorophore of choice in many chemosensor designs, not only because of their exceptional properties as fluorophores, but also as a result of their remarkably rich chemistry. Previously, we reported [52] a dimeric boradiazaindacene, which can be converted into an energy transfer cassette and furthermore into a ratiometric ICT (internal charge transfer) based cation sensor, selective for silver ions, all through simple structural modifications. In that design the two fluorophores were kept very close to each other, so that the through-space EET was nearly 100% efficient, thus creating a large pseudo-Stokes' shift chemosensor. ICT based chemosensors typically have an advantage of two distinct emissive states (analyte-free and analyte-bound), which makes these chemosensors potentially wavelength-ratiometric, that is, internal referencing of the signal is possible, eliminating potential artifacts.

In designing ratiometric chemosensors, one of most important parameters is the magnitude of the range of signal ratios of emission intensities at two different wavelengths for the analyte-free and analyte-bound chemosensor, preferably excited at the isosbestic point. This parameter determines the dynamic range and the sensitivity of the chemosensor to the analyte concentration. A large range of ratios could be obtained, only when the emission peaks for the bound and free chemosensor are well-resolved and if both forms have reasonable emission intensities. However, this ratio is an inherent property of the particular chemosensor-analyte interactions, and, until now, a systematic methodology for improving the signal ratio was unavailable. We now introduce a new strategy in ratiometric chemosensor design which would make this possible: the range of ratios can be significantly improved, if the chemosensor is designed as an energy transfer dyad, and once the interchromophoric distance is carefully adjusted, binding of the analyte increases the spectral overlap between the donor emission

and the acceptor absorption peaks. Thus, more efficient Forster type energy transfer in the bound state results in higher emission intensity for the analyte-bound chemosensor, effectively increasing the signal ratio for the two states. Our design principles are summarized in Figure 75.
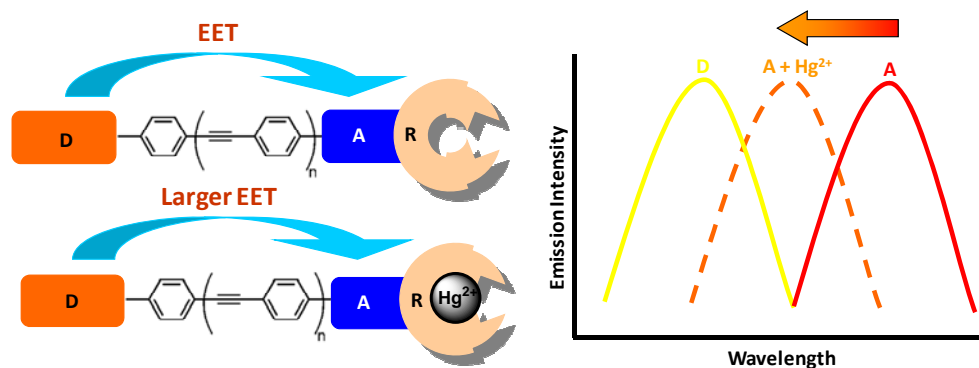
Figure 75. Design principles of the proposed system (n=0, 2, 4).

As we mentioned in the introduction part, there is two factors which can modulate the efficiency of the energy transfer. These are the interchromophoric distance and the spectral overlap between the donor and acceptor units.   Increasing interchromophoric distance between two fluorophores, namely donor and acceptor units will decrease the efficiency of the energy transfer. In our case we keep the interchromophoric distance constant with the aid of rigid phenyl acetylene spacer. And we prepared BODIPY dyads by varying the interchromophoric distance. Second one is the spectral overlap, efficiency of energy transfer increases by spectral overlap. If the emission of donor unit overlaps well with the absorbance of the acceptor unit, energy transfer efficiency increases. There are not many examples in which the energy transfer efficiency is modulated by changing the spectral overlap. As shown in Figure 75, binding of mercuric ion to the receptor unit shows ICT type behavior (detailed explanation can be found in introduction part). As a result of this, absorbance of the acceptor unit blue-shifted while the emission of the donor part remains to be same. This spectral change increases the spectral overlap, thus, causes spectacular change in the efficiency of the energy transfer.

To demonstrate the feasibility of our approach, we set out to synthesize a series of boradiazaindacene dyads, with increasing interchromophoric distance, these target compounds are shown in Figure 76. Besides these we also synthesize reference compound **71** to compare the effect of energy transfer in ratiometric sensing of Hg(II) ion.
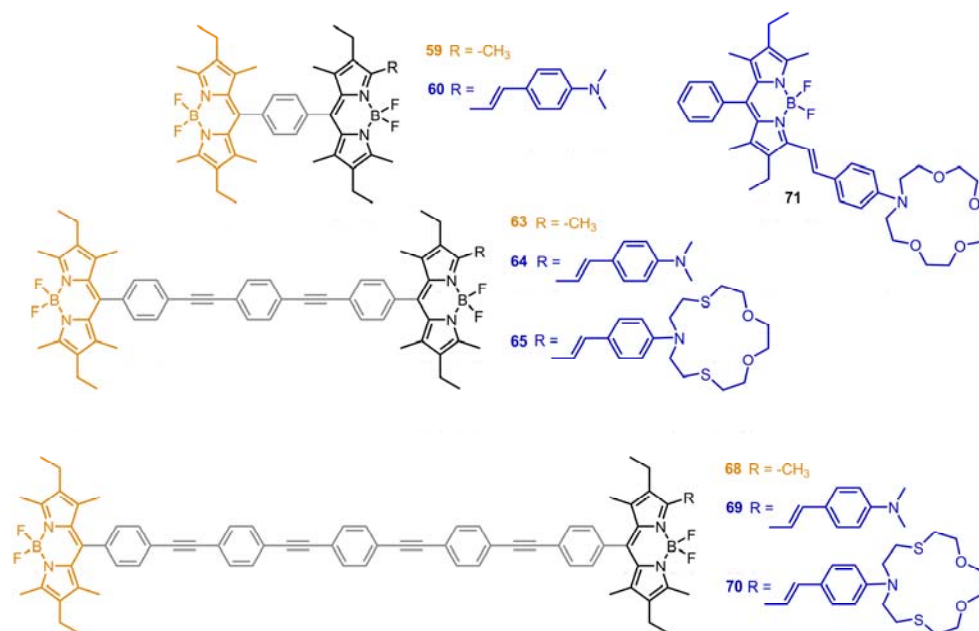
Figure 76. Target Compounds.

In chemosensors in which the metal receptor is an electron donor and also part of the π-system of the chromophore, metal binding always causes a blue shift in the absorption spectrum, and in our systems increase the EET efficiency. In the compound **60**, the energy transfer efficiency was almost 100%, and increasing the interchromophoric distance should decrease the EET efficiency to levels appropriate for cation modulation. Thus, we synthesized new dyes **63**-**70** shown in Figure 76.
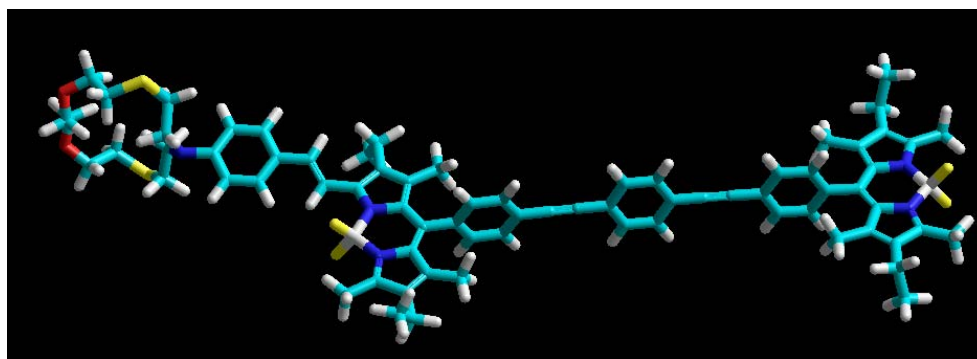
Figure 77. Energy minimized (HyperChem v. 7.5, PM3 semiemprical module) structure of compound **65**. Calculated B-B distance 25.5 Å.
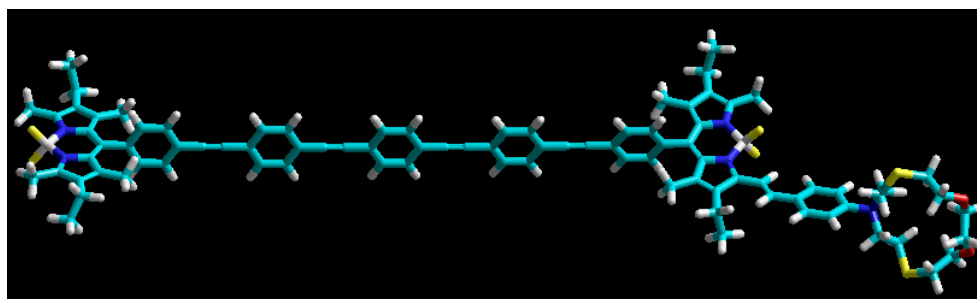
Figure 78. Energy minimized (HyperChem v. 7.5, PM3 semiemprical module) structure of compound **70**. Calculated B-B distance 39.1 Å.

We also run some energy minimization studies by using HyperChem v. 7.5 on these compounds to ensure that we have through space interaction between donor and acceptor units. It is evident that the methyl groups next to the phenyl units ensure the perpendicular orientation of the phenyl ring, thus, blocks any through bond interaction between donor and acceptor units. These findings are in accordance with our experimental findings.

Table 2. Quantum yields of the BODIPY dyads in dilute THF solutions.

Compounds	Quantum yield of dye 1	Quantum yield of dye 2
63	0.63	-
64	0.021	0.17
65	0.029	0.17
65+Hg(II)	0.052	0.41
68	0.59	-
69	0.097	0.12
70	0.13	0.13
70 + Hg(II)	0.078	0.35
71	-	0.16
71+Hg(II)	-	0.40

All dyes were excited at 500 nm, and all spectra were corrected, excitation and emission slits were both set at 5 nm. Rhodamine 6G was used as the reference compound in quantum yield measurements, Quantum yield of rhodamine is 0.95 in ethanol. [99] Corrections for refractive indices were done. The last column refers to the quantum yields of long wavelength emission from the energy acceptor dye.

Quantum yields of the dyes were done by using Rhodamine 6G as the reference compound. In Table 2, dye_1 represents donor part and dye_2 represents the acceptor part. Both compounds **63** and **68** have relatively high quantum yields. After condensation reaction quantum yield of the donor decreases drastically, for chemosensor **65** and **70**, it changes from 0.63 to 0.029 and 0.59 to 0.13 respectively. Calculated B-B distance for **65** is 25.5 Å , and for **70**, it is 39.1 Å. Increasing interchromophoric distance, causes an increase in the quantum yield of the donor part. Increasing the distance will decrease the energy transfer efficiency, as a result of this emission signal which is observed from the donor part increases. To prove our proposal, we need to show that the quantum yield of

the donor should decrease upon binding of Hg(II) to the receptor. The quantum yield of the donor in compound **70** decreases from 0.13 to 0.078, this result shows that we can modulate the energy transfer upon binding of Hg(II). At this stage, we expected to observe higher decrease in the quantum yield of the donor but there is an overlap in the emission signals of the donor part and bound form of the chemosensor, so this value is the sum of two emission signal.

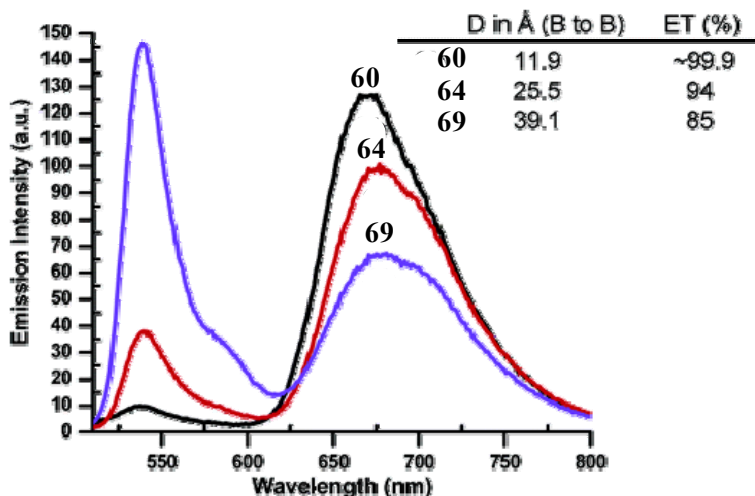|	D in Å (B to B)	ET (%)
60	11.9	~99.9
64	25.5	94
69	39.1	85

Figure 79. EET efficiency as a function of interchromophoric distance: Concentrations of the dyes (**60**, **64**, and **69**) were set at 1.0 M, and the excitation was at 500 nm with 5 nm slit widths. The inset shows the boron to boron distance in Å and the corresponding EET efficiency.

Although, that value is the sum of two emission signals, difference in the quantum yield is quite reasonable. As the distance between the two boradiazaindacene units increase, the emission peak at 540 nm become more prominent. By using this quantum yield data, we calculate the efficiency of energy transfer which is shown in Figure 79. Boron to boron distance in dyads **60**, **64**, and **69** is estimated like 11.9, 25.5, and 39.1 Å (Hyperchem version 7.5, PM3 semiempirical module). For compounds **64**, **65**, **69**, and **70**, the absorbance spectra very clearly show two prominent peaks in the visible region, as expected . The emission spectra of these compounds are very informative. The changes in the emission characteristics reflect the changes in the EET efficiency. In compound **60**, there is very weak emission from the shorter wavelength emitting dye, but in compounds **64** and **69**, a progressively larger fraction of excitation

energy appears as emission at 540 nm (Figure 79). This is also in accordance with the decreased emission intensity at the longer wavelengths (670 nm). Energy transfer efficiencies were calculated using quantum yields of emission.

In order to obtain a cation responsive chemosensor, we took advantage of our modular design and switching to a dithiaazacrown-substituted benzaldehyde instead of 4-dimethylaminobenzaldehyde, we obtained compounds **65, 70** and **71**. The specific dithiazacrown we selected, is reportedly selective for Hg(II) ions in a range of solvents. We made titration experiments for each of these compounds to show that by changing the energy transfer efficiency, we can change the dynamic range. Experiments on compound **65** are shown below;

As expected, absorbance spectra of the compound **65** show two prominent peaks in the unbound form; these are 530 and 640 nm respectively. The one at 530 nm corresponds to the donor part and the other one which is at 640 nm corresponds to the acceptor part. Stock solutions are prepared in THF solution, the concentration of the dye kept at 1 μM. Stock solutions of the cations prepared by using the perchlorate salts as their THF solutions, then diluted with THF to obtain desired concentration of the cation. Bodipy dyad is titrated with Hg(II) at increasing concentrations (0, 1.0, 2.0, 3.0, 4.0, 5.0, 10, 15, 20, 25 μM). Binding of the Hg(II) ion to the receptor part causes approximately 70 nm blue shift, due to the ICT type mechanism. And the receptor reaches its saturation point at 20 μM concentration. There is small enhancement in the absorbance of donor part, this is due to the overlap between the donor absorbance and absorbance of the bound chemosensor.

Emission spectra also correlate well with the absorbtion spectra, binding of the Hg(II) causes 80 nm blue shift and the quantum yield of the acceptor part for compound **65** increases from 0.17 to 0.41. In this case, we also expect to see a decrease in the emission signal of the donor part.

Figure 80. Absorbance spectra of compound **65** in the presence of increasing Hg(II) concentrations (0, 1.0, 2.0, 3.0, 4.0, 5.0, 10, 15, 20, 25 μM). The concentration of the chemosensor was 1.0 μM.
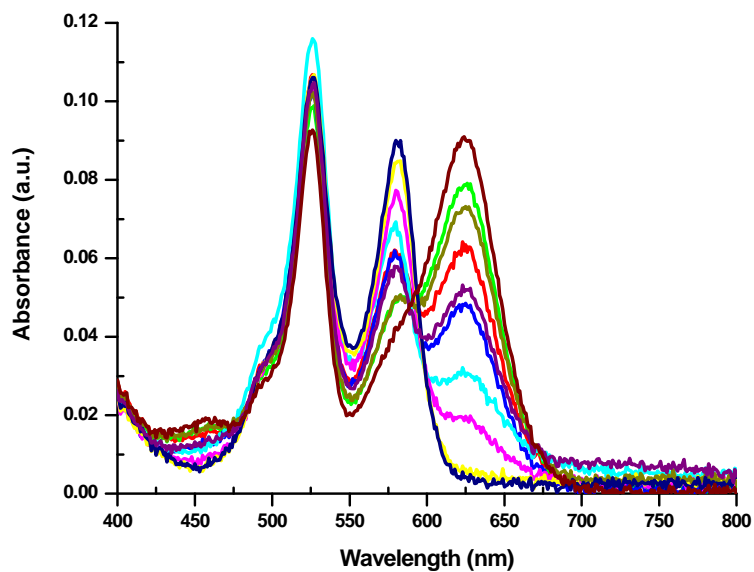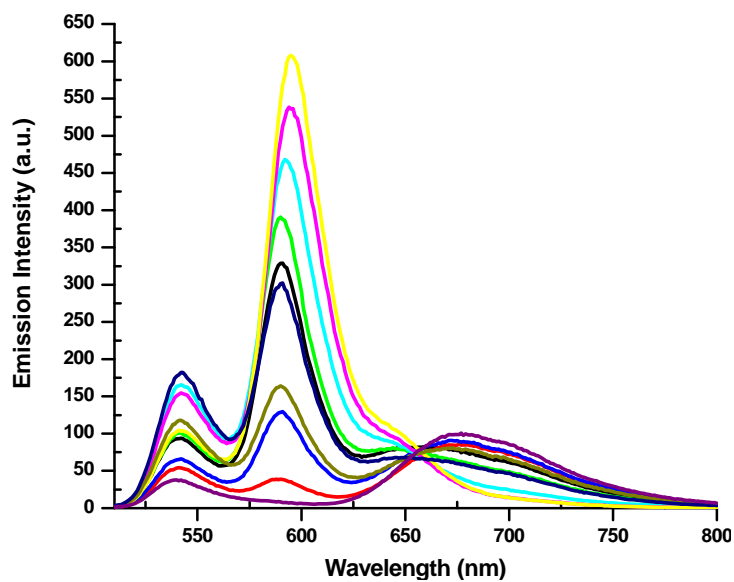

Figure 81. Emission spectra of compound **65** in the presence of increasing Hg(II) concentrations (0, 1.0, 2.0, 3.0, 4.0, 5.0, 10, 15, 20, 25 μM). Excitation wavelength 500 nm with 5 nm slit widths, and spectra were corrected. The concentration of the chemosensor was 1.0 μM.

However, it can be seen in figure 81, donor emission overlaps with the bound form of the chemosensor. This situation causes small increase in the emission signal of the donor part. Selectivity studies also carried out for compound **65**
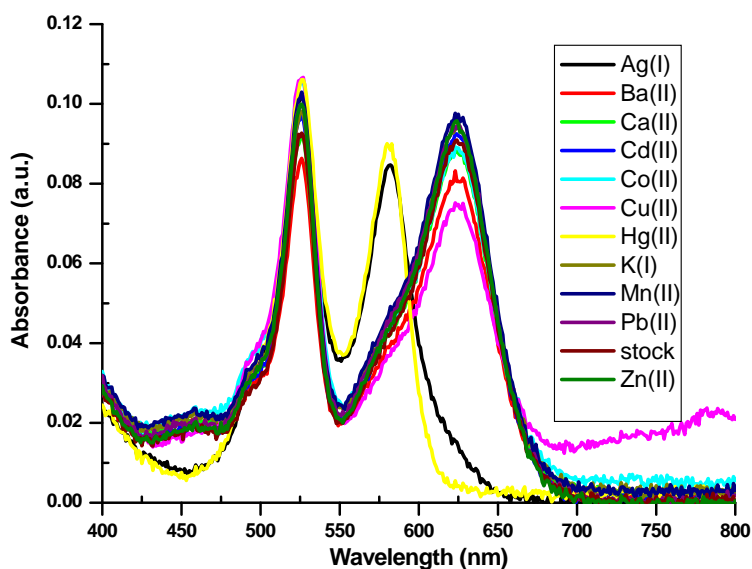

Figure 82. Absorbance spectra of compound **65** in the presence of various cations (cation concentrations 50 µM). The concentration of the chemosensor was 1.0 µM.

Among the cations tested, the compound **65** showed high affinity towards Hg(II) while it shows small affinity towards Copper (II) and the other cations. In this case, Ag(I) ion is exceptional, it shows almost identical affinity with Hg(II). This is due to the hard-soft interaction and the shape of the macrocycle. But absence of Ag(I) ion is quite low where the Hg(II) ion is quite abundant, thus we developed ratiometric chemosensor for Hg(II). Also the emission experiments were carried out for the same solutions. Dye concentration is kept constant at 1.0 µM, and cation concentration in each solution is 50 µM. this value is 2.5 times higher than the saturation concentration of the chemosensor. Interestingly, Ag(I) does not show same effect in the emission spectra. If we were to calculate the ratio between the emission values at 600 and 700 nm, we will definitely see that our

96
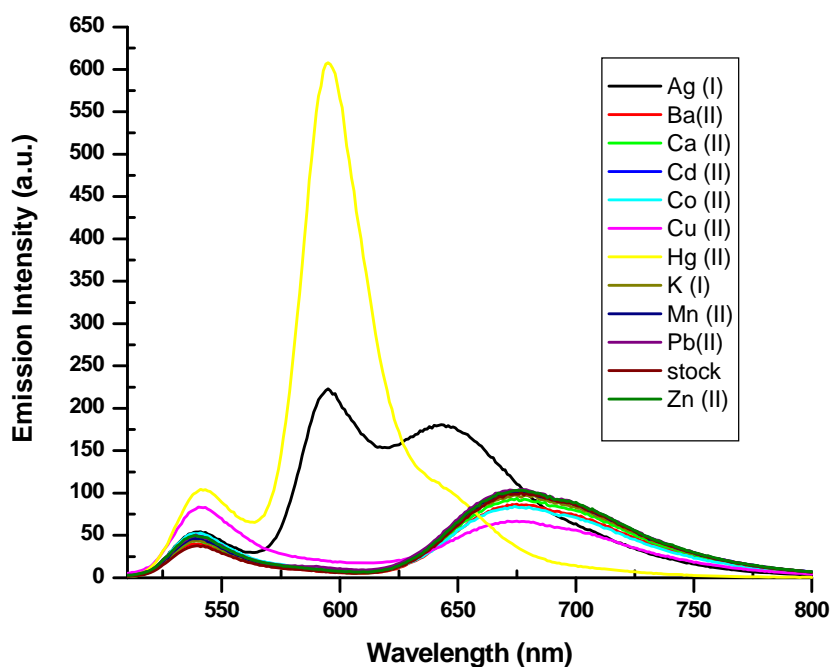
Figure 83. Emission spectra of compound **65** in the presence of various cations (cation concentrations 50 µM). Excitation wavelength 500 nm with 5 nm slit widths, and spectra were corrected. The concentration of the chemosensor was 1.0 µM.
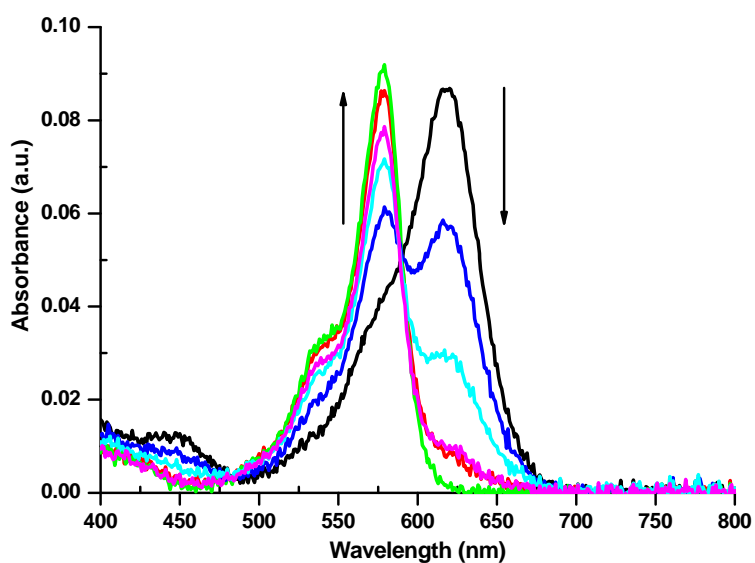

Figure 84. Absorbance spectra of compound **71** (reference compound) in the presence of increasing Hg(II) concentrations (0, 5.0, 10, 15, 20, 25 µM). The concentration of the chemosensor was 1.0 µM.

chemosensor is highly selective towards Hg(II) over other cations tested in THF solution (See Figure 83). We also synthesized reference compound **71**, to show the enhancement which arises from FRET. Dye concentration is kept constant at 1 μM , and again titrated with various concentarions of Hg(II). Reference compound shows almost identical results with acceptor part of the compound **65** and **70**. We could not excite this reference compound at 500 nm, while there is almost absorbtion of the dye. Thus, we excited the chemosensor **71** at the isosbestic point which is at 600 nm. Isosbestic point is the place where absorption peaks of the bound and the unbound form intersects each other. These findings show one of the major advantages of our system, our system has large Stokes` shift. While we can excite our chemosensors at 500 nm and get emission signal from the acceptor part at 680 nm, in the reference compound, chemosensor should be excited at 600 nm to get reasonable emission signal. Also the ration between
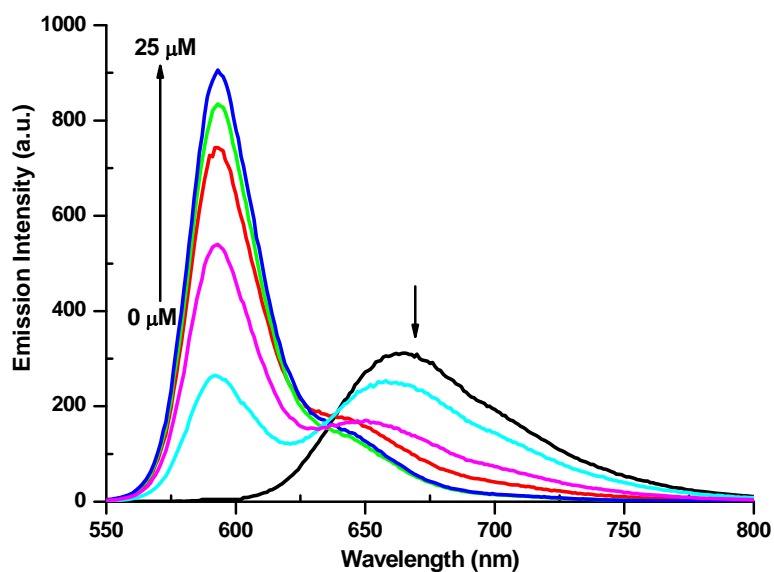

Figure 85. Emission spectra of compound **71** (reference compound) in the presence of increasing Hg(II) concentrations (0, 5.0, 10, 15, 20, 25 μM). Excitation wavelength 500 nm with 5 nm slit widths, and spectra were corrected. The concentration of the chemosensor was 1.0 μM.

emission maximums of the bound and the unbound form of the chemosensor is quite low. This result also decreases the dynamic range of the chemosensor. Absorbtion and emission spectra of **71** at various Hg(II) concentrations are shown in Figure 84 and 85. We have shown the correlation between energy transfer efficiency and distance in Figure 79. We measured B-B distance by using HyperChem v 7.5. According to these calculations at 39.1 Å B-B distance, we observed 85% energy transfer efficiency for Compound **70**. And energy transfer efficiency is calculated simply by the ratio between the quantum yield of the donor in the presence of acceptor and quantum yield of donor part without acceptor. Finally, we choose compound **70** for further characterization. By increasing the distance between donor and the acceptor units, we decrease the energy transfer efficiency. Now, if we increase the spectral overlap by Hg(II) binding, we can increase energy transfer from donor to acceptor, and due to this enhancement, we can also increase the dynamic range. This is the first developed strategy for the controlled enhancement of dynamic range.
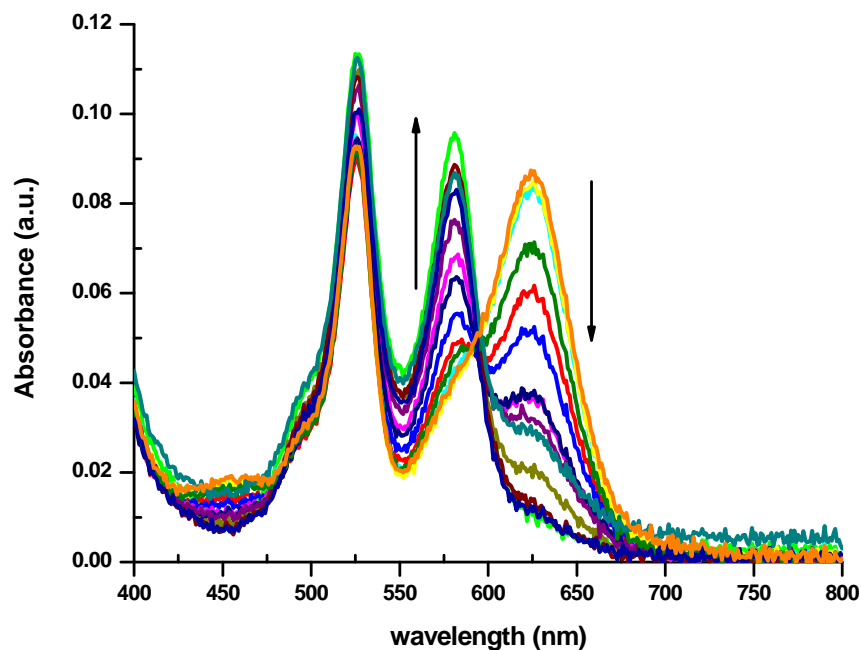

Figure 86. Absorbance spectra of compound **70** in the presence of increasing Hg(II) concentrations (0, 0.5, 0.75, 1.0, 2.0, 3.0, 4.0, 5.0, 7.5, 10, 12.5, 15, 20, 25 μM). The concentration of the chemosensor was 1.0 μM.

Compound **70** showed similar absorbtion and emission characteristics with compound **65**. In Figure 86, we have shown the absortion spectrum of the compound 70, in which binding of Hg(II) causes almost 50 nm hypsochromic shift which is consistent with ICT nature of our acceptor part. In this case, we also prepared 1 μM solution of the dye and later titrated with Hg(II) ion (Hg(II) solution prepared from its perchlorate salt by dissolving in THF). Hg(II) concentrations were 0, 0.5, 0.75, 1.0, 2.0, 3.0, 4.0, 5.0, 7.5, 10, 12.5, 15, 20, 25 μM, respectively. A clear isosbestic point is observed at 590 nm. Isosbestic point is characteristic feature of the ratiometric chemosensors. And ratiometric chemosensors have distinct advantages over other types of sensors.
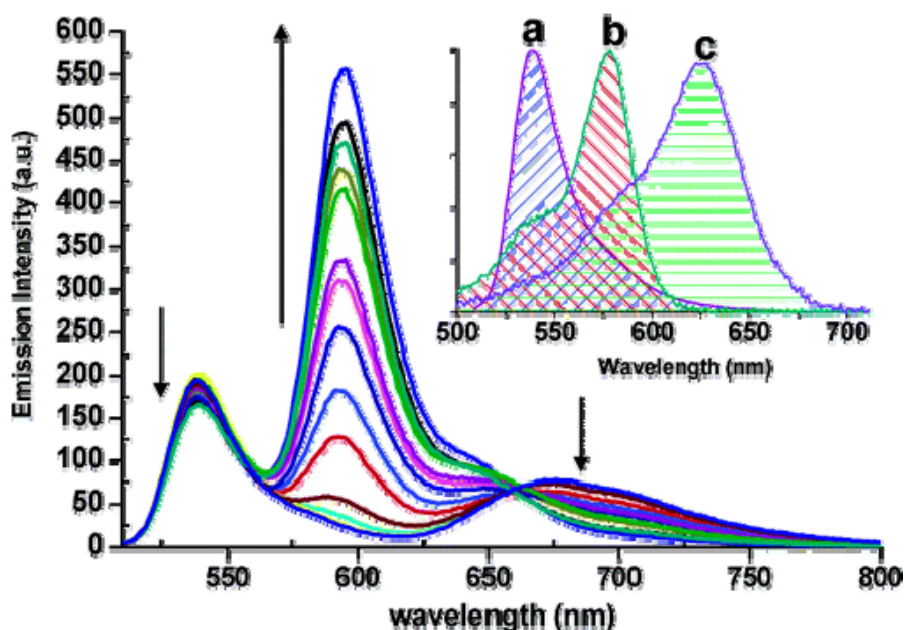
Figure 87. The emission response of the dyad **70** in THF (1.0 μM) to an increasing concentration (0-25 μM) of Hg(II) ions. A small decrease in the intensity at 540 nm is indicative of larger EET. The inset shows the increasing spectral overlap on metal binding: The emission peak (a) of the compound **68** and absorption peak of metal-bound compound (b) and free (c) **71** were normalized while keeping the peak ratios between **71**-Hg and free **71** unchanged. The absporption peaks were moved 7 nm to account for the spectral difference between **71** and **70**.

One of these advantages is that we can signal the absorbance or the emission of the bound form at different wavelength. Emission spectra of the compound **70** are shown in Figure 87. Here, we can see three point ratiometric chemosensor. Although, the change at 540 nm is not so high, there is still reasonable change in that wavelength due to the enhancement in the energy transfer efficiency. It is important to note that emission signal at 540 nm which corresponds to the emission signal from donor part is the sum of donor emission and the emission signal of the bound form. but, there still quite good decrease in the emission signal of the donor part. Binding of Hg(II) ion to the receptor part creates spectacular change in the emission spectra. Acceptor part has broad emission which has maximum around 680 nm, mercuric ion binding causes, approximately, 70 nm hypsochromic shift. Inset of the figure shows an experimental evidence for our proposal which was summarized in Figure 75. In that figure, "a" represents emission of the donor, "b" represents the absorbance of the acceptor in the bound state (Hg(II) binding) and "c" shows the absorbance of the acceptor in the unbound state. In the initial state, there is small overlap between donor emission and the acceptor absorbance, but in the bound state, overlap integral between donor emission and acceptor absorbance increases which is directly proportional with the energy transfer efficiency, this is simply proof of our principle. There are many energy transfer systems which are modulated according to the change in the distance between donor and acceptor units. But modulation of energy transfer by changing the spectral overlap is unique to this study.

Distance modulated systems are much effective than the systems that we have developed, but in addition to the modulation our system also provides an increase in the dynamic range. Thus, increases the sensitivity and provides wide-range analyte detection. Our system is designed to work in organic media such as THF, but, chemosensors should also act in aqueous media for the signaling of the biologically important analytes. In this part, we developed a new idea to increase the dynamic range. This principle can easily be extended to aqueous media after appropriate structural modifications.

Figure 88 shows the Hg(II) selectivity of our chemosensor. Hg(II) causes 35 fold ratio change in the emission signal which is one of the best one among Hg(II) sensors in literature. Among the cations tested, after Hg(II) ion only Ag(I) shows small enhancement in the emission spectrum. Other competitor ions such as Pb(II), Cu(II), Cd(II) don't induce any change both in emission and absorption spectra. So, our system can be used as a Hg(II) selective probe. In this case we kept the dye concentration at 1 µM, and added to this solution from 1 mM metal stock solutions while keeping the cation concentration at 50 µM in the solution. In all cases excitation wavelength was 500 nm, which simply shows the large Stoke`s shift in our system. Ratio is simply calculated from the emission signal.
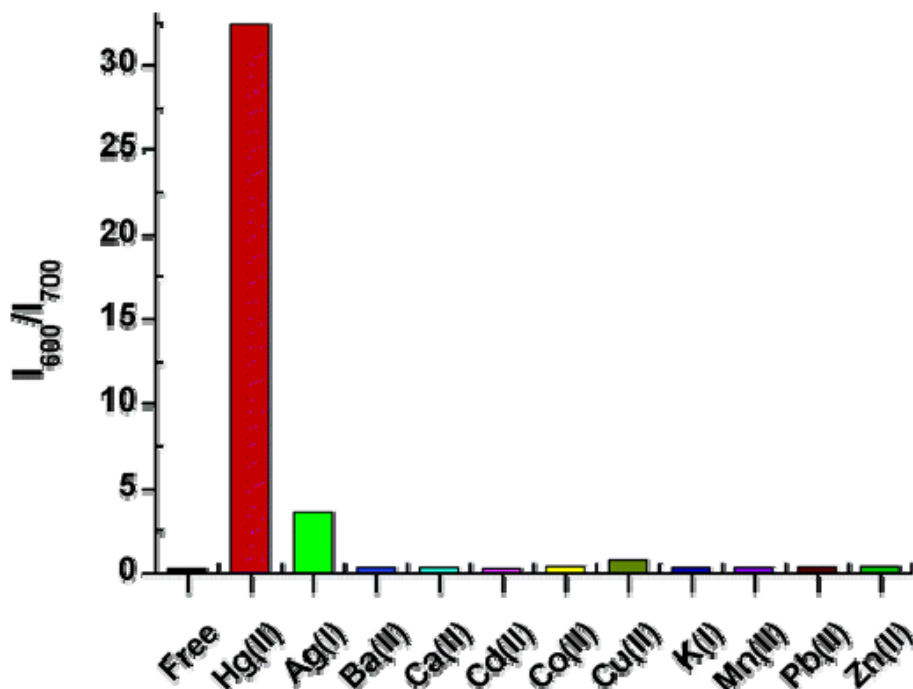

Figure 88. Emission ratios (I_{600}/I_{700}) for the boradiazaindacene dyad **70** (1.0 µM) on excitation at 500 nm. Hg(II) causes the largest spectral shift, and hence results in the most efficient energy transfer for the bound state. All metal ions were at 50 µM concentration. The data were collected in THF and metals were introduced as perchlorates, except for silver (triflate).

The ratio between the emission signal of the bound form which is at 600 nm is divided by the same value at 700 nm which corresponds to the emission signal from the unbound form. this calculation is done for every cation tested. Hg(II) ion causes largest ratio change and as a result of this most efficient energy transfer is observed.

For the detailed absorbtion and emission data, see appendix A, in that part we have shown the absorbance and emission response of chemosensor **70** towards various cations.

We performed Benesi-Hildebrand analysis on the emission data (See Appendix B). We followed the emission data at 595 nm. Binding constant for Hg(II) was determined to be 4.5×10^{-7} M (K_d) in THF. Least square analysis was performed on the emission data which obtained at 595 nm (corresponds to the emission signal of the bound form).
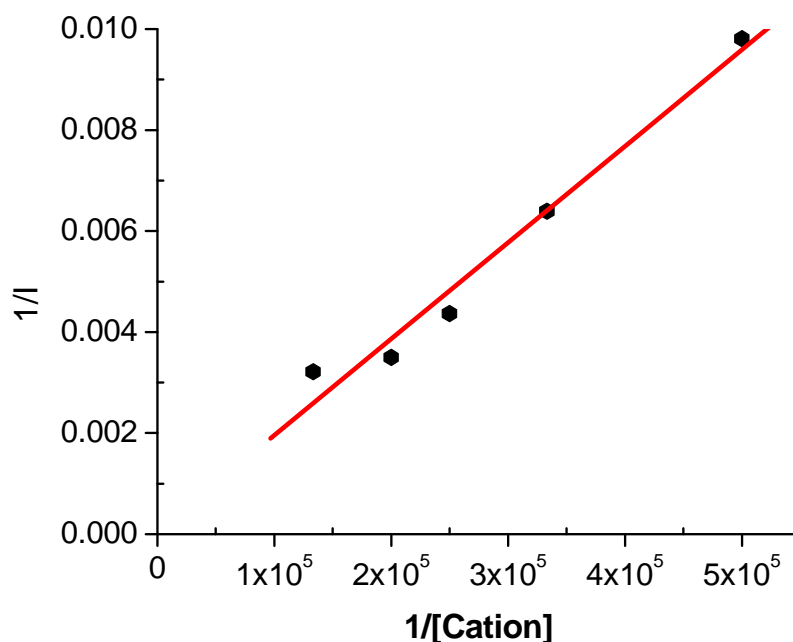

Figure 89. Benesi-Hildebrand analysis of compound **70** at different Hg(II) concentrations with the emission data collected at 595 nm.

Result of the least square analysis follows:

Equation; $Y = AX + B$, $A_0 = 23.8013$ (emission data of the bound form at 595 nm)
$Y = 1.91 \times 10^{-8} X + 5.23 \times 10^{-05}$

$K = 1/(B*Ao) = 2.20 \times 10^{+06}$ (K_a)(binding constant for Hg(II))

$SD = 1/(SD*Ao) = +/- 82.9$

	Value	Error
A	5.23E-05	5.56E-04
B	1.91E-08	1.79E-09

R	SD	N	P
0.98702	5.07E-04	5	0.00177

Now, if we were to calculate the peak emission ratios using the emission intensity values at 600 and 700 nm, for the reference compound **71**, a ratio of 2.8 is obtained.
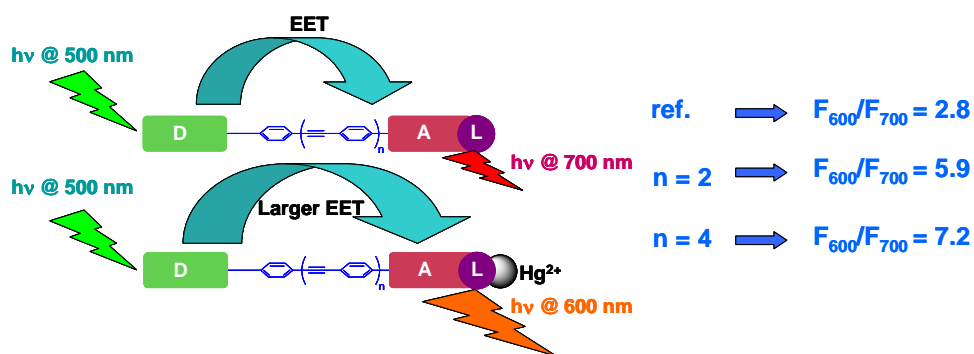

Figure 90. Proposed mechanism for the modulation of the dynamic range.

Modulated EET yields higher values for this ratio, the values are 5.9 for compound **65** and 7.2 for compound **70**. This situation means that the cation modulated excitation energy transfer, through increased spectral overlap, generates a large enhancement of signal ratios, which translates to drastically improved sensitivity to metal ion concentrations. Thus, we satisfactorily demonstrate that in judiciously designed energy transfer dyads, chemosensors of larger intensity ratio changes can be obtained, if the binding of the analyte modulates the energy transfer efficiency. We are confident that in due course this general and modular approach in ratiometric chemosensor design would lead to novel and useful chemosensors for many biologically and environmentally relevant analytes.

3.3 Double Clicking a Two-Station [2]Catenane

Mechanically interlocked molecules, such as bistable catenanes and rotaxanes constitute some of the most intriguing candidates to serve as nanoscale switches and machines in the fields of nanoelectronics and nanoelectromechanical systems (NEMS). The advantages of using mechanically interlocked molecules in the fields of molecular electronics and machines stem from the abilities of their components to undergo controllable relative mechanical motions in response to external stimuli. In a bistable catenane, for example, the competitive binding affinities of one ring with the two recognition sites that are grafted on the other one allows a circumrotary or linear motion of the first ring along the backbone of the latter.

Thus, a large-amplitude molecular mechanical motion can be produced within a mechanically interlocked molecule without impairing its molecular structure. The necessary conditions for generating these highly controllable molecular actuations in a bistable rotaxane is a large difference in the binding affinities of the ring component for two sites on the dumbbell component and their complete reversal in two different states of the molecule. A free energy difference greater than 1.2 kcal mol^{-1} between the two translational isomers of a bistable rotaxane in its ground state ensures that, at room temperature, 90% of the ring resides around one of the two recognition sites in preference to the other. In order to induce motion of the ring component within such skewed bistable rotaxanes, a variety of external stimuli, such as, chemical, electrochemical, and photoelectrochemical inputs have been employed with considerable success. Until recently, the bistable [2]catenanes were synthesized by a template-directed "clipping" of one ring component using the recognition site grafted onto the other ring component as a template for the second ring. The Advent of Cu(I)-catalyzed "click" chemistry has unfurled a much simple-way of making the mechanically interlocked bistable [2]catenanes from preformed [2]pseudorotaxanes, the dumbbell component of which can be cyclized into a second macrocycle. The synthesis of a bistable [2]catenane **79**•2PF$_6$ from its pseudorotaxane precursor **77** (Figure 91), using "click" chemistry, its thermally activated mechanical switching

process which scrambles the original isomer into two co-conformations, as well as its electrochemical response, are all described in this section.
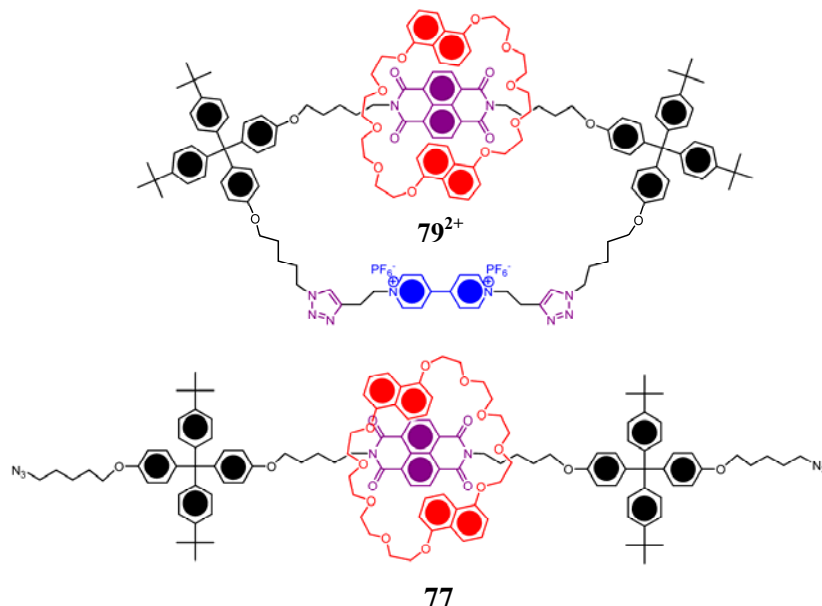

Figure 91. Structural formulas of the two-station [2]catenane **79²⁺** and the corresponding [2]pseudorotaxane **77**.

The bistable [2]catenane **79²⁺** is composed of a π-electron rich bis-1/5dioxynaphthalene[38]-C10 (1/5DNP[38]C10) ring which is interlocked with a second ring containing two π-electron deficient stations — namely, a naphthalene diimde (NpI) unit and a 4-4′-bipyridinium (BIPY²⁺) unit — which are separated by two bulky tetraarylmethane groups, acting as pseudo-stoppers for the 1/5DNP38C10 ring at ambient temperature. The [2]catenane was produced (Figure 92) in 25% yield from its pseudorotaxane **77** precursor by two Cu(I)-catalyzed 2,3-dipolar cycloadditions between the two azide groups on both ends of **77** and two acetylene groups surrounding the BIPY²⁺ unit in **76²⁺**. The monotosylate **73** was synthesized following literature procedures. Synthesis of the NpI derivative **74** was accomplished in 82% yield by carrying out a Mitsunobu reaction between NpI **72** and alcohol **73** in the presence of

diethylazodicarboxylate (DEAD) and PPh$_3$. The resulting ditosylate derivative **74** was then converted quantitatively into the corresponding diazide **77** by treating it with NaN$_3$ at 80˚C for 16 h. The pseudorotaxane **77** was prepared in 15% yield by slipping the 1/5DNP38C10 **78** ring onto the NpI thread **75** over the bulky tetraarylmethane groups on either side of the NpI unit at an elevated temperature.
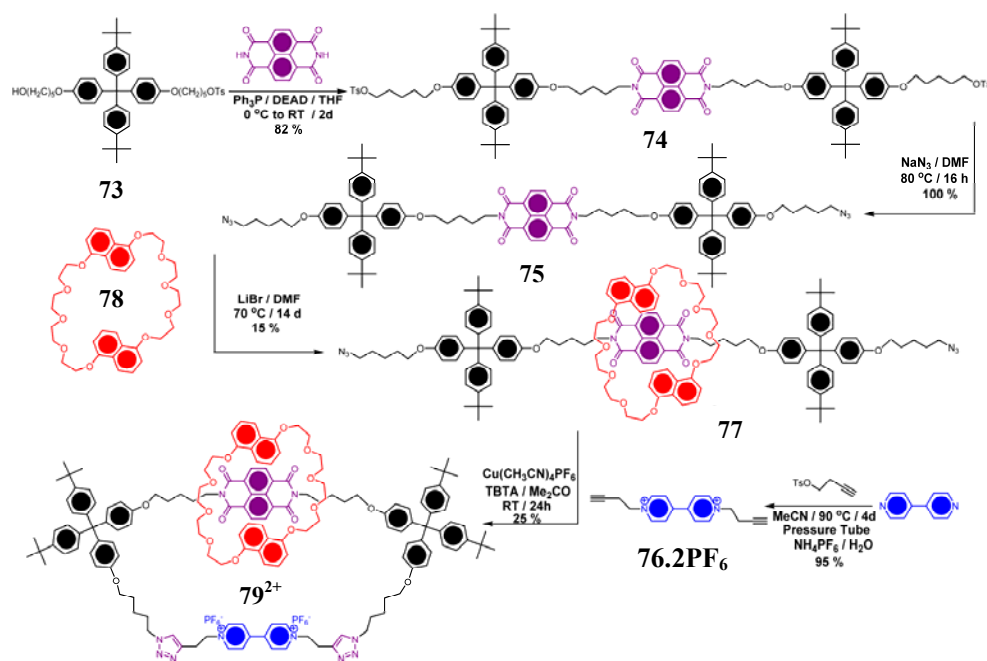

Figure 92. The synthesis of the [2]catenane **79**·2PF$_6$.

The ^{1}H NMR spectral analysis of the dumbbell **75**, pseudorotaxane **77**, and [2]catenane **79**$^{2+}$ shows (Figure 93) encapsulation of the NpI unit by the 1/5DNP38C10 **78** ring in the pseudorotaxane as well as in the catenane, a process which is evident from the up-field shift of 4H signals of the NpI unit from 8.75 ppm in the dumbbell **75** to 8.26 ppm in **77** and 8.22 ppm in **79**$^{2+}$. The fact that there is no difference in the chemical shifts of the four NpI Hs in **77** and **79**$^{2+}$ confirms that the 1/5DNP38C10 still encircles the NpI unit in the catenane **79**$^{2+}$ at the ambient temperature, establishing its structural integrity. Thermal activation of the [2]catenane **79**$^{2+}$ at 70˚C over 60 h. shows (Figure 94) its isomerization to

form the two possible co-conformations — one in which the 1/5DNP38C10 **78** ring still encircles the NpI unit, another in which the crown ether encircles the BIPY^{2+} unit by virtue of its circumrotation over the tetraarylmethane groups. The scrambling of the two co-conformations has been monitored by ^{1}H NMR spectra recorded (Figure 94) at room temperature at certain time intervals during which the catenane **79**$^{2+}$ was warmed at 70˚C.
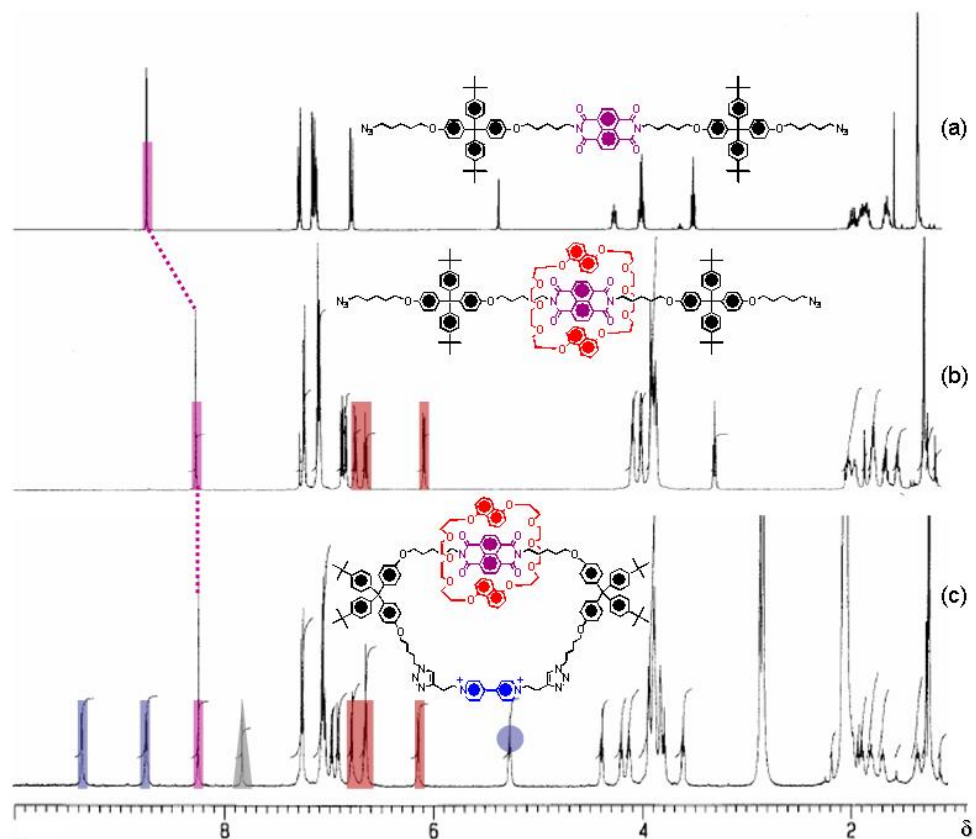

Figure 93. ^{1}H NMR spectra (500 MHz, room temperature) of (a) the NpI diazide **75** in CDCl$_3$, (b) the corresponding [2]pseudorotaxane **77** in CDCl$_3$, and (c) the [2]catenane **79**$^{2+}$ in (CD$_3$)$_2$CO. The chemical shifts of the signature Hs are annotated.

In the [2]catenane 79^{2+}, the chemical shifts of the methylene Hs adjacent to the triazole groups, triazole Hs, NpI H, and β-Hs of the $BIPY^{2+}$ units appear at 4.96, 7.55, 8.17, and 8.20 ppm, respectively. After warming the catenane 79^{2+} the ^{1}H NMR spectra showed emergence of additional downfield peaks at 5.06, 7.82, 8.51, and 8.57 ppm which correspond to chemical shifts of the methylene Hs adjacent to the triazole groups, triazole Hs, NpI H, and β-Hs of the $BIPY^{2+}$ units,
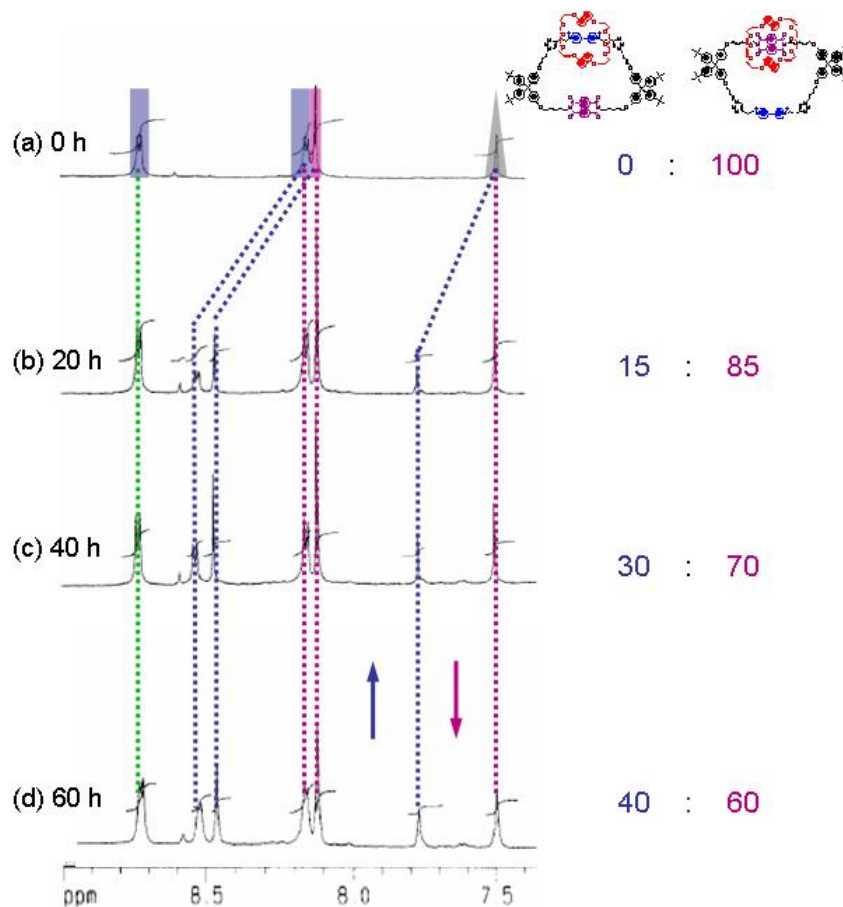
Figure 94. ^{1}H NMR spectra (500 MHz, CD$_3$CN, room temperature) of the [2]catenane 79^{2+} after heating the solution at 70°C for (a) 0 h, (b) 20 h, (c) 40 h, and (d) 60 h. The spectrum (a) recorded before heating the sample shows the presence of only one co-conformation in which 1/5DNP38C10 ring encircles the NpI unit. The thermal activation produces the other co-conformation having the crown ether ring encircling the $BIPY^{2+}$ unit, as observed from the emergence of the corresponding NMR peaks in (b), (c), and (d).

110

respectively. The ratio of the peaks' intensities reached an equilibrium at 60:40 in favor of the NpI isomer after 60 h. The energy barrier for circumrotation is estimated 27±3 kcal/mol and the *ΔG°* between the two co-conformations is only 0.3 kcal/mol. The high energy barrier for 1/5DNP38C10 ring's movement over the tetraarylmethane groups explains the presence of just one isomer at room temperature, Whereas the *ΔG°* between the two co- conformations is virtually zero, rendering both isomers almost equally stable.
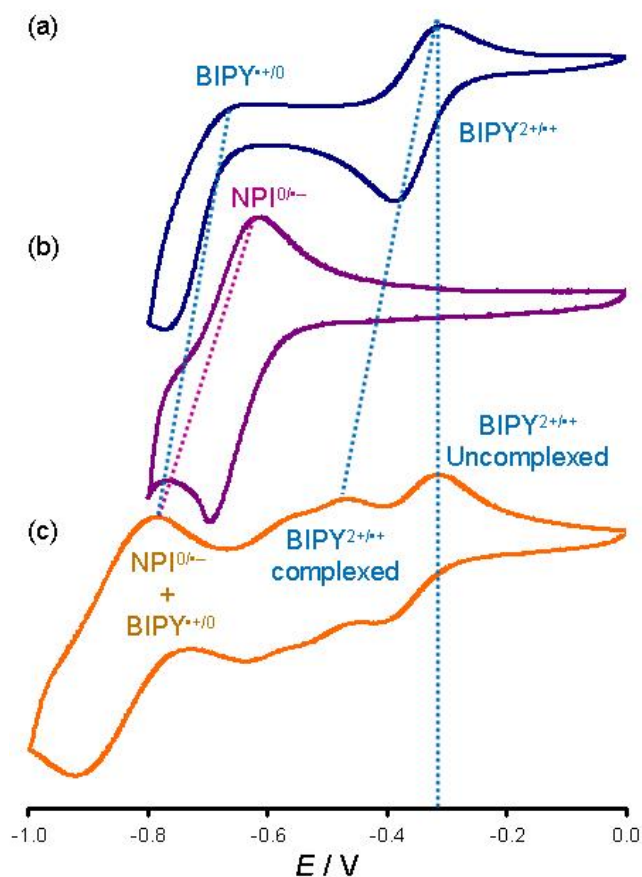
Figure 95. Cyclic voltammograms (0.1 M TBAPF6 / MeCN, vs SCE, 100 mVs– 1) of (a) the BIPY2+ derivative **76^{2+}** (2 mM), (b) the NpI derivative **75** (2 mM), and (c) [2]catenane **79^{2+}** (1 mM) after heating at 70˚C for 60 h. which generated a 60:40 mixture of the two co-conformations.

Cyclic voltammetry (CV) of the catenane 79^{2+} after warming at 70°C for 60 h. as well as of the dumbbell **75** and BIPY^{2+} **76** confirm (Figure 95) the presence of both co-conformations at ca. 60:40 ratio. The CV of the catenane 79^{2+} (Figure 95c) shows that ca. 60% of the BIPY^{2+} unit is reduced to BIPY$^{\bullet+}$ at –0.33 mV — a potential which is the same for the first reduction of a free-BIPY^{2+} unit (Figure 95a) — while the other 40% is being reduced at more negative potentials (–0.47 to –0.55 V), suggesting BIPY^{2+} unit's encapsulation by the π-electron rich 1/5DNP38C10 ring in the latter co-conformation. The second reduction of the BIPY^{2+} unit to BIPY^0 and the reduction of the NpI unit are shifted toward more negative potentials, observations that are commensurate with encapsulation of both units by the 1/5DNP38C10 ring. Neither of the isomers of the catenane 79^{2+}, however, could be switched to the other one by electrochemical inputs because of the presence of the bulky tetraarylmethane groups on both sides of the NpI and BIPY^{2+} units.

In conclusion, we have demonstrated the synthesis of a nondegenerate [2]catenane, using Cu(I)-catalyzed 2,3-dipolar cycloadditions between an acetylene and an azide group. The presence of a sterically bulky group on either side of the π-electron deficient recognition units in one ring impedes the mechanical movement of the mechanically interlocked 1/5DNP[38]C10 ring at room temperature or by electrochemical inputs, even although the free energy difference between the two isomers is negligible. Nonetheless, introduction of a smaller group between the NpI and BIPY^{2+} should allow mechanical switching of the crown ether to produce a true bistable [2]catenane in near future.

CHAPTER 4

CONCLUSION

In the first part of thesis, we have introduced a general strategy for large pseudo-Stokes' shift, ratiometric chemosensors, utilizing efficient energy transfer has been introduced. Yet, the synthesis is highly straightforward on account of the symmetry of the first precursor. In just one step, this symmetrical precursor can be transformed into an efficient RET system, where the choice of the ligand-carrying aldehyde also determines the selectivity of the resulting chemosensor. Considering the multitude of choices in ligand selection and the large number of energy transfer casettes operating in aqueous solutions, one can be confident that this powerful approach can be extended to polar protic solvents, including water, to yield a new class of chemosensors with practical applications in many sensing fields. Research towards these ends is in progress.

In the second part, cation-modulated excitation energy transfer, through increased spectral overlap, generates a large enhancement of signal ratios, which translates into drastically improved sensitivity to metal-ion concentrations. Thus, it has been satisfactorily demonstrated that, in judiciously designed energy transfer dyads, chemosensors of larger intensity ratio changes can be obtained, if the binding of the analyte modulates the energy transfer efficiency. In due course this general and modular approach in ratiometric chemosensor design will lead to novel and useful chemosensors for many biologically and environmentally relevant analytes.

In the final part, the synthesis of a nondegenerate [2]catenane, using Cu(I)-catalyzed 2,3-dipolar cycloadditions between acetylene and azide functions has been described. The presence of a sterically bulky group on either side of the π-electron deficient recognition units in one ring impedes the mechanical movement of the interlocked 1/5DNP38C10 ring at room temperature or by electrochemical inputs, even although the free energy difference between the two isomers is negligible. Nonetheless, introduction of a smaller group between the NpI and BIPY^{2+} should allow mechanical switching of the crown ether to produce a bistable [2]catenane in near future.

REFERENCES

[1] Lehn. J.-M.; Atwood, J.L.; Davies, J.E.D.; MacNicol, D.D.; Vögtle, F. *Comprehensive Supramolecular Chemistry*, Pergamon, Oxford, UK, **1996**.

[2] Lehn. J.-M. *Supramolecular Chemistry*, VCH, Weinheim, Germany, **1995**.

[3] Cram, D.J. *Angew. Chem. Int. Ed.*, **1986**, *25*, 1039-1134.

[4] Steed, J.W.; Turner, D.R.; Wallace, K.J. *Core Concepts in Supramolecular Chemistry and Nanochemistry*, John Wiley&Sons, Ltd., **2007**.

[5] Beer, P.D.; Gale, P.A.; Smith, D.K. *Supramolecular Chemistry*, Oxfrod, New York, **1999**.

[6] Sessler, J.L.; Lawrence, C.M.; Jayawickramarajah, J. *Chem. Soc. Rev.*, **2007**, *36*, 314-325.

[7] Ma, J.C.; Dougherty, D.A. *Chem. Rev.*, **1997**, *97*, 1303-1324.

[8] Hunter, C.A.; Lawson, K.R.; Perkins, J.; Urch, C.J. *J. Chem. Soc., Perkin Trans. 2,* **2001**, 651-669.

[9] Schneider, H.-J. *Encylopedia of Supramolecular Chemistry*, Vol. 2, Steed, J.W.; Atwood, J.L.; Dekker, M. New York, NY, USA, **2004**, 1550-1556.

[10] Southall, N.T.; Dill, K.A.; Haymet, A.D.J. *J. Phys. Chem.*, **2002**, *106*, 521-523.

[11] Fischer, E. Ber. *Deutsch. Chem. Ges.*, **1894**, *27*, 2985.

[12] Beer, P.D.; Chen, Z.; Drew, M.G.B.; Gale, P.A. *J. Chem. Soc., Chem. Commun.*, **1994**, *19*, 2207-8.

[13] Beer, P.D.; Chen, Z.; Grieve, A.; Haggit, *J. Chem. Soc., Chem. Commun.*, **1994**, *20*, 2413-14.

[14] Beer, P.D.; Blackburn, C.; McAleer, J.F.; Sikanyika, H. *Inorg. Chem.,* **1990**, *29(3)*, 378-81.

[15] Black, C.B.; Andrioletti, B.; Try, A.C.; Ruiperez, C.; Sessler, J.L. *J. Am. Chem. Soc.*, **1999**, *121*, 10438-10439.

[16] Shiratori, H.; Ohno, T.; Nozaki, K.; Osuka, A. *Chem. Commun.*, **1999**, *21*, 2181-2182.

[17] DeSilva, A.P.; Gunaratne, H.Q.N.; Gunnlaugsson, T.; Huxley, A.J.M.; McCoy, C.P.; Rademacher, J.T.; Rice, T.E. *Chem. Rev.*, **1997**, *97*, 1515-1566.

[18] Valeur, B.; Leray, I. *Coord. Chem. Rev.*, **2000**, *205*, 3-40.

[19] De silva, A.P.; De silva S.A. *J. Chem Soc. Chem. Commun.* **1986**, 1709.

[20] Akkaya, E.U.; Huston, M.E.; Czarnick, A.W. *J. Am. Chem. Soc.* **1990**, 112, 3590-3593.

[21] DeSilva, A.P.; Gunaratne, H.Q.N.; Gunnlaugsson, T. *Chem. Commun.* **1990**, 1967-1969.

[22] Bourson, J.; Pouget, J.; Valeur, B. *J. Phys. Chem.* **1993**, *97*, 4552.

[23] Huston, M. E.; Akkaya, E. U.; Czarnik, A. W. *J. Am. Chem. Soc.* **1989**, *111*, 8735-8737.

[24] Vance, D. H.; Czarnik, A. W. *J. Am. Chem. Soc.* **1994**, *116*, 9397-9398.

[25] Matsumoto, T.; Urano, Y.; Shoda, T.; Kojima, H.; Nagano, T. *Org. Lett.* **2007**, *9*, 3375-3377.

[26] Coskun A. ; Baytekin, B.; Akkaya, E.U. *Tetrahedron Lett.,* **2003**, *45*, 5649-5651.

[27] Callan, J.F.; de Silva, A.P.; Magri, D.C. *Tetrahedron*, **2005**, 61, 8551-8588.

[28] Bourson, J.; Valeur, B. *J. Phys. Chem.* **1989**, 93, 3871.

[29] Le´tard, J.F.; Lapouyade, R.; Rettig, W. *Pure Appl. Chem.* **1993**, *65*, 1705.

[30] Rurack, K.; Bricks, J.L.; Kachkovski, A.; Resch, U. *J. Fluoresc.* **1997**, *7*, 63.

[31] Mateeva, N.; Enchev, V.; Antonv, L.; Deligeorgiev, T.; Mitewa, M. *J. Incl. Phenom.* **1995**, *93*, 323.

[32] Martin, M.M.; Plaza, P.; Dai Hung, N.; Meyer, Y.H.; Bourson, J.; Valeur, B. *Chem. Phys. Lett.* **1993**, *202*, 425.

[33] Martin, M.M.; Be´gin, L.; Bourson, J.; Valeur, B. *J. Fluoresc.* **1994**, *4*, 271.

[34] Jonker, S.A.; Van Dijk, S.I.; Goubitz, K.; Reiss, C.A.; Schuddeboom, W.; Verhoeven, J.W. *Mol. Cryst. Liq. Cryst.* **1990**, *183*, 273.

[35] Minta, A.; Tsien, R.Y. *J. Biol. Chem.* **1989**, *264*, 19449.

[36] Coskun, A.; Deniz, E.; Akkaya, E.U. *Org. Lett.*, **2005**, *7(23)*, 5187-5189.

[37] Sandanayake, K. R. A. S.; Imazu, S.; James, T. D.; Mikami, M.; Shinkai, S. *Chem. Lett.* **1995**, 139.

[38] Takeuchi, M.; Mizuno, T.; Shinmori, H.; Nakashima, M.; Shinkai, S. *Tetrahedron* **1996**, *52*, 1195.

[39] Wan, CW.; Burghart, A.; Chen, J.; Bergstrom, F.; Johansson, L.B.; Wolford, M.F.; Kim, T.G.; Topp, M.R.; Hochstrasser, R.M.; Burgess, K. *Chem. Eur. J.* **2003**, *9*, 4430-4441.

[40] Bandichhor, R.; Petrescu, A.D.; Vespa, A.; Kier, A.B.; Schroeder, F.; Burgess, K. *J. Am. Chem. Soc.* **2006**, *128*, 10688-10689.

[41] Wagner, R. W.; Johnson, T. E.; Lindsey, J. S. *J. Am. Chem. Soc.* **1996**, *118*, 11166.

[42] Sapsford, K.E.; Berti, L.; Medintz, I.L. *Angew. Chem. Int. Ed.*, **2006**, *45*, 4562-4588.

[43] Azov, V.A.; Schlegel, A.; Diederich, F. *Angew. Chem. Int. Ed.* **2005**, *44*, 4635-4638.

[44] Albers, A.E.; Okreglak, V.S.; Chang, C.J. *J. Am. Chem. Soc.,* **2006**, *128*, 9640-9641.

[45] Onagi, H.; Rebek, J. Jr. *Chem. Commun.* **2005**, 4604-4606.

[46] Yamada, K.; Nomura, Y.; Citterio, D.; Iwasawa, N.; Suzuki, K. *J. Am. Chem. Soc.,* **2005**, *127*, 6956-57.

[47] Yoon, S.; Albers, A.E.; Wong, A.P.; Chang, C.J. *J. Am. Chem. Soc.*, **2005**, *127*, 16030-16031.

[48] Nolan, E.M.; Lippard, S.J. *J. Am. Chem. Soc.*, **2003**, *125*, 14270-14271.

[49] Coskun, A.; Yilmaz, M.D.; Akkaya, E.U. *Org. Lett.*, **2007**, *9*, 607-609.

[50] Chen, C.T.; Huang, W.P. *J. Am. Chem. Soc.*, **2002**, *124*, 6246-6247.

[51] Peng, X.; Du, J.; Fan, J.; Wang, J.; Wu, Y.; Zhao, J.; Sun, S.; Xu, T. *J. Am. Chem. Soc.*, **2007**, *129*, 1500-1501.

[52] Coskun, A.; Akkaya, E.U. *J. Am. Chem. Soc.*, **2005**, *127*, 10464-10465.

[53] Rurack, K.; Kollmannsberger, M.; Daub, J. *Angew Chem. Int. Ed.*, **2001**, *40*, 385-387.

[54] Yang, R.H.; Chan, W.H.; Lee, A.W.M.; Xia, P.F.; Zhang, H.K.; Li, K. *J. Am. Chem. Soc.*, **2003**, *125*, 2884-2885.

[55] Woodroofe, C.C.; Lippard, S.J. *J. Am. Chem. Soc.*, **2003**, *125*, 11458-11459.

[56] Ajayaghosh, A.; Carol, P.; Sreejith, S. *J. Am. Chem. Soc.*, **2005**, *127*, 14962-14963.

[57] Taki, M.; Wolford, J.L.; O`Halloran, T.V. *J. Am. Chem. Soc.*, **2004**, *126*, 712-713.

[58] Maruyama, S.; Kikuchi, K.; Hirano, T.; Urano, Y.; Nagano, T. *J. Am. Chem. Soc.*, **2002**, *124*, 10650-10651.

[59] J.-M. Lehn, J.-M.; Sonveaux, E.; Willard, A.K. *J. Am. Chem. Soc.*, **1978**, *100*, 4914.

[60] Metzger, A.; Lynch, V.M., Anslyn, E.V. *Angew. Chem. Int. Ed. Engl.* **1997**, *36*, 862.

[61] Mizukami, S.; Nagano, T.; Urano, Y,; Odani, A.; Kikuchi, K. *J.Am. Chem. Soc.* **2002**, *124*, 3920.

[62] Anzenbacher, P., Jr.; Jursıkova , K.; Sessler, J. L. *J. Am. Chem. Soc.* **2000**, *122*, 9350.

[63] Ward, C. J.; Patel, P.; James, T. D. *Chem. Lett.,* **2001**, 406.

[64] Black, C. B.; Andrioletti, B.; Try, A. C.; Ruiperez, C.; Sessler, J.L. *J. Am. Chem. Soc.* **1999**, *121*, 10438.

[65] Lee, D. H.; Im, J. H.; Son, S. U.; Chung, Y. K.; Hong, J.-I. *J.Am. Chem. Soc.* **2003**, *125*, 7752.

[66] Lee, H.N.; Xu, Z.; Kim, S.K.; Swamy, K.M.K.; Kim, Y.; Kim, S.-J.; Yoon, J. *J. Am. Chem. Soc.* **2007**, *129*, 3828-3829.

[67] Treibs, A.; Kreuzer, F.-H. *Justus Liebigs Ann. Chem.*, **1968**, *718*, 208.

[68] Haugland, R.P. *in Handbook of Molecular Probes and Research Products*, Molecular Probes, Inc., 9th edn, **2002**.

[69] Atilgan, S.; Ekmekci, Z.; Dogan, A.L.; Guc, D.; Akkaya, E.U. *Chem. Commun.*, **2006**, 4398-4400.

[70] Yogo, T.; Urano, Y.; Ishitsuka, Y.; Maniwa, F.; Nagano, T. J. *Am. Chem. Soc.*, **2005**, *127*, 12162-12163.

[71] Harriman, A.; Izzet, G.; Ziessel, R. *J. Am. Chem. Soc.,* **2006**, *128*, 10868-10875.

[72] Turfan, B.; Akkaya, E.U. *Org. Lett.*, **2002**, *4*, 2857-2859.

[73] Yilmaz, M.D.; Bozdemir, O.A.; Akkaya, E.U. *Org. Lett.*, **2006**, *8*, 2871.

[74] Camerel, F.; Bonardi, L.; Schmutz, M.; Ziessel, R. *J. Am. Chem. Soc.*, **2006**, *128*, 4548-4549.

[75] Camerel, F.; Ulrich, G.;Barbera, J.; Ziessel, R. *Chem. Eur. J.*, **2007**, *13*, 2189-2200.

[76] Hattori, S.; Ohkubo, K.; Urano, Y.; Sunahara, H.; Nagano, T.; Wada, Y.; Tkchanko, N.V.; Lemmetyinen, H.; Fukuzimi, S. *J. Phys. Chem. B*, **2005**, *109*, 15368-15375.

[77] (a) Pentecost, C.D.; Tangshaivang, N.; Cantrill, S.J.; Chichak, K.S.; Peters, A.J.; Stoddart, J.F. *J. Chem. Ed.*, **2007**, *84*, 855-859. (b) Cantrill, S.J.; Chichak, K.S.; Peters, A.J.; Stoddart, J.F. *Chem. Commun.*, **2005**, 3394-3396. (c) Chichak, K.S.; Cantrill, S.J.; Pease, A.R.; Chiu, S.–H.; Cave, G.W.V.; Atwood, J.L.; Stoddart, J.F. *Science*, **2004**, *304*, 1308-1312.

[78] Anelli, P. L.; Ashton, P.R.; Ballardini, R.; Balzani, V.; Delgado, M.; Gandolfi, M.T.; Goodnow, T.T.; Kaifer, A.E.; Philp, D.; Pietraszkiewicz, M.; Prodi, L.; Reddington, M.V.; Slawin, A.M.Z.; Spencer, N.; Stoddart, J.F.; Vicent, C.; Williams, D. *J. Am. Chem. Soc.,* **1992***, 114,*193-218*.*

[79] (a) Collier, C.P.; Mattersteig, G.; Wong, E.W.; Luo, Y.; Beverly, K.; Sampaio, J.; Raymo, F.M.; Stoddart, J.F.; Heath, J.R. *Science*, **2000**, *289*, 1172-1175. (b) Amabilino, D.B.; Stoddart, J.F. *Chem. Rev.,* **1995**, *95*, 2725-2828.

[80] (a) Fujita, M.; Aoyagi, M.; Ibukuro, F.; Ogura, K.; Yamaguchi, K. *J. Am. Chem. Soc.*, **1998**, *120*, 611-612. (b) Cesario, M.; Dietrich-Buchecker, C.O.; Guilhem, J.; Pascard, C.; Sauvage, J.-P. *J. Chem. Soc., Chem. Commun*., **1985**, 244-245.

[81] Sambrook, M.R.; Beer, P.D.; Wisner, J.A.; Paul, R.L.; Cowley, A.R. *J. Am. Chem. Soc.*, **2004**, *126*, 15364-15365.

[82] Clegg, W.; Gimenez-Saiz, C.; Leigh, D.A.; Murphy, A.; Slawin, A.M.Z.; Teat, S.J. *J. Am. Che. Soc.*, **1999**, *121*, 4124-4129.

[83] Amabilino, D.B.; Ashton, P.R.; Reder, A.S.; Spencer, N.; Stoddart, J.F. *Angew. Chem. Int. Ed.*, **1994**, *33*, 1286-1290.

[84] (a) Chong, L.; Culotta, E.; Sudgen, A. *Science*, **2000**, *288*, 5643-. (b) Ismagilov, R.F.; Schwartz, A.; Bowden, N.; Whitesides, G.M. *Angew. Chem. Int. Ed.*, **2002**, *41*, 652-.

[85] Frey, E. *Chem. Phys. Chem.*, **2002**, *3*, 270-.

[86] (a) Gilbert, A.; Baggot, J. *Essentials of Molecular Photochemistry*, Blackwell, Oxford, **1991**. (b) Balzani, V.; Scandola, F. *Supramolecular Photochemistry*, Horwood, Chichester, **1991**.

[87] (a) Kaifer, A.E.; Gómez-Kaifer, M. *Supramolecular Electrochemistry*, Wiley-VCH, Weinheim, **1999**. (b) Cordova, E.; Bissell, R.A.; Spencer, N.; Ashton, P.R.; Stoddart, J.F.; Kaifer, A.E. *J. Org. Chem.*, **1993**, *58*, 6550-. (c) Armaroli, N.; Balzani, V.; Collin, J.-P.; Gavina, P.; Sauvage, J.-P; Ventura, B. *J. Am. Chem. Soc.*, **1999**, *121*, 4397.

[88] Collin, J.-P.; Dietrich-Bucheker, C.O.; Gavina, P.; Jimenez-Molero, M.C.; Sauvage, J.-P. *Acc. Chem. Res.*, **2001**, *34*, 477.

[89] (a) Huang, T. J.; Brough, B .; Ho, C.-M.; Liu, Y.; Flood, A. H.; Bonvallet, P. A.; Tseng, H.-R.; Stoddart, J . F.; Baller, M.; Magonov, S . *Appl. Phys. Lett.* **2004**, *85*, 5391–5393. b) Liu, Y.; Flood, A. H.; Bonvallet, P. A.; Vignon, S . A.; Northrop, B . H.; Tseng, H.-R.; Jeppesen, J. O.; Huang, T. J.; Brough, B.; Baller, M.; Magonov, S.; Solares, S. D.; Goddard, W. A.; Ho, C.-M.; Stoddart, J. F. *J. Am. Chem. Soc*. **2005**, *127*,9745–9759.

[90] Berna, J.; Leigh, D.A.; Lubomska, M.; Mendoza, S.M.; Perez, E.M.; Rudolf, P.; Teobaldi, G.; Zerbetto, F. *Nat. Mater.,* **2005**, *4*, 704-710.

[91] Jimenez-Molero, M.C.; Dietrich-Bucheker, C.O.; Sauvage, J.-P. *Angew. Chem. Int. Ed.*, **2000**, *39*, 3284-3287.

[92] a) Ahuja, R. C.; Caruso, P.-L.; Mubius, D .; Wildburg, G .; Ringsdorf, H.; Philp, D.; Preece, J. A., Stoddart, J. F. *Langmuir*, **1993**, *9*, 1534–1544. b) Ahuja, R.C.; Caruso, P.-L.; Möbius, D.; Philp, D.; Preece, J.A.; Ringsdorf, H.; Stoddart, J.F.; Wildburg, G. *Thin Solid Films*, **1996**, *285*, 671–677 c) Brown, C.L.; Jonas, U.; Preece, J. A.; Ringsdorf, H.; Seitz, M.; Stoddart, J. F. *Langmuir*, **2000**, *16*, 1924–1930 d) Asakawa, M.; Higuchi, M.; Mattersteig, G.; Nakamura, T.; Pease, A. R.; Raymo, F. M.; Shimizu, T.; Stoddart, J. F. *Adv. Mater.*, **2000**, *12*, 1099–1102.

[93] Collier, C. P.; Mattersteig, G .; Wong, E. W.; Luo, Y.; Beverly, K.; Sampaio, J.; Raymo, F. M.; Stoddart, J . F.; Heath, J. R. *Science*, **2000**, *289*, 1172–1175.

[94] Luo, Y.; Collier, C. P.; Jeppesen, J. O.; Nielsen, K. A.; Delonno, E.; Ho, G.; Perkins, J.; Tseng, H.-R.; Yamamoto, T.; Stoddart, J. F.; Heath, J. R. *ChemPhysChem*, **2002**, *3*, 519–525.

[95] Green, J.E.; Choil, J.W.; Boukai1, A.; Bunimovich, Y.; Johnston-Halperin, E.; DeIonno, E.; Luo, Y.; Sheriff, B.A.; Xu, K.; Shin, Y.S.; Tseng, H.-R.; Stoddart, J.F. and Heath, J.R. *Nature*, **2007**, *445*, 414-417.

[96] Ulrich, G.; Ziessel, R. *J. Org. Chem.* **2004**, 69, 2070-2083.

[97] Niu, C.R.; Jiang, H.; Wu, C. T. *Chinese Chem. Lett.* **1998**, 9, 17-20.

[98] Hsung, R. P.; Babcock, J. R.; Chidsey, C. E. D.; Sita, L. R. *Organometallics* , **1995**, *14*, 4808.

[99] Du, H.; Fuh, R. A.; Li, J.; Corkan, A.; Lindsey, J. S. *Photochem. Photobiol.* **1998**, *68*, 141-142.

[100] Coskun, A.; Akkaya, E.U. *J. Am. Chem. Soc.*, **2006**, *128*, 14474-14475.
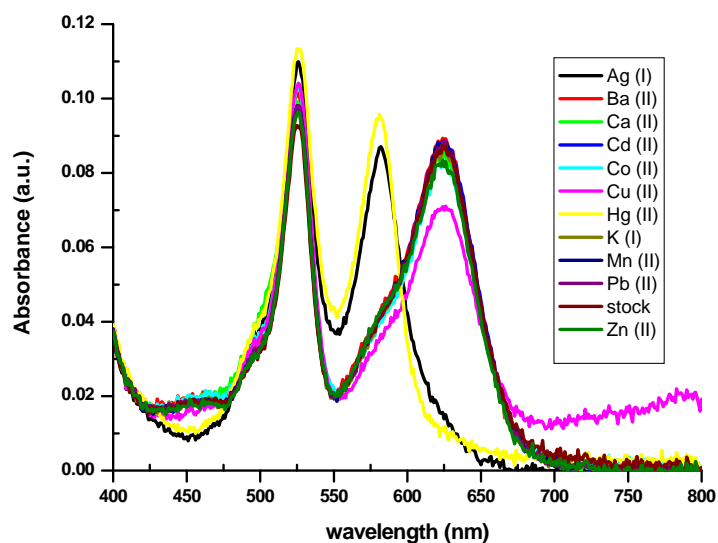
Figure 96. Absorbance spectra of compound **70** in the presence of various cations (cation concentrations 50 μM). The concentration of the chemosensor was 1.0 μM.
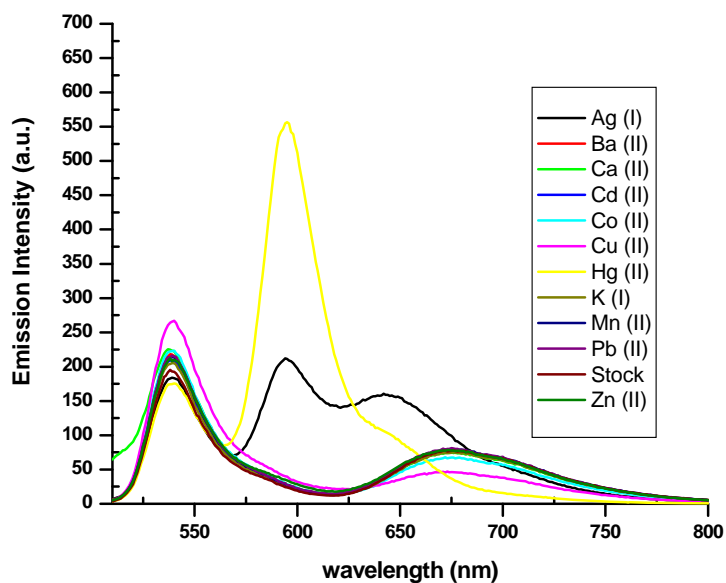
Figure 97. Emission spectra of compound **70** in the presence of various cations (cation concentrations 50 μM). Excitation wavelength 500 nm with 5 nm slit widths, and spectra were corrected. The concentration of the chemosensor was 1.0 μM.

APPENDIX B

Benesi-Hildebrand Analysis;
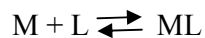
$$M + L \rightleftharpoons ML$$

$$K_a = \frac{[ML]}{[M][L]} \quad (B.1)$$

Let Y_o be the absorbance or the fluorescence intensity of the free ligand. In the fluorometric experiments, the absorbance at the excitation wavelength should be less than ca. 0.1. Then, at a given wavelength, Y_o is proportional to the concentration c_L :

$$Y_o = a \times c_L \quad (B.2)$$

And in the presence of an excess of cation such that the ligand is fully complexed, Y reaches the limiting value Y_{lim};

$$Y_{lim} = b \times c_L \quad (B.3)$$

In spectrophotometry, a and b are the products of the absorbtion pathlength by the molar absorbtion coefficients of the ligand and the complex, respectively. In spectrofluorometry, a and b are proportional to the molar absorbtion coefficients (at the excitation wavelength) and the fluorescence quantum yields of the ligand and the complex, respectively.

After addition of a given amount of cation at a concentration c_M, the absorbance or the fluorescence intensity becomes

$$Y = a[L] + b[ML] \quad (B.4)$$

Mass balance equations for the ligand and cation are

$$cL = [L] + [ML] \quad (B.5)$$

$$cM = [M] + [ML] \quad (B.6)$$

From equations B.1 and B.6, it is easy to derive the usual relation

$$\frac{Y - Y_o}{Y_{lim} - Y} = K_a[M] \quad (B.7)$$

This relationship can be used to determine K_s under the condition that the concentration in free cation [M] can be approximated to the total concentration c_M: $(Y-Y_o) / (Y_{lim}-Y)$ is plotted as a function of c_M, and the plot should be linear and slope yields K_s.

When Y_{lim} is not measurable because full complexation cannot be attained at a reasonable concentration of cation, it is better to use the following relation:

$$\frac{Y_0}{Y-Y_0} = \frac{a}{K_s[M]} + \alpha \qquad \text{(B.8)}$$

Where $\alpha = a / (b-a)$. It is convenient to plot $Y_o / (Y - Y_o)$ versus $1 / c_M$ provided that the approximation $[M] \approx c_M$ is valid. The ratio of the ordinate at the origin to the slope yields K_s. Such a plot is called a double-reciprocal plot or a *Benesi-Hildebrand* plot.

Quantum Yield Calculations;

Quantum yield calculations were carried out by using following formula;

$$\frac{\Phi_{sample}}{\Phi_{reference}} = \frac{area^{sample}}{area^{reference}} \times \frac{n^2_{sample}}{n^2_{reference}} \times \frac{1 - 10^{-abs(reference)}}{1 - 10^{-abs(sample)}}$$

Φ= Quantum yield

Area= area under the curve

n= refractive index of the solvent
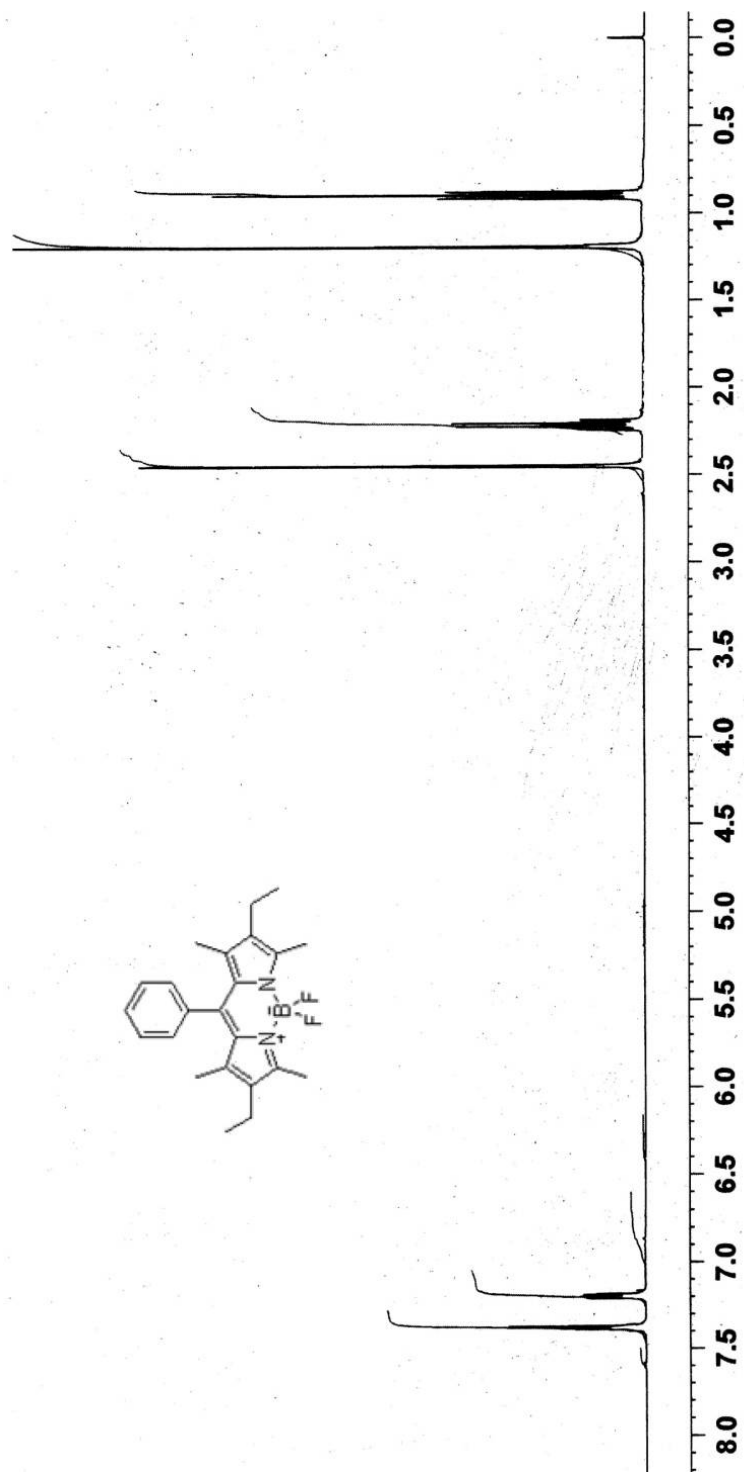
Figure 98. ^{1}H-NMR spectrum (400 MHz, CDCl$_3$, 298 K) of compound **57**
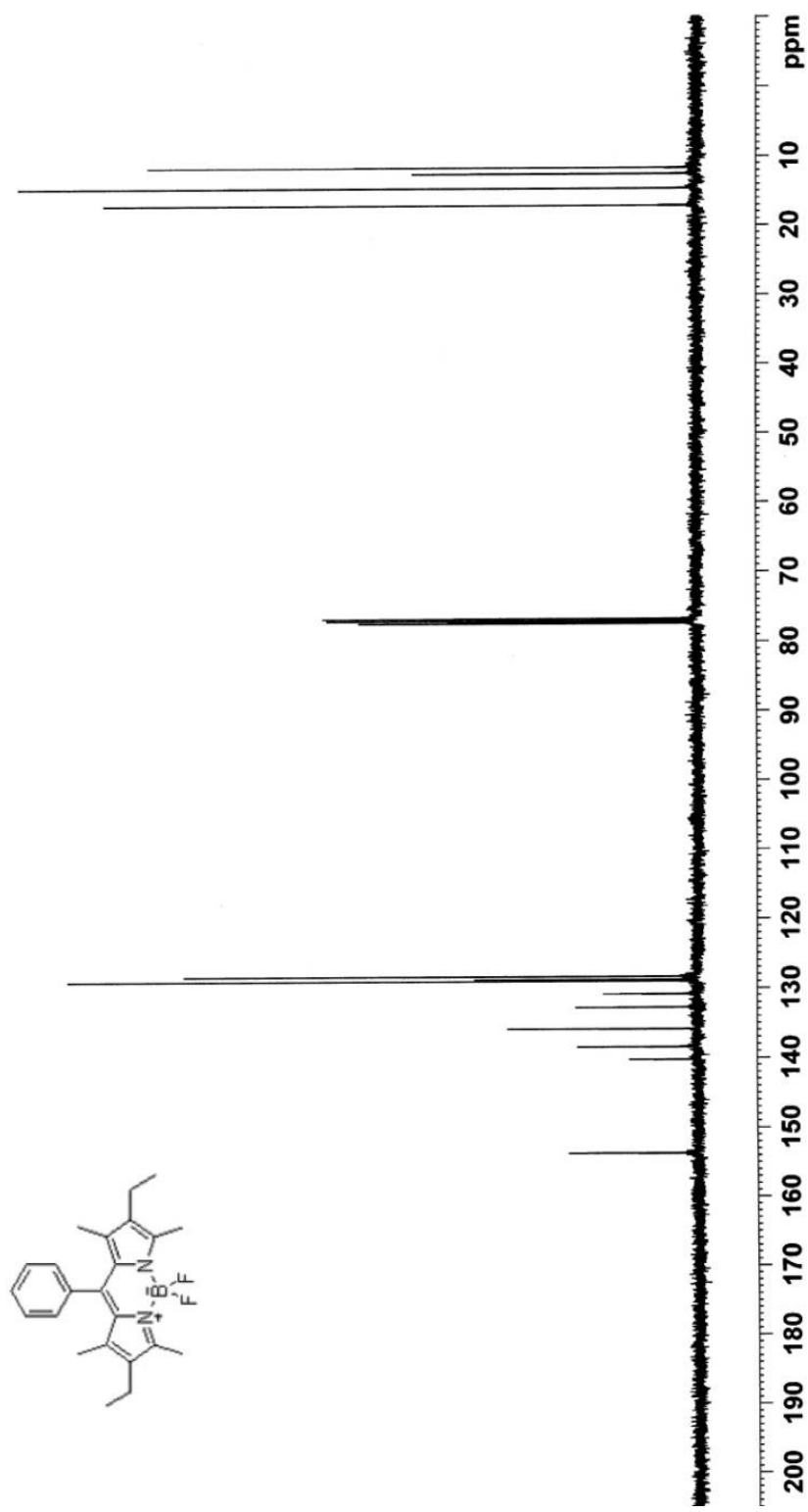
Figure 99. ^{13}C-NMR spectrum (400 MHz, CDCl$_3$, 298 K) of compound **57**
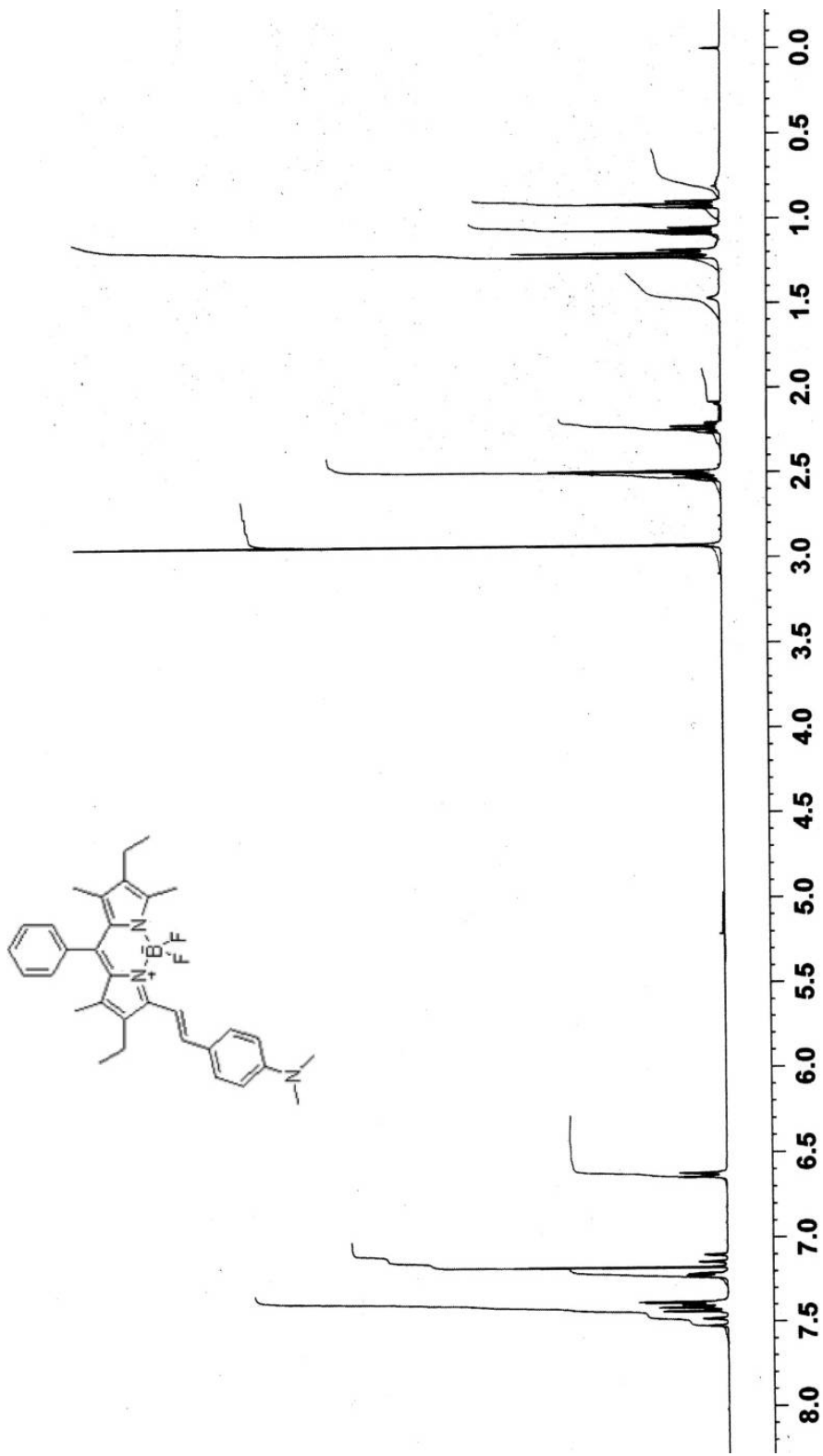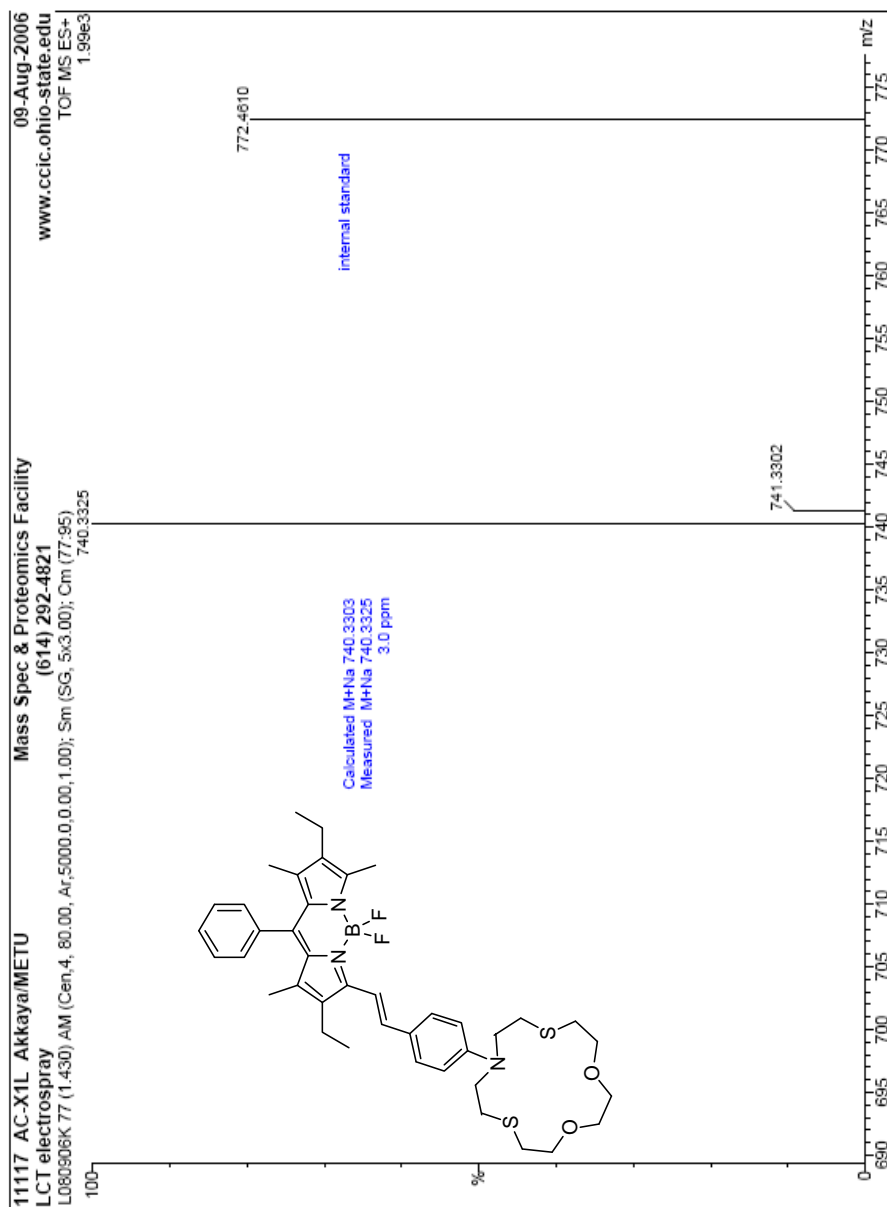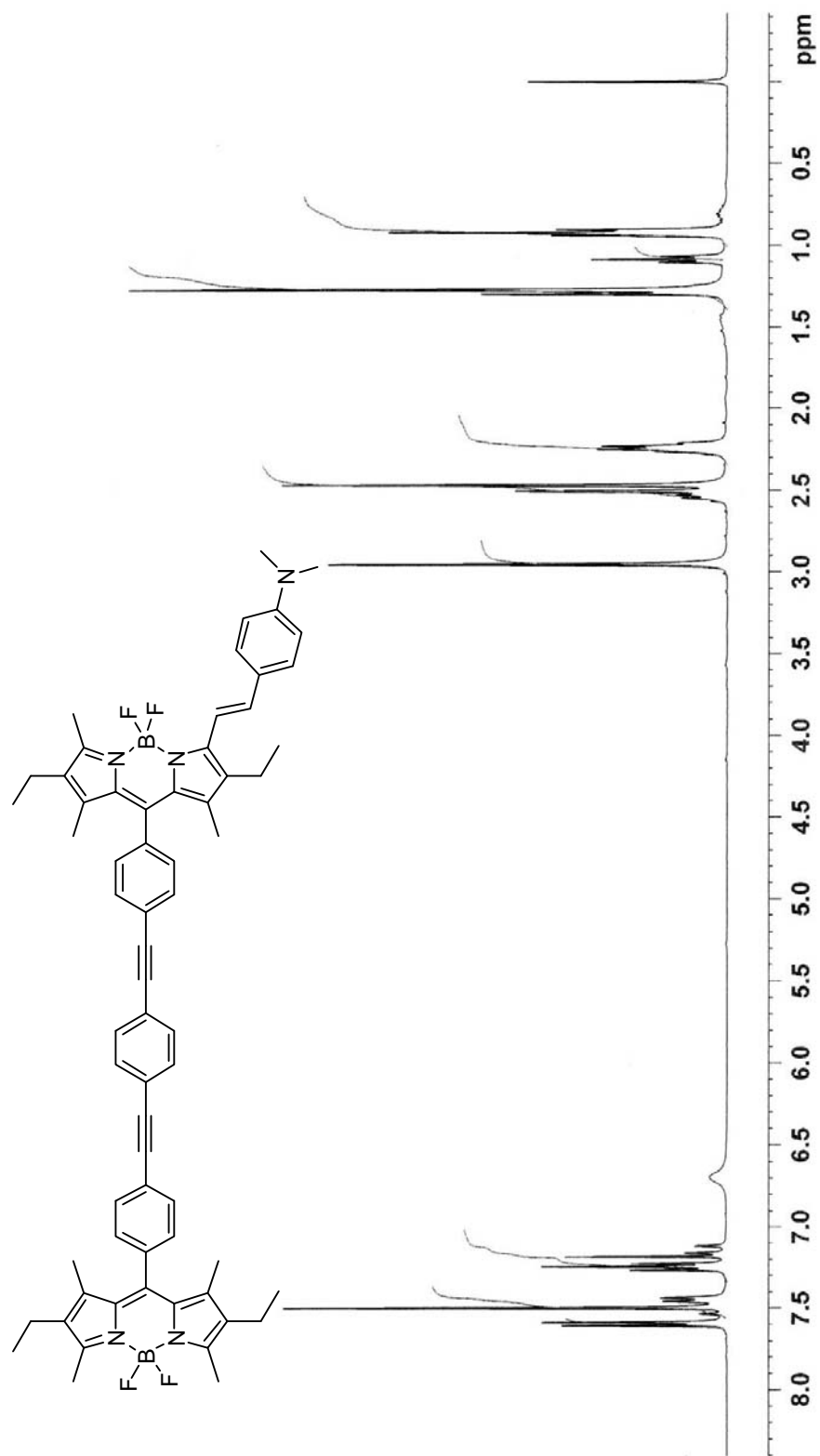
Figure 100. ^{1}H-NMR spectrum (400 MHz, CDCl$_3$, 298 K) of compound **58**
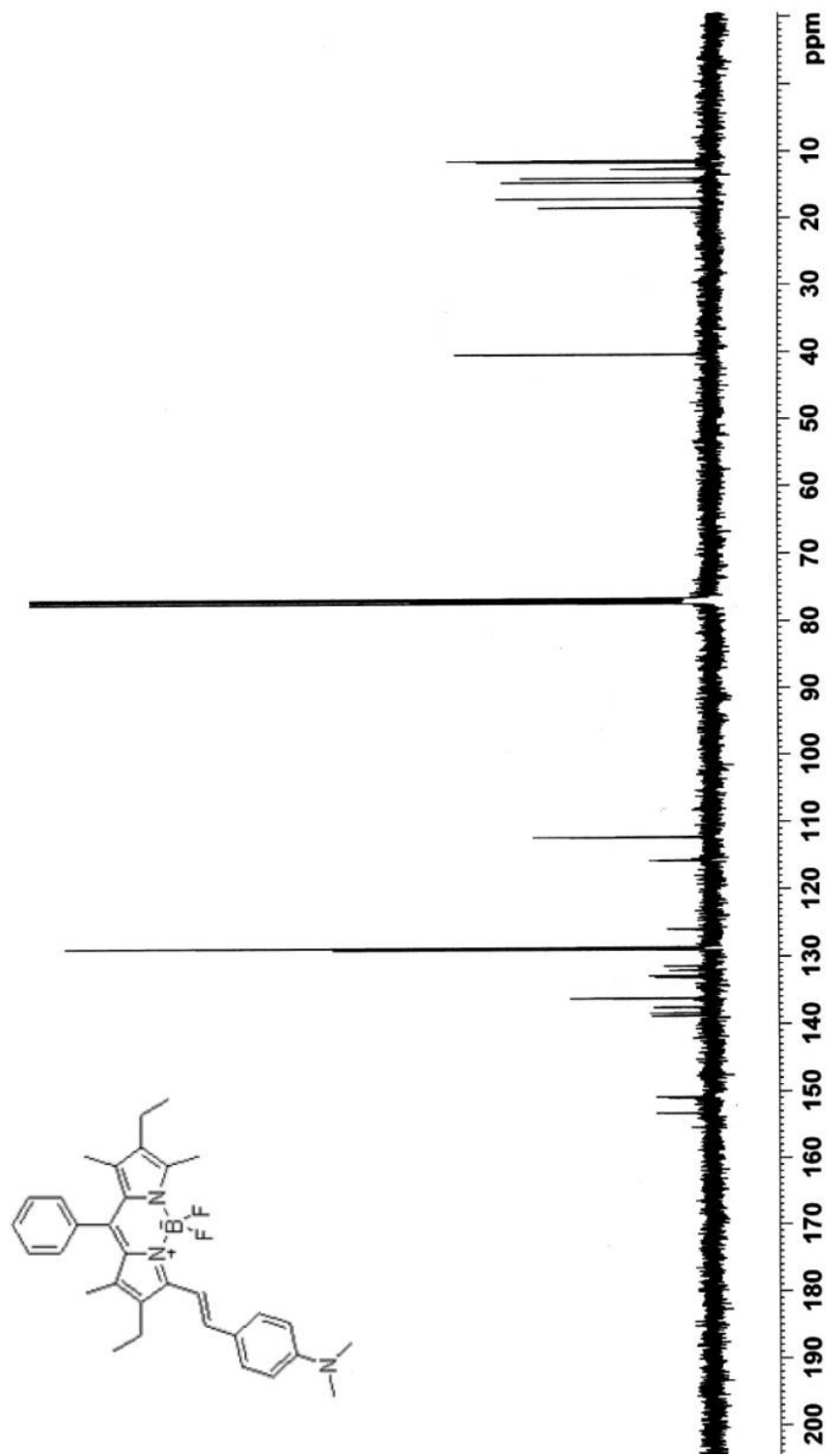
Figure 101. ^{13}C-NMR spectrum (400 MHz, CDCl$_3$, 298 K) of compound **58**
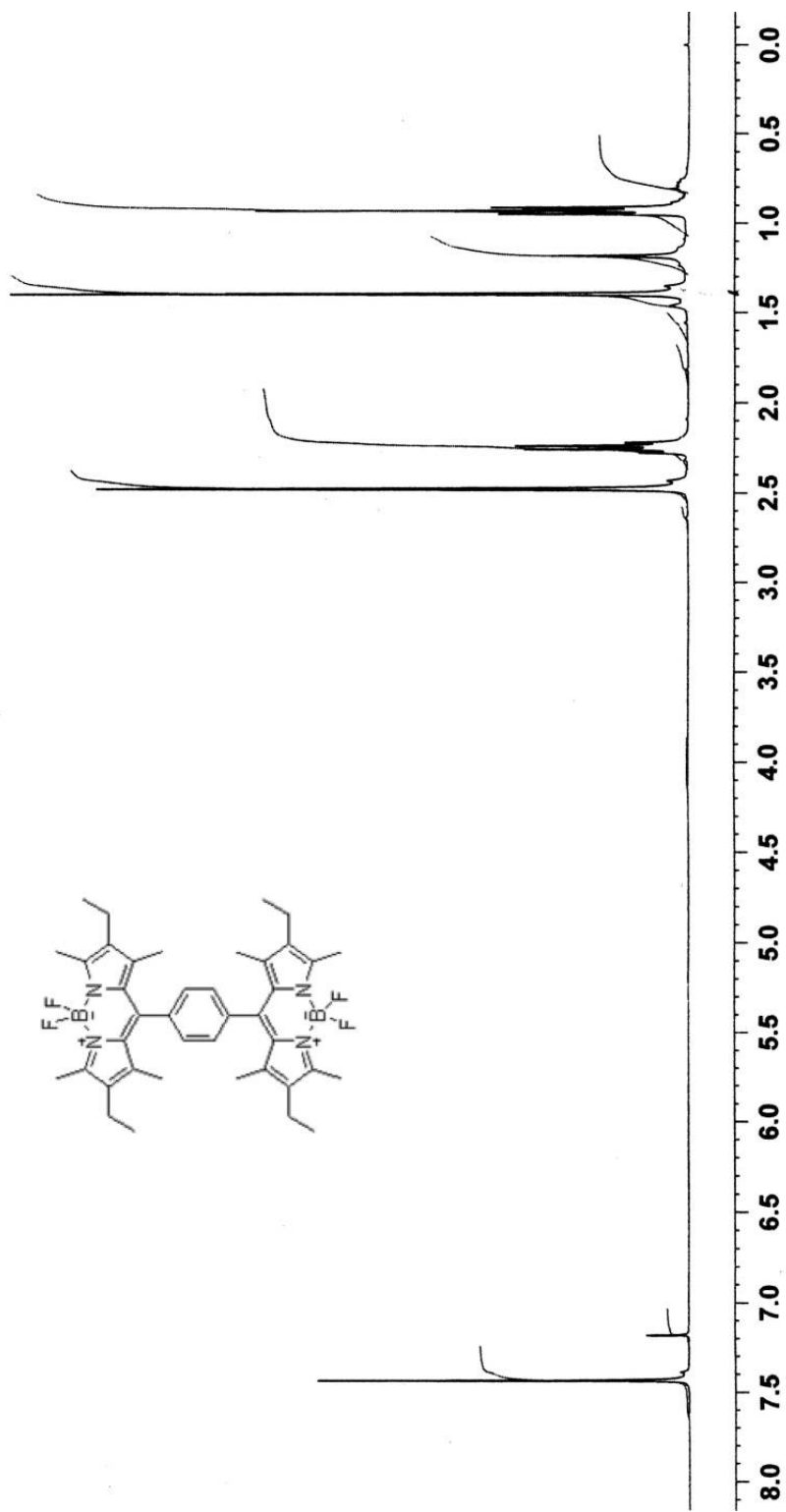
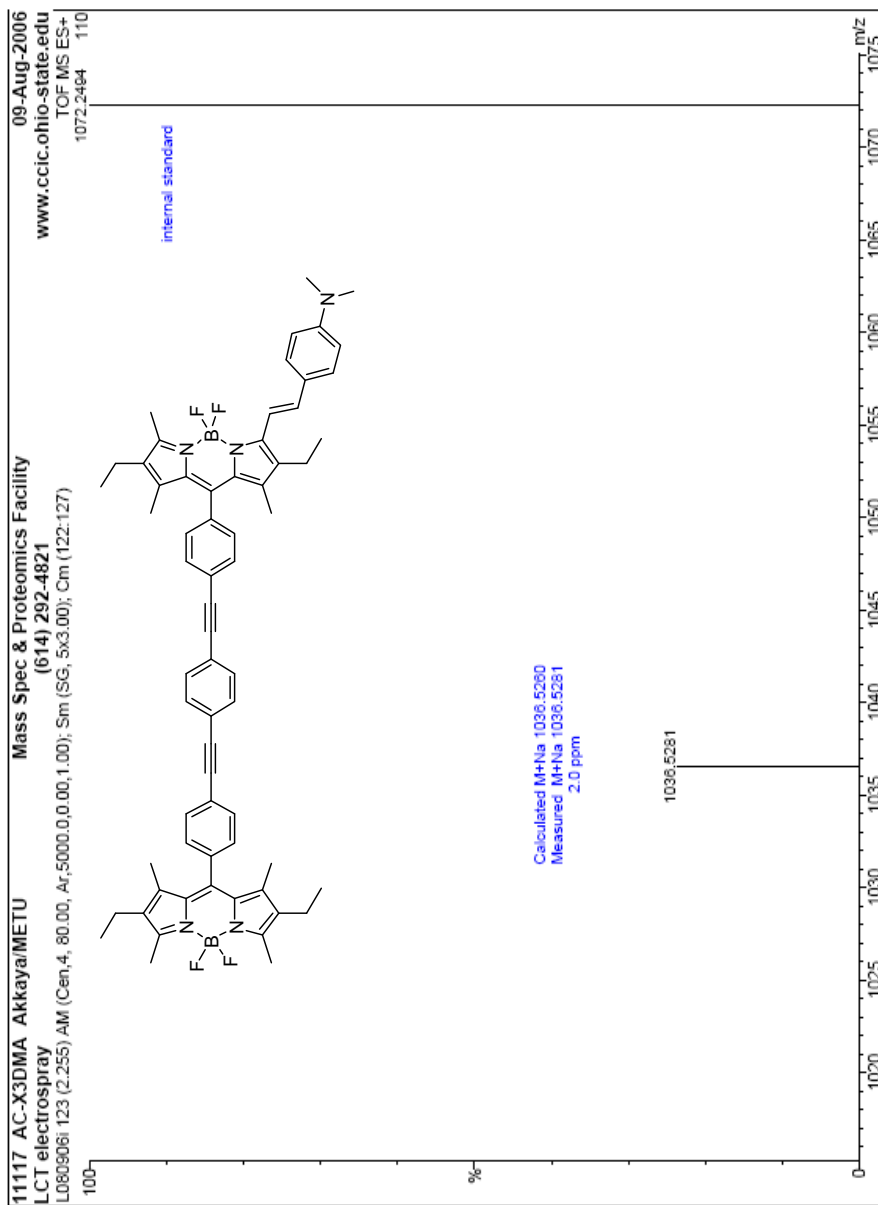Figure 102. ^{1}H-NMR spectrum (400 MHz, CDCl$_3$, 298 K) of compound **59**

129
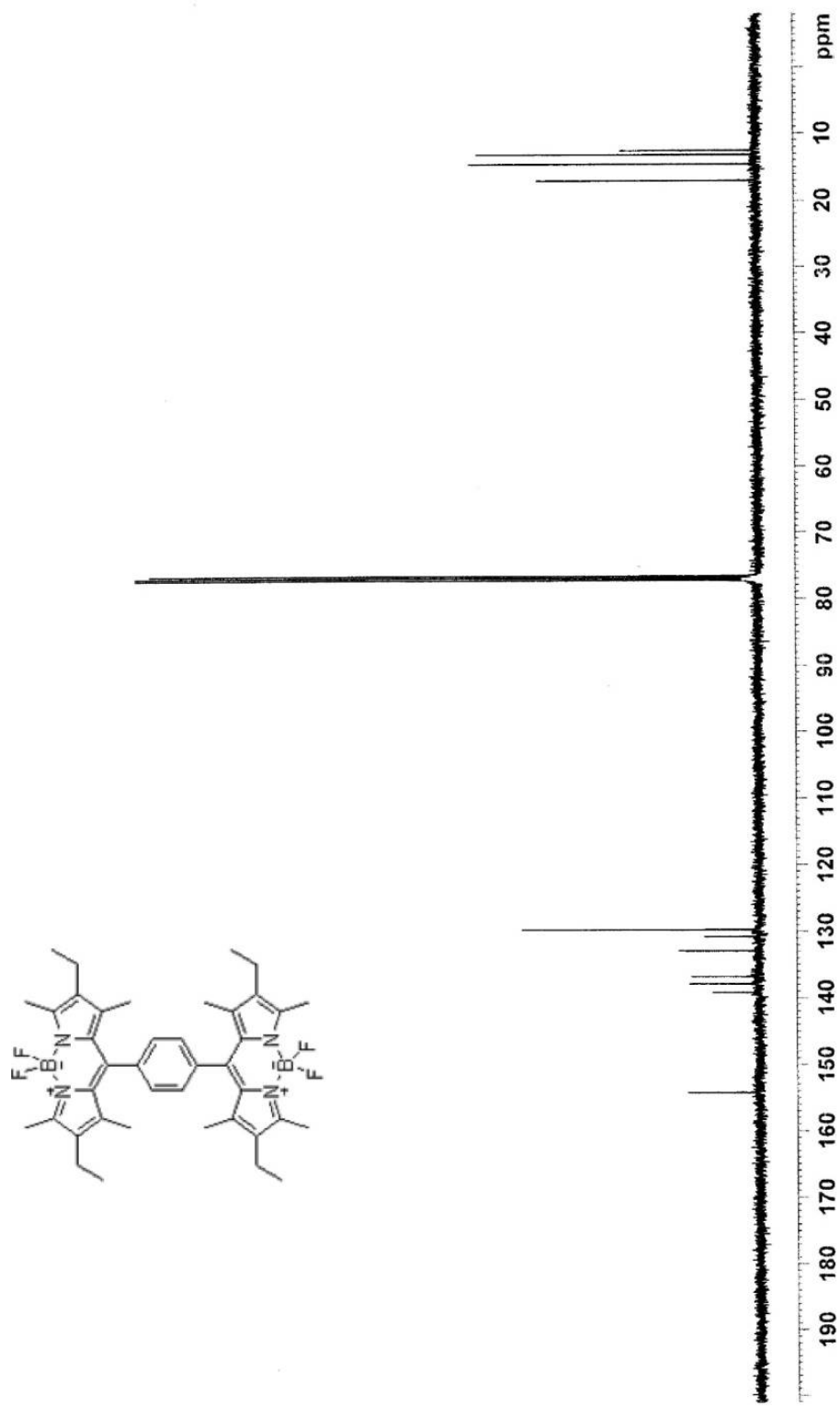
Figure 103. ^{13}C-NMR spectrum (400 MHz, CDCl$_3$, 298 K) of compound **59**
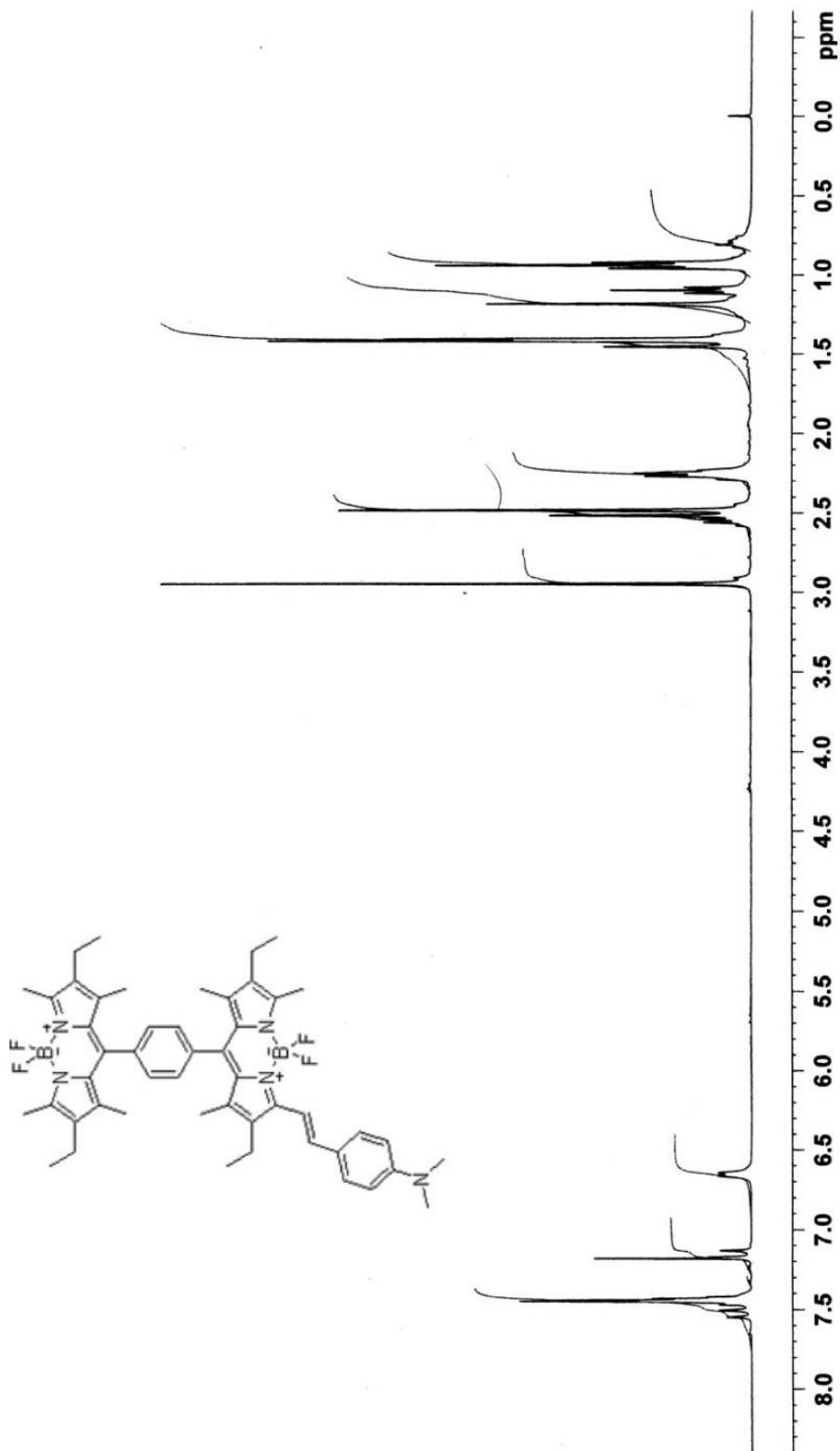
Figure 104. ^{1}H-NMR spectrum (400 MHz, CDCl$_3$, 298 K) of compound **60**

131
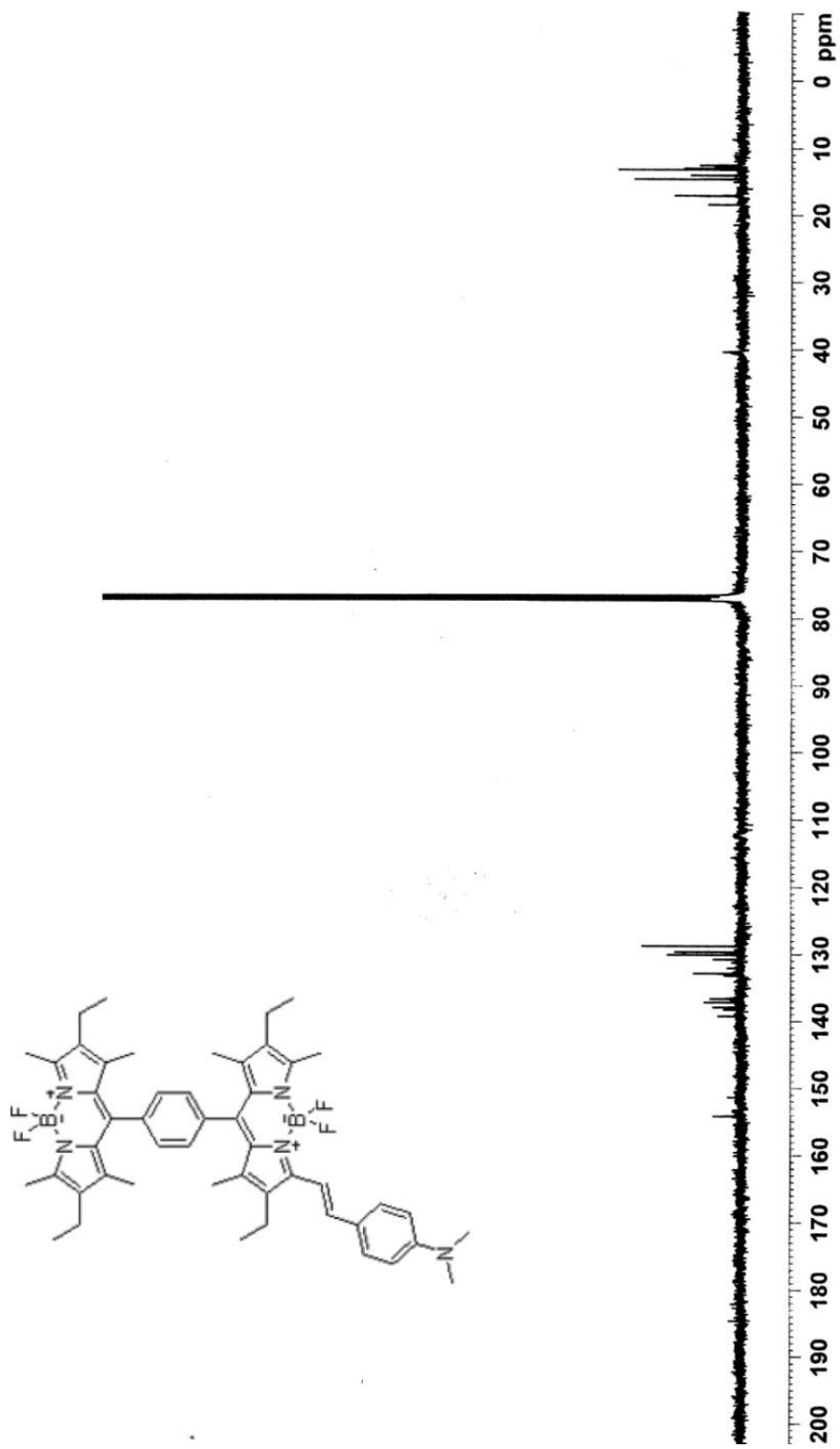
Figure 105. ^{13}C-NMR spectrum (400 MHz, CDCl$_3$, 298 K) of compound **60**

132
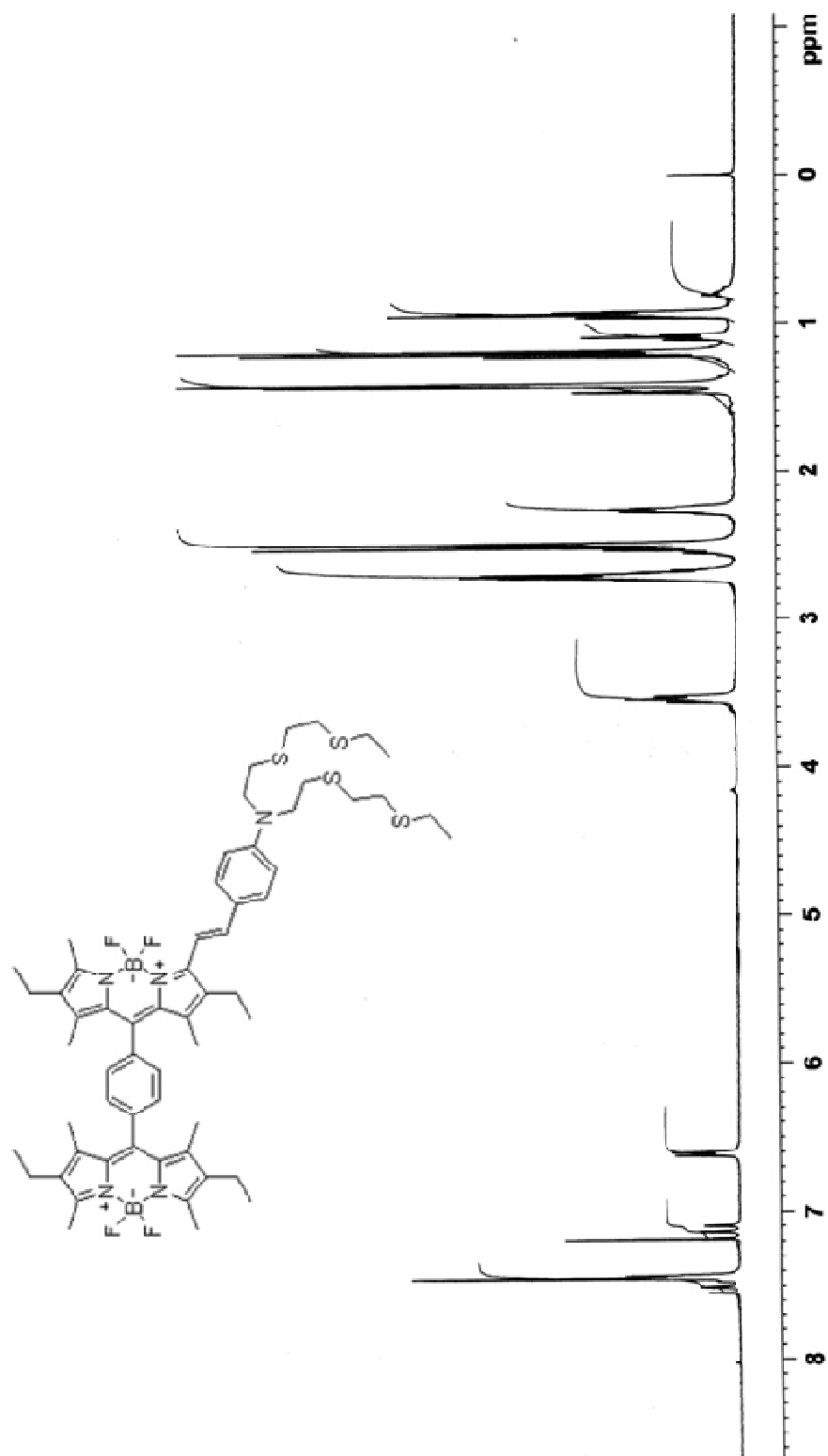
Figure 106. ^{1}H-NMR spectrum (400 MHz, CDCl$_3$, 298 K) of compound **61**
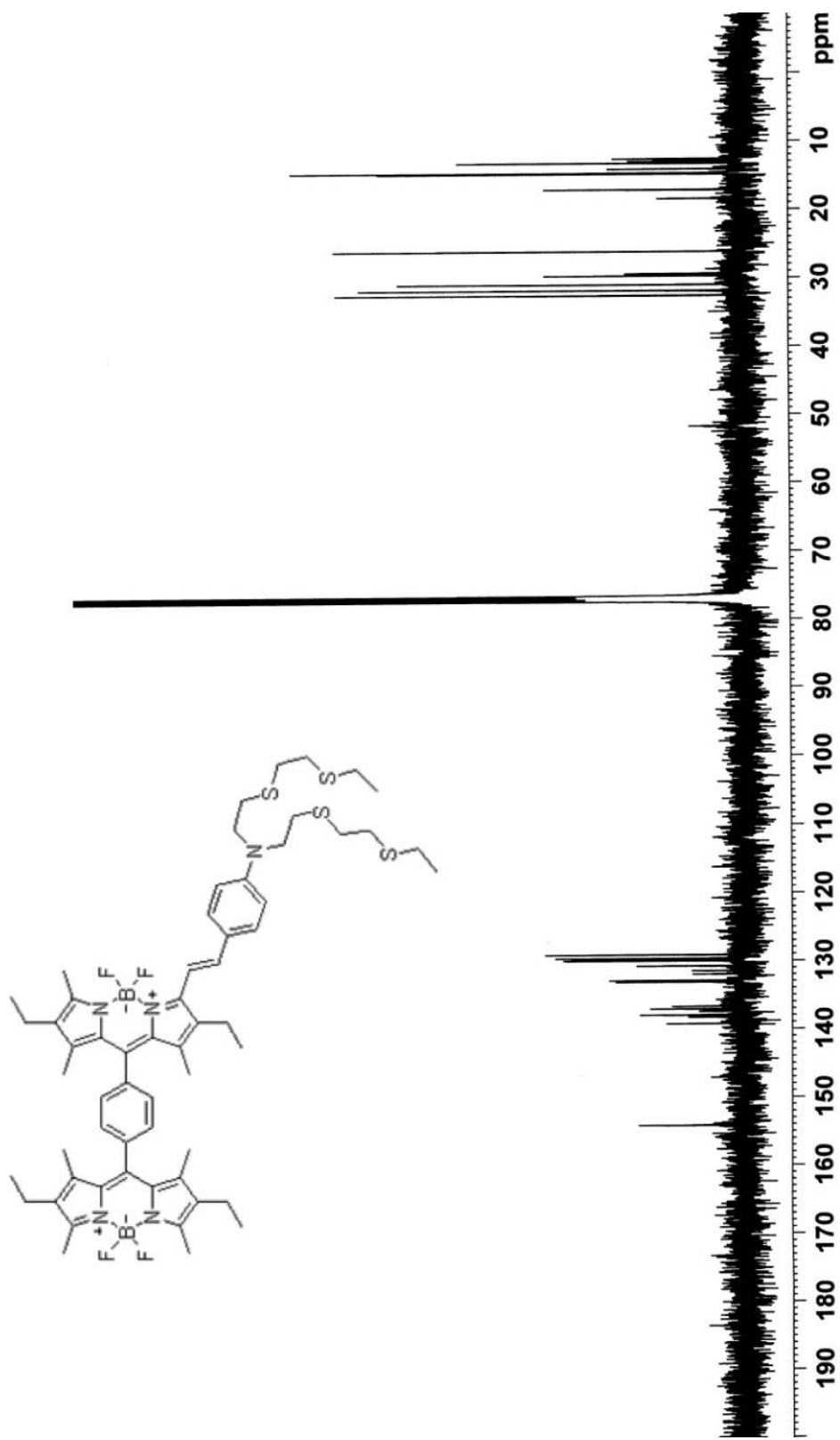
Figure 107. ^{13}C-NMR spectrum (400 MHz, CDCl$_3$, 298 K) of compound **61**

134
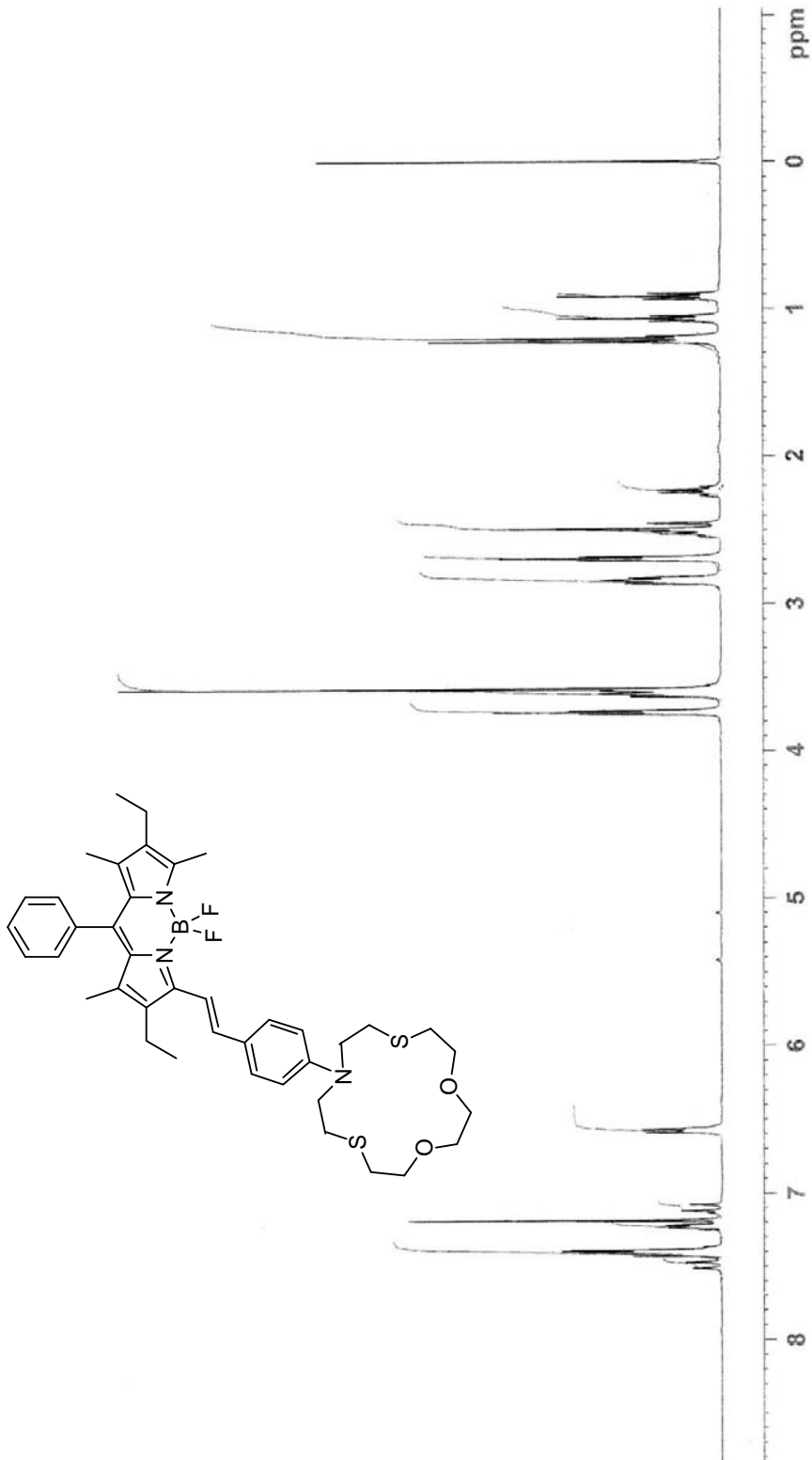
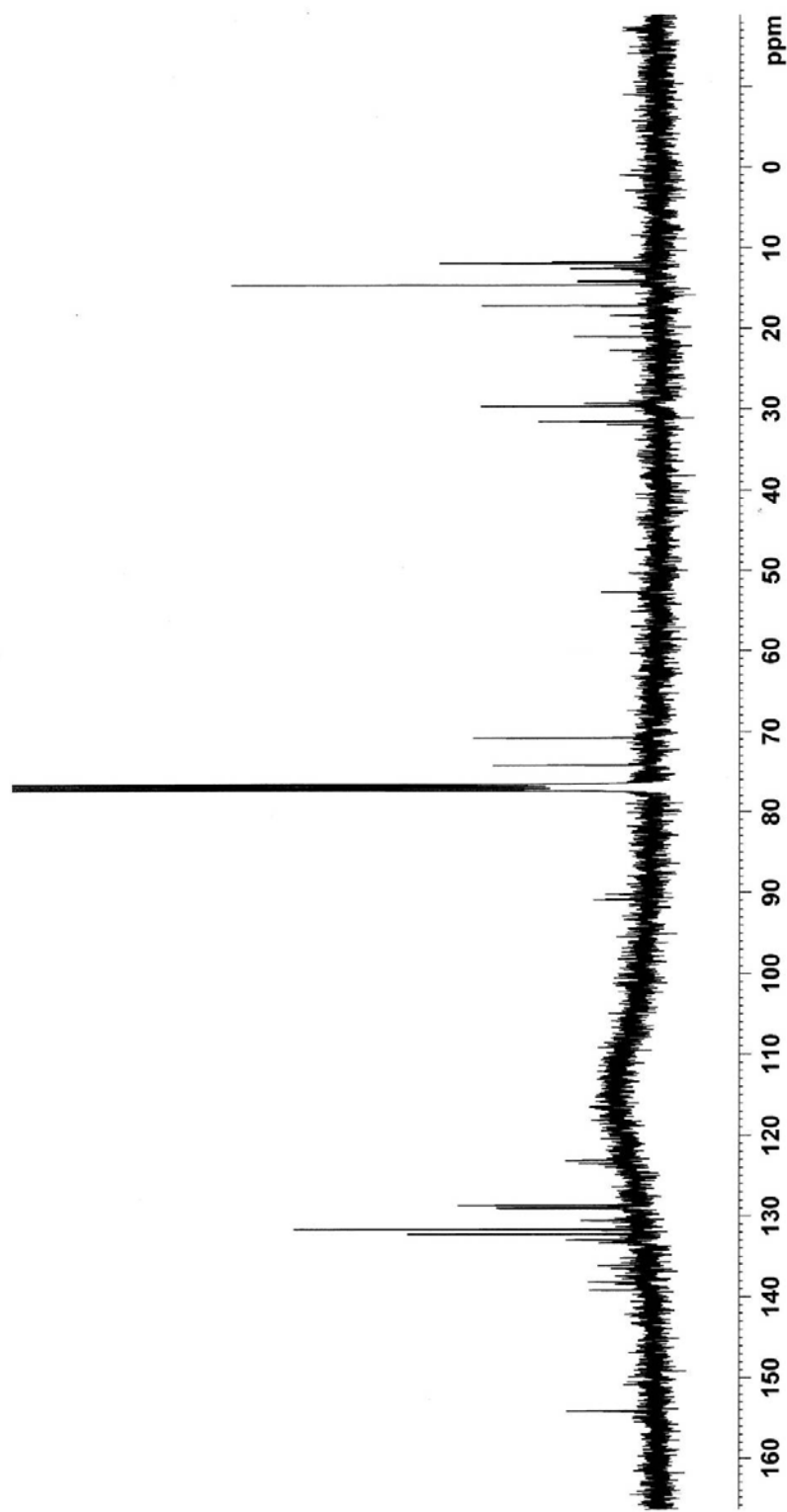Figure 108. ^{1}H-NMR spectrum (400 MHz, CDCl$_3$, 298 K) of compound **71**

135
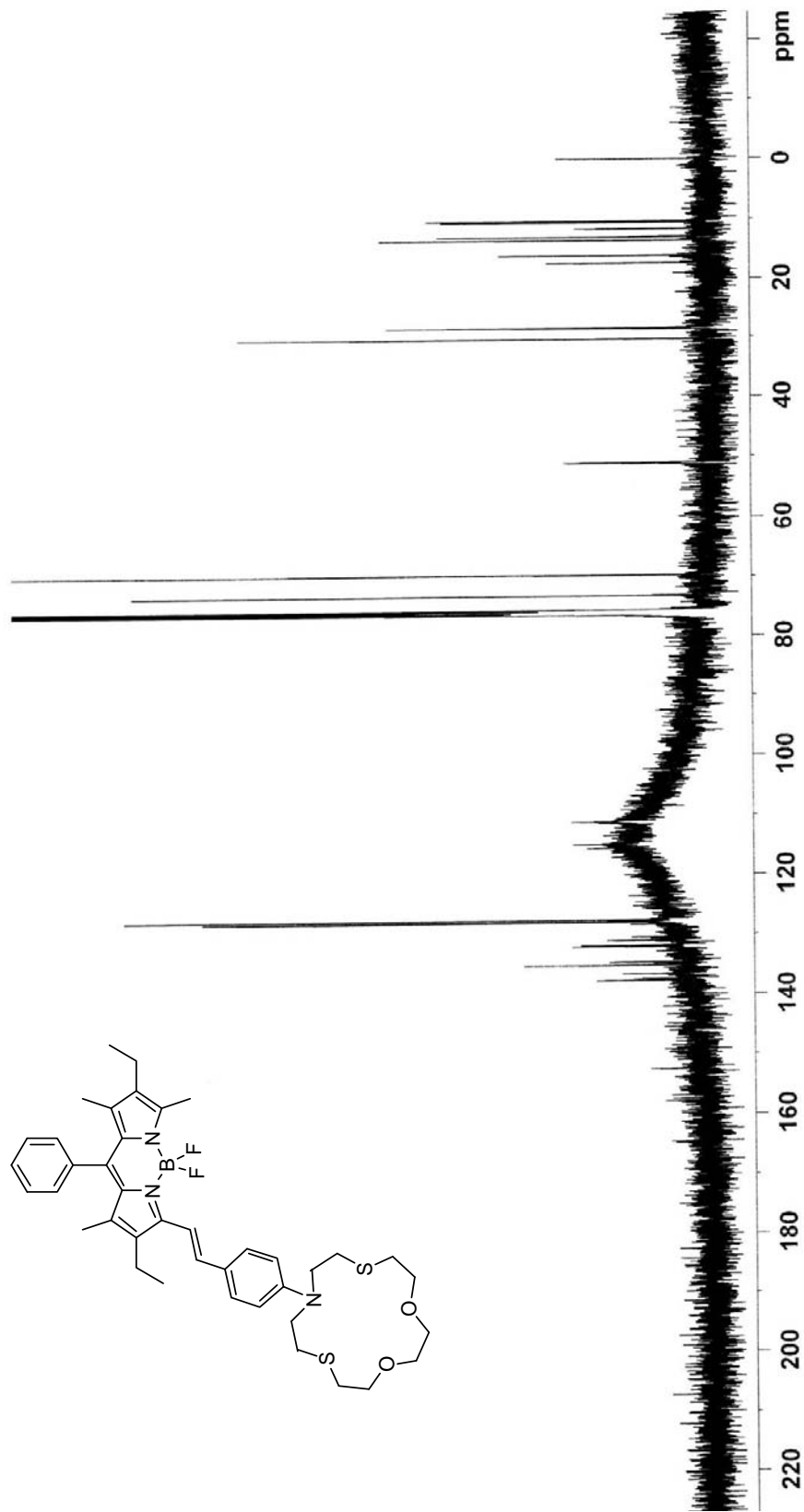
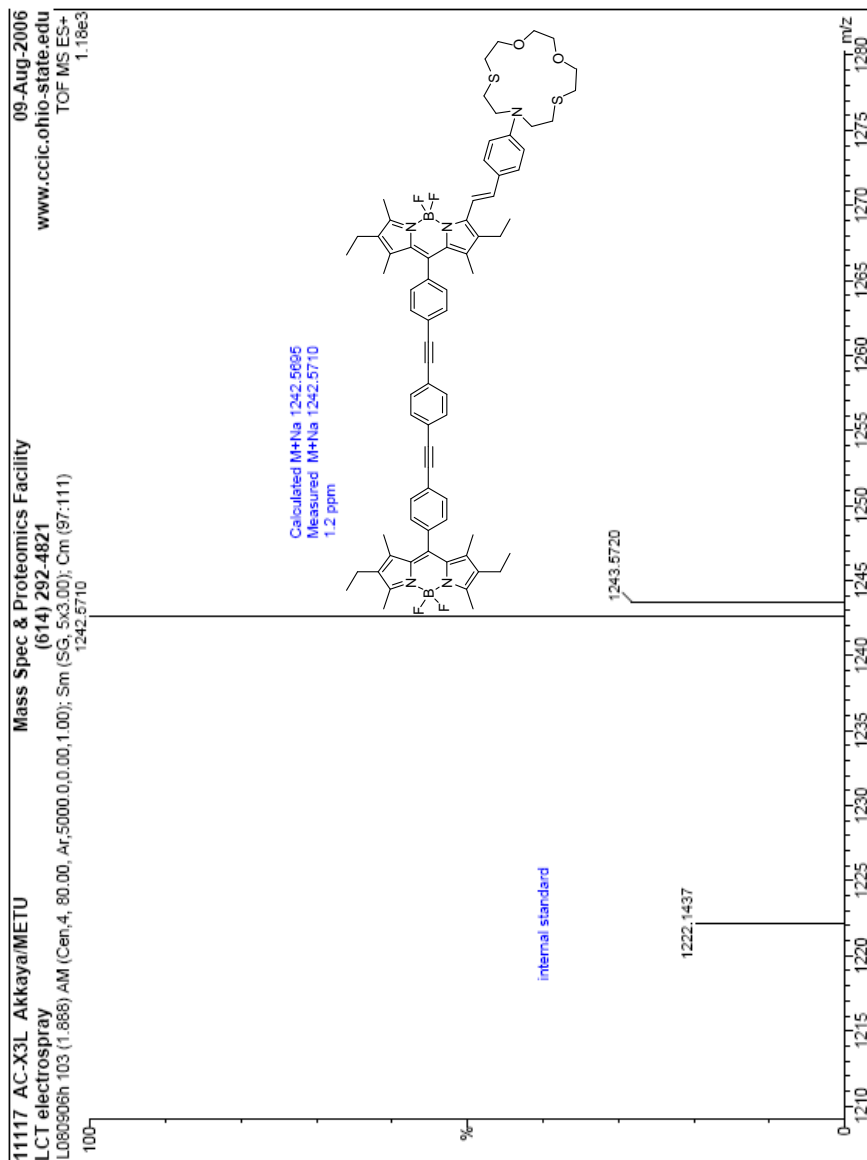Figure 109. ^{13}C-NMR spectrum (400 MHz, CDCl$_3$, 298 K) of compound **71**

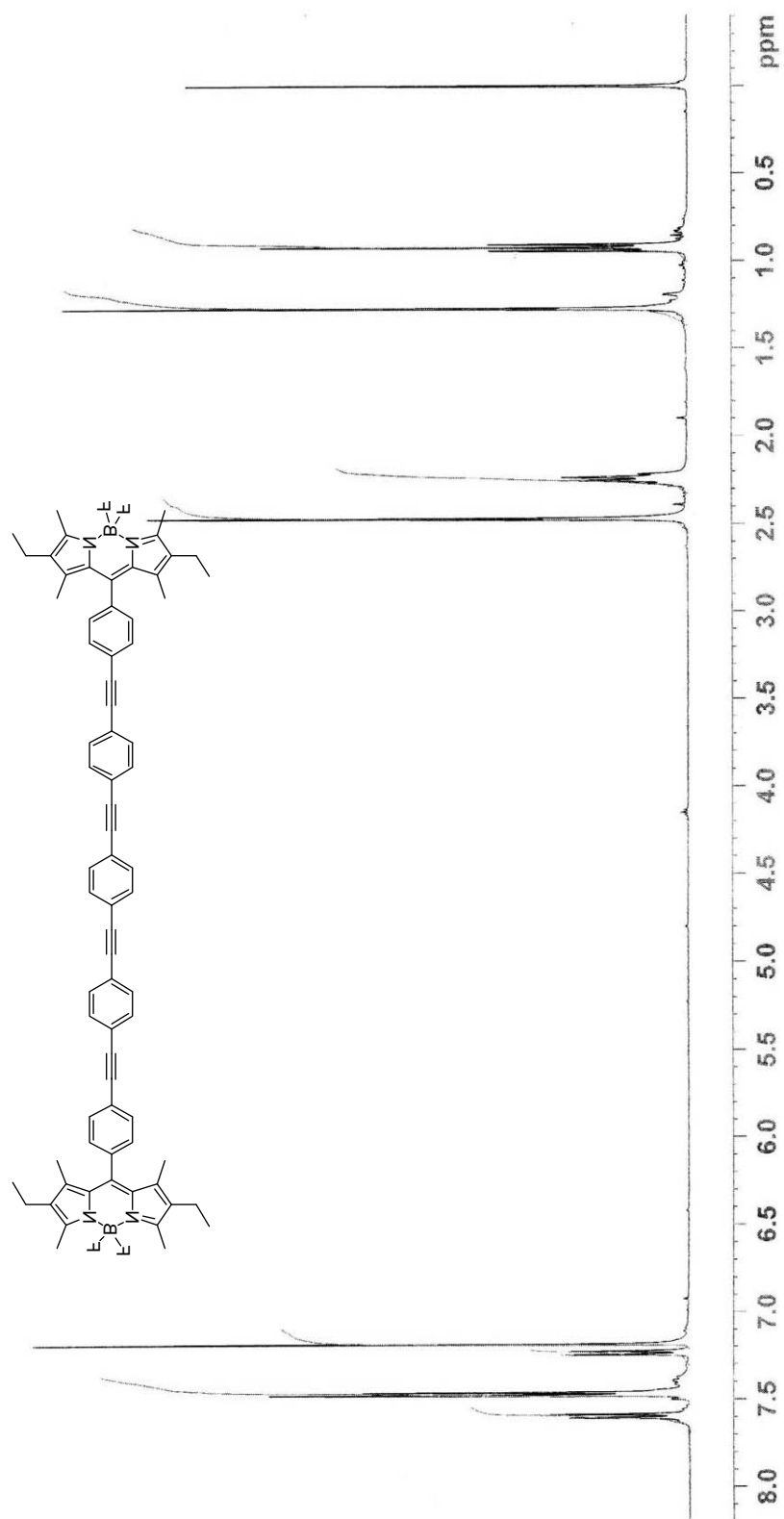Figure 110. ESI-HRMS of compound **71**, calcd for [M+Na] 740.3303 found 740.3325
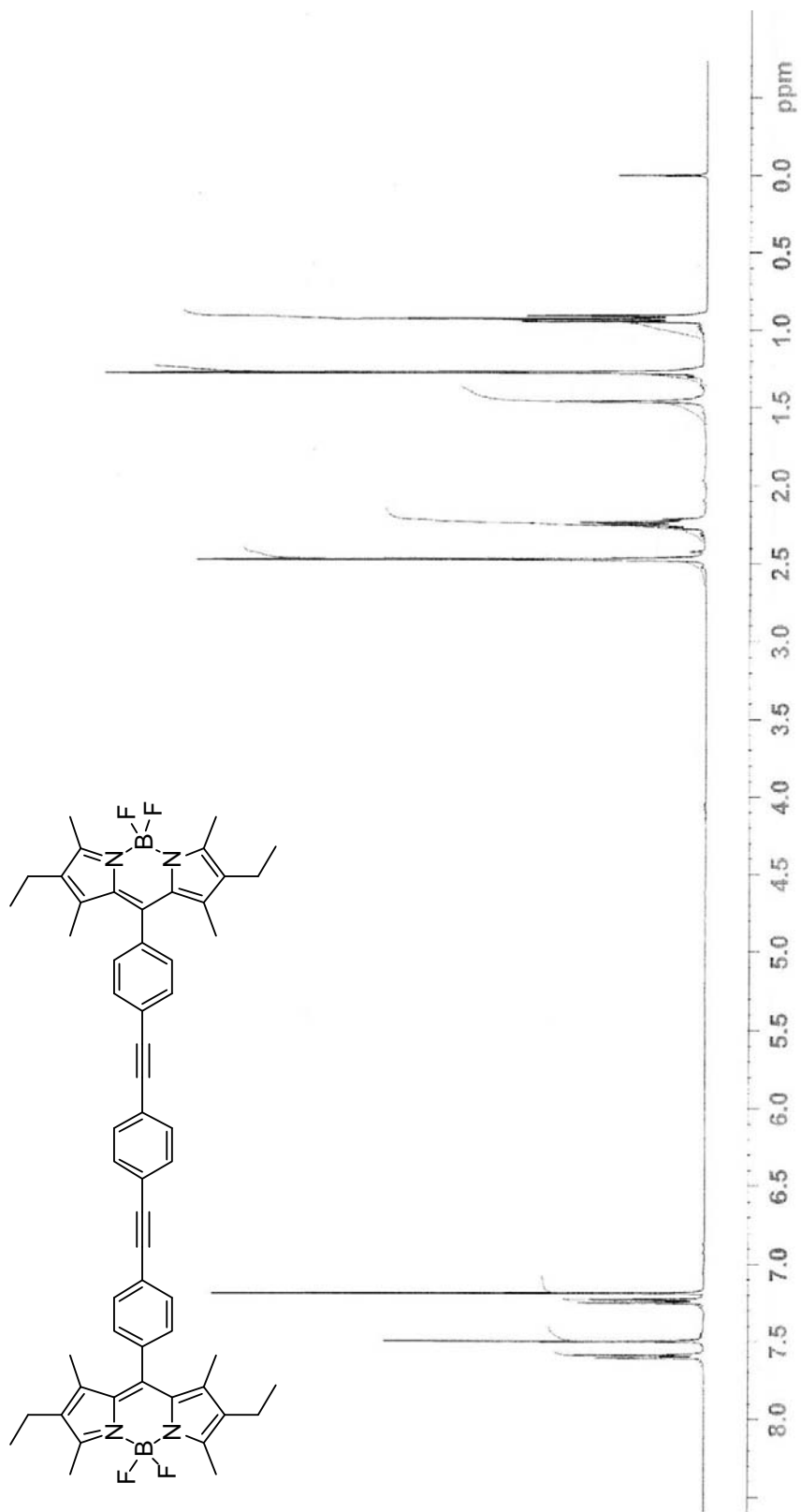
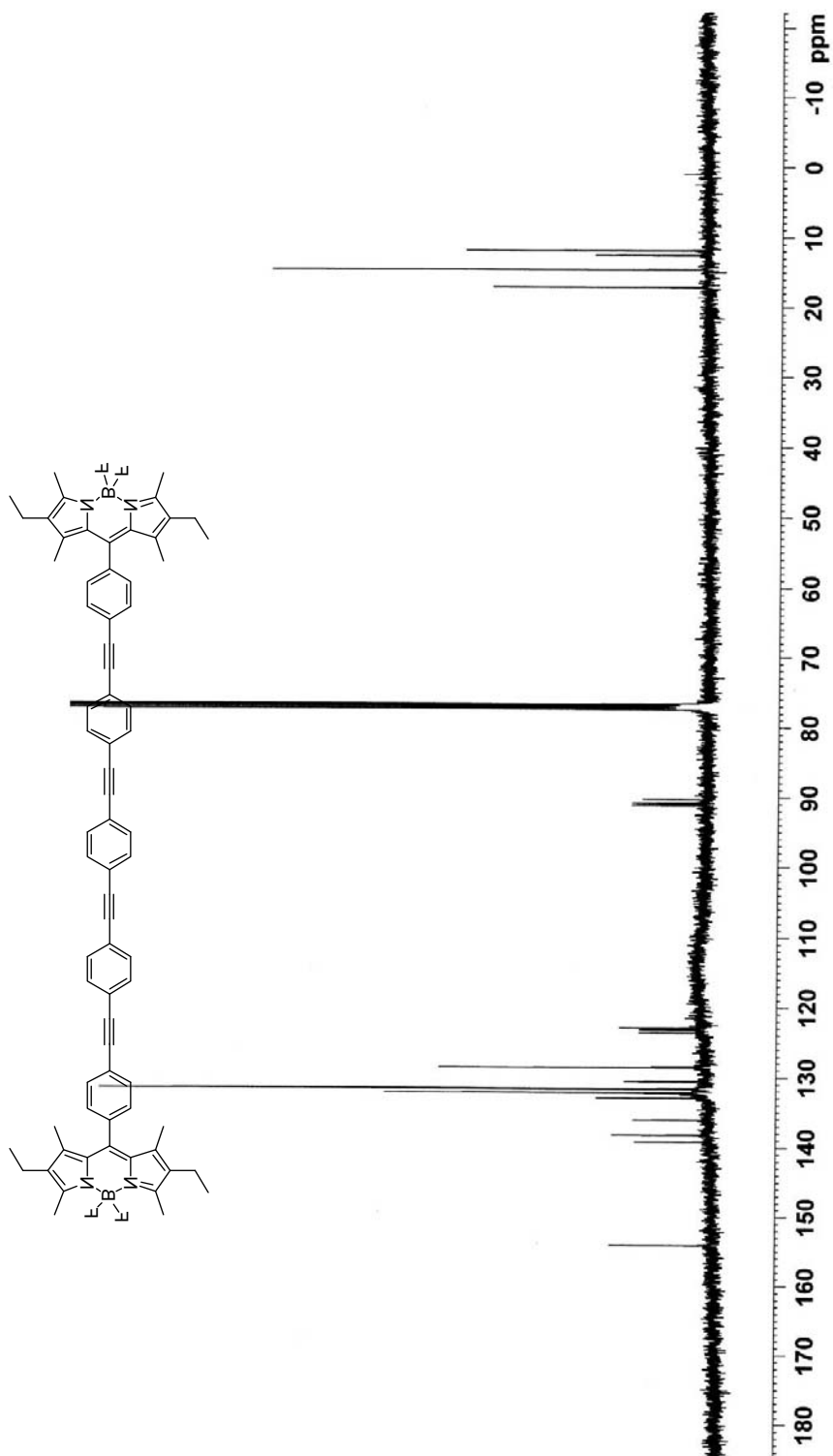Figure 111. ¹H-NMR spectrum (400 MHz, CDCl$_3$, 298 K) of compound **63**
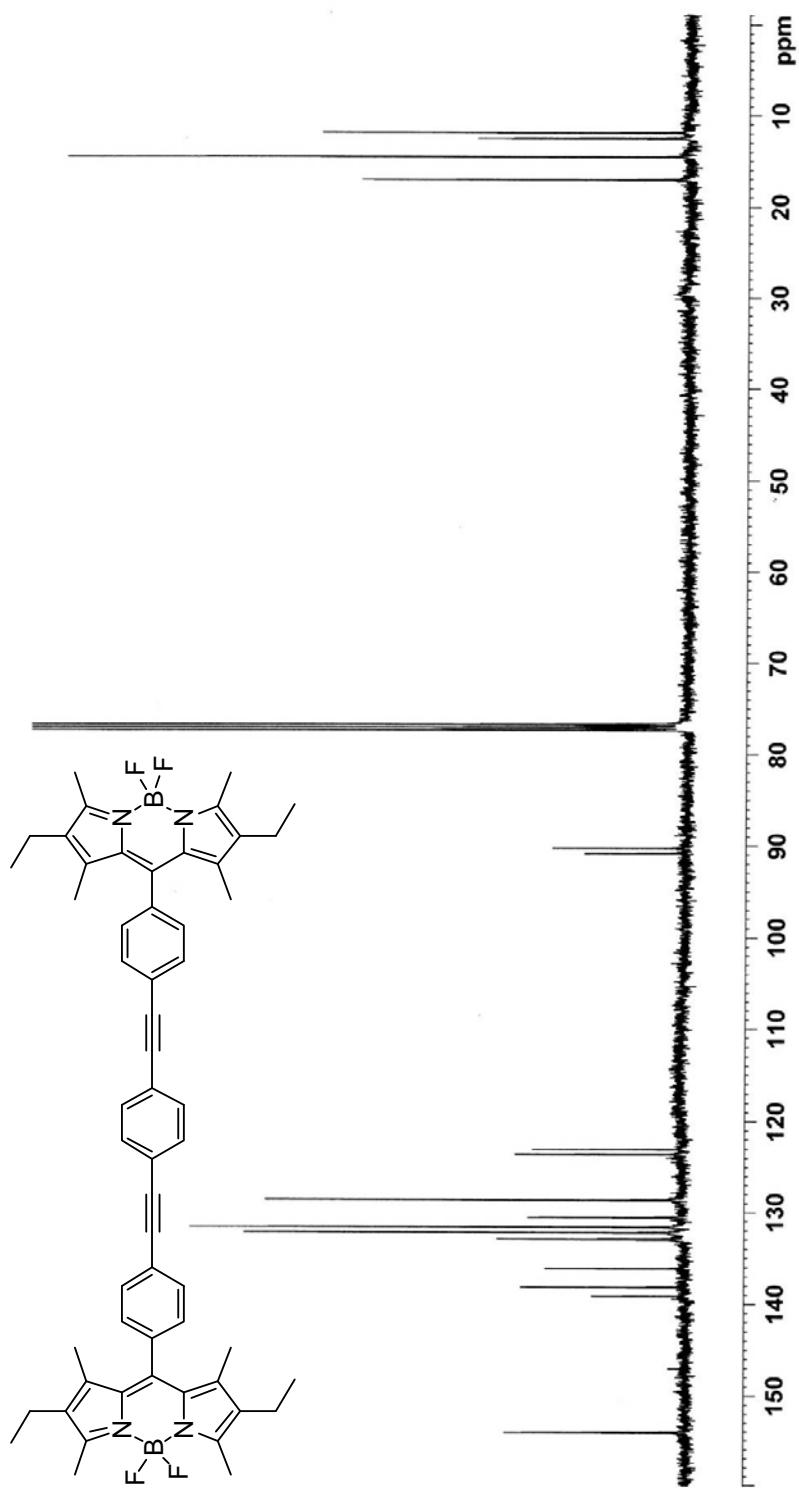
Figure 112. ^{13}C-NMR spectrum (400 MHz, CDCl$_3$, 298 K) of compound **63**

139
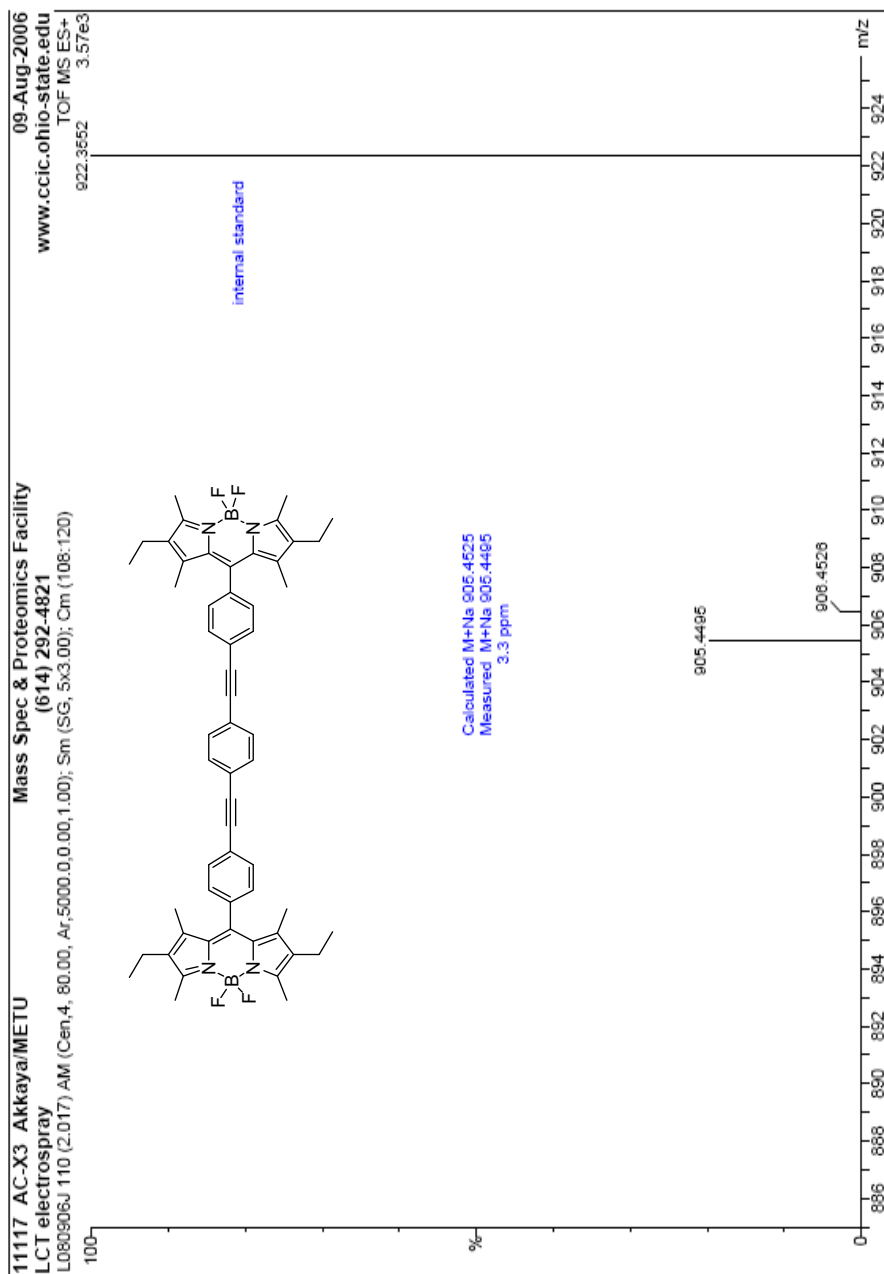
Figure 113. ESI-HRMS of compound **63**, calcd for [M+Na] 905.4525 found. 905.4495

Figure 114. ^{1}H-NMR spectrum (400 MHz, CDCl$_3$, 298 K) of compound **64**

141
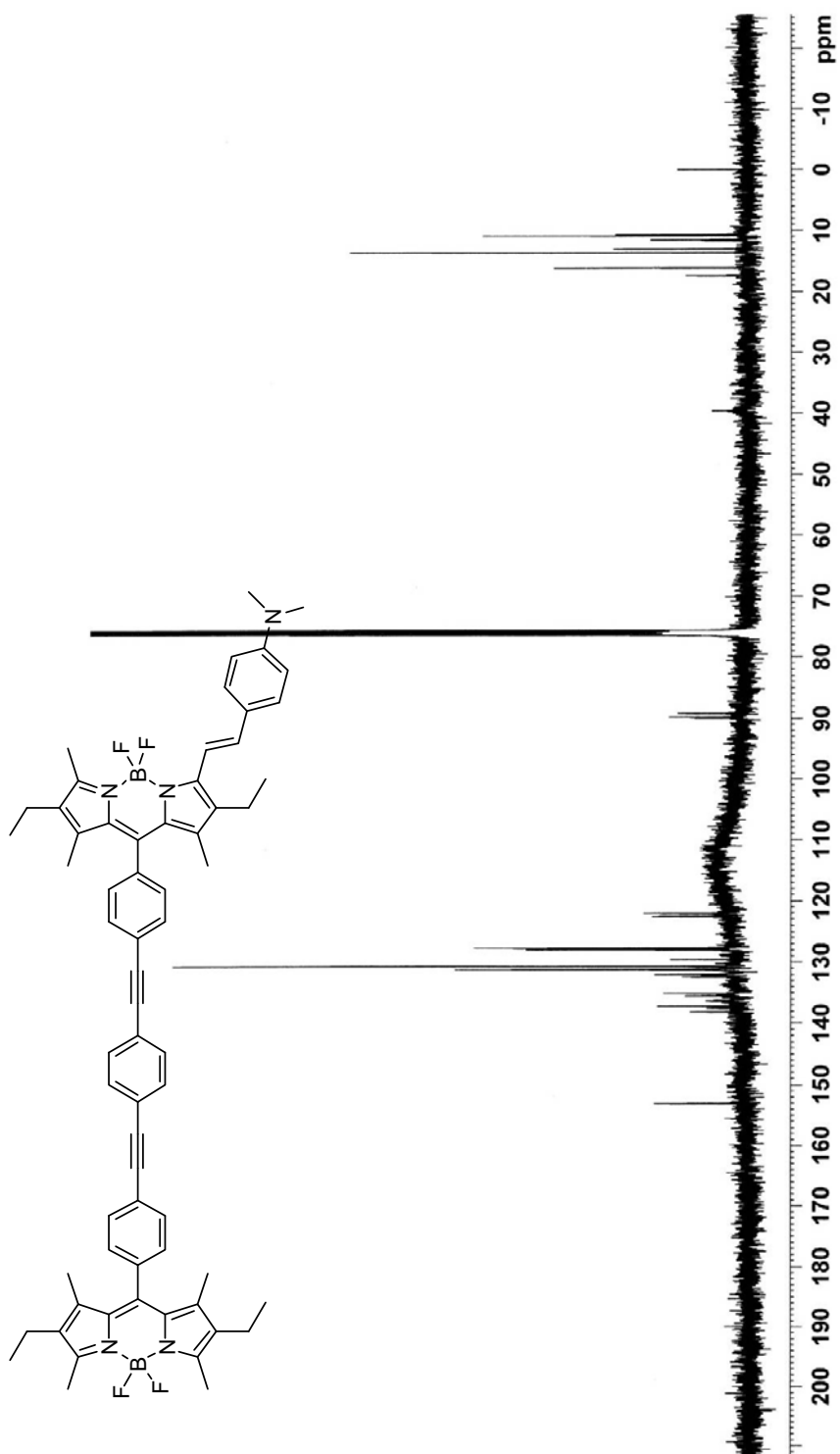
Figure 115. ^{13}C-NMR spectrum (400 MHz, CDCl$_3$, 298 K) of compound **64**

142
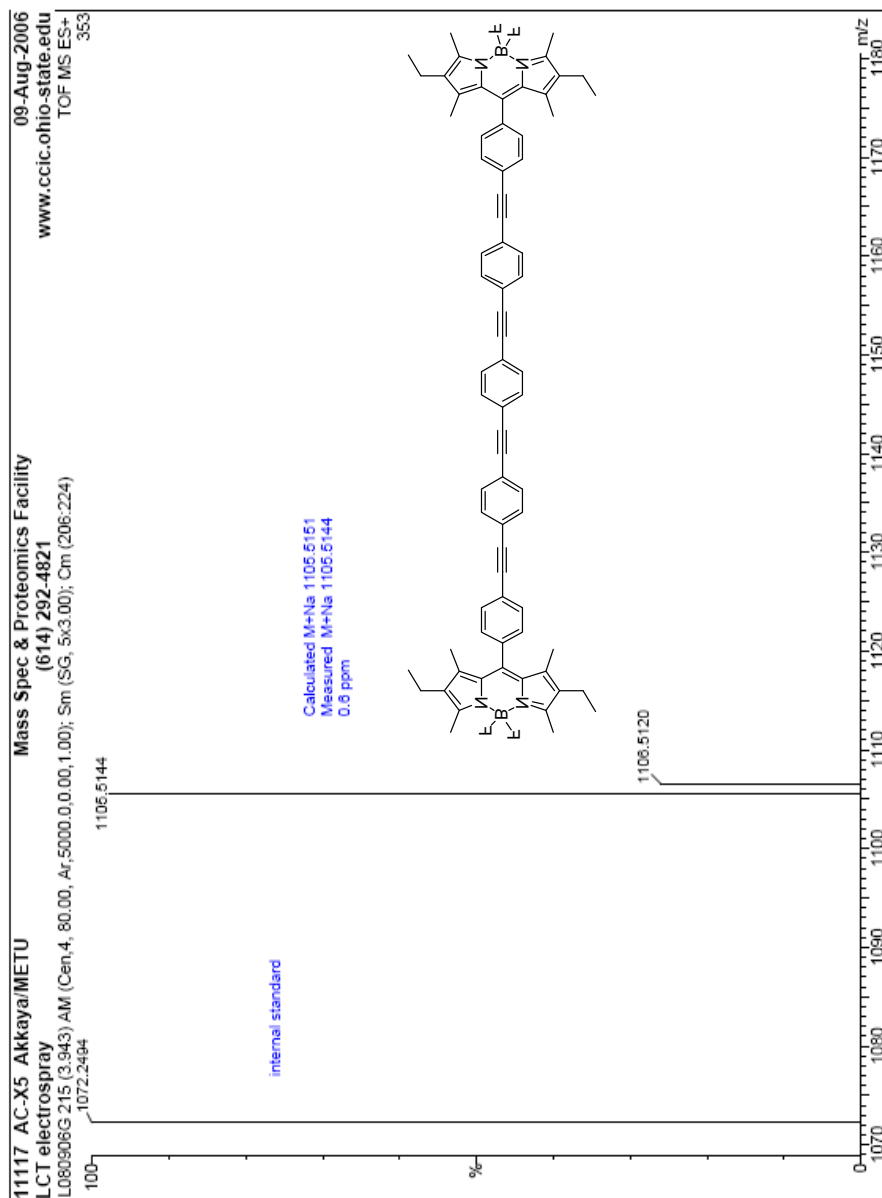
Figure 116. ESI-HRMS of compound **64**, calcd for [M+Na] 1036.5260 found 1036.5281
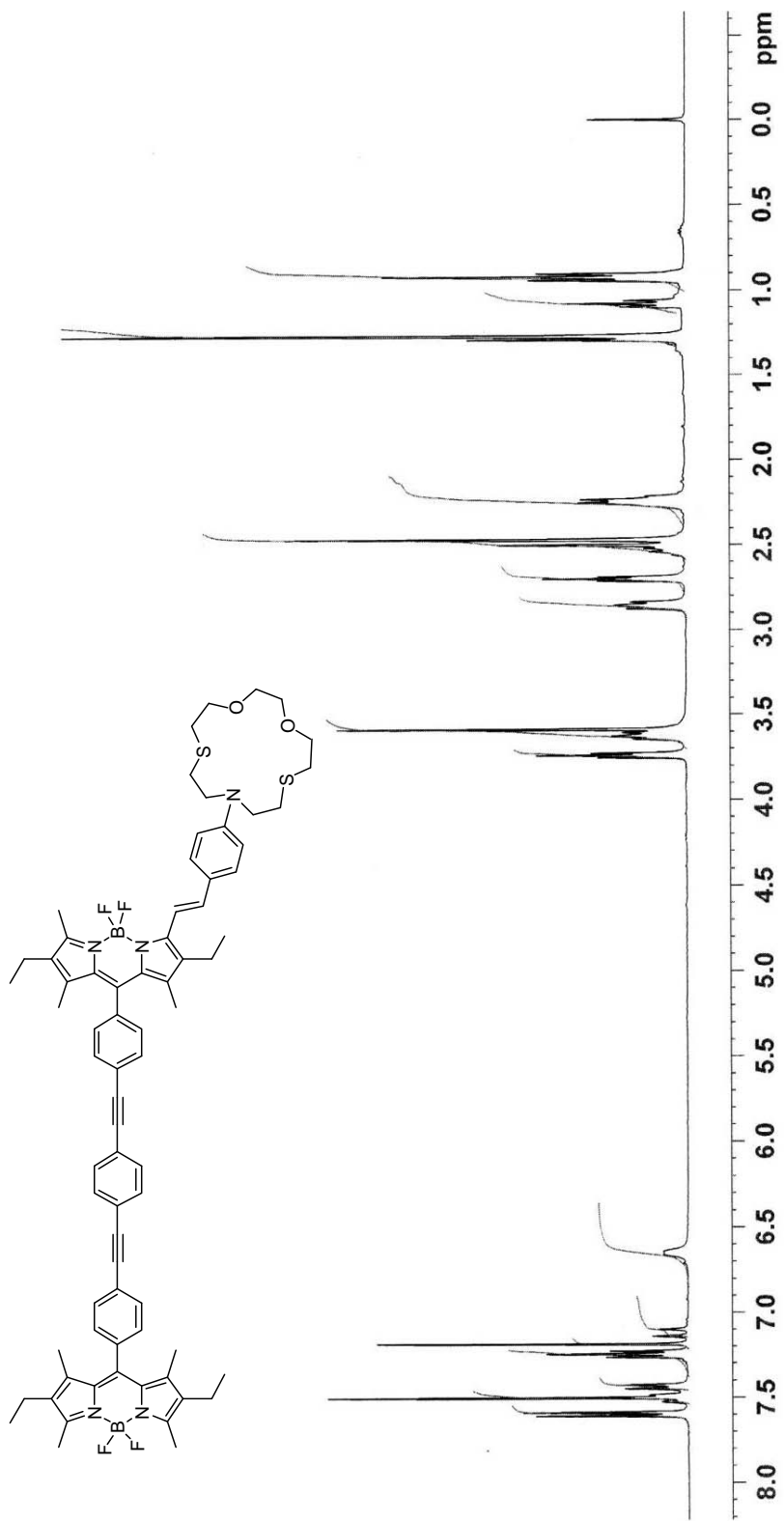
Figure 117. ¹H-NMR spectrum (400 MHz, CDCl₃, 298 K) of compound **65**

Figure 118. ^{13}C-NMR spectrum (400 MHz, CDCl$_3$, 298 K) of compound **65**

Figure 119. ESI-HRMS of compound **65**, calcd for [M+Na] 1242.5695 found 1242.5710

Figure 120. ^{1}H-NMR spectrum (400 MHz, CDCl$_3$, 298 K) of compound **68**

147

Figure 121. ^{13}C-NMR spectrum (400 MHz, CDCl$_3$, 298 K) of compound **68**

148

Figure 122. ESI-HRMS of compound **68**, calcd for [M+Na] 1105.5151 found 1105.5144
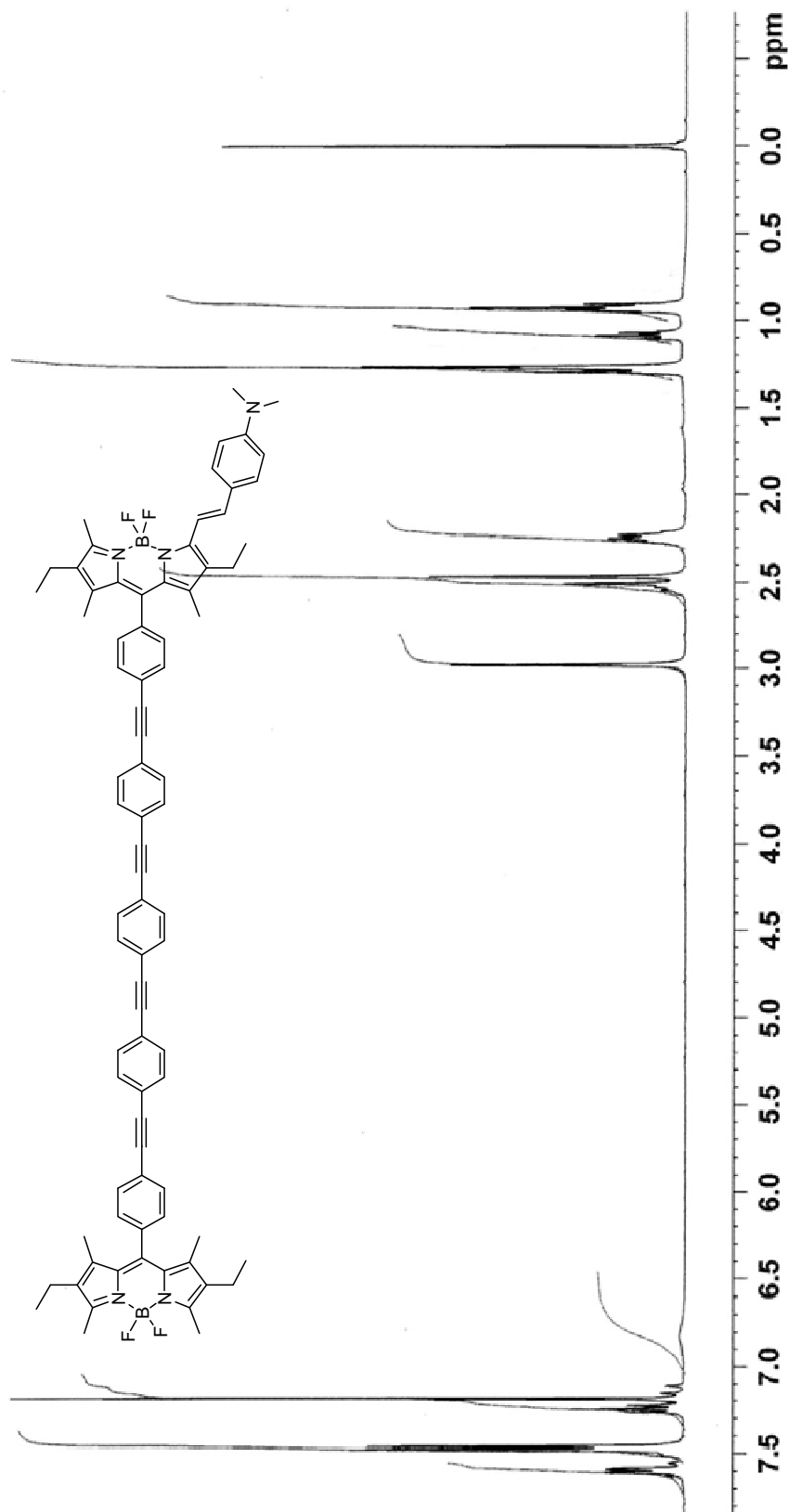
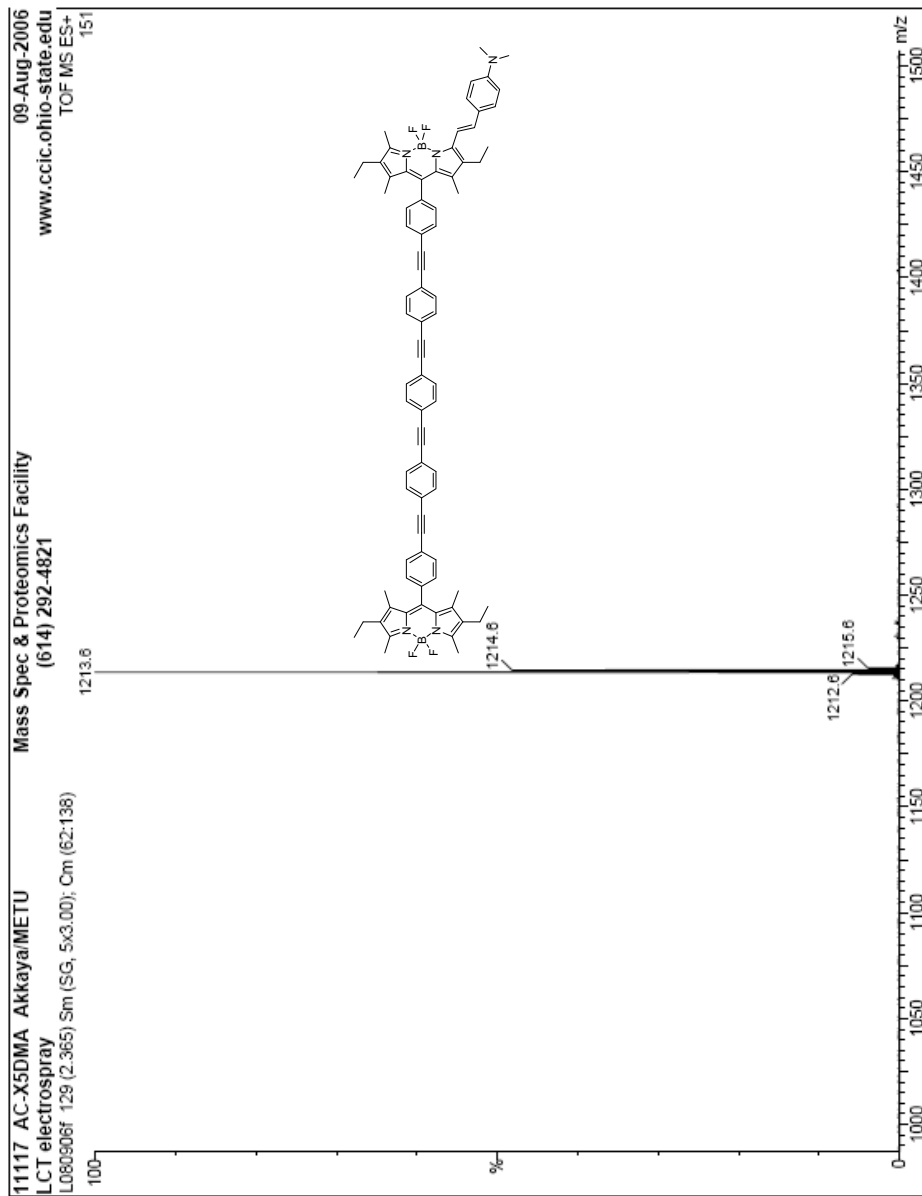Figure 123. ^{1}H-NMR spectrum (400 MHz, CDCl$_3$, 298 K) of compound **69**

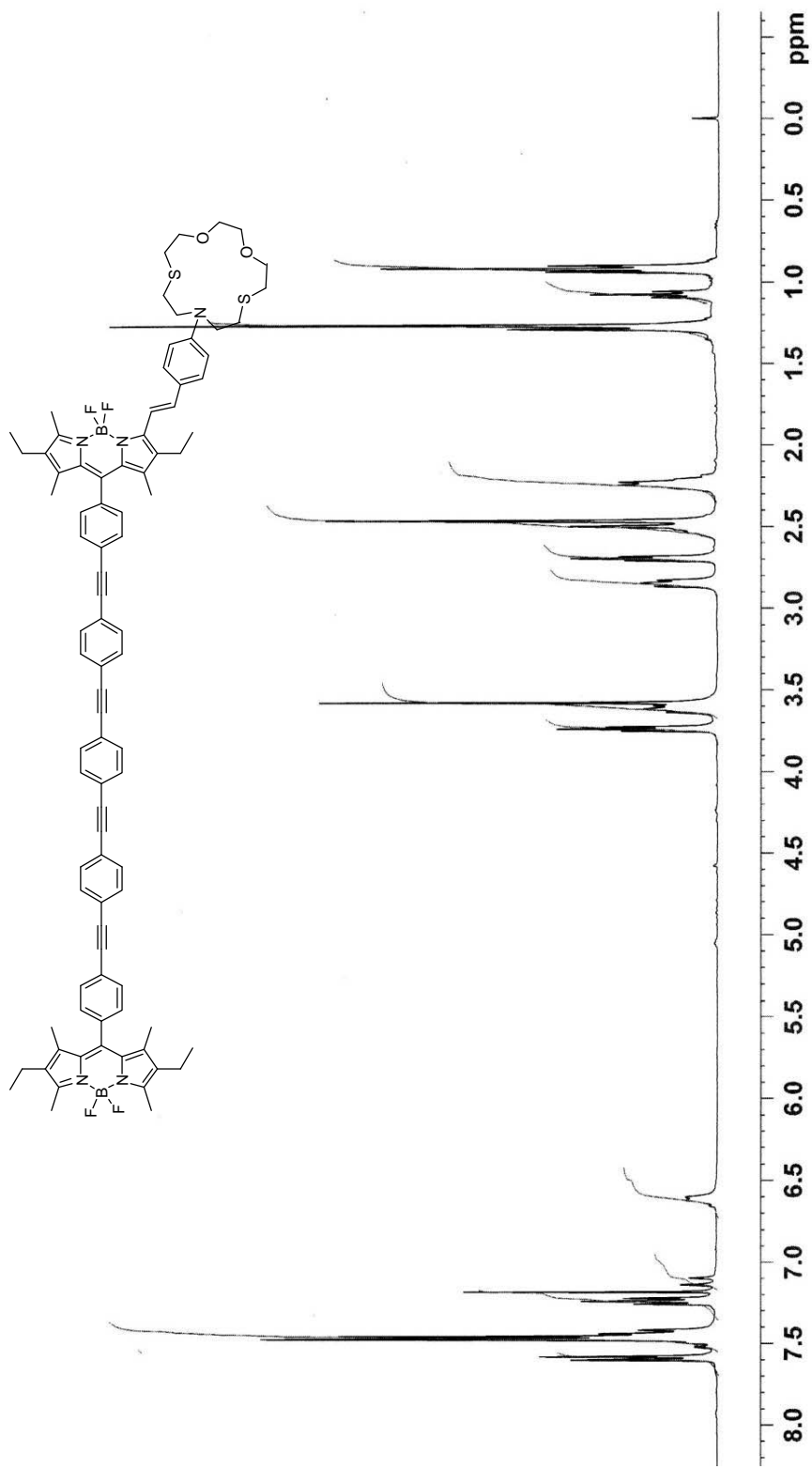Figure 124. ESI-HRMS of compound **69**, calcd for 1213.5988 found 1213.6049

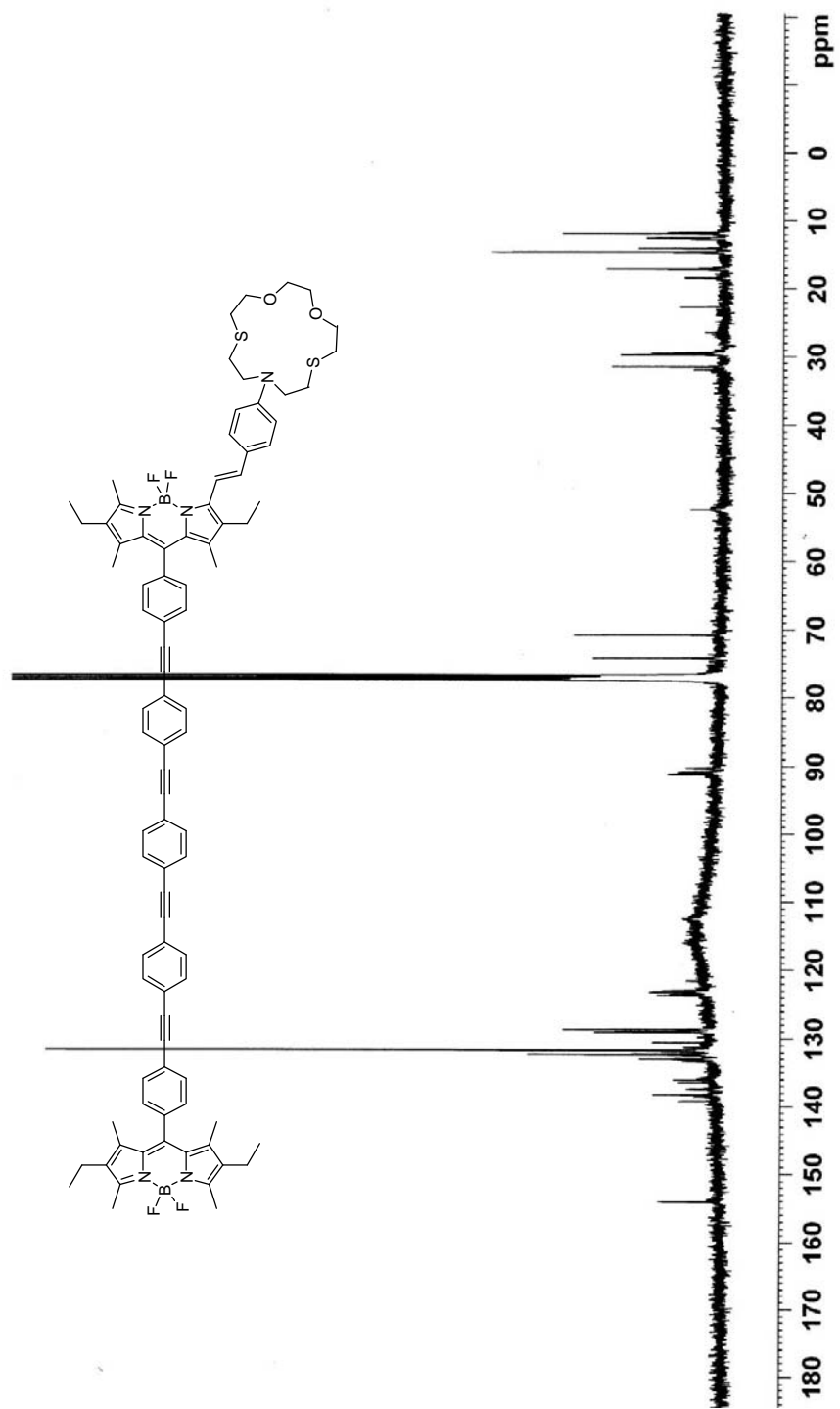Figure 125. ^{1}H-NMR spectrum (400 MHz, CDCl$_3$, 298 K) of compound **70**

Figure 126. ^{13}C-NMR spectrum (400 MHz, CDCl$_3$, 298 K) of compound **70**
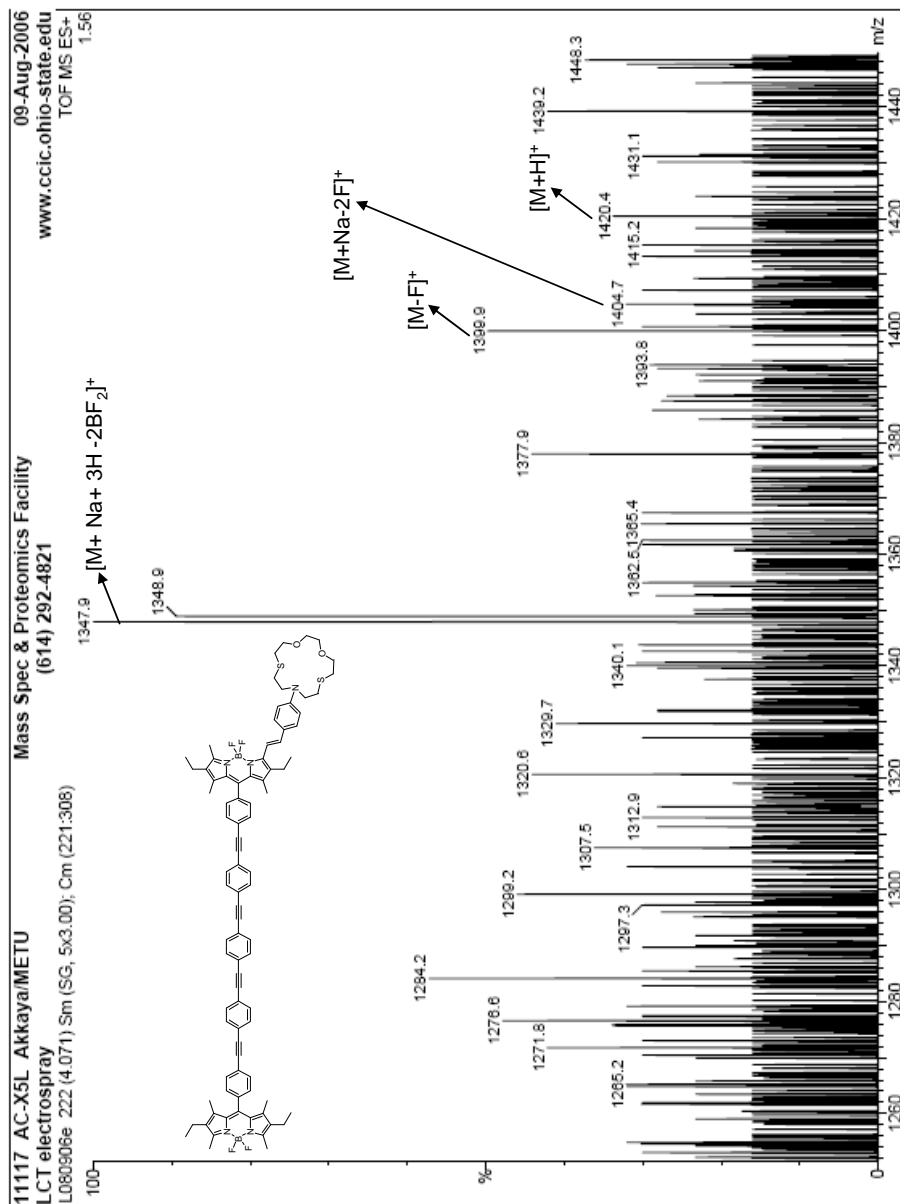
153

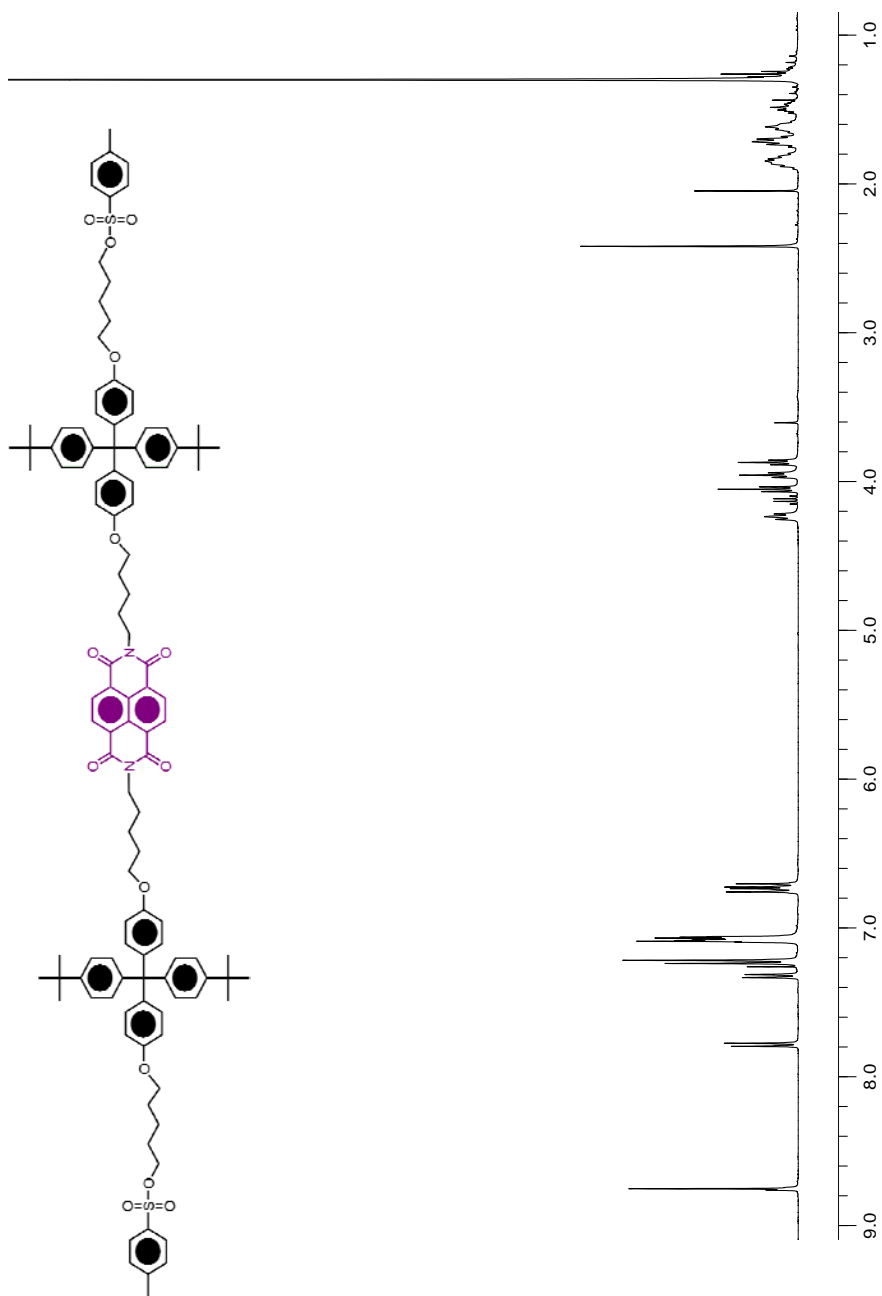Figure 127. ESI-HRMS of compound **70**, calcd for [M+ Na+ 3H- 2BF$_2$] 1347.6434 found. 1347.9

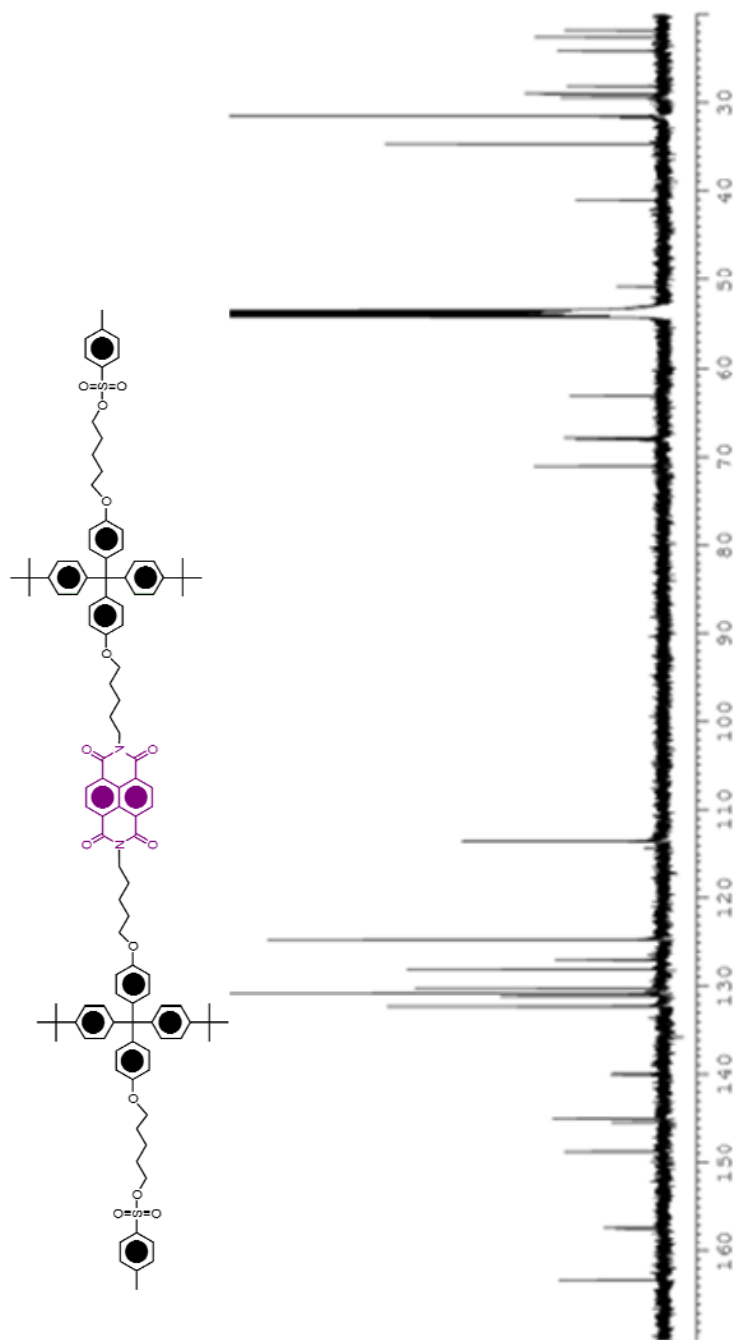Figure 128. ^{1}H-NMR spectrum (400 MHz, CDCl$_3$, 298 K) of compound **74**

Figure 129. ^{13}C-NMR spectrum (600 MHz, CD$_2$Cl$_2$, 298 K) of compound **74**
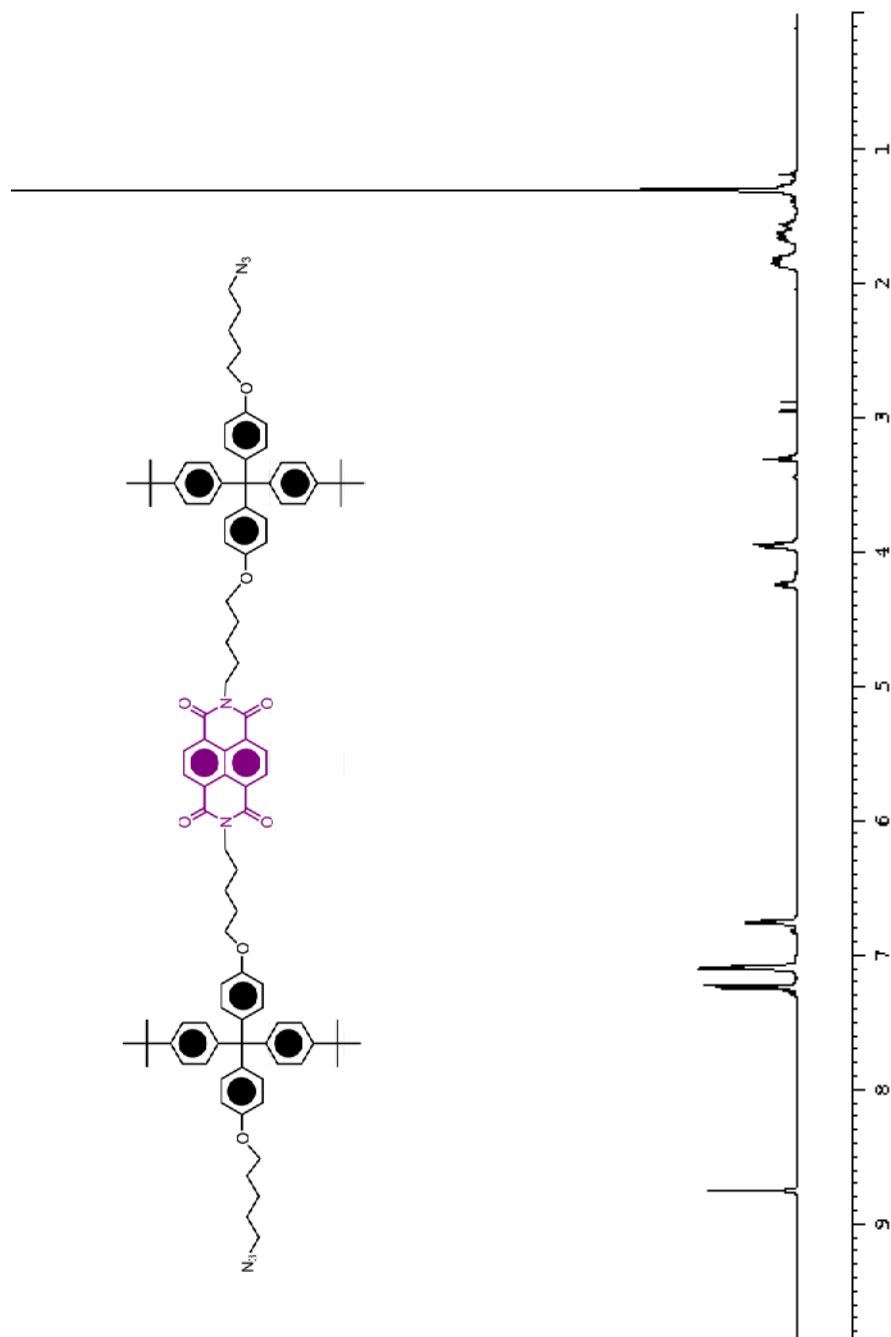
Figure 130. ^{1}H-NMR spectrum (500 MHz, CDCl$_3$, 298 K) of compound **75**

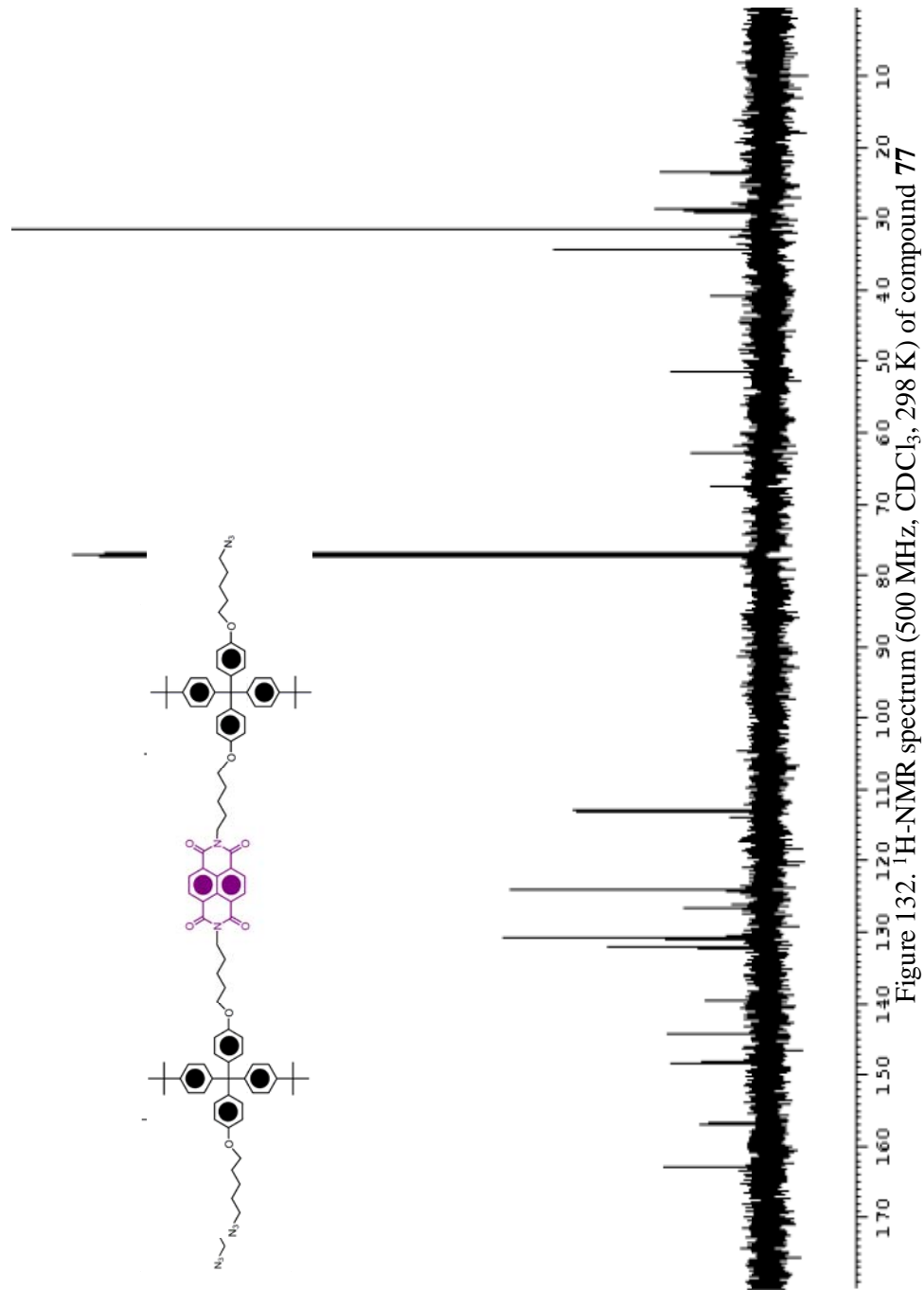Figure 132. ^{1}H-NMR spectrum (500 MHz, CDCl$_3$, 298 K) of compound **77**

158

Figure 131. ^{13}C-NMR spectrum (500 MHz, CDCl$_3$, 298 K) of compound **75**
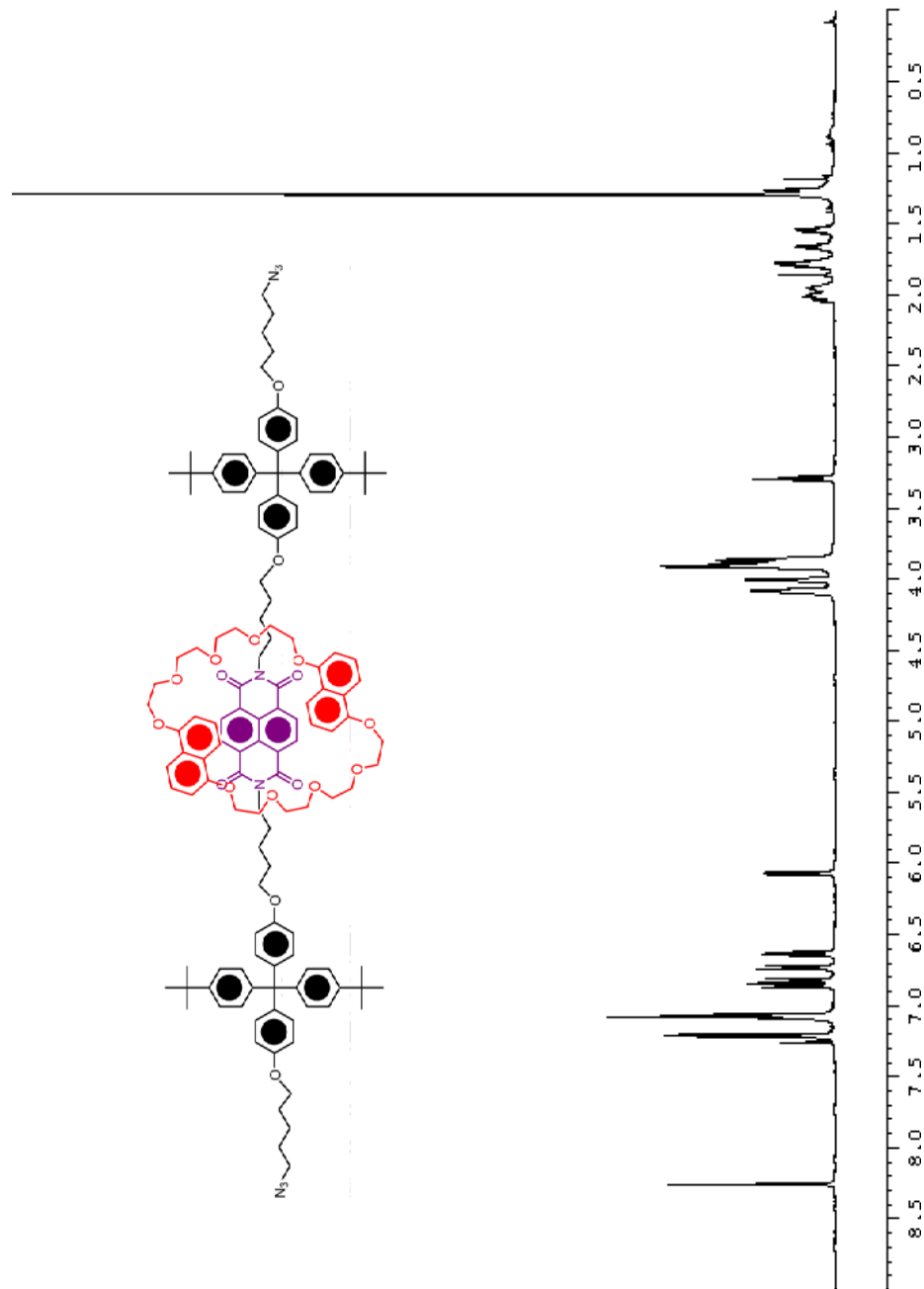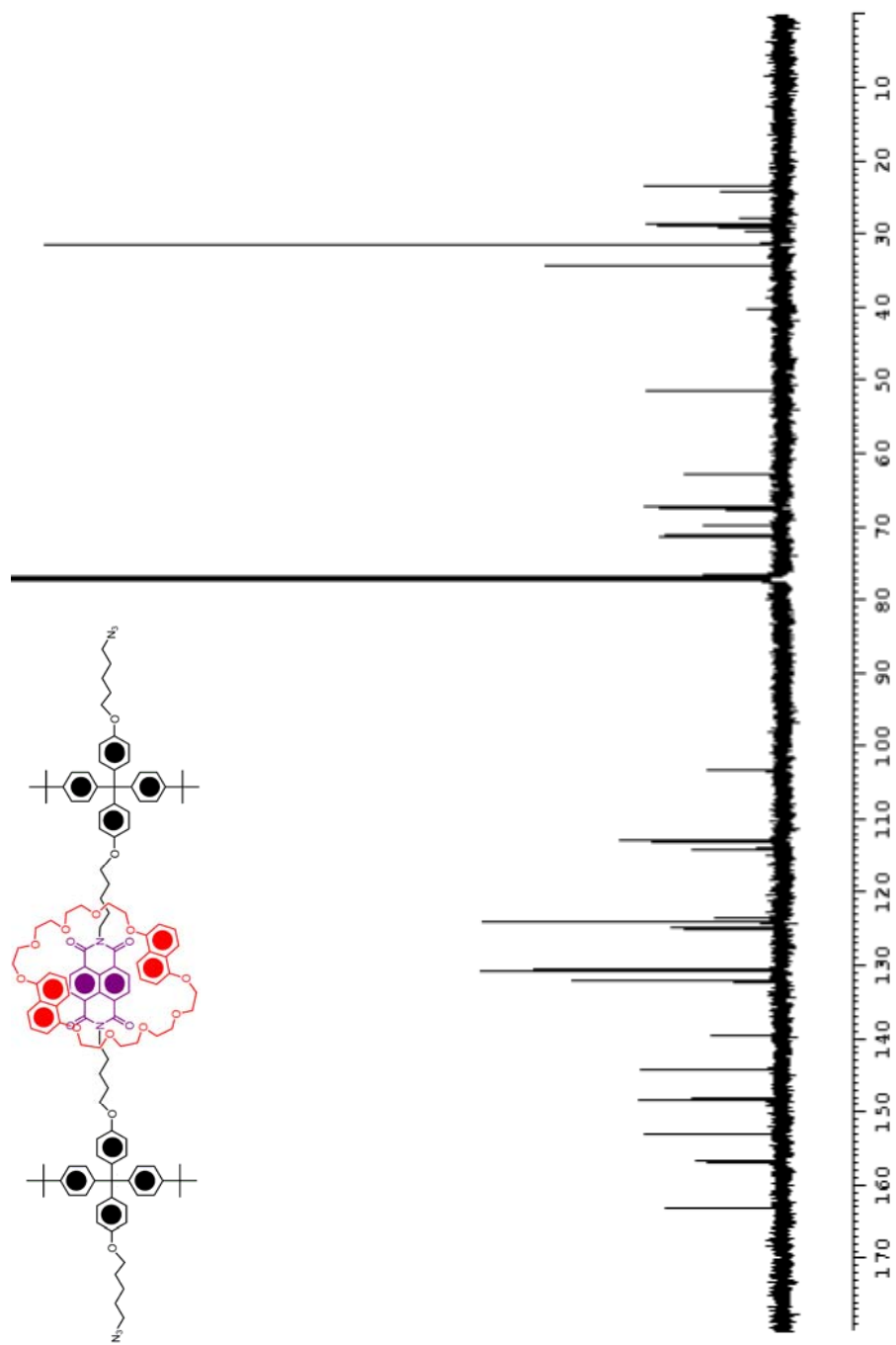
Figure 133. ^{13}C-NMR spectrum (500 MHz, CDCl$_3$, 298 K) of compound **77**

160

Figure 134. ^{1}H-NMR spectrum (500 MHz, CD$_3$CN, 298 K) of compound **76.2PF$_6$**
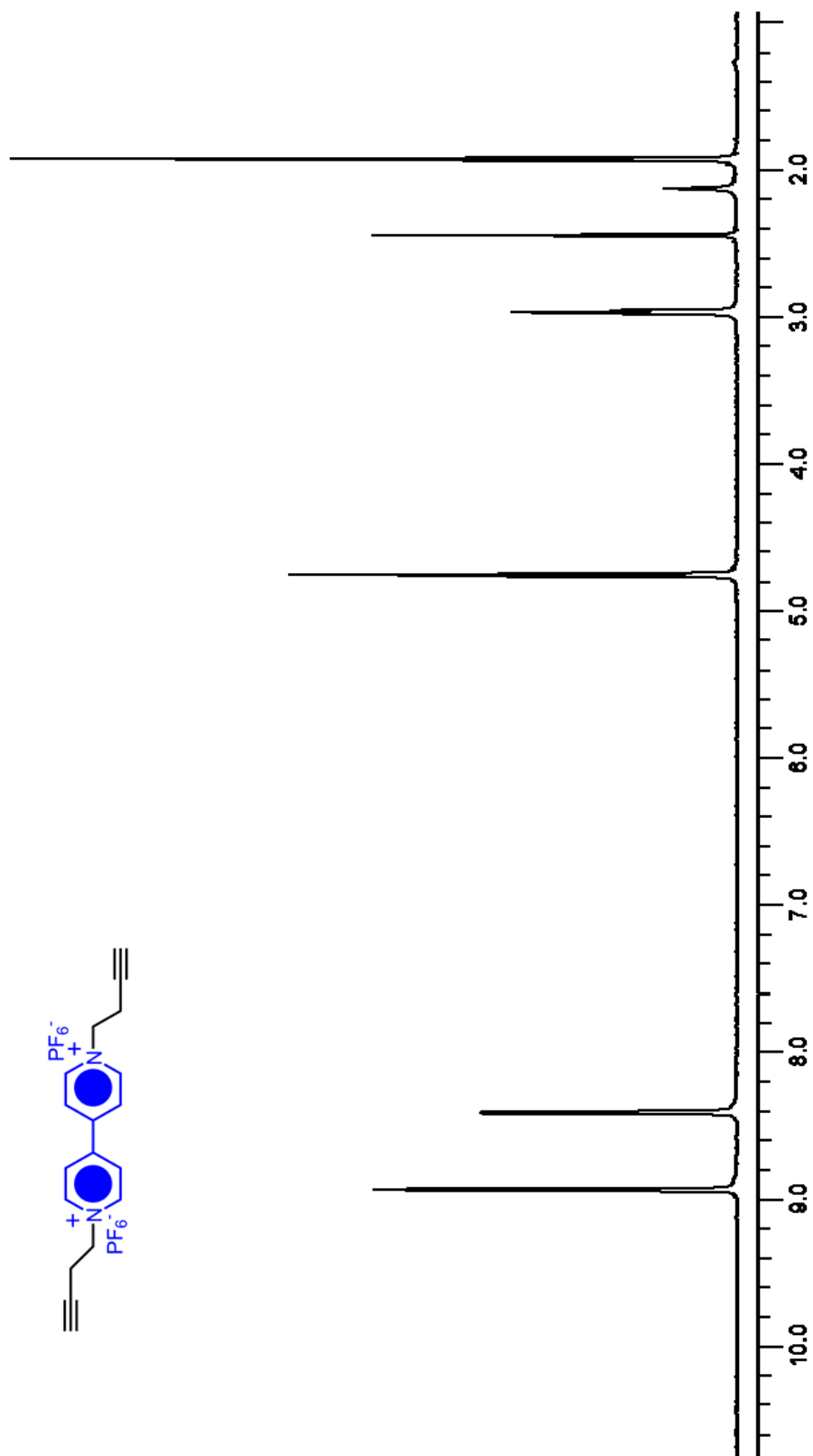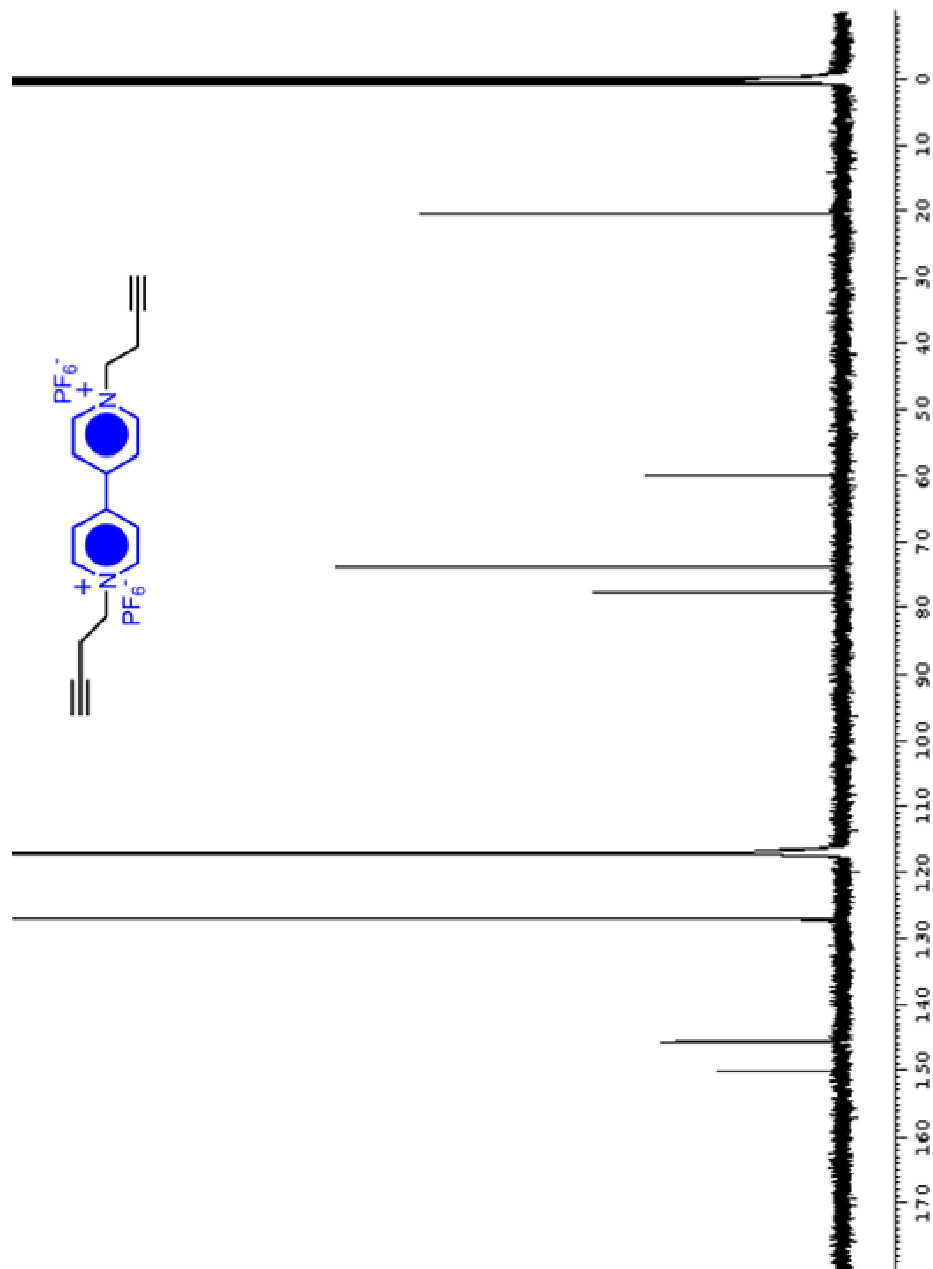
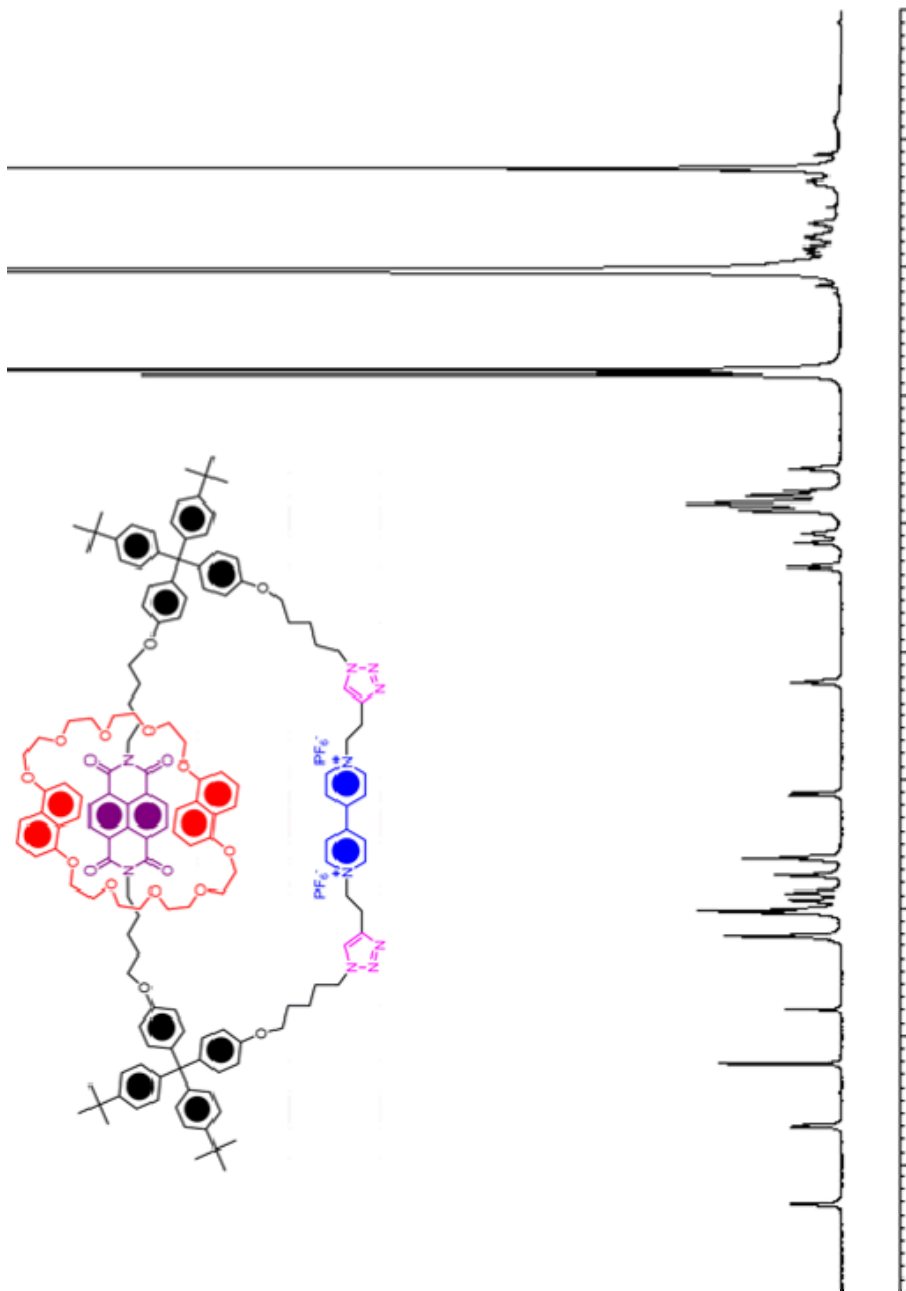Figure 135. ^{13}C-NMR spectrum (500 MHz, CD$_3$CN, 298 K) of compound **76.2PF$_6$**

Figure 136. ^{1}H-NMR spectrum (500 MHz, CD$_3$COCD$_3$, 298 K) of compound **79**$^{2+}$
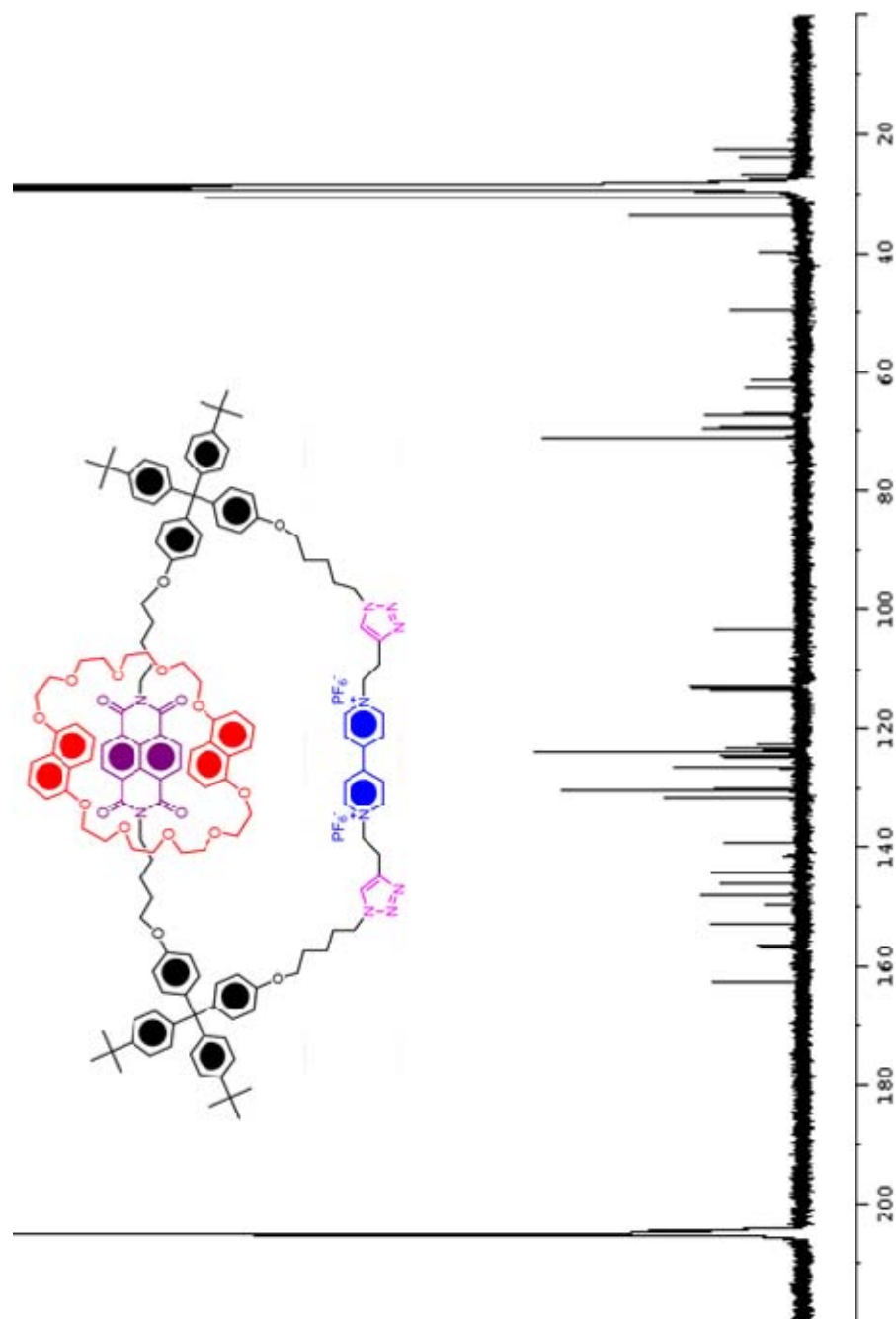
Figure 137. ^{13}C-NMR spectrum (500 MHz, CD$_3$COCD$_3$, 298 K) of compound **79^{2+}**

164

VITA

Ali Coşkun

Research Assistant, Middle East Technical University, 2001-2007

Birth Date: 13/09/1979

Education

Ph.D,Middle East Technical University (M.E.T.U.), Department of Chemistry, 2003-2007,Current CGPA; 3.79/4.00

M.Sc. degree, Middle East Technical University, Department of Chemistry, 2001-2003, CGPA; 3.86/4.00

Bachelors degree, Middle East Technical University, Department of Chemistry 1999-2001 CGPA; 3.67/4.00

Hacettepe University, Department of Chemsitry , 1996-1999

Research Experience

Visiting Scholar, University of Califonia, Los Angeles , Department of Chemistry and Biochemistry. Prof. Dr. J. Fraser Stoddart,   September 2006-March 2007.

Novel Fluorescent Energy Transfer Casettes and Chemosensors Based on Boradiazaindacene Derivatives: ***Ph.D.***, Prof. Dr. Engin U. Akkaya, Ali Coşkun, Middle East Technical University, Chemistry Department, September 2003-2007.

Time resolved Fluorescence Spectrophotometer education program (one week), London, Ontario/Canada, 10/2004

Novel Supramolecular Ion Sensing Systems and Their Application in Molecular Logic Gates; **M.Sc. Thesis**, Prof. Dr. Engin U. Akkaya, Ali Coşkun, Middle East Technical University, Chemistry Department, September 2003.

Teaching Assistant, Organic Chemistry and General Chemistry Student Laboratory, september 2001-

Enzymatic oxidation of dyes which are hydrolyzed from cotton during the continuous washing process and its application on continuous washing system; **Internship**, Bayer AG, Leverkusen, Germany, 06-09/2001.

Synthesis and the Characterization of the camphor derivatives of biologically active1,4-dihydropyridines; **Undergraduate reserach project**, Prof. Dr. Ayhan S. Demir, Prof. Dr. İdris M. Ahmedov, Ali Coşkun, Middle East Technical University, Chemistry Department, 2000-2001.

Enzymatic oxidation of dyes which are hydrolyzed from cotton during the continuous washing process; **Internship**, Bayer AG, Leverkusen, Germany, 06-09/2000.

Removal of Toxic Heavy Metal Ions from Turkish Lignite Coal; **Research Project**, Doç. Dr. Bekir Salih, Ali Coşkun, Hacettepe University, Chemistry Department , Ankara/TURKEY 1999.

Scholarship and Achivements

Scientific and Research Council of Turkey (TUBITAK), Young Scientist Growth Program, Research Scholarship, 2006

Scientific and Research Council of Turkey (TUBITAK), Ph.D scholarship, March 2004-

Head of graduate student council of M.E.T.U, September 2004

M.E.T.U., Prof. Dr. Mustafa N. Parlar Education and Research Foundation, M.Sc Thesis of the Year Award, November 2003

M.E.T.U Graduate Student Council member, September 2003

M.E.T.U. Chemistry Department, head of Graduate Students, September2003

Scientific and Research Council of Turkey (TUBITAK), M.Sc scholarship, March 2002-September 2003

Graduation Degree, High Honour Student, June 2001

Ranked first among all 51 graduates of the bachelor's degree programs in Chemistry Department 2000-2001 academic year.

Conference and Meetings

Joint International Symposium on Macrocyclic and Supramolecular Chemistry, June 25-30, 2006, Victoria, BC, Canada, Signal Ratio Amplification via Modulation of Resonance Energy Transfer, Ali Coşkun, Engin U. Akkaya.

XXX International Symposium on Macrocyclic Chemistry, July 17-21, 2005, Dresden, Germany, Molecular Half Subtractor Based on Boradiazaindacene Emission via PET and ICT Processes Within a Single Molecule, Ali Coşkun, Erhan Deniz, Engin U. Akkaya.

8th Conference on Methods and Applications of Fluorescence, August 24-27, 2003, Praque, Czech Republic, Towards Novel Fluorescent Chemosensors for Anions, Ali Coskun, Neslihan Saki, and Engin U. Akkaya.

XVII. National Chemistry Conference, 8-11 September 2003, İstanbul, Application of New Boradiaza-s-indacene Derivatives in Anion sensing and Molecular Logic Gates, Ali Coşkun, Engin U. Akkaya.

Publication

1.   Novel fluorescent chemosensor for anions via modulation of oxidative PET: A remarkable 25-fold enhancement of emission, Coskun A. ; Baytekin, B.; Akkaya, E.U. *Tetrahedron Lett.,* **2003**, 45, 5649-5651.
2.   Difluorobora-s-diazaindacene dyes as highly selective dosimetric reagents for fluoride anions, Coskun A. ; Akkaya, E.U. *Tetrahedron Lett.,* **2004**, 45, 4947-4949.
3.   Three-Point Recognition and Selective Fluorescence Sensing of L-DOPA Coskun, A.; Akkaya, E. U. *Org. Lett*., **2004**, 6(18), 3107-3109.

4.   Cation modulation of carbonyldipyrrinone (CDP) fluorescence: emission-ratiometric sensing of calcium, Coskun, A.; Deniz, E.; Akkaya, E.U., J. Mater. Chem., 2005, 27-28 ,2908-2912.

5.   Ion Sensing Coupled to Resonance Energy Transfer: A Highly Selective and Sensitive Ratiometric Fluorescent Chemosensor for Ag(I) by a Modular Approach, Coskun, A.; Akkaya, E.U., *J. Am. Chem. Soc.* ; **2005**; 127(30); 10464-10465.

6.   Effective PET and ICT Switching of Boradiazaindacene Emission: A Unimolecular, Emission-Mode, Molecular Half-Subtractor with Reconfigurable Logic Gates, Coskun, A.; Deniz,E.; Akkaya, E.U.; *Org. Lett.*; **2005**; 7(23); 5187-5189.

7.   Acenaphtopyrrolone-dipicolylamine derivative as selective and sensitive chemosensor for IIB cations, Coskun, A.; Yilmaz, M.D.; Akkaya, E.U.; *Tetrahedron Lett.* ; **2006**; 47 (22); 3689-3691.

8.   Signal Ratio Amplification via Modulation of Resonance Energy Transfer: Proof of Principle in an Emission Ratiometric Hg(II) Sensor,   Coskun, A.; Akkaya, E.U., *J. Am. Chem. Soc.* ; **2006**; 128(45); 14474-14475.

9.   Bis(2-pyridyl)-Substituted   Boratriazaindacene   as   an   NIR-Emitting Chemosensor for Hg(II), Coskun, A.; Yilmaz, M.D.; Akkaya, E.U., *Org. Lett*.; **2007**; 9(4); 607-609.

10.   A sensitive fluorescent chemosensor for anions based on a styryl-boradiazaindacene framework, Coskun, A.; Deniz, E.; Akkaya, E.U. *Tetrahedron Lett.*, **2007**, *48*, 5359-5361.